ANALYTICAL AND EXPERIMENTAL INVESTIGATION FOR DISTORTION-INDUCED FATIGUE IN STEEL BRIDGES

Project No. TPF-5(189)

By

Amanda Sue Hartman

Submitted to the graduate degree program in Civil Engineering
and the Graduate Faculty of the University of Kansas
in partial fulfillment of the requirements for the degree of
Doctor of Philosophy.

Committee Chairman _____
Dr. Caroline Bennett

Committee Members _____
Dr. Stanley Rolfe

_____
Dr. Adolfo Matamoros

_____
Dr. Ron Barrett-Gonzalez

_____
Robert Lyon

Date Defended: _____

The Dissertation Committee for Amanda Sue Hartman certifies that this is the approved version of the following dissertation:

ANALYTICAL AND EXPERIMENTAL INVESTIGATION FOR DISTORTION-INDUCED FATIGUE IN STEEL BRIDGES

Committee Chairman

_____
Dr. Caroline Bennett

Committee Members

_____
Dr. Stanley Rolfe

_____
Dr. Adolfo Matamoros

_____
Dr. Ron Barrett-Gonzalez

_____
Robert Lyon

Date Approved: _____

EXECUTIVE SUMMARY

Distortion-induced fatigue has been extensively studied; however, retrofit techniques currently used are expensive and/or time consuming to implement. These retrofit techniques primarily fall into two categories—stiffening or softening the weak web-gap region. The University of Kansas has developed an innovative stiffening technique that is economical to implement. This technique requires two angles providing attachment between the connection plate and girder web with a plate placed on the other side of the web to distribute out-of-plane forces (called angles-with-plate retrofit). Another appealing aspect of the angles-with-plate retrofit is the minimal traffic disruption required during retrofit application. Through analytical and experimental testing, the angles-with-plate retrofit has been shown to be effective in halting or slowing distortion-induced fatigue crack growth.

This dissertation is divided into five parts and appendices. The first two parts are an analytical investigation of parameters influencing distortion-induced fatigue and current retrofit techniques on a full-scale bridge in Abaqus. Parts 3-5 are analytical and experimental investigations of the angles-with-plate retrofit on a 9.1 m [30 ft.] test bridge. Each part within the document contains particular formatting associated with published or expected publishing requirements.

Part 1: Effects of Lateral Bracing Placement and Skew on Distortion-Induced Fatigue

Part 2: Distortion-Induced Fatigue in Steel Bridges: Causes, Parameters, and Fixes

Part 3: Experimental Investigation of Distortion-Induced Fatigue Repair in a 9.1 m [30 ft.] Bridge System

Part 4: Parametric Retrofit Analysis for Distortion-Induced Fatigue in a 9.1 m [30 ft.] Bridge System

Part 5: Innovative Retrofit Technique for Distortion-Induced Fatigue Cracks in Steel Girder Web Gaps

Part 1 was published in the Journal of the Transportation Research Board No. 2200, Volume 1. This research was presented at the 7th International Bridge Engineering Conference in December 2012 in San Antonio, Texas. Part 2 was published in the conference proceedings of

the American Society of Civil Engineers/Structural Engineering Institute (ASCE/SEI) Structures Congress held in Orlando, Florida in May 2010. Parts 3 and 4 are intended for future publication. Part 5 has been accepted for presentation and potential proceedings publication for the 7th New York City Bridge Conference in August 2013 in New York City, New York.

ACKNOWLEDGEMENTS

First of all, I would like to thank all of those at the University of Kansas that made this dissertation possible. Without the guidance, support, and expertise of Drs. Caroline Bennett, Adolfo Matamoros, and Stanley Rolfe, this research and completed dissertation would not have been possible. Additionally, I would like to thank Dr. Ron Barrett-Gonzalez and Robert Lyon for their contributions to my research and education. Several undergraduates made this research possible including Nathan Hickey, Andy Petz, Riley Piles, Zach Olson, and Patricia Aguiar who assisted with construction and data collection. Finally, I would like to thank all those graduate students who contributed to this work including Heidi Hassel, Chris Adams, Say Hak Bun, Temple Richardson, Jack Przywara, Alisha Elmore, and Katie McElrath.

I would like to gratefully acknowledge funding support from the Kansas Department of Transportation (KDOT), University of Kansas Transportation Research Institute (KU TRI), and Transportation Pooled Fund Study TPF 5(189) participants.

Lastly, I would like to thank Kyle Hartman, my husband, for his unending support and encouragement throughout all of my education.

TABLE OF CONTENTS

APPENDIX D: FINITE ELEMENT MODELING DATA

APPENDIX E: EXPERIMENTAL DATA

LIST OF FIGURES

PART 1: EFFECTS OF LATERAL BRACING PLACEMENT AND SKEW ON DISTORTION-INDUCED FATIGUE

PART 2: DISTORTION-INDUCED FATIGUE IN STEEL BRIDGES: CAUSES, PARAMETERS, AND FIXES

PART 3: EXPERIMENTAL INVESTIGATION OF DISTORTION-INDUCED FATIGUE REPAIR IN A 9.1 M [30 FT.] BRIDGE SYSTEM

PART 4: PARAMETRIC RETROFIT ANALYSIS FOR DISTORTION-INDUCED FATIGUE IN A 9.1 M [30 FT.] BRIDGE SYSTEM

PART 5: INNOVATIVE RETROFIT TECHNIQUE FOR DISTORTION-INDUCED FATIGUE CRACKS IN STEEL GIRDER WEB GAPS

APPENDIX A: TEST SPECIMEN SPECIFICATIONS

APPENDIX B: CALIBRATION CONSTANTS

N/A

APPENDIX C: LOADING PROTOCOL

N/A

APPENDIX D: FINITE ELEMENT MODELING DATA

APPENDIX E: EXPERIMENTAL DATA

LIST OF TABLES

APPENDIX A: TEST SPECIMEN SPECIFICATIONS

APPENDIX B: CALIBRATION CONSTANTS

APPENDIX C: FINITE ELEMENT MODELING DATA

N/A

APPENDIX D: EXPERIMENTAL DATA

APPENDIX E: EXPERIMENTAL DATA

Part 1

EFFECTS OF LATERAL BRACING PLACEMENT AND SKEW ON DISTORTION-INDUCED FATIGUE

A.S. Hartman[1], H.L. Hassel[2], C.A. Adams[3], C.R. Bennett[4], A.B. Matamoros[5], and S.T. Rolfe[6]

ABSTRACT

Due to the structural configuration of skewed steel bridges, girders at the same station are likely to experience different bending moments and deflections. Resulting differential deflections between adjacent girders leads to out-of-plane secondary stresses, which often results in a fatigue-critical connection between the cross frames and the girders. For this reason skewed steel bridges are particularly susceptible to distortion-induced fatigue.

This research explored the importance of lateral bracing placement in protecting bridges against distortion-induced fatigue. High-resolution three-dimensional finite element analyses of a bridge with multiple brace and skew configurations were performed to examine the relationships between skew angle, lateral bracing placement, and stresses at regions susceptible to distortion induced fatigue cracking. Bridges with skew angles of 0, 20, and 40 deg. and cross frames spaced at both 4.58 m (15 ft) and 9.15 m (30 ft) were investigated. Lateral bracing configurations examined included cross frames staggered perpendicular to the web of the girders as well as cross frames parallel to the support skew.

The analysis conducted found maximum stresses in the web-gap occurred in positive moment regions, but not necessarily in regions of highest differential deflection. The location of maximum stress demand was in the top web-gap region in configurations with cross frames parallel to skew, but in the bottom web-gap region when cross frames were staggered. Furthermore, skew angle and cross frame spacing slightly increased the maximum stress for parallel to skew cross frame arrangements.

University of Kansas, 1530 W. 15th St., Lawrence, KS 66045
[1] Amanda S. Hartman, Graduate Research Assistant
[2] Heidi L. Hassel, Graduate Research Assistant
[3] Chris A. Adams, Graduate Research Assistant
[4] Caroline R. Bennett, PhD, Assistant Professor, University of Kansas, crb@ku.edu
[5] Adolfo B. Matamoros, PhD, Associate Professor, University of Kansas, abm@ku.edu
[6] Stanley T. Rolfe, PhD, A.P. Learned Distinguished Professor, University of Kansas, srolfe@ku.edu

INTRODUCTION

Distortion-induced fatigue is a failure mechanism found in many steel girder bridges built prior to the mid-1980s. Common practice prior to 1980, in accordance with American Association of State Highway and Transportation Officials (AASHTO) Specifications, was to provide positive connection between transverse connection plates and girder webs; however, rarely was positive connection provided between the plates and girder flanges creating a web-gap region. As a bridge is loaded and girders deflect differing amounts, large secondary stresses can develop in the web-gap region resulting in a connection detail that is vulnerable to fatigue failure.

Previous research [1,2] has related fatigue vulnerability to differential deflection between girders, and examined factors that influence the differential deflections in skewed bridges. The primary objective of this research was to determine the effect skew and lateral brace placement have on stresses and differential deflections to better understand distortion-induced fatigue in steel bridges.

BACKGROUND

DISTORTION-INDUCED FATIGUE

Distortion-induced fatigue is an undesired consequence initially born from an attempt to solve an existing fatigue problem in steel bridges. Prior to 1980, it was common to deliberately not attach connection stiffeners to girder flanges in an effort to avoid creating additional fatigue details. Several fatigue failures in tension flanges of European bridges in the 1930's reinforced the desire to avoid introducing imperfections and discontinuities in regions of high tensile stresses by not welding connection stiffeners to tension flanges [3]. However well intentioned, high stress concentrations in the web-gap region resulted from out-of-plane distortion in the absence of positive connection between the flange and transverse connection stiffener.

Most often, distortion-induced fatigue occurs at connections of transverse structural members [4]. Lateral braces between adjacent girders, connected to girder webs through transverse connection plates, are required to prevent instability during construction and aid in lateral load transfer between girders; however, web-gaps between connection plates and girder flanges are the most common location for fatigue cracking. As load is applied, differential deflection occurs between adjacent steel girders. Because the top flange is restrained from

lateral displacement by the concrete deck and the bottom flange is free to rotate, distortion occurs in the relatively flexible region of the unsupported web between the flange and connection stiffener (Fig. 1).

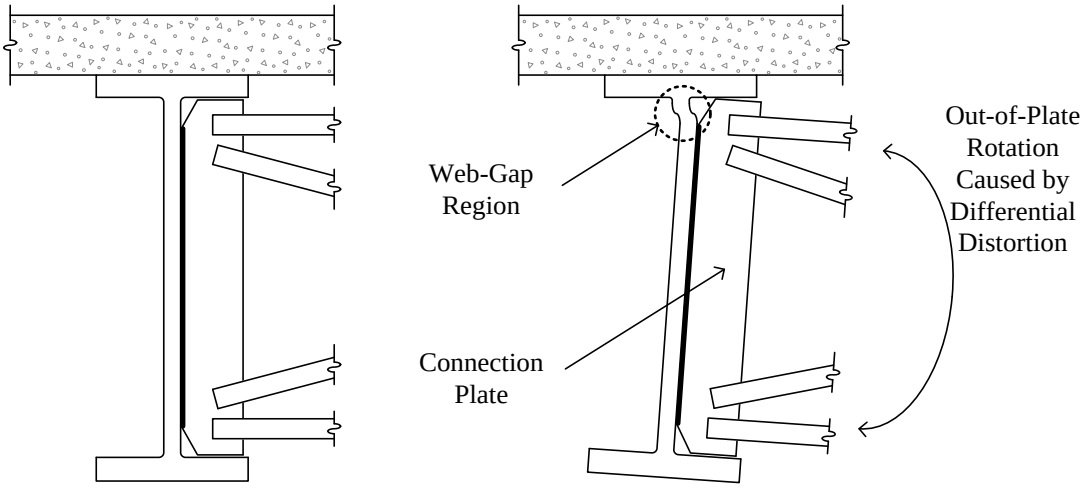

FIGURE 1 Girder cross-section before and after differential displacement.

With web-gap distortion accounting for the majority of fatigue cracks in bridges across the United States, there is a substantial body of literature [4-8] including analytical and experimental studies investigating the expected performance of and repair methods for steel bridge girders subjected to distortion-induced fatigue. There has been much discussion about the location along a girder's length where fatigue cracks in the web-gap region are most likely to form. A literature review conducted as part of this study did not show agreement between various studies due to the number of possible bridge geometric configurations [2, 4, 9-14].

There is repeated disagreement concerning the region within continuous-span bridges most likely to experience distortion-induced fatigue cracking. Roddis and Zhao [4] state that cracking in unskewed (i.e., right) bridges most frequently occurs in positive moment regions of bridge girders where differential girder deflections and out-of-plane bending moments are greatest. Conversely, Khalil et al. [9] investigated a skewed bridge with X-type cross frames, and found that eight out of nine cracks due to differential deflections between adjacent girders occurred in the negative moment region. It should be noted that while there is evidence that distortion-induced fatigue may be problematic in negative bending regions of bridges [9, 10], this limit state is more likely to occur if the bridge is skewed.

Several parameters have been found to have significant effects on bridge girder differential deflections. These parameters, examined using staggered diaphragms susceptible to

web-gab distortion, include: girder spacing, angle of skew, span length, and deck thickness [2]. Increasing skew angle tends to increase distortion-induced fatigue as quantified by increased differential deflection [10], except in situations where the truck length approaches the span of the bridge [2]. Longer spans decrease differential deflections as the bridge is more flexible in the vertical direction and more uniform lateral load distribution between girders can occur. Berglund and Schultz [2] found a linear relationship between differential deflection and girder spacing.

SKEWED BRIDGES

Bridge supports are often skewed to accommodate complicated highway alignments, and the skew angle of the bridge influences distortion-induced fatigue demand placed on bridge girders. AASHTO Specifications [15-17] allow bracing to be installed parallel to the skew angle if skew is less than 20 deg. (Fig. 2a). However, when the skew angle is greater than 20 deg., lateral connections and braces become too flexible due to longer brace lengths [18]. Because of this, AASHTO [15-17] specifies that bracing must be installed perpendicular to girders' webs for bridges skewed more than 20 deg.

Bracing may either be non-staggered (Fig. 2b) or staggered (Fig. 2c), and it has been shown that stagger has an effect on the susceptibility of a bridge to fatigue cracks [11, 12]. However, conflicting conclusions have again been noted in the literature. Barth and Bowman [11] reported that non-staggered diaphragms were more susceptible to fatigue cracking than comparable staggered diaphragm configurations. Conversely, Fraser, Grondin, and Kulak [12] reported that when diaphragms were in a staggered configuration, fatigue cracks were found to be more pronounced than in bridges with unstaggered bracing.

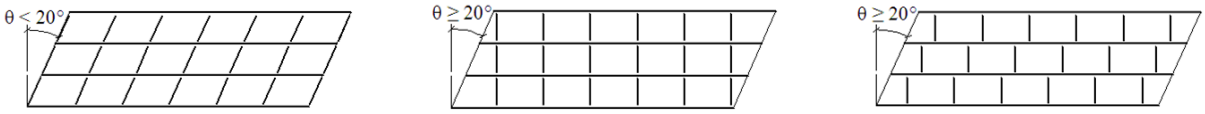

(a) **(b)** **(c)**

FIGURE 2 Cross frame arrangements (a) Skew < 20°, cross frames placed parallel to skew; (b) Skew ≥ 20°, non-staggered cross frames placed perpendicular to web; (c) Skew ≥ 20°, staggered cross frames placed perpendicular to web.

HOT SPOT STRESS ANALYSIS

Estimates of remaining fatigue life for welded structures are commonly based on a nominal stress distribution away from the point of crack initiation. Because high stress gradients occur in the vicinity of welds and nominal stresses cannot be easily determined in regions of complex geometry [14, 19], AASHTO [17] S-N curves are not accurate predictors of fatigue life in these applications. To overcome this problem, analysis techniques have been developed to estimate the number of fatigue cycles to crack initiation using stress results from Finite Element (FE) analyses. One such method is Hot Spot Stress (HSS) analysis.

Hot Spot Stress analysis is defined as the sum of bending and membrane stresses at a structural discontinuity [20]. Membrane stress is taken as the stress resulting from the effect of axial load only (axial load divided by an area). This analysis technique utilizes either a one-point procedure or a two-point extrapolation procedure to estimate the level of stress at the weld toe. The process of HSS analysis begins with calculating stress at a predetermined distance away from the weld toe. This distance is usually calculated based on plate thickness and/or weld length, and must be sufficiently far from the weld toe so that stresses are not influenced by the high stress gradients commonly observed at weld toes.

Although stresses are taken at points away from the weld toe, HSS analysis is dependent on mesh, element type, and extrapolation technique [21], which are important limitations. Despite limitations, HSS analysis is needed to examine distortion-induced stresses in steel bridge girders because nominal stress cannot be determined with confidence using closed form solutions, and was used in this study.

MODELING METHODOLOGY

PARAMETERS FOR STUDY

Among the many parameters known to affect distortion-induced fatigue cracking in steel bridges, skew angle and cross frame placement are two widely varied parameters. To investigate the effects of skew and lateral brace placement on distortion-induced fatigue performance of steel bridges, three skew angles were chosen for study: 0, 20, and 40 deg. Cross frame spacing was also varied, with spacings of 4.58 m (15.0 ft) and 9.15 m (30.0 ft). AASHTO [17] does not allow cross frames to be placed parallel to the skew angle in bridges with skew angles over 20

deg., therefore, it was necessary to evaluate bridges with cross frames placed parallel to skew as well as placed perpendicular to the girder webs and staggered. There are several bridges in existence that have cross frames placed parallel to skew, with skew angles beyond 20 deg. Additionally, it is worthwhile to investigate the effect of this parameter on bridge response to better understand the parameters that affect distortion-induced stresses in steel bridges. Therefore a 40 deg. bridge was also analyzed. A total of ten finite element models (Table 1) were created for analysis.

TABLE 1 Finite Element Models

Skew Angle	Parallel to Skew		Staggered	
	4.575 m (15 ft)	9.150 m (30 ft)	4.575 m (15 ft)	9.150 m (30 ft)
0	X	X		
20	X	X	X	X
40	X	X	X	X

BRIDGE SPECIFICATIONS

Bridge dimensions chosen for analysis were adapted from American Iron and Steel Institute (AISI) Example 2 [22]. The bridge consisted of two 27.5 m (90.0 ft) continuous spans with girder spacing of 3.05 m (10.0 ft). Positive and negative cross-section dimensions as well as an elevation of the bridge are shown in Fig. 3. This bridge was chosen for study because its complete design is widely available to interested readers, its typicality for two-span continuous bridge structures, and its use in other scientific articles to illustrate bridge engineering concepts [23].

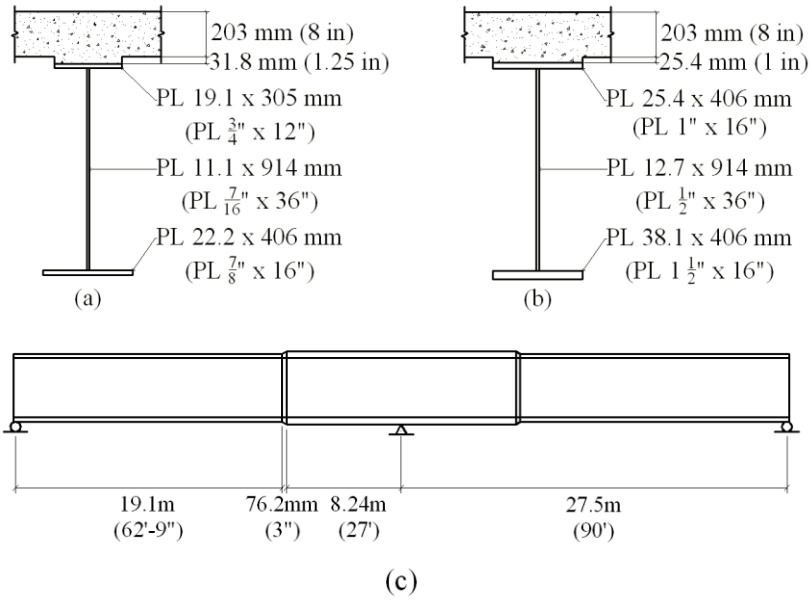

FIGURE 3 (a) Positive girder cross-section. (b) Negative girder cross-section. (c) Location of positive and negative cross-sections.

Four different cross frame placements were considered: parallel to the angle of skew and staggered perpendicular to the girder web for 4.58 m (15.0 ft) and 9.15 m (30.0 ft) spacing. Cross frame arrangements have been presented in Fig. 4, shown with 4.58 m (15.0 ft) spacing. The dashed lines in Fig. 4 represent the cross frames that were removed to form the 9.15 m (30.0 ft) spacing arrangement.

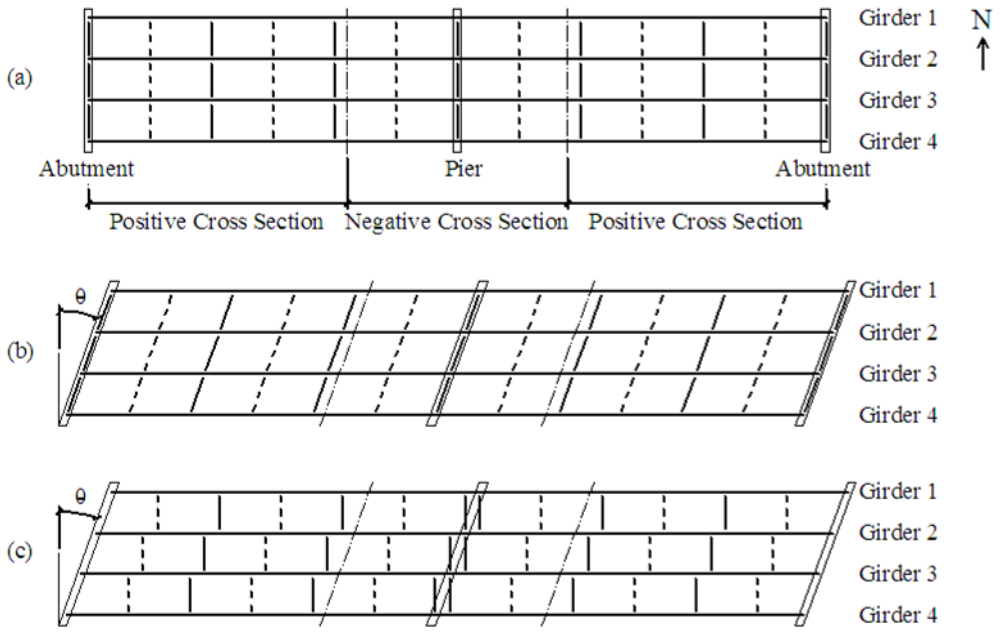

FIGURE 4 (a) Right bridge cross frame locations; (b) Skewed bridge parallel to skew cross frame locations; (c) Skewed bridge staggered cross frame locations.

Cross frame members were designed based on slenderness in compression with a maximum effective slenderness ratio, KL/r, of 140 [24]. For the right bridge and the 20 deg. skewed bridge with cross frames parallel to the skew, L102 X 102 X 15.9 mm (L4 X 4 X 5/8) brace elements were chosen with slenderness ratios 100 and 106 respectively. The 40 deg. skewed bridge with cross frames placed parallel to the skew required WT 152 X 365 (WT 6 X 25) brace elements with a slenderness ratio of 97.9 to counteract the longer unbraced length due to the high degree of skew. All bridges with cross frames perpendicular to the web required utilized the same cross frames modeled in the right bridge.

To reflect construction constraints in a realistic manner, the connection plates for the skewed cross frames were modeled as bent rectangular plates. Bent connection plates allow for adequate welding around all sides perpendicular to the web, instead of attempting welds at acute angles. Connection plate dimensions are shown in Fig. 5.

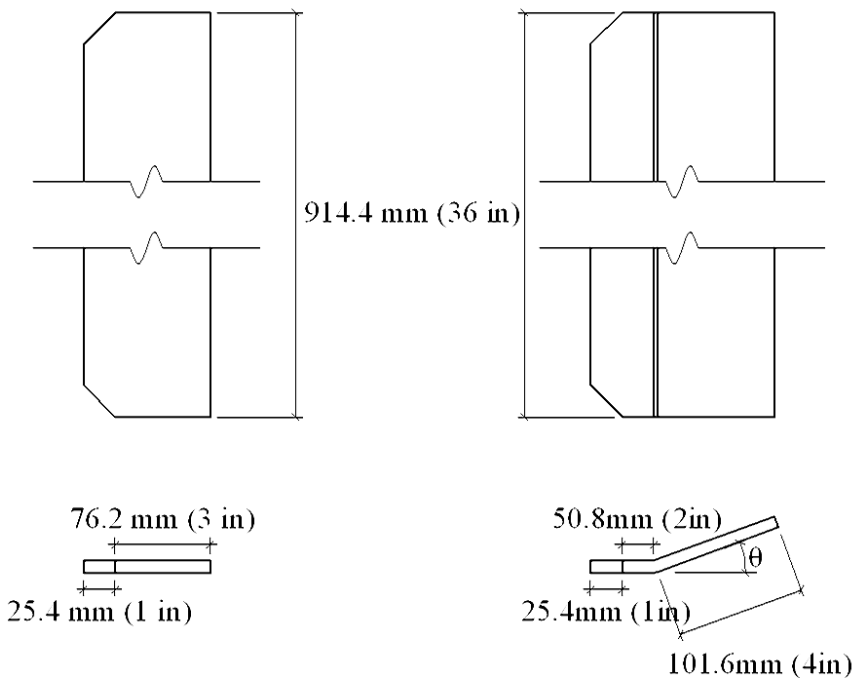

FIGURE 5 Connection plate details.

FINITE ELEMENT MODELING

A detailed analytical investigation was completed for each bridge using the commercially available FE modeling software ABAQUS v.6.8-2. Each three-dimensional model was composed of five main parts: deck, girder top flanges and concrete haunch, girder webs, girder bottom flanges, and cross frames. These parts were needed to create densely meshed web-gap regions, but simplified meshes and elements away from the areas under investigation. The adopted modeling strategy simplified the structure, while allowing for detailed analyses of areas of interest. Model parts were rigidly connected using surface-to-surface tie constraints. Element types, mesh sizes, constraints, and boundary conditions remained constant between models.

The deck was modeled using a linear-elastic material and four-node shell elements (S4R) with a mesh size of approximately 1.07 m (3.50 ft). Shell elements were chosen for the deck to improve computational efficiency. The reinforced concrete deck elements were eight inches thick and loaded on the top surface using a pressure load.

The load was applied over a 2.14 m (7.00 ft) width of deck centered over the third girder, and was continuous over the entire length of the bridge. The loaded section skewed along with the skew angle of the bridge, but the total area did not change. A 10.3 Pa (0.0015 ksi) pressure

was used for a total load magnitude of 1220 kN (274 kips). The load chosen produced stress values large enough to make comparisons more meaningful and readily apparent to the reader. It should be noted that load placement was not studied as a varied parameter in this article, although it is recognized that it would likely have an effect on distortion-induced stresses. Instead, load placement was held constant so that valid comparisons could be made between lateral brace placements and skew angles.

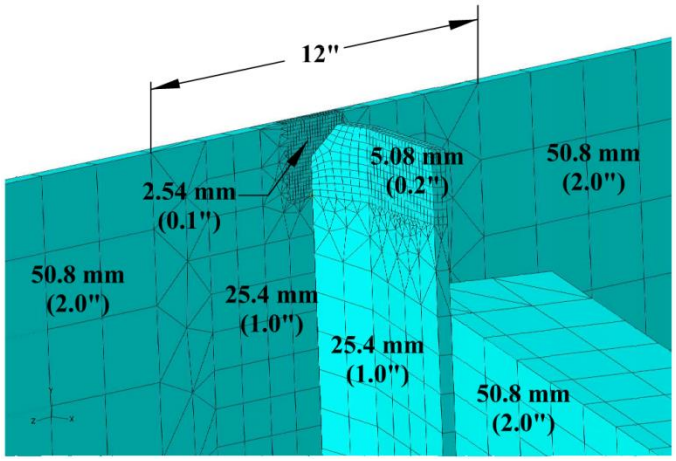

FIGURE 6 Mesh seed sizes for finite element models.

Eight-node, linear brick elements (C3D8R) were utilized in the girders, concrete haunch, and cross frames. The concrete haunch was modeled using brick elements instead of shell elements so that large shell elements with a constant depth could be used to define the primary surface of the deck. The top flange, concrete haunch, and bottom flange were meshed using a 50.8 mm (2.00 in.) mesh throughout. The web was meshed using small elements near the connection of the cross frames and then decreased in density away from the connection regions (Fig. 6). Regions of tetrahedral mesh were used between areas with different sizes of structured, hexagonal mesh to allow the elements to transition from one size to another. Cross frames were also meshed with a variety of element sizes to optimize efficiency of the models (Fig. 6).

Transition regions, 76.2 mm (3.0 in) wide, were used in the top flange, web, and bottom flange where the girder transitioned between positive and negative cross-sections. This region was meshed using a tetrahedral 50.8 mm (2.0 in) mesh. The transition was assumed to have

negligible effects on overall bridge analysis because the region occurred at a point of minimal moment in the girder and was not located near a point of interest.

Each two-span bridge was modeled as continuous, pinned at the interior pier, and supported by rollers at the abutments. The boundary conditions of the FE models were approximated by applying restraints over a 152 mm (6.00 in) long section of the bottom flange centered over both abutments and the interior pier.

STRESS ANALYSIS – HOT SPOT STRESS ANALYSIS

In determining stresses for comparison, it is critical to have a consistent 'measuring stick'. Fatigue is generally based on nominal stresses; however, this was not seen as practical for the complex geometry associated with web-gap regions. Maximum tensile principal stress, a 3-D stress, was the chosen basis for comparison between bridge configurations. It was considered critical in determining distortion-induced fatigue vulnerability to account for stresses in all three directions, capturing both nominal and out-of-plane stresses.

Due to the complex geometry of the web-gap region, HSS one-point procedure was used as a consistent method for determining stresses, rather than the absolute maximum stress. According to this procedure, a point was chosen away from the weld toe or connection to determine stresses that are comparable in nature. For this analysis, stresses were obtained at a distance of 0.20 in. (approximately half the web thickness) away from the edge of the connection plate on the web as seen in Fig. 7. Stresses for all nodes along the path were obtained, and the maximum along this path was chosen for each cross frame. This procedure provided a consistent comparison even as the stress distribution in the web-gap changed between models.

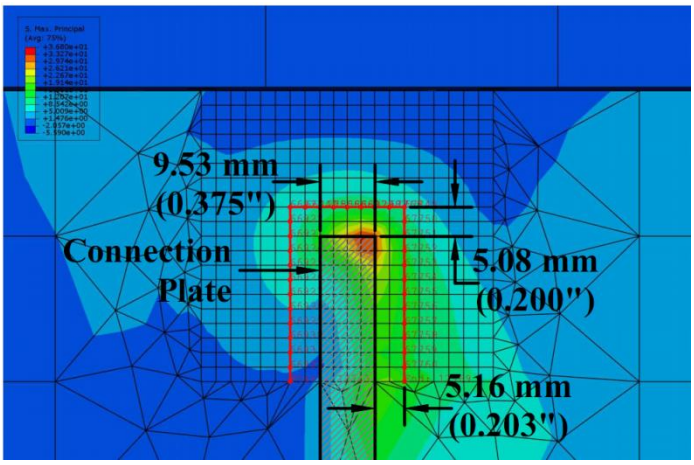

FIGURE 7 Hot spot stress analysis path (in red).

RESULTS

ABSOLUTE AND DIFFERENTIAL GIRDER DEFLECTION

Vulnerability to fatigue failure in areas surrounding the web-gap has previously been considered to be directly related to the amount of differential deflection between adjacent girders. Therefore, the effect of skew angle, girder arrangement, and girder spacing on girder deflection and differential deflection between girders were evaluated in this study.

Vertical girder deflection at each cross frame location was determined using FE models. In all cases, the largest absolute and differential deflections were located in the positive moment regions, near the center of each span. Consistently, the loaded girder (Girder 3) experienced the most deflection. Fig. 8 shows the deflection profile for all four girders in the 40 deg. skewed model, with cross frames positioned parallel to the skew angle every 4.58 m (15.0 ft). Deflection of Girder 2 was restrained by the north exterior girder (Girder 1), and therefore did not experience as much deflection as Girder 4. Differential deflection between girders ordered from highest to lowest in magnitude was as follows: Girder 1 to 2, Girder 2 to 3, Girder 3 to 4. These results were consistent regardless of skew angle or cross frame arrangement in all models evaluated.

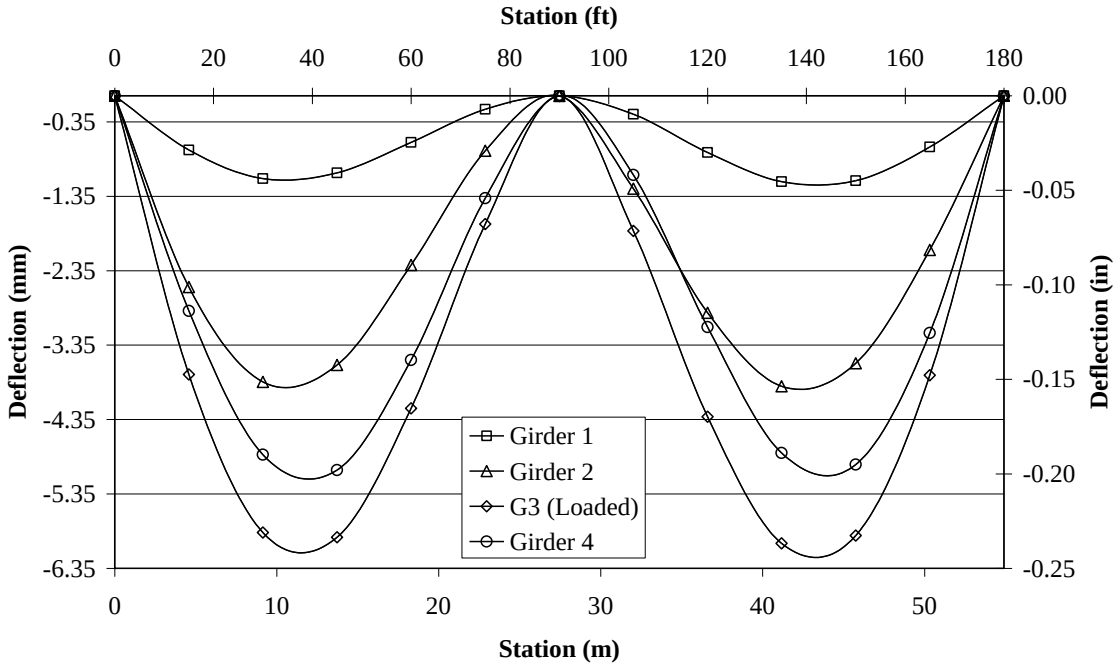

FIGURE 8 Deflected profile of girders from 40 deg. skewed model, cross frames positioned parallel to skew, spaced at 4.58 m (15 ft).

RELATIONSHIP BETWEEN DEFLECTION AND STRESSES

One maximum principal stress value was extracted, using HSS analysis, for the top and bottom of each web-to-cross frame connection. Both stress and differential deflection quantities were highest in positive moment regions, but the differential deflections did not reliably correlate with the location of highest stress. Differential deflection was found to be greatest between Girders 1 and 2, but none of the highest stresses occurred in this region. The highest stresses for the parallel to skew bridges occurred at the connections for the cross frames between Girders 3 and 4, which was found to be the area of lowest differential deflection. In this study, differential deflection was not found to be a reliable predictor of the location of high web-gap stress, although it has commonly been adopted as such in previous studies [2].

Because maximum principal stresses were used for comparison, one would expect stresses in the web-gap region to be affected by the amount of bending stress in the girders. In this analysis, the largest principal stresses were found in Girders 2, 3, and 4, and the location of maximum stress was in the positive bending moment region towards the center of the span, consistent with areas of high bending moment.

Although differential deflection between Girders 3 and 4 was found to be much smaller than that between Girders 2 and 3, the stresses were found to be consistently higher in Girder 4. This was likely due to tensile forces on the south side of Girder 2 (the side closest to the loaded girder) being balanced by tensile forces on the north side of Girder 2. Therefore, if two cross frames were attached to a girder across from each other, stresses tended to balance and drop in magnitude. This is consistent with what Kansas Department of Transportation (KDOT) has observed in the field, as well as research performed by Fraser, Grondin, Kulak, and D'Andrea [12, 13].

BRIDGES WITH CROSS FRAMES PLACED PARALLEL TO SKEW ANGLE

Results from bridge models with cross frames placed parallel to skew as well as the right bridge were compared to determine the effects of skew angle and cross frame spacing on stress demand. The top web-gap region of the exterior girder adjacent to the loaded girder (Girder 4) was found to have the highest stress demand in all six models, with the stress magnitude in the interior girder adjacent to the loaded girder (Girder 2) slightly lower.

SKEW ANGLE

Effect of skew angle on maximum stress magnitude was evaluated in bridges with cross frames placed parallel to the skew. Maximum stress at each cross frame along the length of the girder was determined from analytical models. Fig. 9 shows the value of maximum stress in Girder 4 (the girder with highest magnitude of stress demand) increased with skew angle, although only slightly. Research performed by Jajich and Schultz [10] also found distortion-induced fatigue susceptibility increased with skew angle. A similar trend was noted for bridge models with the larger, 9.15 m (30.0 ft), cross frame spacing. The increase in stress demand between the right bridge and 20 deg. skew models was found to be 13% for the 4.58 m (15.0 ft) spacing and 6% for the 9.15 m (30.0 ft) cross frame spacing. Increase in stress demand between the 20 and 40 deg. skew models was only found to be 4% for the 4.58 m (15.0 ft) spacing and 6% for the 9.15 m (30.0 ft) cross frame spacing.

Maximum stress in the interior girder adjacent to the loaded girder (Girder 2) behaved in an opposite manner. Stress on the south face (the face connected to the loaded girder) decreased with skew angle, although only slightly. Currently AASHTO Specifications [17] prohibit

construction of bridges with cross frames aligned parallel to the skew angle when the skew angle is greater than 20 deg. This research showed that for the bridge configurations analyzed, the increase in maximum principal stress was not significant between bridges with 20 and 40 deg. skew angles under the applied loading.

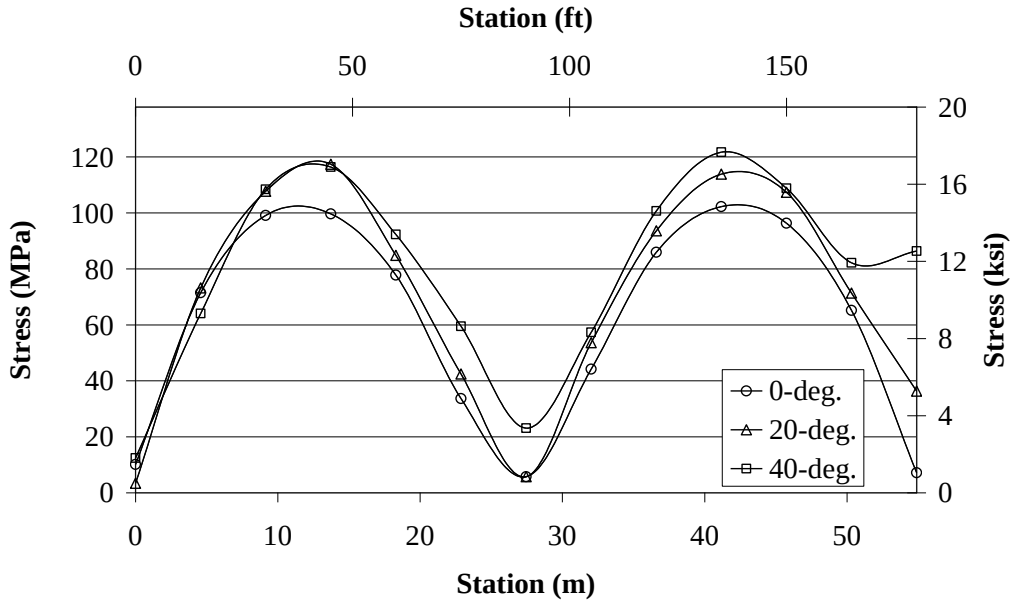

FIGURE 9 Maximum stress in top web-gap region of Girder 4-North at each cross frame location in. parallel to skew models with 4.58 m (15 ft) spacing.

EFFECT OF CROSS FRAME SPACING

Cross frame spacing was found to be proportional to maximum principal stress in bridges with cross frames placed parallel to the skew angle. Doubling cross frame spacing from 4.58 m to 9.15 m (15.0 ft to 30.0 ft) increased the maximum principal stress demand in each skewed bridge model by less than 10%. Therefore, cross frame spacing in a bridge with cross frames placed parallel to skew was found not to have a significant effect on stresses in the web-gap region. It is important to remember that the bridge evaluated was only loaded in the vertical direction. Effects of cross frame spacing may be more significant if similar models with alternative load configurations were evaluated.

EFFECT OF STAGGERED CROSS FRAMES

Staggering the cross frames, in accordance with AASHTO Specifications [17], tended to increase differential deflections because the cross frames were located at different stations on each girder.

Comparing the results from the models with staggered cross frames to the models with cross frames placed parallel to skew, it was observed that although staggering the cross frames caused the location of maximum stress to change drastically, the magnitude of maximum stress changed by less than 1%.

Maximum stresses in the models with staggered cross frames occurred in the positive moment region of the loaded girder (Girder 3) in the bottom web-gap region. In addition to increasing differential deflection, staggering the cross frames caused the bottom of the girder to displace transversely in reverse curvature along the length of the beam. At the top of the girder, the constraint imposed by the slab suppressed this mode of deformation. It is hypothesized that this change in girder response (as compared to models with cross-frames placed parallel to the skew) was the reason maximum stress demands were found in the bottom web-gap region in configurations with staggered cross frames. Fig. 10 shows a cross frame between Girders 3 and 4 in the 40 deg. skewed model with cross frames placed both parallel to the skew angle and staggered at the same station along the girder. The deflection scale and contouring levels are identical in both figures.

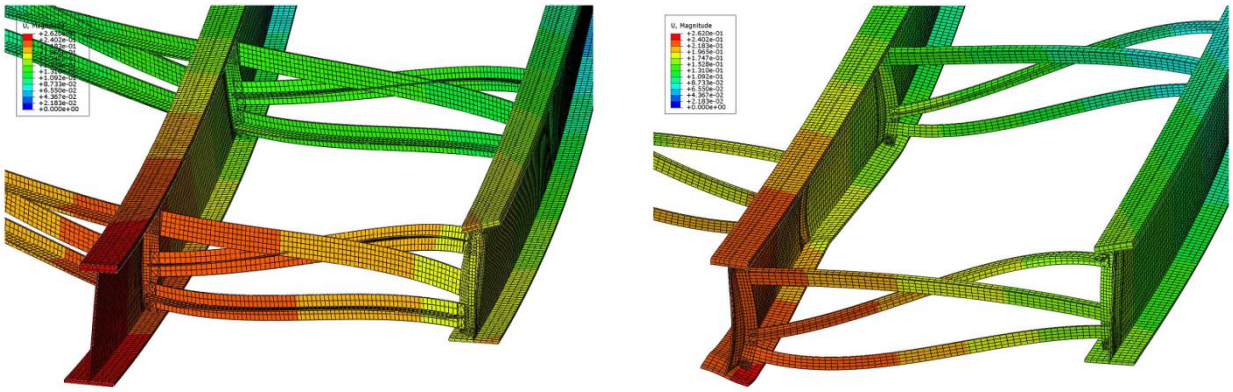

(a) (b)

FIGURE 10 Deflected shape of 40 deg. skewed bridge with 4.58 m (15.0 ft) cross frame spacing and: (a) Cross frames placed parallel to skew; (b) Staggered cross frames. Deck removed from view for clarity.

The spacing between cross frames on opposite sides of a girder, i.e., the amount of stagger, was directly influenced by angle of skew. Fig. 4c shows cross frame layout for the models with staggered cross frames. When two cross frames were in close proximity on opposite sides of the web, stresses acting on both sides tended to cancel each other out and reduced the

tensile stress in this area. As skew angle approached 45 deg., cross frames on opposite sides of the web became more evenly spaced and alternating transverse displacement (reverse curvature effect) was increased. The maximum stress value was found in the 40 deg. skew model with 4.57 m (15.0 ft) spacing. Stresses in all of the models dropped significantly (over 20%) when the cross frame spacing was changed from 4.58 to 9.15 m (15.0 to 30.0 ft). This behavior was due to decreased restraint resulting from fewer cross frames, leading to lower stress concentrations in the web-gap region. In models with staggered cross frames, the maximum principal stress shifted from the girders adjacent to the loaded girder to the loaded girder itself. Maximum principal stress was no longer in the exterior girder because it did not have cross frames on both sides of the web causing reverse curvature. Staggered models showed more complicated behavior than models with cross frames placed parallel to the angle of skew. The magnitude of stress in the web-gap region was significantly altered due to amount of stagger (directly related to the skew angle) and the number of cross frames.

CONCLUSIONS

The parametric study described in this paper investigated the effects of skew and lateral brace placement on stresses and differential deflections of a steel girder bridge. Specifically, skew angle, cross frame spacing, and cross frame arrangement were considered. Results of the study can be summarized as follows:

1. Differential deflection and stress were found to be proportional, although differential deflection did not predict the row of cross frames corresponding with the highest stress demand.
2. Maximum differential deflections and stresses occurred in positive moment regions for all of the bridges modeled.
3. Maximum stresses consistently occurred in the top web-gap region of the exterior girder adjacent to the loaded girder (Girder 4) in bridges with cross frames placed parallel to skew angle.
4. Maximum stresses consistently occurred in the bottom web-gap region of the loaded girder (Girder 3) in bridges with staggered cross frames. Therefore, it was found that bottom web-gaps should not be neglected in analysis, and should be considered during fatigue life assessment of existing structures.

5. Bridges with cross frames placed parallel to the skew angle and those with staggered cross frames behaved very differently, although the maximum stress was found to be similar for both brace placements considered.
6. In bridges with cross frames placed parallel to the skew angle, increased cross frame spacing slightly increased the maximum stress in the bridge.
7. Stagger and cross frame spacing had a large impact on the stresses in the web-gap region of bridges with staggered cross frames, although the stress values did not increase proportionally to skew angle.
8. In bridges with staggered cross frames, the restraint placed on the girder was found to be a significant parameter.

Since many bridges built prior to the mid-1980s are susceptible to distortion-induced fatigue, it is important to recognize bridges, and specific locations within bridges, prone to this type of failure in an effort to extend useful life through monitoring and repair of critical details. Although much research has been performed to identify regions of maximum differential deflections and to evaluate the influence of bridge geometry on differential deflection, little prior work has been done to quantify web-gap stresses or relate differential deflections to stresses. This paper has attempted to provide a link to further guide bridge engineers in identifying details susceptible to distortion-induced fatigue cracking. It is hoped that improving current understanding of the effects of lateral brace placement and skew angle will guide judicious and deliberate implementation of lateral bracing schemes in future bridge designs.

ACKNOWLEDGEMENTS

The authors are grateful for support from the Kansas Department of Transportation (KDOT) and the University of Kansas Transportation Research Institute (KU TRI). The authors would also like to acknowledge support provided through Pooled Fund Study TPF-5(189), which includes the following participating State DOTs: Kansas, California, Iowa, Illinois, New Jersey, New York, Oregon, Pennsylvania, Tennessee, Wisconsin, and Wyoming, as well as the Federal Highway Administration.

REFERENCES

[1] Cousins, T.E. and Stallings, J.M. (1998). "Laboratory Tests of Bolted Diaphragm-Girder Connections." *Journal of Bridge Engineering*, 3(2), 56-63.

[2] Bergland, E. and Schultz, A. (2006). "Girder Differential Deflection and Distortion-Induced Fatigue in Skewed Steel Bridges." *Journal of Bridge Engineering*, 11(2), 169-177.

[3] Fisher, J.W. and Keating, P.B. (1989). "Distortion-Induced Fatigue Cracking of Bridge Details with Web Gaps." *Journal of Constructional Steel Research,* 12(3-4), 215-228.

[4] Roddis, W.M.K. and Zhao, Y. (2001). "Out-of-Plane Fatigue Cracking in Welded Steel Bridges: Why It Happened and How It Can Be Repaired." *Welding Innovation*, 27(2), 2-7.

[5] Lindberg, A.Y. and Schultz, A.E. (2007). "Incorporation of Fatigue Detail Classification of Steel Bridges into the Minnesota Department of Transportation Database: Final Report." *St. Paul: Minnesota Department of Transportation: Research Services Section.*

[6] Keating, P. (1994). "Focusing on Fatigue." *Civil Engineering (N.Y.)* 64(11), 54-57.

[7] Connor, R.J. and Fisher, J.W. (2006). "Identifying Effective and Ineffective Retrofits for Distortion Fatigue Cracking in Steel Bridges Using Field Instrumentation." *Journal of Bridge Engineering,* 11(6), 745-752.

[8] Fisher, J.; Jian, J.; Wagner, D; and Yen, B. (1990). "Distortion-Induced Fatigue Cracking in Steel Bridges." *NCHRP Report #336, Transportation Research Board (TRB).*

[9] Khalil, A., Wipf, T.J., Greimann, L., Wood, D.L., and Brakke, B. (1998). "Retrofit Solution for Out-of-Plane Distortion of X-Type Diaphragm Bridges." *Transportation Conference Proceedings, Iowa Department of Transportation,* 99-102.

[10] Jajich Jajich, D. and Schultz, A.E. (2003). "Measurement and Analysis of Distortion-Induced Fatigue in Multigirder Steel Bridges." *Journal of Bridge Engineering*, 8(2), 84-91.

[11] Barth (Grider), A.S. and Bowman, M.D. (2001). "Fatigue Behavior of Welded Diaphragm-to-Beam Connections." *Journal of Structural Engineering*, 127(10), 1145-1152.

[12] Fraser, R.E.K., Grondin, G.Y., and Kulak, G.L. (2000). "Behavior of Distortion-Induced Fatigue Cracks in Bridge Girders." *Structural Engineering Report No. 235*.

[13] Grondin, G.Y., Fraser, R., and D'Andrea, M. (2002). "Testing and Evaluating of Fatigue Damaged Girders." *4th Structural Specialty Conference of the Canadian Society for Civil Engineering*.

[14] Roddis, K.W.M. and Zhao, Y. (2003). "Finite-Element Analysis of Steel Bridge Distortion-Induced Fatigue." *Journal of Bridge Engineering*, 8(5), p 259-266.

[15] American Association of State Highway and Transportation Officials (AASHTO). (2002). *Standard Specifications for Highway Bridges*, Washington, D.C.

[16] American Association of State Highway and Transportation Officials (AASHTO). (2004). *Standard Specifications for Highway Bridges*, Washington, D.C.

[17] American Association of State Highway and Transportation Officials (AASHTO). (2007). *Standard Specifications for Highway Bridges,* Washington, D.C.

[18] Wang, L. and Helwig, T.A. (2008). "Stability Bracing Requirements for Steel Bridge Girders with Skewed Supports." *Journal of Bridge Engineering*, 13(2), 149-157.

[19] Kim, M.H. and Kang, S.W. (2008). "Testing and analysis of fatigue behaviour in edge details: a comparative study using hot spot structural stresses." *Proceedings of the Institution of Mechanical Engineers, Part C: Journal of Mechanical Engineering*

Science, 22(12), 2351-2363.
[20] Marquis, G. and Kahonen, A. (1996). "Fatigue testing and analysis using the hot spot method." *VTT Publications*, 239, p 3-35.
[21] Maddox, S.J. (2002). "Hot-Spot Stress Design Curves for Fatigue Assessment of Welded Structures." *International Journal of Offshore and Polar Engineering*, 12(2), 134-141.
[22] AISI Example 2: Two-Span Continuous Composite I Girder (1997). *American Iron and Steel Institute*.
[23] Barth, K.E., Hartnagel, B.A., White, D.W., and Barker, M.G. (2004). "Recommended Procedures for Simplified Inelastic Design of Steel I-Girder Bridges." *Journal of Bridge Engineering*, 9(3), 230-242.
[24] Steel Bridge Design Handbook: Example 2A, 3rd Edition Load and Resistance Factor, *National Steel Bridge Alliance*.

Part 2

DISTORTION-INDUCED FATIGUE IN STEEL BRIDGES: CAUSES, PARAMETERS, AND FIXES

H.L. Hassel[1], A.S. Hartman[2], C.R. Bennett[3], A.B. Matamoros[4], and S.T. Rolfe[5]

ABSTRACT

Distortion-induced fatigue in steel bridges is a continuing problem for bridge engineers. Accordingly, a cumulative review and discussion of scholarly literature on this topic as well as focused analytical research aimed at studying bridge system performance when various retrofit techniques are applied to connection details are described.

Driving forces behind distortion-induced fatigue are presented, including the effects of bridge system geometry and specific detail geometries. Retrofit techniques including positive attachment, back-up transverse stiffeners, slotted connection stiffeners, and removal of lateral brace elements were studied analytically to determine effectiveness. Results from finite element analyses are presented showing relative success of various retrofit techniques. Appropriateness of retrofit techniques under various conditions is also disseminated.

INTRODUCTION

Steel bridges designed prior to the mid-1980s were not always detailed in a manner consistent with current industry standards. Many steel bridges of this era were constructed with cross frames connected to the girder web through transverse connection plates; however, no positive connection was provided between the transverse connection plates and girder flanges. As differential deflection occurred between bridge girders under live loading, lack of connection tended to allow cross frames to pull or push on the girder web, resulting in large cyclic secondary stresses in the weak web gap region. This phenomenon is termed distortion-induced fatigue.

University of Kansas, 1530 W. 15th St., Lawrence, KS 66045
[1] Heidi L. Hassel, Graduate Research Assistant
[2] Amanda S. Hartman, Graduate Research Assistant
[3] Caroline R. Bennett, PhD, Assistant Professor, University of Kansas, crb@ku.edu
[4] Adolfo B. Matamoros, PhD, Associate Professor, University of Kansas, abm@ku.edu
[5] Stanley T. Rolfe, PhD, A.P. Learned Distinguished Professor, University of Kansas, srolfe@ku.edu

Many of these aging bridges now require regular inspection and repair to address cracking due to distortion-induced fatigue. To adequately understand and effectively retrofit such bridges, it is important to examine and compare commonly used retrofit techniques. It is also important to consider the effects retrofits have on the bridge from a system-oriented perspective, rather than considering isolated connections outside of their context. This paper provides an extensive literature review of the causes, parameters, and potential fixes associated with distortion-induced fatigue as well as a finite element study on the effectiveness of common retrofit techniques. The objective of this research was to investigate stress reduction resulting from retrofit techniques and compare the success of each in multiple bridge configurations to identify techniques most suitable for a given bridge geometry.

BACKGROUND

DISTORTION-INDUCED FATIGUE OVERVIEW

Lateral bracing in steel girder bridges stabilizes girders during construction, provides resistance to transverse loading, and helps distribute live loading laterally between girders (Tedesco et al. 1995). During the 1930's several failures occurred in European bridges resulting from welds between connection stiffeners and girder tension flanges (Fisher and Keating 1989). In an effort to prevent fatigue damage, common practice was to provide no positive attachment between connection stiffeners and girder flanges.

Lack of connection creates a weak web gap region susceptible to out-of-plane distortions and fatigue. Uneven loading of girders at equal stations along the bridge induce differential deflections between adjacent girders causing rotation of lateral bracing members. Because the girder top flange is restrained by the deck, out-of-plane displacement is concentrated in the flexible web gap region. Resulting secondary stresses in the web gap can lead to distortion-induced fatigue. Although current AASHTO (2007) specifications require positive attachment between transverse stiffeners and girder flanges, bridges constructed prior to 1980 are at risk of experiencing damaged due to distortion-induced fatigue.

PARAMETERS AFFECTING DISTORTION-INDUCED FATIGUE

It has proven difficult to form conclusions from the body of literature concerning the region of bridges most vulnerable to distortion-induced fatigue. Roddis and Zhao (2001) found that

distortion-induced fatigue cracks most frequently occurred in positive bending moment regions where differential girder deflection and out-of-plane bending moments were highest. Conversely, Khalil et al. (1998) observed eight of nine fatigue cracks discovered occurred in the negative moment region in a bridge under investigation. The issue is further complicated by conflicting literature as to whether the web gap region adjacent to the top or bottom girder flange tends to be at greater risk. Fisher et al. (1990) concluded that cracks are most likely to form in web gaps adjacent to the girder top flange unless staggered diaphragms are used.

Bridge Geometry

Distortion-induced fatigue is a complicated issue largely influenced by bridge geometry. Skew angle, span length, girder spacing, and deck thickness influence differential deflection between adjacent girders and therefore, affect distortion-induced fatigue. Decreased span length and increased girder spacing both amplify differential deflection, except when the bridge span approaches truck length. As girder length increases and the bridge becomes increasingly flexible, lateral bracing more effectively distributes load between girders, and the bridge displaces vertically with less differential deflection (Berglund and Schultz 2006).

Bridge supports are often skewed to accommodate highway alignments. At equal stations along skewed bridges, each girder is subjected to varied bending moment and deflection under uniform loading. Increasing skew angle increases the bridges differential deflection and susceptibility to distortion-induced fatigue (Berglund and Schultz 2006). Skew angle also influences lateral bracing configuration.

Lateral Bracing Configuration

Lateral bracing helps distribute live loads among girders and therefore impact the resulting differential deflections and web gap stresses in multi-girder steel bridges. There are numerous lateral bracing configurations because brace type and placement can both be varied widely. Use of cross braces instead of bent-plate diaphragms have been shown to significantly reduce maximum differential deflection (Li and Schultz 2005). Furthermore, K-type truss diaphragms have proven to create smaller secondary stresses in web gaps than X-type cross frames (Fisher et al. 1990).

Multiple lateral brace configurations may be used in skewed bridges, including braces placed parallel to the skew angle, perpendicular to the girders' webs, and staggered. Cross frames or

diaphragms placed parallel to skew angle and directly across from each other is optimal, but not always practical. Back-to-back bracing members have a balancing effect on out-of plane bending stresses (Barth and Bowman 2001). Placing cross frames parallel to skew angle allows lateral bracing members to be attached to adjacent girders at equal points along the member where girders are subjected to equal bending moments and deflection under uniform loading. At high skew angles, braces placed parallel to skew angle tend to become excessively long and flexible and therefore less effective at distributing load. Current AASHTO (2007) Specifications require that lateral bracing members in bridges with skew angles great than 20 deg. be placed perpendicular to girder webs. In such bridges, lateral bracing can be either non-staggered or staggered. Non-staggered, back-to-back brace placement allows brace forces to utilize the balancing effect, but braces are attached to extremely different points along each girder which increases the differential deflection braces undergo. Therefore, braces are often staggered. Fraser et al. (2000) reported that fatigue cracks were more pronounced in bridges with staggered diaphragms than in bridges with non-staggered diaphragms, but Barth and Bowman (2001) concluded the opposite. This is yet another conflicting conclusion in the literature describing distortion-induced fatigue in steel bridges.

Ongoing research at the University of Texas in Austin involves the use of half-pipe shapes instead of bent-plate transverse connection stiffeners in skewed bridges with cross frames oriented parallel to skew angle is being investigated. Initial results indicate the proposed connection detail stiffens the connection significantly, allowing cross frame spacing to be increased due to higher efficiency of fewer cross frames. A stiffer connection combined with a reduced number of cross frames dramatically decreases bridge susceptibility to distortion-induced fatigue (Quadrato et al. 2009).

LOCAL WEB GAP GEOMETRY

Web gap geometry is thought to influence the amount of secondary stresses induced in the web gap region. According to a survey conducted by Fisher et al. (1990), the web gap length (the vertical dimension between the inside of the flange and the weld attaching the connection stiffener) typically ranges from 6.35 to 102mm [0.250 to 4.00in]. Web gaps must absorb the out-of-plane displacement. Since smaller web gaps have less space and material to absorb this

displacement, the risk of distortion-induced fatigue cracking is increased with decreased web gap length (Fisher et al. 1990).

DISTORTION-INDUCED FATIGUE RETROFIT TECHNIQUES

Out-of-plane distortion or other secondary stresses at fatigue sensitive details are responsible for an estimated 90% of all fatigue cracking in steel bridges (Connor and Fisher 2006). Therefore, repair and retrofit techniques have been developed to enhance fatigue life of steel bridges including stiffening, softening, or removal of connection elements.

STIFFENING OR SOFTENING OUT-OF-PLANE CONNECTION ELEMENTS

Numerous studies have concluded that fatigue performance can be enhanced by either stiffening the web gap or softening the restraint on the connection; although no guidance is provided in literature as to which solution is more appropriate for a given bridge configuration. Fisher et al. (1990) showed that positive attachment reduced secondary stresses in the web gap region by reducing the magnitude of out-of-plane displacement in the girders web. Positive connection can be accomplished using methods such as welds, bolts, epoxy, and/or angles. When welding is used, field weld quality is a concern because overhead welding is required. Angles or WT shapes can be attached to the connection plate and flange to reduce stress concentrations. Bolting to the top flange of the girder may be difficult to implement because the concrete deck must be removed; however, Jones et al. (2008) identified a method using stud-welding wherein a bolted angle connection could be made without deck removal. Stiffness of the connection elements used must also be considered as it has been shown to influence effectiveness (Connor and Fisher 2006).

Softening restraint provided by the connection also tends to reduce stresses in the web gap region. Loosening the connection bolts between the stiffener and girder web when a bolted connection is used may reduce both stresses and out-of-plane distortion (Khalil et al. 1998). Another softening technique involves removal of a portion of the transverse stiffener plate, lengthening the web gap. A hole is drilled in the connection plate and a slot is flame cut between the girder web and connection plate.

Removal of Lateral Brace Elements

An additional method of eliminating secondary stresses in web gap regions is to remove lateral brace elements altogether. In composite bridges, interior lateral braces may not be required due to stability provided by the concrete deck. However, lateral bracing may still be needed at supports to transfer lateral loads. Although removal of bracing has been shown to eliminate secondary stresses in web gaps, this technique has been shown to increase differential deflections between adjacent girders by as much as 25% (Tedesco et al. 1995) and bending moments by as much as 15% (Stallings et al. 1999). Therefore, removal may not be advisable unless the bridge under consideration was designed with a high capacity reserve. Another disadvantage of lateral brace removal is that temporary bracing would be required during deck replacement.

Other Improvement Methods

Several methods have been shown to improve fatigue life of welds including shot peening, hammer peening, laser peening, and ultrasonic impact treatment (UIT). These weld treatment methods aim to induce residual compressive stresses at the weld toe resulting in reduced tensile stress ranges experienced at critical details. Additionally, applications of Carbon Fiber Reinforced Polymers (CFRP) to welded details have been shown to improve fatigue life by reducing the stress demand at the weld toe (Kaan et al. 2008).

After a fatigue crack has initiated, growth can be retarded by drilling a hole at the tip of the crack, reducing the stress concentration and increasing the fatigue life. Crack-stop holes can be used in combination with other methods such as cold expansion or pretensioned bolts which introduce residual compressive stresses at the edges of the hole. A combination of retrofits is also practical because space limitations in connection geometry often do not allow for properly sized crack-stop holes and undersized holes must be used.

Modeling Methodology

Studied Parameters

Four commonly used retrofit techniques were implemented in a right (nonskewed) bridge to determine the effects on secondary stresses in the web gap region and other changes induced in retrofitted bridges. Retrofit techniques modeled included positive attachment, back-up stiffeners,

slotted connection stiffeners, and interior cross frame removal. Schemes were implemented on a local and global scale meaning that in "local" models only the most highly stresses regions were retrofitted, whereas all web gap regions were retrofitted in "global" models. The four rows of cross frames producing the highest stresses and treated in local retrofit models were the third and fourth set of cross frames from either end in the positive moment region of the bridge.

Because back-up stiffeners are more often used in skewed bridges with staggered cross bracing members, the effects of this particular retrofit technique were investigated in a 40 deg. skewed bridge with staggered cross frames as well as the right bridge. Three retrofitting schemes were modeled. A partial depth, 305mm [12.0in] stiffener was used on the top flange and bottom flange, and a model with a full depth stiffener fully fixed to both the top and bottom flanges was also used.

BRIDGE DESCRIPTION

The bridge used for analysis was modeled after American Iron and Steel Institute (AISI) Example 2 (1997). The design of this bridge is widely available and has been used in other scholarly research as geometry representative of a typical bridge to illustrate bridge design concepts (Barth et al. 2004). The bridge consists of two 27.4m [90.0ft] continuous spans with four girders spaced at 3.05m [10.0ft]. The cross sections used in the bridge are shown in Fig. 1.

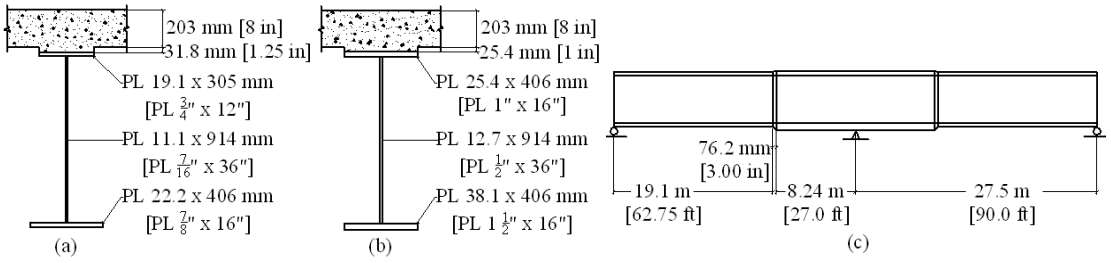

Figure 1. (a) Positive girder cross-section. (b) Negative girder cross-section. (c) Location of positive and negative cross-sections.

X-type cross frames were spaced every 4.58m [15.0ft] along the girders. Fig. 2 shows the plan view of both the right bridge and the skewed bridge. Cross frames were designed based on a maximum slenderness ratio (KL/r value) of 140 to resist compressive forces since no horizontal loads were applied to the bridge. Equal leg angles, L102x102x15.9mm [L4x4x5/8in] were chosen for brace elements.

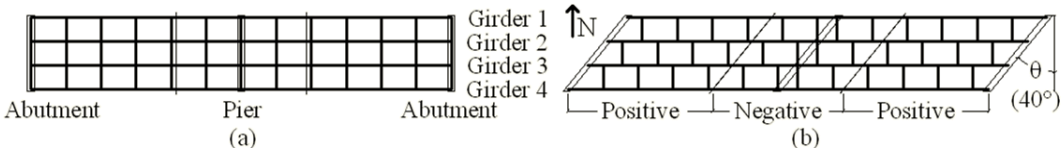

Figure 2. Plan view of (a) Right, nonskewed bridge. (b) Skewed, staggered bridge.

FINITE ELEMENT MODELING

Three-dimensional linear-elastic finite element (FE) models were completed using ABAQUS v.6.8-2, commercially available FE software. Each of the four bridge girders were composed of three main parts: bottom flange, web, and top flange with concrete haunch. Other components of the model included cross frames and concrete deck. Various mesh densities were used within the model to develop fine meshes in localized regions with coarse meshes elsewhere. Parts were connected using surface-to-surface tie constraints. Young's moduli were taken as 200GPa [29,000ksi] and 24.9GPa [3605ksi] for steel and concrete, respectively. Poisson's ratio was taken as 0.30 for steel and 0.15 for concrete. Support conditions were applied over a length of 152mm [6.00in] to the bottom flanges of each girder. Pinned conditions were applied to the interior pier while roller conditions were applied at abutments.

Four-node shell elements (S4R) with mesh size of approximately 1.07m [3.50ft] comprised the 203mm [8.00in] thick concrete deck. A pressure of 10.3Pa [0.00015ksi] was applied over a 2.14m [7.00ft] width spanning the entire length of Girder 3. This load was chosen to produce meaningful and noticeable stress responses. Although load placement would be expected to have an effect on distortion-induced fatigue stresses, load was held constant throughout all models to draw valid comparisons between applied retrofits.

Girders, cross frames, and concrete haunches were modeled using eight-node brick elements (C3D8R). Top flanges, bottom flanges, and concrete haunches were meshed at a density of 50.8mm [2.00in]. Girder webs were comprised of various mesh sizes to create very dense meshes in the web gap regions (see Fig. 3). Transitions between structured hexagonal meshes were accomplished through the use of four-node linear tetrahedron elements (C3D4). Mesh density of the connection stiffeners was also varied to refine output in the web gap region (see Fig. 3).

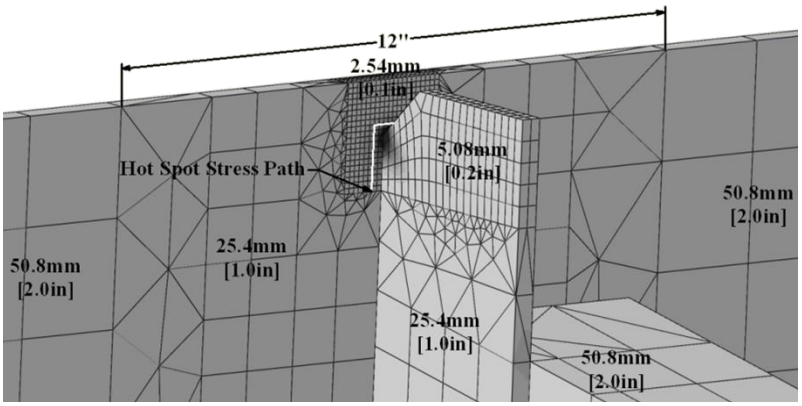

Figure 3. Mesh sizes and Hot Spot Stress path.

In order to transition between negative and positive girder dimensions, a 76.2mm [3.00in] region of four-node tetrahedron elements (C3D4) was utilized in the concrete haunch, top flange, web, and bottom flange. Course web mesh size of 50.8mm [2.00in] was applied to the transition regions. This overall modeling strategy was employed to accurately capture system and local response of the bridges studied, while maintaining a reasonable level of computational efficiency needed to accomplish a parametric investigation. Each 3-D bridge model included approximately 750,000 elements and 2.75 million degrees of freedom.

RETROFIT TECHNIQUES

Effectiveness of four retrofit techniques in reducing secondary stresses in the web gap regions was investigated. Those studied included positive attachment, back-up transverse stiffeners, slotted connection stiffeners, and interior cross frame removal. The no-retrofit configuration and the first three of these retrofits are shown in Fig. 4.

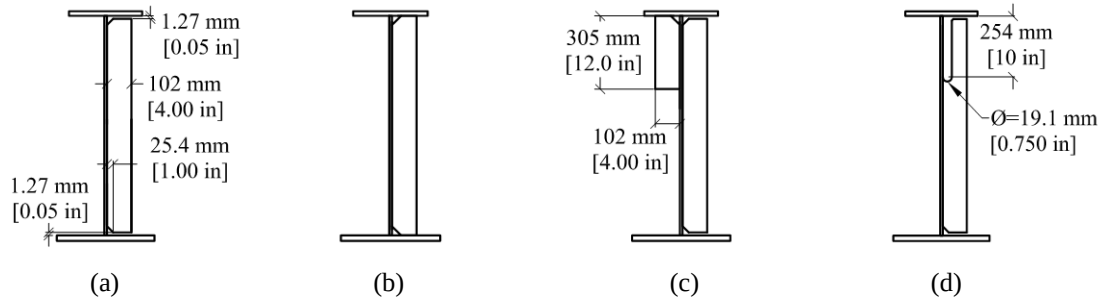

Figure 4. (a) No-retrofit stiffener. (b) Positively attached stiffener. (c) Back-up transverse stiffener. (d). Slotted connection stiffener.

Positive attachment was accomplished by removing the 1.27mm [0.0500in] gaps between the stiffener and flanges and using surface-to-surface tie constraints between the transverse stiffener and both top and bottom flanges. The back-up stiffener was modeled with the same thickness and width as the transverse stiffener plate, but the length was varied. Surface to surface ties were used to connect the back-up stiffener to both the web and adjacent girder flange(s), depending on the configuration used. Back-up stiffeners were meshed identically to no-retrofit connection stiffeners.

Slot dimensions were chosen based on space limitations and suggestions found in the literature surveyed (Fisher et al. 1990 and Fisher and Keating 1989). A slot length of 254mm [10in] was sized to be 20 times the largest web thickness. The hole diameter at the end of the slot was limited to 19.1mm [0.750in] by geometric constraints in the stiffener plate. In practice, the hole should be sized to facilitate a smooth surface so that new areas of stress concentration are not created (Zhao and Roddis 2007). The densely meshed region in both the stiffener and web were extended beyond the slot by 50.8mm [2.00in] so that detailed results could be viewed in the lengthened web gap region.

HOT SPOT STRESS ANALYSIS

Hot Spot Stress (HSS) analysis was utilized to compare stresses induced in bridge web gaps. HSS was chosen over absolute maximum stress because it is less mesh dependant and has be shown to be more reliable in regions of complex geometry. Because the web gap region experiences a complex three-dimensional stress field, maximum principal stress was deemed optimal for comparing stresses in this study. Numerous HSS techniques have been developed, however a simple one point extraction procedure was used herein. The procedure involved determining stress values a set distance from the weld toe and comparing them directly. Stress values were collected a distance of approximately half of the web thickness, 5.08mm (0.200in), from the weld toe on all three sides of each transverse stiffener in the densely meshed region of the girder web as shown in Fig. 3.

RESULTS

All four retrofit techniques studied reduced the web gap stress at applied locations. However, the extent to which each retrofit extended the bridge's fatigue life varied significantly.

Table 1 presents the maximum principal web gap stress in each of the right bridge models determined using Hot Spot Stress analysis as well as the percentage change from the no-retrofit model. Location of maximum principal HSS in the right bridge model with no retrofit was observed to be in the top web gap of Girder 4 in the positive moment regions (Fig. 2). Second most highly stressed region was the top web gap of Girder 2 in the positive moment regions.

Table 1. Maximum web gap stresses determined using Hot Spot Stress analysis, right bridge.

	Locally Applied Retrofit		**Globally Applied Retrofit**	
Retrofit Description	***Stress MPa [ksi]***	***% Change from no-retrofit model***	***Stress MPa [ksi]***	***% Change from no-retrofit model***
No Retrofit	103 [14.9]			
Positive Attachment	80.7 [11.7]	-21%	52.5 [7.62]	-49%
Back-Up Stiffener	86.0 [14.8]	-1%	69.2 [14.4]	-3%
Slotted Stiffener	102 [12.5]	-16%	99.4 [10.1]	-33%
Cross Frame Removal	98.5 [14.3]	-4%	45.4 [6.58]	-56%

Vertical girder deflection at each cross frame was also extracted from the analytical models and differential deflection between adjacent girders at every cross frame location (or location of cross frame removal) was computed. The differential deflection between Girders 3 and 4 was deemed most critical due to the location of maximum principal stress in the bridge, although this was not found to be the location of highest differential deflection, Δ. Results and percent change from the no-retrofit model are shown in Table 2.

Table 2. Maximum differential deflection between Girder 3 and 4, right bridge.

	Locally Applied Retrofit		**Globally Applied Retrofit**	
Retrofit Description	***Δ mm [10^{-3} in]***	***% Change from no-retrofit model***	***Δ mm [10^{-3} in]***	***% Change from no-retrofit model***
No Retrofit	0.249 [9.82]			
Positive Attachment	0.222 [8.74]	-11%	0.169 [6.66]	-32%
Back-Up Stiffener	0.408 [9.16]	-5%	0.570 [8.07]	-18%
Slotted Stiffener	0.233 [16.1]	64%	0.205 [22.5]	129%
Cross Frame Removal	0.532 [21.0]	114%	0.773 [30.4]	210%

LOCAL VS. GLOBAL RETROFIT TECHNIQUES

All retrofits were more successful at reducing the maximum web gap stress in the bridge when applied globally rather than locally. Globally-applied retrofits reduced the magnitude of stress demand by more than twice as much as local retrofits. Localized retrofit techniques reduced the stress where the retrofit was applied, but stresses in untreated areas of the bridge remained potentially problematic. In models with slotted stiffeners and removed cross frames stresses in untreated areas actually increased, although maximum stress in the entire bridge decreased. Maximum principal stress at each cross frame location in the top web gap of Girder 4 in models with the local retrofit are shown in Fig 5. These findings emphasize the importance of treating distortion-induced fatigue on a system level rather than focusing on localized regions in the bridge. Though local retrofitting may theoretically be a cost-saving approach, it was not found to be practical due to disagreement in the literature concerning the location of maximum stresses in bridges, as well as the possibility of transferring distortion-induced fatigue risk to other connections.

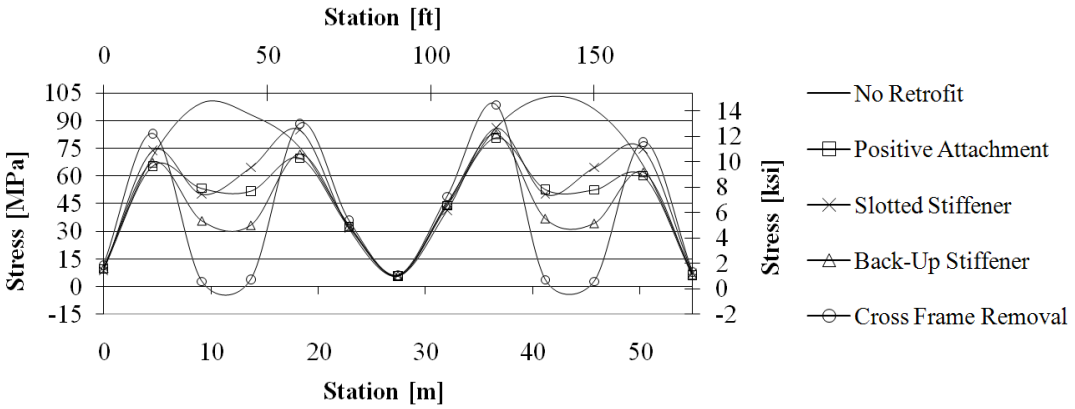

Figure 5. Maximum principal Hot Spot Stress in the top web gap of Girder 4 at each cross frame location in models with the local retrofit.

POSITIVE ATTACHMENT

Positively attaching the transverse stiffener to both the top and bottom flange reduced stresses in the web gap region, thereby extending fatigue life of the connection detail. It decreased both differential deflection and Hot Spot Stress in the bridge. Of the four retrofitting schemes analyzed, it reduced differential deflection the most and produced the second highest reduction in stress. Connections made between the transverse stiffener plates and girder flanges

are not expected to be completely rigid in practice, which may decrease the effectiveness of this retrofit technique from that found in the FE models.

BACK-UP STIFFENER

The back-up stiffener was not found to be an effective retrofit when applied to a right, nonskewed bridge. Although it decreased web gap stresses generated in the exterior girders where applied, the stress in Girder 2 increased. Therefore the overall maximum principal stress in the bridge did not decrease significantly.

The no-retrofit, skewed staggered model produced the highest Hot Spot Stresses in the bottom web gaps of the loaded girder in the positive moment regions. Though the location of maximum stress was different than in the right bridge, results were consistent with those of Fisher et al. (1990). Data for HSS in the web gap region and differential deflection between Girder 3 and 4 are shown in Table 3. Results for a locally retrofitted bridge were consistent with those determined using a right bridge.

Table 3. Maximum prinicpal Hot Spot Stress and differential deflection between Girder 3 and 4 for skewed, staggered bridge with global retrofit.

Retrofit	Stress MPa [ksi]	*% Change from no-retrofit model*	Δ mm [10^{-3} in]	*% Change from no-retrofit model*
No Retrofit	100 [14.6]		1.06 [41.8]	
Top Partial Stiffener	103 [15.0]	3%	0.954 [37.6]	-10%
Bottom Partial Stiffener	51.2 [7.43]	-49%	1.02 [40.0]	-4%
Full Depth Stiffener	35.9 [5.20]	-64%	0.896 [35.3]	-16%

The top partial stiffener was not effective in reducing stress in the bridge because it was not applied at locations of maximum stress. Both the bottom partial stiffener and the full depth stiffener significantly reduced the maximum principal stress in the bridge by almost 50%. All three retrofit schemes reduced differential deflection.

SLOTTED TRANSVERSE STIFFENER

Removal of a portion of the transverse stiffener significantly increased differential deflection as much as 129% in some areas but reduced the maximum principal stress in the bridge, illustrating that differential deflection alone cannot necessarily predict the bridge's susceptibility

to distortion-induced fatigue. Literature reviewed noted increased out-of-plane displacement resulting from utilization of the slot retrofit technique as much as four times the original value (Zhao and Roddis 2007). Therefore, the maximum out-of-plane displacement along the path used for HSS analysis was determined at each cross frame location. Out-of-plane displacement increased significantly and magnitudes in retrofitted models were as much as five times larger than in the model with no retrofit. Though out-of-plane displacement increased, the magnitude remained small (under 0.762 mm [0.0300 in]) and therefore, was not regarded as detrimental for this structure.

CROSS FRAME REMOVAL

Complete removal of interior cross frames eliminated the web gap region and associated stress concentrations, reducing the maximum principal HSS in the bridge by 56%. In this study, cross frame removal was most effective at reducing stresses at the original cross frame locations, but may not be suitable for all bridges. Because interior cross frames were no longer present to help distribute traffic loading among adjacent girders, the differential deflection increased by as much as 210% at some locations. Though the increase was large, it was not considered problematic because the maximum girder deflection increased by less than 0.500mm [0.0200in].

CONCLUSIONS

A thorough review of existing literature concerning the causes of distortion-induced fatigue, parameters which influence a bridge's susceptibility to secondary stresses generated in the web gap regions, and retrofits that can extend the remaining fatigue life of the bridge is presented. A finite-element analysis involving four retrofits including positive attachments, back-up transverse stiffeners, slotted connection stiffeners, and cross frame removal was conducted. Conclusions of this study can be summarized as follows:

1. Generally speaking, retrofit techniques should be applied on a global basis. Retrofitting every connection in the bridge reduced the maximum stress more than twice as much as only treating the most highly stressed regions.
2. Connection stiffening techniques reduced the amount of differential deflection between adjacent girders, but connection softening techniques and cross frame removal increased differential deflection.

3. Positive attachment reduced differential deflection by the greatest amount and reduced the maximum principal stress in the bridge by almost 50%.
4. Back-up stiffeners were found to not be suitable for right, nonskewed bridges, but were extremely effective in skewed, staggered bridges. Globally applied back-up stiffeners were found to reduced the maximum stress in the bridge (originally found in the positive moment regions) most when either partial depth and attached to the bottom web gap region or full depth were used.
5. Partial removal of the transverse stiffener through use of a slot technique reduced the stress concentrations in the web gap region by over 30%.
6. Cross frame removal reduced secondary stresses in the web gap regions over 55% and was the most effective of the retrofits studied, although removal may not be a practical solution for all bridges.

Many bridges are susceptible to distortion-induced fatigue and identification of effective retrofits is essential to extending useful life. Finite element analysis performed demonstrates the importance of considering the bridge as a system rather than individual connections in an isolated sense, when evaluating performance of retrofit techniques. Bridge parameters not only affect the bridges' fatigue risk, but success of repair and retrofit schemes. This study highlighted the importance of quantifying stresses in the bridge rather than using differential deflection alone to predict fatigue risk. Findings of this analysis are intended to help further guide bridge engineers in selecting and implementing retrofits in steel girder bridges.

ACKNOWLEDGEMENTS

The authors are grateful for support from the Kansas Department of Transportation (KDOT) and the University of Kansas Transportation Research Institute (KU TRI). The authors would also like to gratefully acknowledge support provided through Pooled Fund Study TPF-5(189), which includes the following participating State DOTs: Kansas, California, Iowa, Illinois, New Jersey, New York, Oregon, Pennsylvania, Tennessee, Wisconsin, and Wyoming, as well as the Federal Highway Administration.

REFERENCES

American Iron and Steel Institute (AISI) Example 2: Two-Span Continuous Composite I Girder

(1997). *American Iron and Steel Institute*.

American Association of State Highway and Transportation Officials (AASHTO). (2007). *Standard Specifications for Highway Bridges,* Washington, D.C.

Barth (Grider), A.S. and Bowman, M.D. (2001). "Fatigue Behavior of Welded Diaphragm-to-Beam Connections." *Journal of Structural Engineering*, 127(10), 1145-1152.

Barth, K.E., Hartnagel, B.A., White, D.W., and Barker, M.G. (2004). "Recommended Procedures for Simplified Inelastic Design of Steel I-Girder Bridges." *Journal of Bridge Engineering*, 9(3), 230-242.

Berglund, E. and Schultz, A. (2006). "Girder Differential Deflection and Distortion-Induced Fatigue in Skewed Steel Bridges." *Journal of Bridge Engineering*, 11(2), 169-177.

Connor, R. J. and Fisher, J. W. (2006). "Identifying Effective and Ineffective Retrofits for Distortion Fatigue Cracking in Steel Bridges Using Field Instrumentation." *Journal of Bridge Engineering*, 11(6), 745-752.

Fisher, J. W., Jian, J., Wagner, D. C., and Yen, B. T. (1990). "Distortion-Induced Fatigue Cracking in Steel Bridges." *National Cooperative Highway Research Program Report #336,* Transportation Research Board, National Research Council, Washington, D. C.

Fisher, J.W. and Keating, P.B. (1989). "Distortion-Induced Fatigue Cracking of Bridge Details with Web Gaps." *Journal of Constructional Steel Research,* 12(3-4), 215-228.

Fraser, R.E.K., Grondin, G.Y., and Kulak, G.L. (2000). "Behavior of Distortion-Induced Fatigue Cracks in Bridge Girders." *Structural Engineering Report No. 235*.

Jones, J., Bennett, C., Matamoros, A., Rolfe, S., and Roddis, K. (2008). "Fighting fatigue in steel bridges," TR News, Transportation Research Board (TRB), Nov/Dec, Issue 259.

Kaan, B., Barrett, R., Bennett, C., Matamoros, A., and Rolfe, S. (2008). "Fatigue Enhancement of Welded Coverplates Using Carbon-Fiber Composites." Proc. of the 2008 ASCE/SEI Structures Congress, Vancouver, ABC, April 24-26, 2008.

Khalil, A., Wipf, T. J., Greimann, L, Wood, D. L, and Brakke, B. (1998). "Retrofit Solution for Out-of-Plane Distortion of X-Type Diaphragms Bridges." *Transportation Conference Proceedings, Iowa Department of Transportation*, 99-102.

Li, H. and Schultz, A. E. (2005). "Analysis of Girder Differential Deflection and Web Gap Stress for Rapid Assessment of Distortional Fatigue in Multi-Girder Steel Bridges." *Final Report 2005-38,* Minnesota Department of Transportation, St. Paul, MN.

Quadrato, C., Battistini, A., Helwig, T., Engelhardt, M., and Frank, K. "Effect of Cross Frame Connection Details on Stability of Steel Bridges with Skewed Supports." University of Texas, Austin. http://www.aisc.org/assets/0/1209478/1209480/1271820/39248d5d-83ad-4575-ae4c-4672c2486359.pdf [accessed 12/16/2009].

Roddis, W.M.K. and Zhao, Y. (2001). "Out-of-Plane Fatigue Cracking in Welded Steel Bridges: Why It Happened and How It Can Be Repaired." *Welding Innovation*, 27(2), 2-7.

Stallings, J. M., Cousins, T. E., and Stafford, T. E. (1999). "Removal of Diaphragms from Three-span Steel Girder Bridges." *Journal of Bridge Engineering*, 4(1), 63-70.

Tedesco, J.W.; Stallings, J. M.; and Tow, D.R. (1995). "Finite Element Method Analysis of Bridge Girder-Diaphragm Interaction." *Computers and Structures*, 56(2-3), 461-473.

Zhao, Y. and Roddis, W. M. K. (2007). "Fatigue Behavior and Retrofit Investigation of Distortion-Induced Web Gap Cracking." *Journal of Bridge Engineering*, 12(6), 737-745.

Part 3

EXPERIMENTAL INVESTIGATION OF DISTORTION-INDUCED FATIGUE REPAIR IN 9.1 M [30 FT.] TEST SYSTEM

Amanda Hartman[1], S.M. ASCE
Caroline Bennett[2], M. ASCE
Adolfo Matamoros[3], A.M. ASCE
Stan Rolfe[4], Hon. M. ASCE

ABSTRACT

With infrastructure in the United States deteriorating at an alarming rate, repair of existing roadway bridges is critical for state highway agencies to responsibly allocate scarce resources. For steel bridges that were constructed prior to the mid-1980s, distortion-induced fatigue cracking can be a significant problem. Retrofit or repair techniques currently used in the field may not completely halt crack growth and/or can be expensive to implement. A distortion-induced fatigue repair technique that is commonly implemented in the field is to provide positive connection between the transverse connection plate and girder flange. However, this technique often requires partial removal of the concrete deck to access the top of the flange to make the connection.

To address these concerns, an innovative retrofit technique developed at the University of Kansas was analyzed to determine its effectiveness as a distortion-induced fatigue repair its suitability for field implementation. A different approach was also taken by the authors where a retrofit termed "angles-with-plate" utilized two angle segments and a backing plate to connect the girder connection plate and the web.

To investigate the performance of this retrofit, a 9.1-m [30-ft] long three-girder test bridge was constructed and tested under fatigue loading to develop, and subsequently repair, distortion-induced fatigue cracking. A total of 12 test trials were performed with varying load ranges to assess the effectiveness and applicability of the angles-with-backing plate retrofit. In

[1] Amanda Hartman, Graduate Research Assistant, University of Kansas, 1530 W. 15th St., Lawrence, KS 66045
[2] Caroline Bennett, PhD, PE, Associate Professor, University of Kansas, 1530 W. 15th St., Lawrence, KS 66045
[3] Adolfo Matamoros, PhD, Professor, University of Kansas, 1530 W. 15th St., Lawrence, KS 66045
[4] Stan Rolfe, PhD, PE, A.P. Learned Distinguished Professor, University of Kansas, 1530 W. 15th St., Lawrence, KS 66045

addition to assessing retrofit performance, crack growth as well as girder deflections and strains were monitored. It was found that retrofit application significantly reduced web-gap rotation, while the diagonal cross frame angle framing into the top web-gap experienced a significant increase in tensile strain. When implemented with crack arrest holes, the angle-with-backing plate performed well at mitigating distortion-induced fatigue cracking in steel girders.

INTRODUCTION

During and prior to the 1970s, many steel bridges were constructed without significant knowledge of structural fatigue. Due to several structural failures in Europe when cross frame or diaphragm connection plates were welded to tension flanges in the 1930s (Fisher and Keating 1989), common practice until 1985 was to not weld connection plates to the tension flange. Although the intention of this detailing practice was to prevent similar failures to those that occurred in European steel bridges, this lack of connection initiated an area of significantly high stresses in steel bridge girders leading to rife fatigue cracking in bridges with this detailing. Many steel bridge structures designed and constructed during this time period have exhibited significant fatigue cracking due to distortion-induced fatigue, presenting bridge engineers and management staff with a challenging and expensive situation.

Distortion-induced fatigue commonly occurs at connections of transverse structural members (Roddis and Zhao 2001). Web-gaps that exist between connection plates and girder top flanges are the most common location for fatigue cracking. As a bridge experiences traffic loading, the steel girders undergo different levels of deflection. This results in cross frame members inducing secondary, out-of-plane forces on the adjacent girders that are deforming differently. Since the top flange of the girder is restrained from rotation by the concrete deck and the bottom flange is free to rotate, distortion of the web-gap region occurs which is shown in Figure 1. While secondary forces carried by the cross frames may be low in magnitude, they often translate into significant stresses due to the high flexibility of the web-gap, and due to the presence of a multitude of stress concentrations in the congested geometry of the web-gap region, and fatigue cracking can be expected to occur.

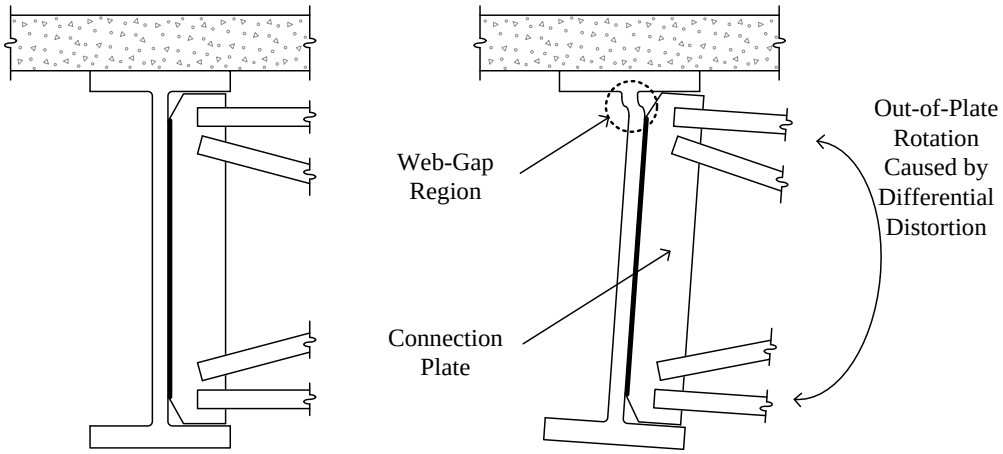

Figure 1: Out-of-plane rotation causing distortion-induced fatigue.

BACKGROUND

In addition to being a common occurrence in steel bridges, distortion-induced fatigue is also a problem that is both difficult and expensive to repair. There are a number of techniques that can be used to retrofit bridges for distortion-induced fatigue, including drilled crack-arrest holes, cross frame removal, slotting the connection plate, utilizing a back-up stiffener, and connecting the connection plate to the girder's top flange. Each of these techniques have associated advantages and disadvantages, and it is useful to bridge engineers and owners to have multiple options from which to choose.

Crack-arrest holes are often drilled at the tips of sharp cracks to halt crack growth as a first line of defense against fatigue crack propagation; however, "hole drilling alone is not effective at stopping fatigue cracks when the cracks are initiated from out-of-plane distortions" (Grondin et al. 2002). Although crack stop holes may temporarily slow or stop crack growth, they are not a permanent fix for cracking due to distortion-induced fatigue. Instead, crack-arrest holes are often used in conjunction with other retrofit techniques such as slotting or providing an alternate load path via a structural repair.

Cross frame removal is another retrofit option that has been examined for distortion-induced fatigue (Tedesco et al. 1995; Roddis and Zhao 2001). The concept of this technique is to remove the lateral connection between adjacent girders which eliminates out-of-plane forces induced by secondary structural members, thus eliminating distortion-induced fatigue. However, when cross-frames are removed from an existing bridge system, consideration should be given

to: (1) effectiveness of the bridge system to laterally distribute live loads; (2) effectiveness of the system to carry wind loading; and (3) future needs regarding deck replacement. While under construction and in negative bending regions post-construction, cross frames provide restraint to prevent lateral-torsional buckling. Due to lateral-torsional buckling considerations, cross frames or other bracing is a necessity during deck replacement and cross-frames generally cannot be removed from negative bending moment regions. Additionally, Tedesco et al (1995) indicated that cross frame removal increases individual girder moment demand by approximately 8-14%, due to lower amounts of live load distribution.

Back-up stiffeners are a retrofit scheme that functions by stiffening the web-gap region, reducing distortion-induced fatigue effects. Placed on the opposite side of the web from the cross frame connection plate, back-up stiffeners are simply transverse stiffeners that strengthen the web-gap and reduce out-of-plane rotation of the web-gap region. Although Hassel et al. (2010) concluded that back-up stiffeners can be highly effective in skewed bridge applications with staggered cross frame layouts, the authors found that these stiffeners are less effective in non-staggered bridges applications where the only potential retrofit locations are on the fascia side of the exterior girders.

Positive connection to the girder flange can be accomplished using several methods. Commonly, angles are used to provide connection between the flange and connection plate by either bolting or welding one leg to the flange and the other to the connection plate (Roddis and Zhao 2003, Fisher et al. 1990). This method was found to be effective at halting fatigue crack initiation and propagation; however, applications of this technique are not without challenges. For example, bolting to the flange is preferred over welding due to the greater fatigue sensitivity at welded details. If the web-gap being repaired is at the top flange of the girder, application of this technique usually requires removal of at least portions of the concrete deck, bringing about significant traffic disruption and expense.

An alternative retrofit technique to traditional means of positive connection has been the subject of a number of investigative efforts at the University of Kansas (Alemdar et al. 2013a; Alemdar et al. 2013b; Przywara 2013). The retrofit described in Alemdar et al. (2013a; 2013b) consisted of two angles which attached the connection plate to the girder web. The angles were used in conjunction with a back plate on the opposite side of the girder web to distribute out-of-plane forces over a large area of the web. Since this retrofit did not require any attachment to the

flange, it eliminated any need for deck removal and can be installed under traffic. This technique, which was termed the "angles-with-plate" retrofit, was evaluated through a series of tests performed on 2.8-m [9.3-ft] long girder-cross frame subassemblies loaded under a demanding distortion-induced fatigue loading protocol. An analytical investigation was performed in parallel to the physical simulations.

The test set-up used in Alemdar et al. (2013a; 2013b) was such that the girder-cross frame subassembly was tested upside-down, with the girder's top flange rotationally restrained to the laboratory strong floor. Cyclic loads were applied through a servo-controlled hydraulic actuator attached to the free end of the cross-frame elements. This test set-up eliminated in-plane bending effects on the test girders and presented a demanding out-of-plane fatigue test. The test set-up used by Alemdar et al. is shown in Figure 2.

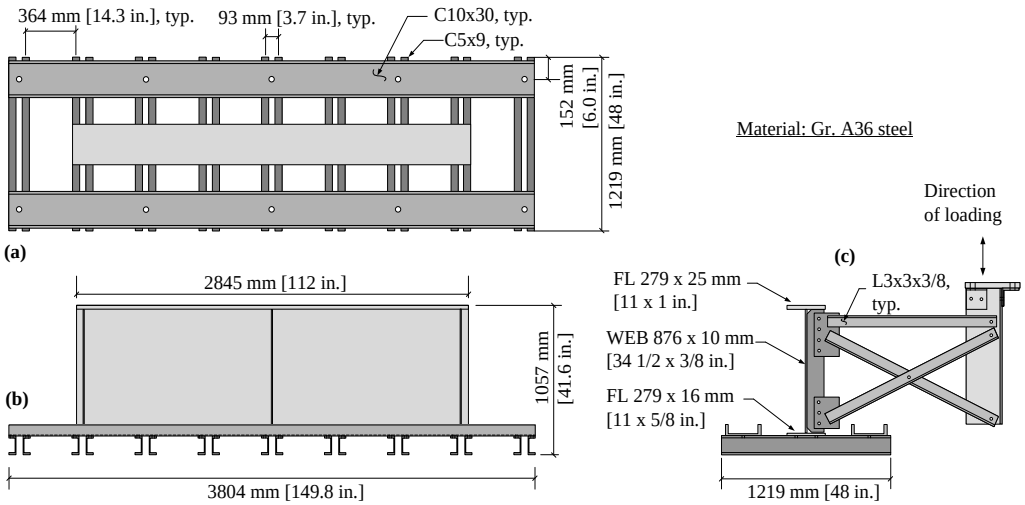

Figure 2: Test set-up for 2.8 m [9.3 ft.] girder sub-assembly testing (Alemdar et al. 2013a; 2013b).

The test set-up and computational models were used to generate an initial set of data for the angles-with-plate retrofit. This showed that the technique was highly effective under pure out-of-plane fatigue loading, reducing web-gap stresses and drastically reducing propensity of crack propagation under distortion-induced fatigue.

OBJECTIVE AND SCOPE

The objective of this study was to investigate the effectiveness of the angles-with-plate retrofit technique initially studied by Alemdar et al. (2013a; 2013b) in reducing distortion-induced

fatigue crack propensity under a more realistic test set-up, wherein both out-of-plane and in-plane effects are considered.

The scope of this study included performing 12 test trials on a three-girder test bridge that was 9.1-m [30-ft] long and included a composite concrete deck. Results from a parallel analytical investigation have been presented in a companion paper. Results of these studies are currently limited to straight, non-skewed bridge girders.

EXPERIMENTAL PROGRAM

Since the goal of this investigation was to evaluate the effectiveness of the angles-with-plate retrofit in a test that captured both in-plane bending effects and secondary stresses from distortion-induced fatigue, a set-up was constructed that included three 9.1-m [30-ft] long girders connected with X-type cross frames at the two simple support locations and at midspan. A concrete bridge deck was cast in sections and was connected to the girders such that it would act compositely. All loads were applied through a 1470 kN [330-kip] servo-controlled hydraulic actuator. The loading end of the actuator was situated over a steel bearing plate centered on the bridge deck. Details regarding the test set-up have been provided in the following sections.

GIRDER SPECIFICATIONS

Test specimen dimensions were primarily based on laboratory space constraints and a sample bridge from American Iron and Steel Institute (AISI) Example 1: Simple-Span Composite I Girder (AISI 1997). Approximately half scale of the AISI sample bridge, the 9.1 m [30 ft.] long girders were comprised of a 16 x 279 mm [5/8 x 11 in.] top flange, 6 x 876 mm [1/4 x 2 ft.-10 1/2 in.] web, and 25 x 279 mm [1 x 11 in.] bottom flange. All girders were supported on rollers to minimize axial forces with a center-to-center span length of 8.7 m [28 ft.-6 in.] between supports. Test section dimensions and girder span with load placement are shown in Figure 3. In the laboratory, the longitudinal axis of the bridge system was oriented east-west which defined the exterior girders as being the north and south girders. At the section shown in Figure 3(a), looking west, the exterior girder shown on the right is the north girder and the left is the south girder.

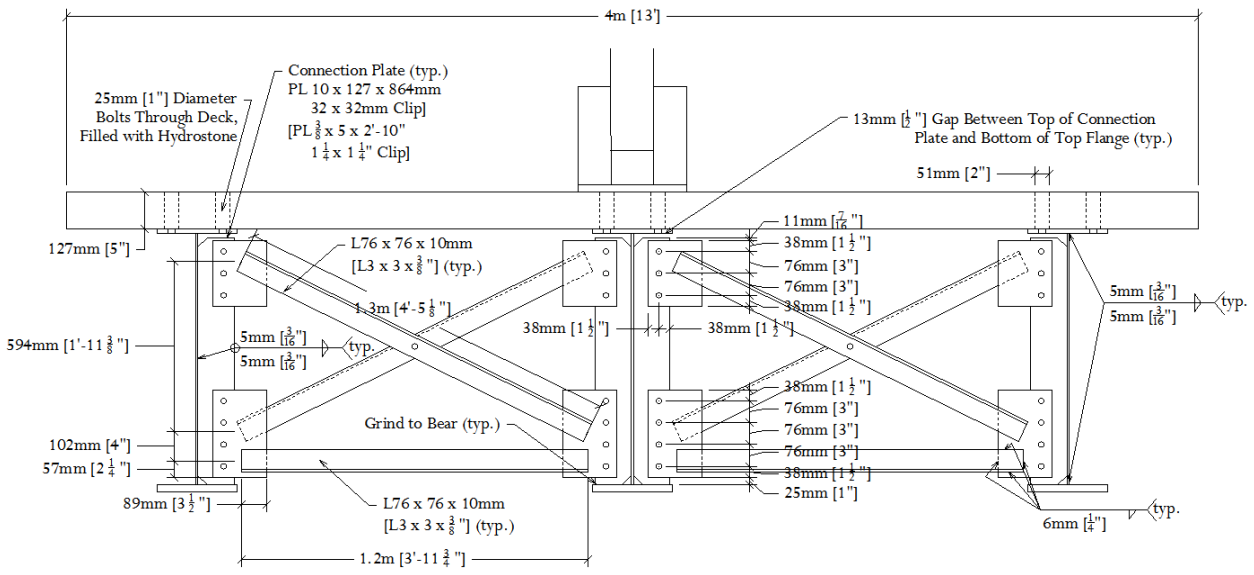

(a)

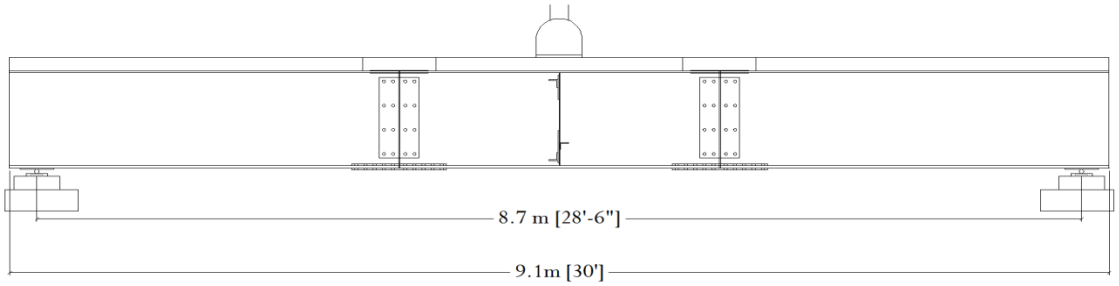

(b)

Figure 3: (a) Dimensions and schematic of test region cross frames. (b) Girder span and load application.

The concrete deck was cast in five sections; 51-mm [2-in.] diameter circular voids were created during the casting procedure, spaced to provide one bolt on either side of the web at a maximum spacing along the girder flange of 432 mm [1 ft.-5 in.]. Complete casting layout has been provided in Appendix A, Figure A. 9. Each portion of deck was cast on using formwork on the ground and then lifted into place after they had been cured. The voids cast into the concrete deck elements matched a hole layout on the top flanges of the girders, providing a location for high-strength structural bolts to be placed through. After the bolts were placed, the remaining void area was filled with Hydrostone. In this manner, horizontal shear transfer was achieved between the steel girders and the concrete deck elements. The compressive strength of the concrete used in the deck was found to range from 267 MPa [3900 psi] to 33 MPa [4800 psi] when tested at 28-days.

LOADING

Cyclic loading was delivered by a MTS 201.70 actuator (1470 kN [330 kips] capacity in compression) powered by a MTS 505.90 90 GPM pump and controlled with a MTS FlexTest II CTC Controller. A 25-mm [1.0-in.] thick steel plate was centered on the bridge deck, and was grouted in place under the footprint of the actuator. The purpose of the steel plate was to distribute the concentrated compressive force delivered by the actuator. Loading was applied at midspan over the interior girder, as shown in schematic in Figure 3. The cyclic loading was applied at rates varying between 1.0 – 2.0 Hz depending on the load range being applied.

RETROFIT SPECIFICATIONS

The investigated retrofit contained two angles providing attachment between the connection plate and girder web with a backing plate on the opposing face of the web. Two L152x152x19 mm [L6x6x3/4 in] angles were bolted to the connection plate and girder web while a 457x457x19 mm [18x8x3/4 in] back plate was used to distribute out-of-plane forces over a large web area, as shown in Figure 4 schematics.

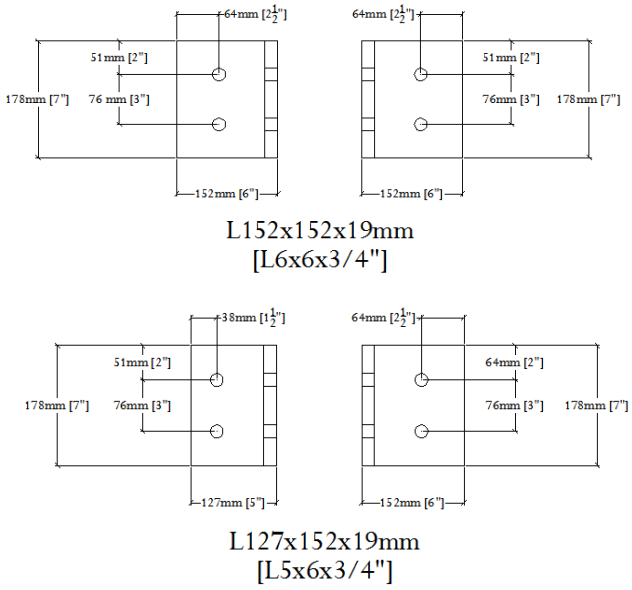

(a)

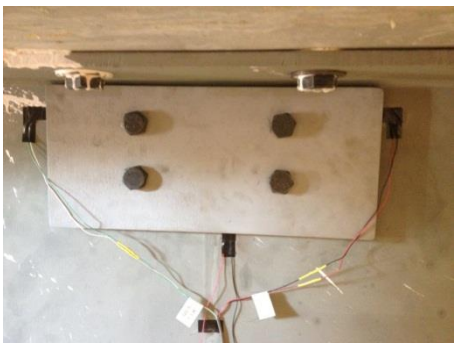

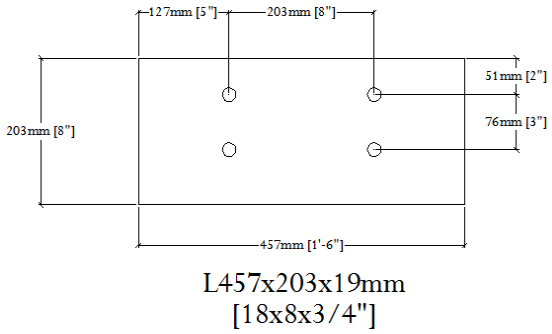

(b)

Figure 4: Retrofit as applied to top web-gap in test specimen.

Due to fit interferences with the cross frame angles, it was necessary that two retrofit angles each have one leg shortened by 25.4 mm [1 in.]. Shim plates were also utilized to avoid weld interference. The bolt layout consisted of a total of six Gr. A325 19-mm [3/4-in.] diameter slip-critical bolts for each retrofit application.

INSTRUMENTATION

The test bridge was instrumented such that strain, vertical deflections, and lateral deflections could be measured through the test sequence. Additionally, load and displacement data were recorded from the actuator using the same data acquisition system as was used for all other sensors. Sensors included the following: load cells, linear variable differential transformers (LVDTs), string potentiometers, Bridge Diagnostics Inc. (BDI) strain transducers, and strain gages. Global bridge response was monitored using load cells, LVDTs, string potentiometers, and strain transducers. Six load cells, one at each girder end, were used to monitor load distribution between girders. Load cells were calibrated using a 6.55V power supply.

LVDTs and string potentiometers were powered using a 15V power supply. Initially, LVDTs were used to monitor vertical girder deflections at midspan as well as lateral displacements for each exterior girder at three different locations along the height of each girder (Figure 5(a)). Since exterior girder deflections included both vertical and lateral displacements, it was found that the LVDT core could not extend and retract freely which resulted in inaccurate deflection measurements. Due to this, four string potentiometers (Figure 5(b)) replaced the original three LVDTs monitoring lateral girder displacements.

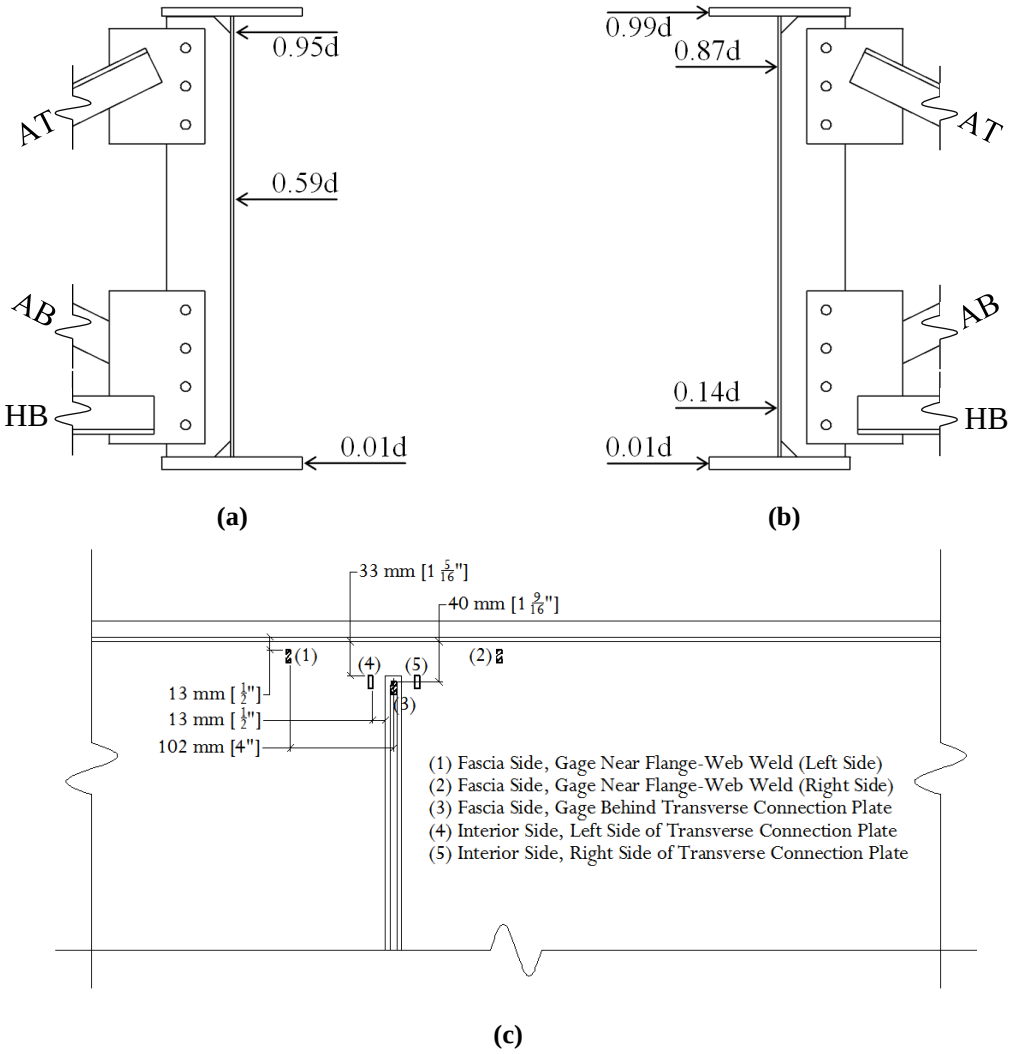

Figure 5: Instrumentation placements for (a) LVDTs, (b) string potentiometers, and (c) strain gages.

Six Bridge Diagnostics, Inc. (BDI) strain transducers were used in the test set-up. Each girder was instrumented with two strain transducers, one placed at top and bottom of each girder web to monitor in-plane bending strains in the three girders. BDI strain transducers were powered with 5V. To avoid local concentrations due to geometry, these were placed 50.8 mm [2 in.] below or above the flanges, and were located a longitudinal distance 654 mm [25 3/4 in.] from the connection plates at midspan.

To monitor strains in the web-gap region, bondable strain gages were included in the bridge instrumentation plan. Bondable strain gages were powered directly through the data acquisition system in a quarter bridge configuration with excitation voltages of 2.5V or 3.3V—strain gages into NI-9219 were powered by 2.5V and strain gages into NI-9236 were powered by

3.3V. In total, 20 Micro-Measurements WK-06-250BG-350 gages were placed in web-gap regions as shown in Figure 5(c). Additionally, bondable strain gages were placed on each cross frame angle at midspan of the girders oriented along the axis of the cross frame member. On the horizontal angle of the cross frame, the gage was placed mid-span. For the diagonal members which were bolted at mid-span, the gages were placed at the quarter-point of the span nearest the exterior girder.

Due to the scale of the project and large sensor array, synchronizing the data was a critical step. , All data were recorded using a single data acquisition system manufactured by National Instruments (NI cDAQ 9188 with NI 9205, NI 9212, NI 9236, and NI 9239 modules). A protocol was written in Labview 2011 to read, compress, and record data in a text file. The quantity of data required an extremely large sampling rate to sufficiently increase the buffer size within the NI cDAQ 9188 chassis. Sampled data were post-compressed to produce an effective sampling rate of approximately 20 samples/second. All appropriate calibration factors were applied within the Labview protocol, such that data written to the measurement file contained appropriate units.

Prior to retrofit application, data were recorded under static load application every 15,000 cycles. Throughout test trials performed on the bridge in the retrofitted state, static data were recorded at the beginning and end of each trial (which usually had a duration of 1.2 million cycles). During data acquisition loading was controlled manually progressing from 0 kN [0 kip] to 356 kN [80 kip] while data were recorded continuously. Raw data were imported into Microsoft Excel and post-processed to examine data at 11 kN [2.5 kip] load increments. As the load range applied to the test bridge was different in various test trials, the maximum load to which data were recorded was increased to 445 kN [100 kip] and then to 534 kN [120 kip], and the corresponding data increment was increased to 22 kN [5 kip].

CRACKING AND INSPECTION

Crack inspection was performed at regular intervals while the bridge was subjected to cyclic loading. Inspection techniques included photographic and visual inspection as well as evaluation of strain measurement data. Zyglo Penetrant (ZL-27A) by Magnaflux and an ultraviolet flashlight were used to see crack openings and tips. When dye penetrant was sprayed on the region of interest during cyclic loading, surface cracks could be seen pulsing under the

ultraviolet light. At each inspection, photographs were taken using a Cannon Rebel XTi DSLR with an 18-55mm lens. Early photographic images contained a small scale taped to the girder web used for determining crack length. Later, photographs were scaled to the previous images to verify crack measurements obtained visually and monitor crack growth.

In addition to visual and photographic inspection, strain gages were monitored through static data collection at 15,000 cycles, 20,000 cycles, and 30,000 cycles, and then every 15,000 cycles until retrofitting at 150,000. Strain readings from gages placed on the fascia side directly behind the connection plate (shown in Figure 5(c)) were compared throughout testing of the bridge in the unretrofitted condition. These gages measured the largest strains and were found to be highly sensitive to cracking in the connection plate-web weld.

As discussed further in the following sections of this paper, it was found that girder cracking first initiated and propagated around the connection plate-web weld in the top web gaps of the south and north girders. These cracks were closely monitored and classified by three different categories: (1) cracks growing down the weld (termed "vertical cracks"), (2) cracks growing out from the weld in the longitudinal direction of the girders (termed "spider cracks"), and (3) cracks extending through the web thickness (termed "through cracks"). Each of these three crack patterns is shown in Figure 6. Additionally, cracking was found near the flange-web weld; these were termed "longitudinal cracks."

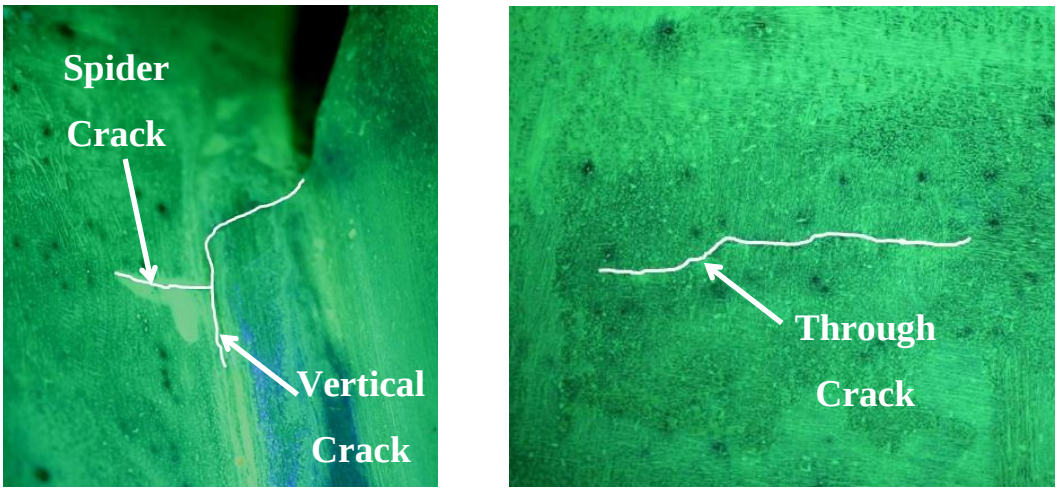

(a) **(b)**

Figure 6: Crack definition for (a) interior side of girder web at cross frame connection plate and (b) exterior or fascia side of girder web.

TEST TRIALS

Twelve test trials were performed on the test bridge which are summarized in Table 1. For each loading protocol on the bridge system, the two exterior girders (the north girder and the south girder) underwent a test trial. The center girder was not listed as undergoing a test trial, since the center girder did not experience any cracking throughout the test sequence. Trial 1 consisted of an unretrofitted specimen in which cracking was allowed to initiate and propagate until a crack length of 24 mm [1 in.] was achieved. Trials 2, 3, 5, and 6 were indicative of the bridge with the exterior girders in the retrofitted condition (sometimes with the addition of crack stop holes), with each trial having a duration of 1.2 million cycles, with the exception of Trial 4. Trial 4 was the only retrofit trial that did not reach 1.2 million cycles, for reasons discussed further in the following sections.

Table 1: Specimen test trials for North (N) and South (S) Girders with Load Range

Trial	Specimen Description	Target Load Range
1N **1S**	Bare specimen	27-267 kN [6-60 kip]
2N **2S**	"Angles-with-plate" retrofit applied in top web-gap	27-267 kN [6-60 kip]
3N **3S**	Same as Trials 2N and 2S: "Angles-with-plate" retrofit applied in top web-gap	36-356 kN [8-80 kip]
4N **4S**	Small drilled holes with "angles-with-plate" applied in top web-gap	44-445 kN [10-100 kip]
5N **5S**	Larger drilled hole with "angles-with-plate" retrofit applied in top web-gap	44-445 kN [10-100 kip]
6N **6S**	Same as Trials 5N and 5S: Larger drilled hole with "angles-with-plate" retrofit applied in top web-gap	53-534 kN [12-120 kip]

The load range applied to the test bridge was varied over the course of the testing sequence to create a highly-demanding test of the angles-with-plate retrofit effectiveness at reducing distortion-induced fatigue crack propensity. The load range applied to the bridge in Trials 1S, 1N, 2S, and 2N was 27-267 kN [6-60 kip] which corresponded to a maximum normal bending stress of 29.6 MPa [4.3 ksi] in the bottom flange of the center girder. This load range was found to produce vertical strains of approximately 250 με – 850 με in the top web-gap regions of the south and north girders, and produced a maximum vertical deflection at midspan

of 2.0 mm [0.077 in.]. Details regarding the strain and deflection measurements under the various load ranges have been provided in Table 2.

Table 2: Specimen trials with load range and bottom flange stresses

Trial	Sample Load kN [kip]	Girder Max. Deflection mm [in.]	Girder Maximum Bottom Flange Stress MPa [ksi]	Uncracked Top Web-Gap Strain Gages (3)/(4 & 5) (με)	Cracked Top Web-Gap Strain Gages (3)/(4 & 5) (με)
1N		0.8 [0.033]	9.7 [1.4]	-705/285-352	-818/252-333
Center	267 [60]	*2.0 [0.077]*	*29.6 [4.3]*	*N/A*	*N/A*
1S		0.8 [0.032]	8.3 [1.2]	-839/522-556	-854/521-556
2N		0.9 [0.034]	9.7 [1.4]	-705/285-352	
Center	267 [60]	*1.9 [0.075]*	*29.6 [4.3]*	*N/A*	
2S		0.8 [0.032]	8.3 [1.2]	-839/522-556	
3N		1.1 [0.044]	13.1 [1.9]	-963/377-468	
Center	356 [80]	*2.3 [0.091]*	*40.0 [5.8]*	*N/A*	
3S		1.1 [0.042]	11.0 [1.6]	-1120/694-742	
4N		1.3 [0.051]	16.5 [2.4]		
Center	445 [100]	*3.4 [0.134]*	*48.3 [7.0]*		
4S		1.4 [0.055]	14.5 [2.1]		
5N		1.4 [0.056]	15.9 [2.3]		
Center	445 [100]	*3.7 [0.145]*	*Bad Data*		
5S		1.3 [0.052]	12.4 [1.8]		
6N		1.5 [0.059]	17.9 [2.6]		
Center	534 [120]	*4.5 [0.178]*	*Bad Data*		
6S		1.6 [0.062]	20.0 [2.9]		

All values in Table 2, with the exception of uncracked strains, are recorded from the end of each Trial. Strains in the uncracked north and south girders were only recorded up to a load of 356 kN [80 kip], and strains in cracked north and south girders were only recorded for Trials 1N and 1S since retrofit application caused gages in the top web-gap to fail. Maximum girder deflection at mid-span was measured directly using an LVDT under each girder. Strain transducer data were used to determine maximum bottom flange bending stress. For each girder, the two strain transducers were used to develop a strain profile. These were placed in the web; however, with the strain profile, bending strains were extrapolated to the bottom flange (the

extreme fiber). Additionally, these strains were not located at midspan so they were modified to represent midspan strains using a linear variation between support and midspan due to single point loading at midspan. Since significant amounts of data were collected, each strain reading is an average of four consecutive data points. All data were averaged in a similar fashion and data for the given maximum load was extracted which resulted in a single set of data for each load.

Three other load ranges were applied in various test trials: 36-356 kN [8-80 kip] (Trials 3S and 3N); 44-445 kN [10-100 kip] (Trials 4S, 4N, 5S, and 5N); and 53-534 kN [12-120 kip] (Trials 6S and 6N). The largest load range used in the test sequence, 53-534 kN [12-120 kip], produced a maximum vertical deflection at midspan under the 53-534 kN [12-120 kip] load range of 4.5 mm [0.178 in.]. An issue with the bottom strain transducer resulted in non-linear data for bending stresses. Extrapolating from previous loading data for the 53-534 kN [12-120 kip] loading, an approximate maximum normal bending stress in the bottom flange of the center was determined to be 57.9 MPa [8.4 ksi].

The load ranges were chosen to be quite large and were significantly higher than what was expected for typical fatigue loadings in an actual bridge structure. Choosing large variation in load range was intended to assess retrofit performance over a full range of load demand that bridge behavior under retrofit application. The authors did not wish to approach the test design by using loadings that would ensure that no crack initiation or propagation would occur under the retrofit. Therefore, it was fully expected that cracking would propagate under the high load demands, even while retrofitted. Changes in crack propagation rates between unretrofitted and retrofitted conditions were therefore key interest to the investigators.

RESULTS AND DISCUSSION

Throughout testing, data were recorded through the instrumentation plan discussed and crack growth was monitored and charted. Changes in bridge behavior and crack propagation were used to evaluate the retrofit effectiveness. Cross frame strains and girder lateral deflections helped to establish changes in bridge behavior while crack inspections were used to track crack propagation.

By comparing cross frame strains with cracked and uncracked girders as well as unretrofitted and retrofitted girders, changes in bridge response were observed. Another response that was monitored was the lateral deflections of the north and south girder profiles. Under retrofit application, girder lateral deflections were found to significantly change. In addition to global bridge response, crack initiation was established through strain gage data while crack propagation was monitored through visual and photographic inspection.

GIRDER CROSS FRAME STRAINS

Strain measurements on individual cross-frame members at mid-span were monitored to establish the amount of out-of-plane force acting on the web-gap as well as to determine the distribution of forces through the cross frame elements. Cross frame labeling notation is shown in Figure 5(a) and 5(b) where angle top (AT) and angle bottom (AB) is where the inclined cross frame angles framing into the top and bottom web-gaps, respectively. The horizontal angle in the cross frame is labeled HB (horizontal bottom).

Figure 7(a) and 7(b) show the effects of crack initiation on cross frame strain measurements. Prior to cracking, cross frame members AT and HB for the north and south girders experienced approximately the same strain in tension while AB experienced a similar strain magnitude in compression. Once cracking occurred in the connection plate-to-web weld of each girder, member AT experienced a reduction in strain of approximately 75 με while HB and AB experienced increases in strain of approximately 50 με. Due to cracking in the top web-gap, less force was transferred into the cross frame member framing into top web-gap, while the remaining members picked up additional load. As crack length increased, cross frame member strain distributions were seen to remain similar, as seen in a comparison of Figure 7(b) and (c).

Figure 7(c) and (d) show the change in strains between unretrofitted and retrofitted conditions after 1.35 million cycles. With the retrofit applied, stiffening the top web-gap, inclined cross frame angles framing into the top web-gap (AT) experienced an increase in tensile strain of more than 50%. Since the inclined cross frame member framing into the top web-gap experienced an increase in strain, both cross frame members framing into the bottom web-gap experienced decreases in strain. Inclined cross frame members framing into exterior girder bottom web-gaps (AB) experienced a decrease in compressive strains while horizontal members framing into the bottom web-gaps (HB) experienced a decrease in tensile strains. Strain

increases in element framing into the top web-gap does not directly provide any information about propensity for crack growth. It does, however, show that the retrofit allows for significantly more force transfer into the web since the cross frame strains were larger when retrofitted as compared with the unretrofitted condition.

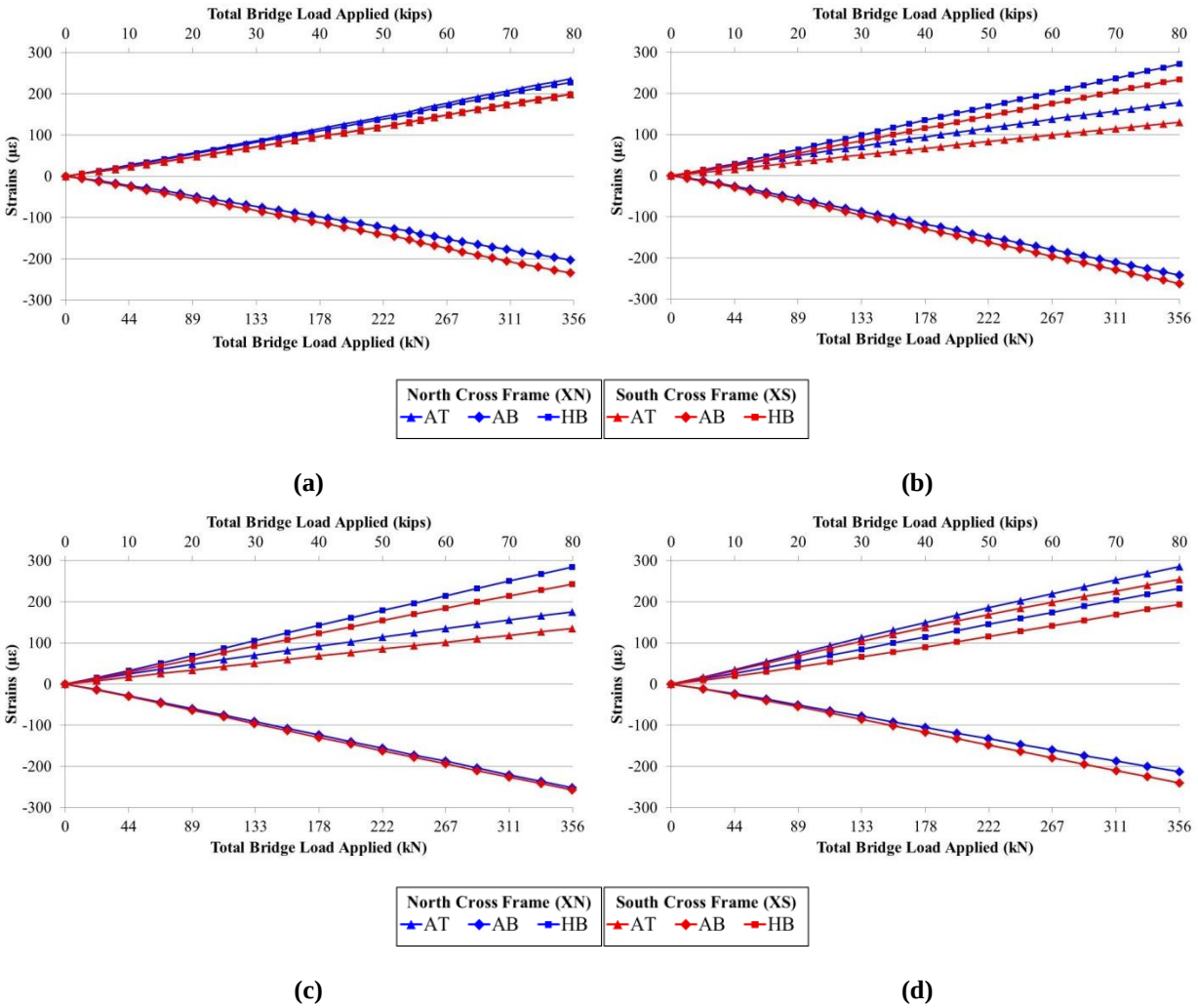

Figure 7: Cross frame strains for (a) uncracked, unretrofitted at 0 cycles, (b) cracked at 150,000 cycles, (c) cracked, unretrofitted at 1.35 million cycles, and (d) cracked, retrofitted at 1.35 million cycles.

LATERAL GIRDER DEFLECTION

With the initial LVDT locations matching placements used in previous 2.8 m [9.3 ft.] girder sub-assembly testing at the University of Kansas (Alemdar et al. 2013a; 2013b), girder lateral

deflections at 150,000 total cycles for both pre- and post-retrofit conditions have been presented in Figure 8.

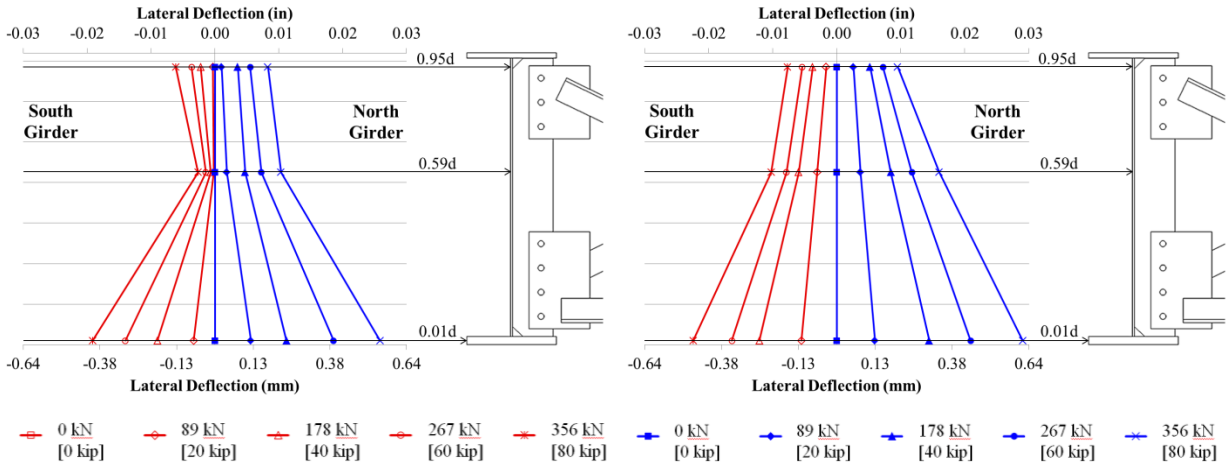

Figure 8: Girder lateral displacements at 150,000 cycles (end of Trials 1S and 1N) for (a) unretrofitted and (b) retrofitted conditions.

Lateral girder deflections of the north girder were found to be similar in shape to those obtained from tests of the 2.8 m [9.3 ft.] girder sub-assemblies (Alemdar et al. 2013a; 2013b). South girder deflections were found to behave a little differently than those from the north girder and the girder sub-assemblies tested by Alemdar et al. (2013a; 2013b). Between the top and middle LVDTs, the south girder hinges inward (less displacement) at mid-height while the north girder and component girders experienced increases in lateral displacement. The larger differential displacement between LVDTs placed at the top and mid-height of the south girder may have contributed to more significant crack growth as seen experimentally.

With the initial LVDT placements, little information could be inferred about the top web-gap displacements; however, girder deflection was found to be nearly linear when the retrofit was applied (Figure 8 (b)). To gain greater information regarding web-gap rotations, four string potentiometers replaced the existing three LVDTs. After 1.35 million cycles (end of Trials 2S and 2N), both pre- and post-retrofit girder lateral displacements can be seen in Figure 9.

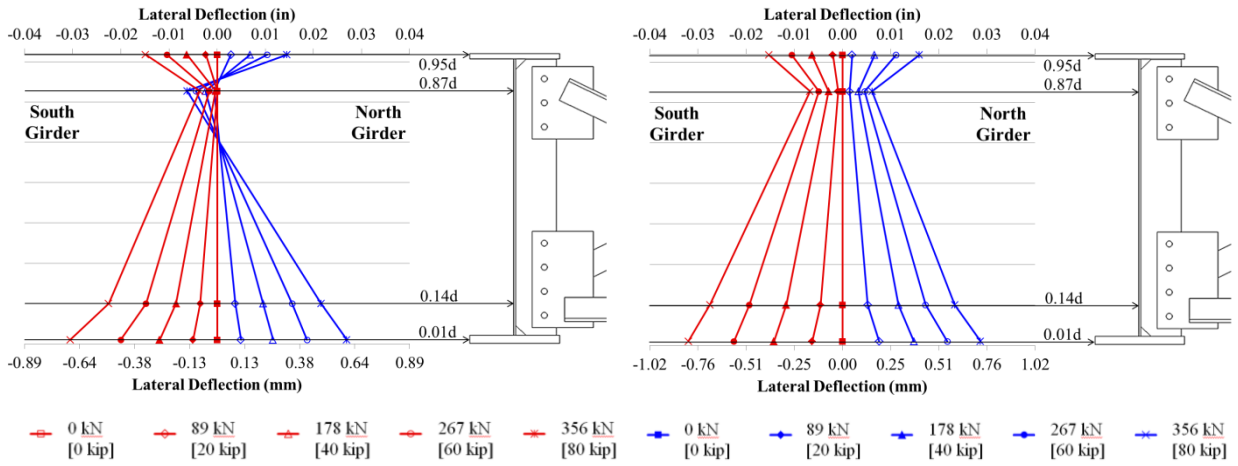

(a) **(b)**

Figure 9: Girder lateral displacements at 1.35 million cycles for (a) unretrofitted and (b) retrofitted conditions.

Revised lateral displacement locations provided an improved description of girder deflections. Without retrofit, significant displacement reversal was found to occur in the top web-gap (Figure 9 (a)) of the north and south girders. Once the retrofit was applied, this reversal was significantly reduced while lateral displacements of girder flanges remained nearly constant. Since web-gap rotation is considered to be a driving factor (Jajich and Schultz 2003) in distortion-induced fatigue cracking, reducing web-gap rotation was anticipated to reduce fatigue susceptibility.

CRACK INITIATION AND PROPAGATION

Crack propagation was of particular importance to the investigators since the primary method for establishing retrofit effectiveness is the ability of the retrofit to significantly slow or halt crack growth. Initially, bondable strain gages placed in the top web gaps on the north and south girders were used to identify potential crack initiation. After initiation was visually confirmed, crack propagation was monitored and charted while the girder was in the unretrofitted condition. Crack lengths were also monitored before and after retrofit applications, providing information regarding crack propagation under the application of the retrofits. Due to the large loads placed on the bridge, change in crack propagation rate was of particular interest. In the following sections crack initiation and propagation have been explained in detail.

CRACK INITIATION

At the beginning of the test sequence (Trials 1S and 1N), the uncracked, unretrofitted test bridge was cycled between 27-267 kN [6-60 kip] at a frequency of 1 Hz. Visual crack inspections were performed every 5,000 cycles while static data from all instrumentation was recorded every 15,000 cycles. Strain gages placed on the fascia side of the north girder (gage 3 in Figure 5(b)) indicated potential cracking at 15,000 cycles. Figure 10 displays the *increase* in strain from -950 με to -1225 με experienced by the gage of interest.

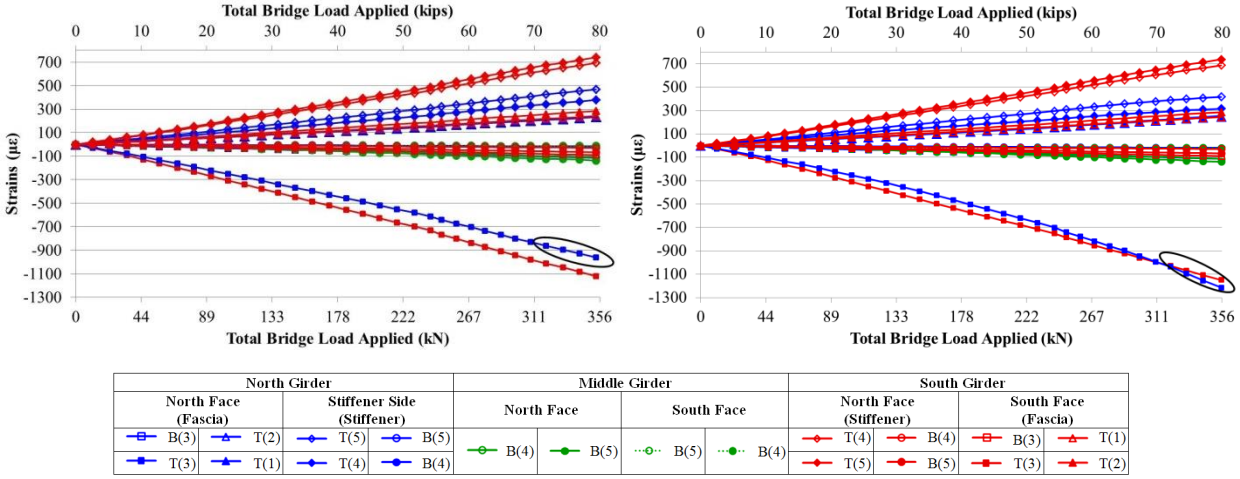

(a) **(b)**

Figure 10: Strains in top web-gaps at (a) 0 cycles and (b) 15,000 cycles. Top web-gap denoted by T in legend and bottom web-gap denoted by B. Number denotes gage location from Figure 5(c).

Although strain gages indicated potential cracking on the north girder, physical inspection found no visible cracking at that point; however, at 20,000 cycles (just 5,000 additional cycles) cracking was visually identified at the connection plate-to-web weld in the north girder. This indicated excellent agreement between the two crack indication / inspection techniques.

CRACK PROPAGATION PATTERN

In Trials 1S and 1N, cracking initiated at the weld near the clip in the transverse connection plate. Cracking progressed diagonally down through the weld until reaching the girder web.

During Trial 1S, cracking progressed down the weld toe in the south girder until branching out into a spider crack. These spider cracks propagated outward away from the

transverse connection plate. On the left side of the transverse connection plate, cracking also progressed down web at the weld toe. North girder cracking progressed slightly differently, in that cracks did not propagate into the web until Trial 2N and did not follow the weld toe. Longitudinal cracks at the flange-web weld were found in Trials 6N and 6S. The point of initiation was unclear for the longitudinal cracking, since the north girder longitudinal cracks were significantly large when discovered at the end of Trial 6N. Table 3 shows the cracking patterns at the end of Trials 6S and 6N.

Table 3: Cracking at End of Trial 6 (6,011,097 Cycles)

	Left Side of Connection Plate	Right Side of Connection Plate
South Girder	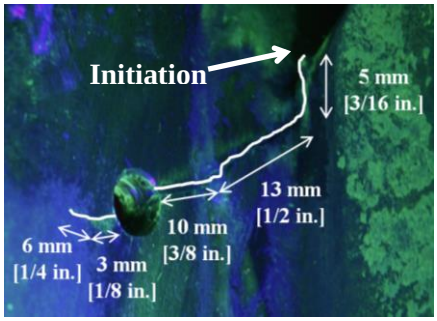 (East)	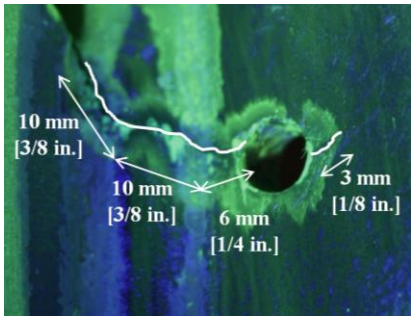 (West)
	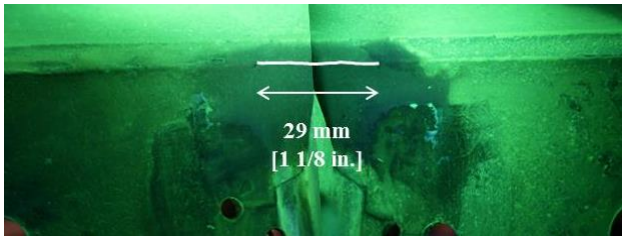	
	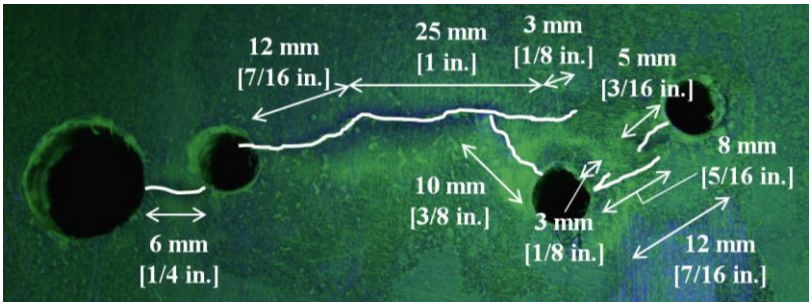	

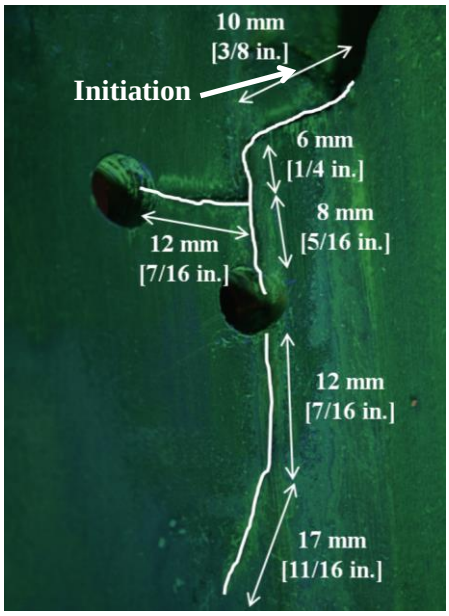

(West)

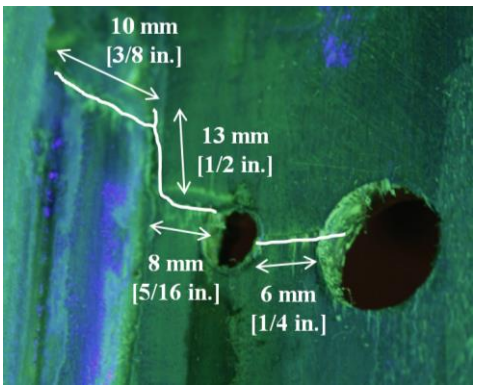

(East)

North Girder

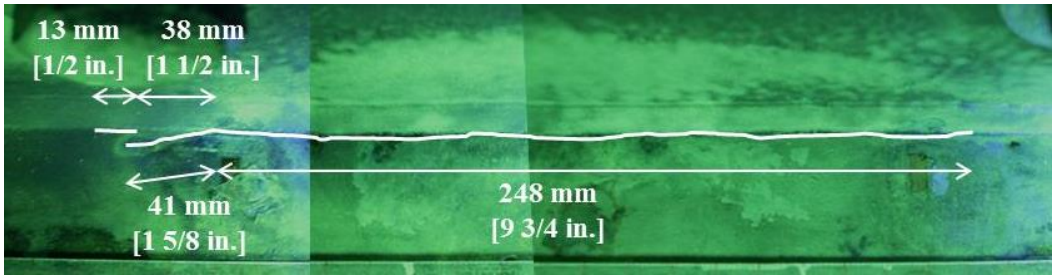

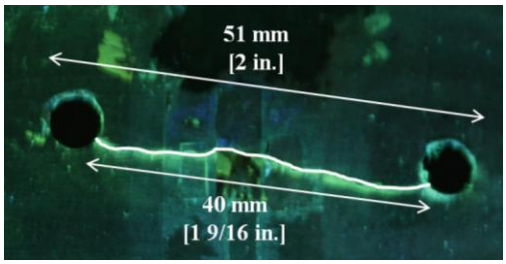

TRIALS 1N-6N CRACK GROWTH (NORTH GIRDER TEST TRIALS)

Crack length is plotted against the total fatigue cycles as shown in Figure 11. The cracks were each categorized as vertical cracks, spider cracks, through cracks, or longitudinal cracks. When holes were drilled at crack tips, an instantaneous jump occurred in the graph that is not connected by a line. For locations where a crack grew into an existing crack-arrest hole, only the crack

propagation was plotted. As shown in Figure 11, an instantaneous jump at the end of that test trial is shown with a solid line to denote the difference between drilling a crack-arrest hole and propagating into a pre-existing hole.

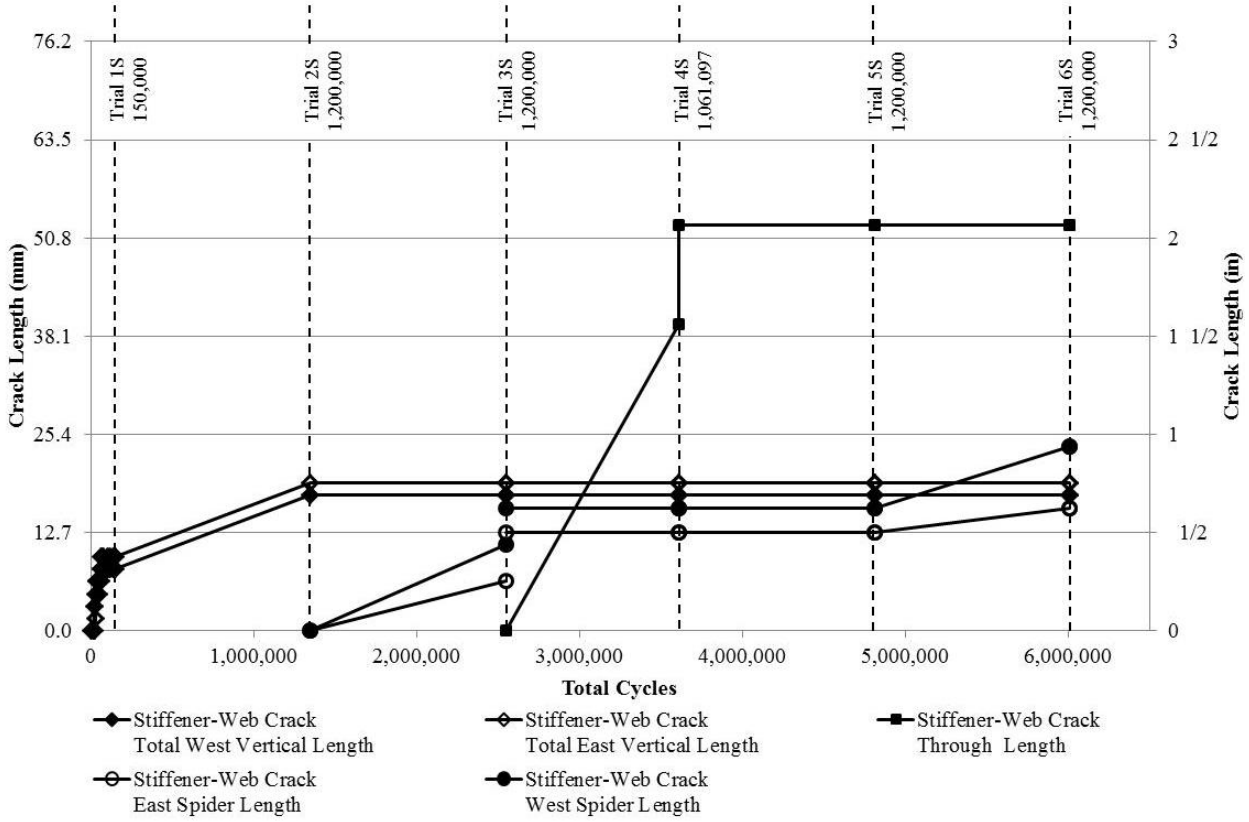

Figure 11: North girder crack growth around transverse connection plate.

Cracking initiated in the north girder at approximately 20,000 cycles during Trial 1N. During Trial 1N, cracking in the north girder reached length of 8 mm [5/16 in.] on the left side (west) and 10 mm [3/8 in.] on the right side (east) of the transverse connection plate. Both cracks propagated diagonally downward through the weld throat, but did not propagate out into the web. Cracking in the north girder stabilized around 65,000 cycles with no further growth during Trial 1N.

With the angles-with-plate retrofit in place during Trial 2N, north girder cracking lengthened under the retrofit application. Based on previous research (Alemdar et al. 2013a; 2013b) and a detailed finite element study of the 9.1 m [30 ft.] test bridge (presented in Part 4 of this thesis), it is postulated that in this extreme situation where the stress demands are high for a

small crack, small amounts of propagation may occur under the retrofit; however, as cracking propagates, this high stress decreases and cracking will slow.

During Trial 3N, cracks again propagated in the north girder. At this point, cracking progressed into the web in the form of a spider crack. Spider crack length out into the web was measured to be 11 mm [7/16 in.] on the west side of the connection plate and 6 mm [1/4 in.] on the east side of the connection plate. Spider crack dimensions provided are in addition to the cracking that occurred through the weld, which is 18-mm [11/16-in.] long on the west side of the connection plate and 19-mm [3/4-in.] long on the east side of the connection plate.

Small crack arrest holes with a 6-mm [1/4-in.] diameter were drilled at the crack tips before the start of Trial 4N, and the angles-with-plate retrofit was reapplied and the load range was increased. Approximately 650,000 cycles into Trial 4N, a faint clicking noise was noticed originating from the connection plate in the north girder. After inspection of strain data, no significant change in bridge response was noticed. However, when the bridge was visually inspected at 1.06 million cycles into Trial 4N, the cross frame between the north and middle girders was found to be cracked completely through at the tab plate, as shown in Figure 12.

Figure 12: North cross frame failure during Trial 4N.

During inspection, there was no evidence of fretting due to the angle-with-plate retrofit. Measured strains in the cross frame element prior to fracture were approximately 375 με, which, based on modulus of elasticity for steel of 200 GPa [29,000 ksi], correlated with an approximate stress of 75 MPa [11 ksi]. It is estimated that the crack started at the bottom corner of the weld toe where the cross frame diagonal member (AT) framed into the tab plate.

Due to the cross frame member failure (member AT) during Trial 4N, the angles-with-plate retrofit was removed and a detailed inspection was performed for the entire test bridge. After inspection, it was noticed that the north girder through-crack developed between the two 6-mm [1/4-in.] diameter crack-arrest holes. However, the spider cracking had not progressed through the crack arrest holes.

Due to the cross frame failure experienced in Trial 4N, Trial 5N was performed as a repeat of Trial 4N. No crack propagation was experienced during Trial 5N; however, at the end of Trial 6N in which the load was increased, a 298 mm [11 3/4 in.] longitudinal crack was discovered at the top flange-to-web weld. Prior to Trial 6N inspection, the last inspection was performed at the end of Trial 5N. At this time, no longitudinal crack was reported; however, ridges at the weld toe and very small crack opening displacements impeded crack detection. It should be noted that the loading applied during Trial 6N was expected to be much larger than typical fatigue bridge loading. Due to this, the final trials were believed to have pushed this specimen well beyond most practical applications.

TRIALS 1S-6S CRACK GROWTH (SOUTH GIRDER TEST TRIALS)

Cracking experienced around the transverse connection plate in the south girder is shown in Figure 13. The same crack definitions were applied as those used in the north girder as described in the previous section. Drilled holes are denoted by an instantaneous jump with no line, and cracks that propagated into an existing hole were denoted by an instantaneous jump with a connecting solid line.

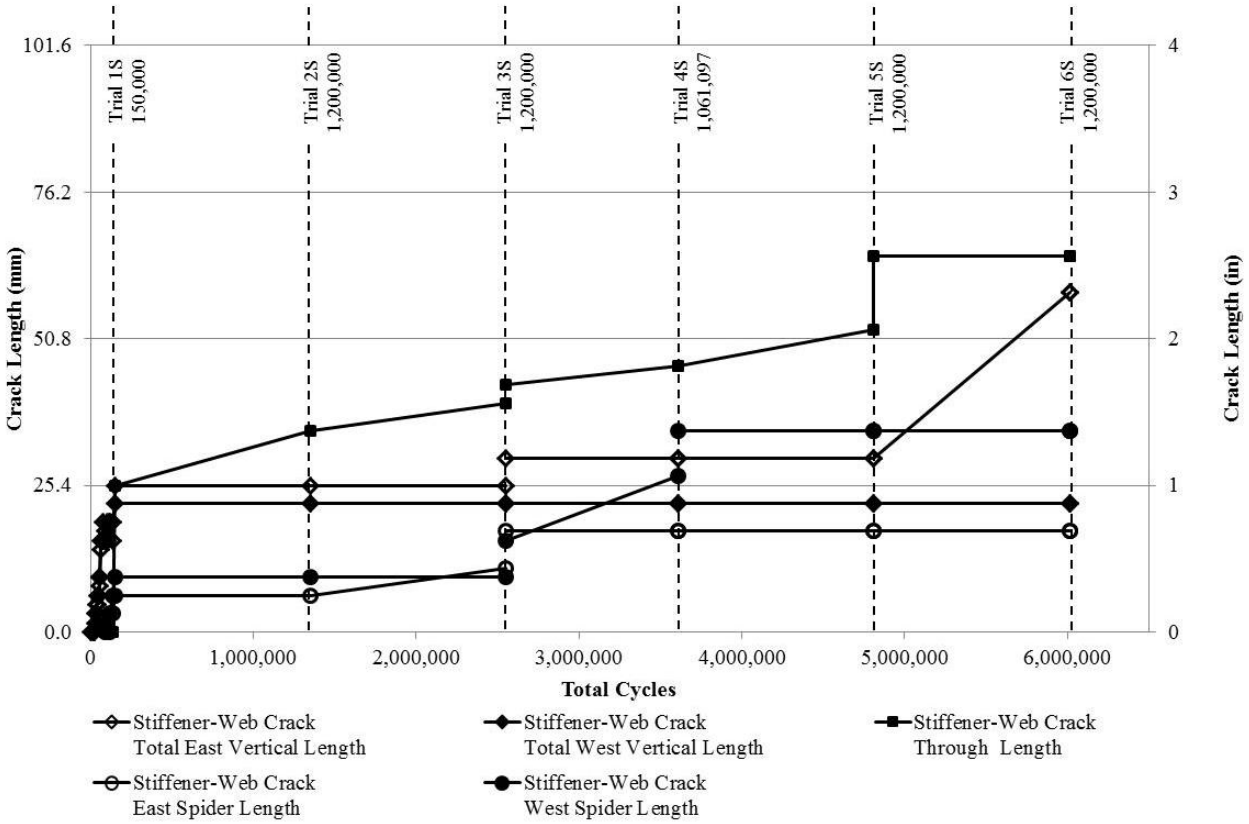

Figure 13: South girder crack growth around transverse connection plate.

Cracking in the south girder initiated during Trial 1S at 30,000 cycles in the unretrofitted condition, approximately 10,000 cycles after north girder cracking initiated. South girder cracking propagated through the weld and into the web at a steady rate until about 75,000 cycles. At this time, vertical cracking down the weld toe slowed. The first evidence of spider cracking began at 105,000 cycles. Between 105,000 and 120,000 cycles, the spider cracking propagated through the web, debonding the strain gage (3) on the fascia side of the south girder. This crack initiation was hidden behind the bonded gage and was first noticed at 150,000 cycles. During Trial 1S, a maximum crack length of 25 mm [1 in.] was reached by the vertical cracking on the left side of the connection plate and also in the through-crack length.

During Trial 2S, under application of the angles-with-plate retrofit, cracking on the interior face of the girder did not change; however, fascia cracking increased by a length 6 mm [1/4 in.]. This crack was formed as a through-thickness crack from the spider cracking seen on the interior side of the girder. The total length of the crack seen on the fascia side was 35 mm [1 3/8 in.] which correlated with the total projected crack length on the interior side of the girder

including the spider crack length (9.5 mm + 6 mm [3/8 in. + 1/4 in.]), connection plate width (9.5 mm [3/8 in.]), and weld width (9.5 mm [3/8 in.]). It is believed that the change in the fascia girder crack length can be attributed to the existing interior crack propagating through the thickness of the girder.

Trial 3S resulted in crack propagation. Spider cracking reached 11 mm [7/16 in.] on the east side of the connection plate and 10 mm [3/8 in.] on the west side of the connection plate. Vertical cracking on the east side of the connection plate did not propagate during Trial 3S. Through-crack length increased by 5 mm [3/16 in.]. At the end of Trial 3S, 6-mm [1/4-in.] diameter crack arrest holes were drilled at the crack tips of the spider cracks and the vertical crack in the south girder.

Trial 4S, was halted due to north cross frame failure as discussed previously. At the end of Trial 4S, minimal crack growth was seen in the through-web crack on the south girder, while the spider crack on the right side (west side) of the south girder grew through the 6-mm [1/4-in.] diameter crack stop hole. At the tip of this extended crack, a 13-mm [1/2-in.] diameter hole was drilled for the start of Trial 5S.

Similar to behavior observed in the north girder, cracking did not propagate under the angles-with-plate retrofit during Trial 5S. Increasing the load during Trial 6S resulted in some crack growth. Along the connection plate-web weld, cracking grew down vertically through the 6-mm [1/4-in.] crack stop hole as seen in Table 3. Careful inspection of the flange-to-web weld resulted in confirmation of a longitudinal crack detected with 29 mm [1 1/8 in.] length on the connection plate side of the web. As with the north girder, loading during this test cycle was larger than expected fatigue loading.

CONCLUSIONS

The objective of this study was to determine the effectiveness of the angles-with-plate retrofit for reducing distortion-induced fatigue propensity when applied to a steel test bridge that included in-plane bending effects as well as out-of-plane effects. The research team's conclusions are as follows:

- Cross frame members framing into the top web-gap experienced an increase in tensile strain of more than 50% when the angles-with-backing plate retrofit was applied to a cracked specimen as compared with an unretrofitted cracked specimen. Application of the angles-with-plate retrofit allows more force to be transferred into the web as compared with an unretrofitted condition. Since crack growth was slowed when retrofitted, the angles-with-plate retrofit combats distortion-induced fatigue cracking even though additional force is being transferred into the web.
- Strain gages placed on the opposing web face at the web-gap location were found to be good tools with which to detect crack initiation in the web-gap region. Significant changes in strain were noticeable just prior to visibly-detectable cracking in the web-gap region.
- Measurements taken with LVDTs and string potentiometers showed that out-of-plane web-gap rotations were significantly decreased after top web-gaps were retrofitted using the angles-with-plates technique, indicating a lower distortion-induced fatigue demand on the web-gap region.
- When the angles-with-plate retrofit was applied over top web-gap regions with existing sharp cracks, crack growth was significantly slowed. Maximum unretrofitted growth was 25 mm [1 in.] over 150,000 cycles at 27-267 kN [6-60 kip] load while maximum retrofitted growth was 11 mm [7/16 in.] over 1,200,000 cycles at 36-356 kN [8-80 kip] load.
- When the angles-with-plate retrofit was applied over top web-gap regions with cracks that had been modified with small crack-arrest holes drilled at the crack tips, crack growth was halted under 44-445 kN [10-100 kip] loading with a maximum longitudinal bending stress due to fatigue of 48.3 MPa [7.0 ksi].

Given the widespread nature of distortion-induced fatigue in existing steel bridge infrastructure, identification of effective, practical, and inexpensive retrofit techniques are in great demand. The angles-with-plate retrofit tested in a large-scale bridge test set-up under demanding cyclic loads exhibited excellent levels of fatigue crack retardation. The angle-with-plate retrofit is an important development in this area, as it does not require deck removal or flange attachment. Development of this retrofit technique has the potential to greatly streamline

the process of repairing steel bridges susceptible to distortion-induced fatigue in a manner that is effective, economical, and easily implementable.

REFERENCES

Alemdar, F., Overman, T., Matamoros, A., Bennett, C., and Rolfe, S. (2013a). "Repairing Distortion-Induced Fatigue Cracks in Steel Bridge Girders using Angles-with-Plate Retrofit Technique, Part I: Physical Simulations." *Journal of Structural Engineering,* ASCE, In Press

Alemdar, F., Nagati, D., Matamoros, A., Bennett, C., and Rolfe, S. (2013). "Repairing Distortion-Induced Fatigue Cracks in Steel Bridge Girders using Angles-with-Plate Retrofit Technique, Part II: Computer Simulations." *Journal of Structural Engineering*, ASCE, In Press.

American Iron and Steel Institute (AISI) Example 1: Simple-Span Composite I Girder (1997). *American Iron and Steel Institute.*

Connor, R. and Fisher, J. (2006). "Identifying Effective and Ineffective Retrofits for Distortion Fatigue Cracking in Steel Bridges Using Field Instrumentation." *Journal of Bridge Engineering,* 11(6), 745-752.

Fisher, J. W., Jian, J., Wagner, D. C., and Yen, B. T. (1990). "Distortion-Induced Fatigue Cracking in Steel Bridges." *National Cooperative Highway Research Program Report #336,* Transportation Research Board, National Research Council, Washington, D. C.

Fisher, J.W. and Keating, P.B. (1989). "Distortion-Induced Fatigue Cracking of Bridge Details with Web-gaps." *Journal of Constructional Steel Research,* 12(3-4), 215-228.

Grondin, G.Y., Fraser, R., and D'Andrea, M. (2002). "Testing and Evaluating of Fatigue Damaged Girders." *4th Structural Specialty Conference of the Canadian Society for Civil Engineering.*

Hassel, H., Hartman, A., Bennett, C., Matamoros, A., and Rolfe, S. (2010). "Distortion-Induced Fatigue in Steel Bridges: Causes, Parameters, and Fixes." *2010 ASCE/SEI Structures Congress Proceedings*. 471-483.

Jajich, D. and Schultz, A.E. (2003). "Measurement and Analysis of Distortion-Induced Fatigue in Multigirder Steel Bridges." *Journal of Bridge Engineering*, 8(2), 84-91.

Nagati, D. (2012). "Repair of Steel Bridge Girders Damaged by Distortion-Induced Fatigue." Master's Thesis, University of Kansas.

Overman, T. (2012). "Analytical Investigation of Repair Methods for Fatigue Cracks in Steel Bridges." Master's Thesis, University of Kansas.

Przywara, J. (2013). "Applications of the Extended Finite Element Method (XFEM) for the Analysis of Distortion-Induced Fatigue Cracking in Highway Bridge Girders." Master's Thesis, University of Kansas.

Roddis, W.M.K. and Zhao, Y. (2001). "Out-of-Plane Fatigue Cracking in Welded Steel Bridges: Why It Happened and How It Can Be Repaired." *Welding Innovation*, 27(2), 2-7.

Roddis, K.W.M. and Zhao, Y. (2003). "Finite-Element Analysis of Steel Bridge Distortion-Induced Fatigue." *Journal of Bridge Engineering*, 8(5), 259-266.

Tedesco, J.W.; Stallings, J. M.; and Tow, D.R. (1995). "Finite Element Method Analysis of Bridge Girder-Diaphragm Interaction." *Computers and Structures*, 56(2-3), 461-473.

Part 4

PARAMETRIC RETROFIT ANALYSIS FOR DISTORTION-INDUCED FATIGUE IN A 9.1 M (30 FT.) TEST BRIDGE

Amanda Hartman[1], S.M. ASCE
Caroline Bennett[2], M. ASCE
Adolfo Matamoros[3], A.M. ASCE
Stan Rolfe[4], Hon. M. ASCE

ABSTRACT

Developing and testing retrofit techniques to halt distortion-induced fatigue cracking of steel bridge structures can be time consuming and expensive. Finite element modeling is a tool that can be used to reduce the expenses associated with testing such retrofits. In this study, the effectiveness of several existing retrofit techniques was examined for the 9.1 m [30 ft.] test bridge to form a series of baseline values against which to evaluate several variations of the "angles-with-plate" retrofit technique under investigation at the University of Kansas.

Existing techniques investigated included a full depth back-up stiffener as well as bolted angles providing positive attachment from the connection plate to the girder flange. The research team developed "angles-with-plate" technique uses two angles and a backing plate attached to the girder web (called angles-with-backing plate retrofit). Through finite element modeling, three variations of the angles-with-backing plate retrofit were investigated in which the thickness was adjusted and stiffeners were added to the angles.

During investigation, two crack patterns were studied with several crack lengths ranging from 25 mm [1 in.] to 203 mm [8 in.]. Cracking studied included a horseshoe crack around the connection plate-web weld and a longitudinal crack at the flange-web weld. For the connection plate-web weld, the stiffened angles-with-backing plate provided the largest stress reduction; however, for the flange-web weld, angles providing positive attachment to the girder flange reduced the stress the most. Based on the analytical results of the investigation, future

[1] Amanda Hartman, Graduate Research Assistant, University of Kansas, 1530 W. 15th St., Lawrence, KS 66045
[2] Caroline Bennett, PhD, PE, Associate Professor, University of Kansas, 1530 W. 15th St., Lawrence, KS 66045
[3] Adolfo Matamoros, PhD, Professor, University of Kansas, 1530 W. 15th St., Lawrence, KS 66045
[4] Stan Rolfe, PhD, PE, A.P. Learned Distinguished Professor, University of Kansas, 1530 W. 15th St., Lawrence, KS 66045

experimental tests at the University of Kansas will explore the stiffened angles-with-backing plate retrofit.

INTRODUCTION AND BACKGROUND

Many steel bridges built prior to 1985 have experienced distortion-induced fatigue caused by lack of positive connection between connection stiffeners and girder flanges. As differential deflection occurs between adjacent bridge girders, the weak web gap region experiences repeated out-of-plane rotation which causes fatigue. Several methods have been used to mitigate distortion-induced fatigue cracking including: crack arrest holes, cross frame removal, back-up stiffeners, positive attachment between transverse connection stiffeners and flanges, and slotting the transverse connection stiffener (Hassel et al. 2010).

In addition to repair techniques currently in practice, the University of Kansas has developed a new retrofit technique which provides additional positive attachment between the transverse connection stiffener and girder web. This technique is termed "angles-with-plate" retrofit. This retrofit has been shown in previous studies to mitigate crack propagation in a 2.8 m [9 ft.] girder sub-assembly (Alemdar et al. 2013a; 2013b). However, the physical and computational simulations conducted in Alemdar et al. (2013a; 2013b) were representative of a test set-up in which the girder was only subjected to out-of-plane bending effects.

Extensive finite element analyses of these retrofit techniques (of both the more traditional techniques and the newly-developed "angles-with-plate" technique) have been conducted at the University of Kansas. Hassel et al. (2010) used Abaqus v.6.8-2 in which full-scale non-skewed and skewed bridges were evaluated with the following techniques: cross frame removal, back-up stiffeners, positive attachment between connection plates and flanges (using two angles), and slotting the connection plate. . When the retrofits were applied at every cross-frame location (excluding cross-frame removal), positive attachment between connection plates and flanges were found to provide the largest reduction in stress around the connection plate-to-web weld. However, this study failed to consider hot spot stresses at the flange-to-web weld. Additionally, the newly-developed angles-with-plate retrofit technique was not analyzed in the bridge models studied by Hassel et al. (2010).

In a separate investigation, a series of computational and physical studies were performed by Alemdar et al. (2013a; 2013b) aimed at evaluating the performance of the angles-with-plate

retrofit when applied on a 2.8-m [9-ft.] long steel girder sub-assembly. This assembly was comprised of a girder segment oriented upside-down with the top flange attached to the concrete strong floor. An upward force was applied to the cross frame to imitate an adjacent girder deflecting downward in a real bridge. At the ends of the 2.8 m [9.3 ft.] girder segment, small angles were attached to the flange that was not connected to the laboratory floor at one end, and at the load frame at the other end. This was intended to simulate, in an admittedly rudimentary fashion, the out-of-plane restraint provided by longitudinal girder continuity in a real bridge system as shown in Figure 1.

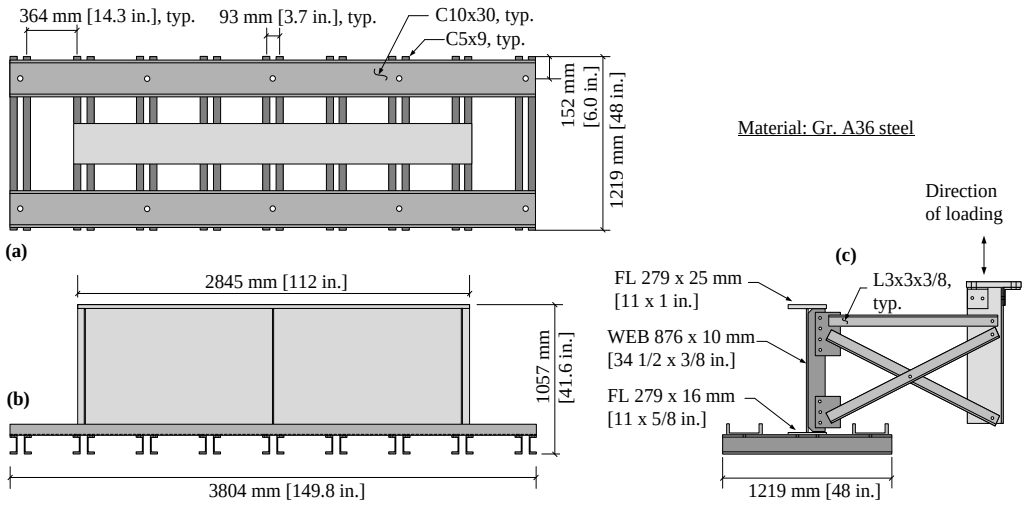

Figure 1: Girder sub-assembly set-up for 2.8 m [9 ft.] testing and finite element modeling (Alemdar et al. 2013a; 2013b).

In the test set-up, the girder flange connected to the concrete floor was intended to represent the top flange in a real bridge that exhibits no flange rotation (e.g. an extremely stiff concrete deck). Finite element modeling followed the actual sub-girder assembly closely, including the flange restraint mechanism.

In a computational parametric study provided in Przywara (2013), the angles-with-plate retrofit and set-up used in Alemdar et al. (2013a; 2013b) was studied extensively by varying angle and plate thicknesses. Thickness variations considered for the angle and plate elements included: 6 mm [1/4 in.], 13 mm [1/2 in.], and 25 mm [1 in.]. With a web thickness of 9.5 mm [3/8 in.], retrofit-to-web thickness ratios of 0.7, 1.3, and 2.7 were examined (Alemdar et al. 2013a; Przywara 2013). For both the flange-to-web weld (hot spot stress path 2, HSS-2) and the

connection plate-to-web weld (hot spot stress path 1, HSS-1), stresses were found to increase at fatigue-susceptible locations as crack length increased, as shown in Figure 2. Retrofit results are shown for stiff (S-S) angles-with-plate (25-mm [1-in.] thick) and flexible (F-F) angles-with-plate (6-mm [1/4-in.] thick) combinations.

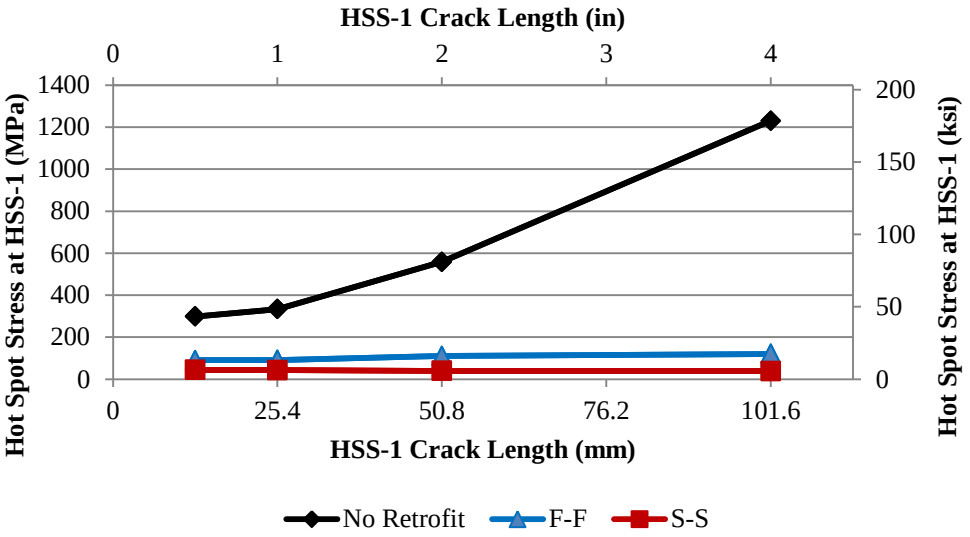

(a)

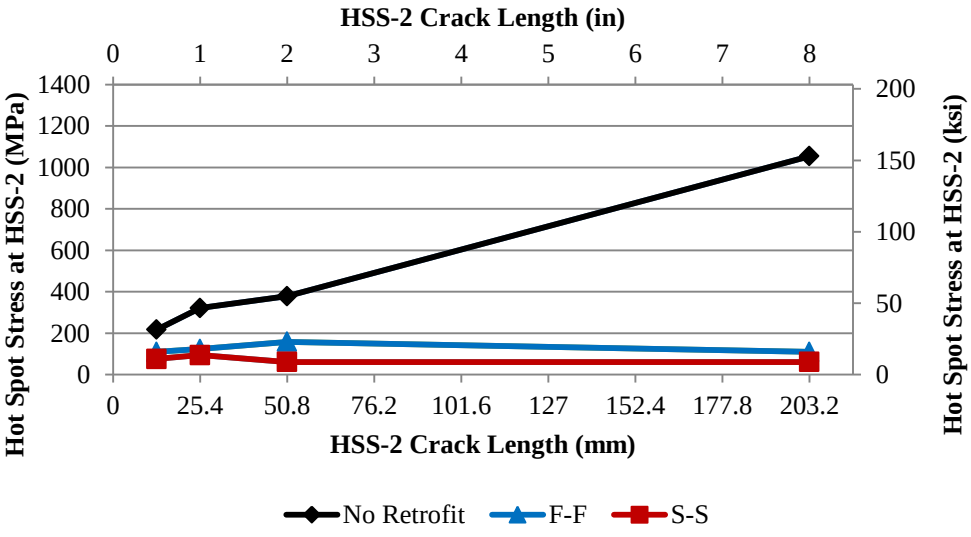

(b)

Figure 2: Hot spot stress at (a) HSS-1 crack and (b) HSS-2 crack for no retrofit, F-F retrofit, and S-S retrofit (Przywara 2013).

For large crack lengths, Przywara (2013) showed that both stiff and flexible angles-with-plate retrofit configurations provided significant reduction in hot spot stresses in both hot spot locations (at the connection plate-to-web weld and at the flange-to-web weld). Retrofitting small cracks did not result in a similar reduction in stress. Additionally, it was found that increasing the retrofit thickness/stiffness caused a slightly larger reduction in hot spot stress; however, this difference was not found to be significant.

Based on the analyses and physical testing outlined in Alemdar et al. (2013), it was found that "the angles-with-plate measure was effective in preventing distortion of the web-gap region, reducing stress demands calculated at the critical points by an order of magnitude." Additionally, experimental testing "showed that there was negligible crack growth when the angles-with-plate retrofit measure was implemented" (Alemdar et al. 2013).

OBJECTIVE AND SCOPE

The primary objective of this study was to analytically evaluate the effectiveness of the new "angles-with-plate" retrofit technique on a 9.1 m [30 ft.] bridge system subjected to both in-plane and out-of-plane bending effects as compared with existing retrofit techniques. The effects crack length on the effectiveness of the angles-with-plate retrofit was investigated, as was the effect of reduced deck stiffness.

The computational simulations presented in this paper corresponded to an experimental test set-up in which a three-girder, 9.1-m [30-ft] long test bridge was tested under fatigue loading. Details regarding the physical tests of the test bridge have been presented in a companion paper.

FINITE ELEMENT MODELING METHODOLOGY

The test bridge geometry described in the companion paper was modeled as faithfully as possible using the commercially-available software Abaqus v.6.10. Screenshots from the bridge model are shown in Figure 3.

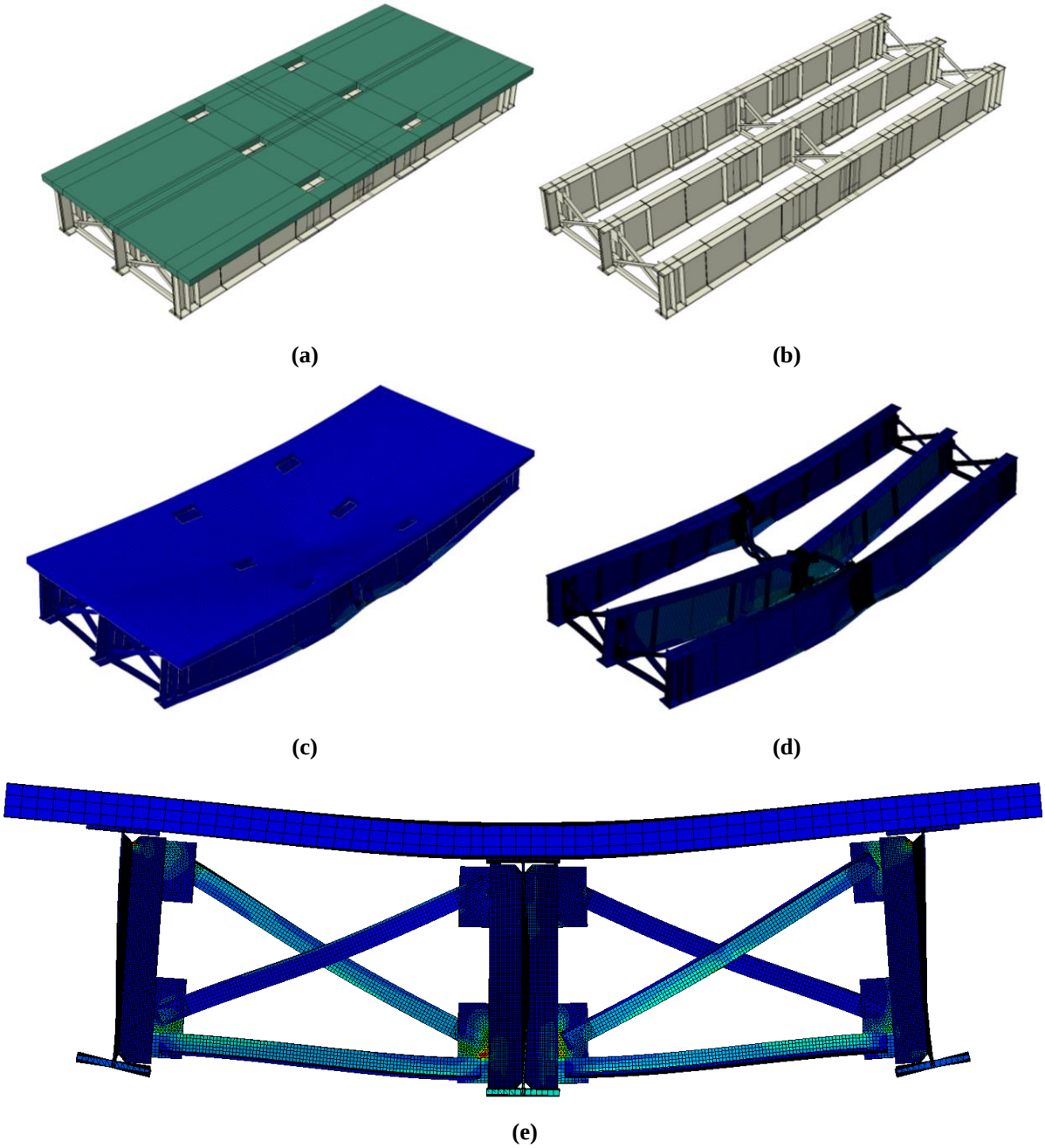

Figure 3: (a) Overall model with concrete deck, (b) overall model without concrete deck, (c) deflected model with concrete deck, deflection scale=425, (d) deflected model without concrete deck, deflection scale=425, and (e) deflected section cut at mid-span, deflection scale=100.

Forty-five finite element models were constructed and analyzed as variations of the baseline test bridge geometry. Models included cracked and uncracked conditions in the top web

gap of the exterior (north and south) girders. Cracked models included either a horseshoe-shaped crack or a longitudinal crack. A modeling test matrix is shown in Table 1.

Table 1: Finite Element Modeling Matrix for Cracks around Stiffener-Web-Weld

	Model Description / Crack Length	No Crack	25 mm [1 in.]	38 mm [1-1/2 in.]	51 mm [2 in.]	64 mm [2-1/2 in.]	76 mm [3 in.]	101 mm [4 in.]	203 mm [8 in.]
Connection Plate-to-Web Cracks	Unretrofitted condition	X	X	X	X	X	X	X	X
	Reduced deck stiffness with unretrofitted condition				X				
	Broken Cross Frame		X						
	Angles-with-plate repair with 19-mm [3/4-in.] thicknesses		X	X	X	X	X		
	Stiffened angles-with-plate repair with 19-mm [3/4-in.] thicknesses		X	X	X	X	X		
	Angles-with-plate repair with 13-mm [1/2-in.] thicknesses		X	X	X	X	X		
	Traditional angles repair connected to flange with 19-mm [3/4-in.] thickness		X	X	X	X	X		
	Back-up stiffener repair placed on fascia side		X	X	X	X	X		
Flange-to-Web C racks	Unretrofitted Condition		X		X		X	X	X
	Angles-with-backing plate repair with 19-mm [3/4-in.] thicknesses		X		X		X	X	X

Horseshoe-shaped (U-shaped) cracks were modeled around the connection plate weld toe having leg lengths from 25.4-76.2 mm [1.0-3.0 in.] and the leg length of the crack was varied in 12.7-mm [0.5-in.] increments. Additionally, two cracks with leg lengths of 101 mm and 203 mm [4.0 in. and 8.0 in.] were also considered. Crack lengths correlated with the vertical length of each leg of the crack. In separate analyses, longitudinal cracks were placed near the flange-to-

web weld. Three longitudinal crack lengths were studied which included: 25mm [1 in.], 51 mm [2 in.], and 76 mm [3 in.].

All bridge components were constructed in Abaqus v.6.10 using three dimensional elements including mostly hexahedral elements (C3D8R) and some tetrahedral elements (C3D4) for transition regions. Each model contained approximately 3 million elements and 10 million degrees of freedom. A dense mesh was applied to the web gap region while other locations within the bridge contained a coarser mesh as shown in Figure 4(a). Based on a convergence study performed on the dense mesh region around the connection plate-web weld, the optimal mesh size of the web gap was determined to be 2.5 mm [0.1 in.] (Figure 4(b)).

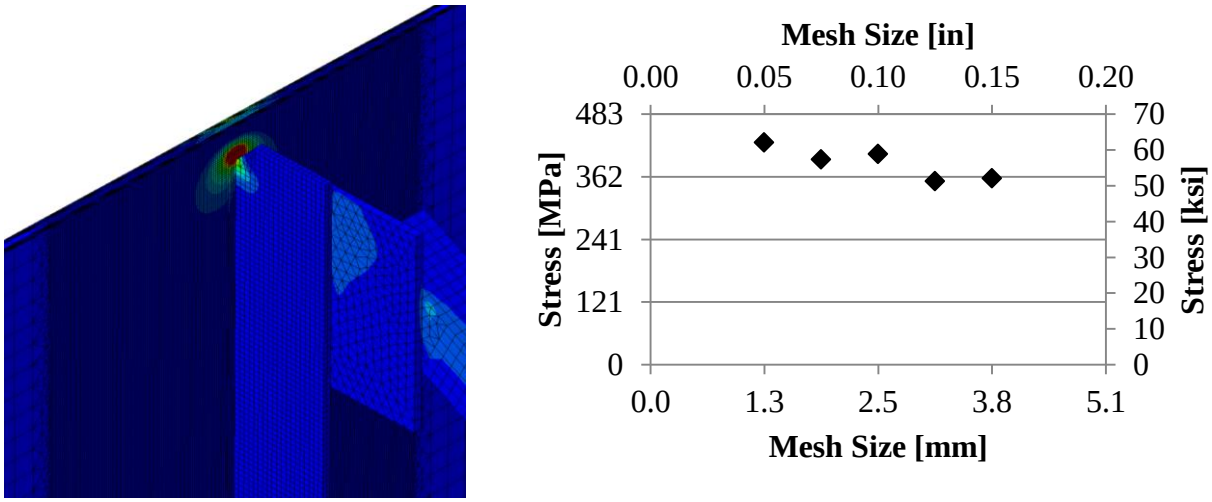

(a) **(b)**

Figure 4: (a) Dense mesh (2.54 mm [0.1 in.]) in web gap region transitions to coarse mesh (25.4 mm [1.0 in.]) and (b) mesh sensitivity study for changing dense region mesh.

Steel and concrete were modeled as linear-elastic materials where the moduli of elasticity for each were taken as 200,000 MPa [29,000 ksi] and 25,000 MPa [3,605 ksi], respectively. Poisson's ratio for steel and concrete were assumed to be 0.3 and 0.2, respectively. For the reduced deck stiffness model, the concrete modulus of elasticity was halved. The entire 9.1 m [30 ft.] test bridge was modeled and assembled in Abaqus v.6.10 using 3D solid elements, including welds, cross frames, stiffeners, and deck.

Since modeling bolts and bolt tension are computationally expensive endeavors, the base model of the test bridge contained surface-to-surface ties at girder splice locations and cross

frame connections. Welds were modeled using surface-to-surface ties and when appropriate, hard contacts were used to prevent parts from moving through one another during loading.

Retrofitted models required further refinement with regard to bolting. To improve computational efficiency, modeled bolt heads and nuts were tied directly to the surfaces in which they were in contact. All other surfaces contained hard contact interactions with a frictional coefficient of 0.35. All bolts were modeled as 19-mm [3/4-in.] diameter which was consistent with those used in the physical tests. For models that included application of retrofits, behavior was desired that would replicate the slip-critical bolt conditions implemented in the physical tests. For the slip-critical connection, an initial bolt pretension step was created in the models that induced a bolt load of 125 kN [28 kip] on each bolt using the bolt load function in Abaqus v.6.10.

Static loading applied in the models correlated with the upper bound load of 267 kN [60 kip] from the first test trial in the physical test sequence (Test Trials 1S and 1N). In the models, this load was spread over two areas of 400x114 mm [15-3/4 x 4-1/2 in.] to represent the application of the load through the two "feet" of the actuator's swivel end. Loading was applied at midspan of the center girder as was done in the physical tests. Due to this load placement, primary regions of interest were found to occur in the top web gaps of the exterior girders. This region of interest was consistent with previous research results obtained for an unstaggered bridge condition in which highest stresses were found to occur in top web gaps for exterior girders (Hartman et. al 2010).

Cracks were modeled using the Extended Finite Element Method (XFEM) in Abaqus v.6.10. Using XFEM, cracks of various shapes could be easily modeled without affecting the mesh in the region of interest. Additionally, cracks could be placed anywhere within elements, not just located at element boundaries. U-shaped cracks (wrapping around the connection plate weld) and longitudinal cracks (along the flange-to-web weld) were modeled using three-dimensional planar elements with a depth larger than the girder web thickness of 6.35 mm [1/4 in.].

An identified limitation to using XFEM is that only two crack tips can exist for one crack. In experimental testing, cracks were found to often branch out into multiple "spider" cracks. This branching cannot be modeled using XFEM; however, even though branched cracks were found to exist experimentally, generally the vertical portion of the crack was observed to

progress down the weld while the branch crack (spider crack) growth slowed (Nagati 2012). In the companion paper in Part 3, only the east side of the south girder connection stiffener has following this pattern; however, cracking in the test bridge is relatively small (less than 51 mm [2 in.] in the horseshoe crack). Due to this, spider cracks were not modeled as they were observed to only temporarily grow until stress concentrations at the weld became larger than the stress concentrations at the spider crack tip. The vertical crack that wrapped around the connection plate-to-web weld was referred to as a horseshoe-shaped crack. In addition to horseshoe-shaped cracking, a separate longitudinal crack was modeled near the flange-to-web weld.

COMPUTING CRACK PROPENSITY: HOT SPOT STRESS ANALYSIS

Traditionally, in-plane fatigue is classified using nominal stresses; however, the three-dimensional stress state in the web gap region cannot accurately be captured using only nominal bending stress. To capture both normal and out-of-plane stresses, maximum principle stresses were extracted from the models. Richardson (2012) and Nagati (2012) found that crack growth closely followed maximum principal hot spot as shown in Figure 5. White lines superimposed on the stress contours in Figure 5 denote crack growth seen experimentally.

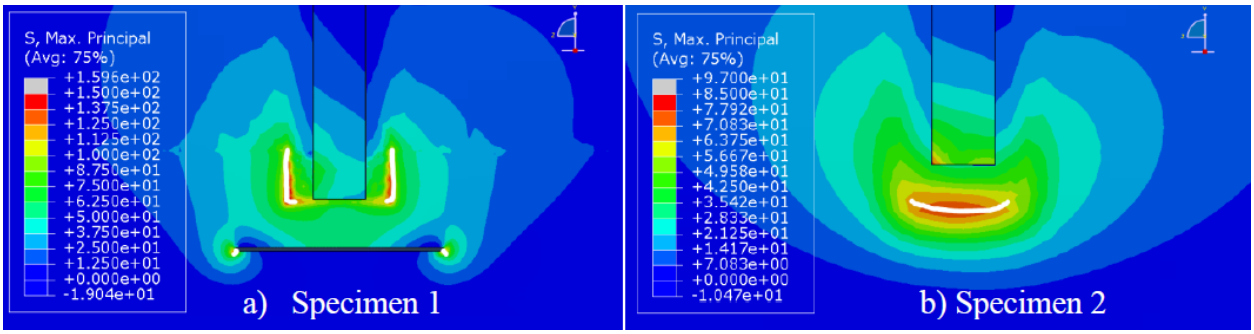

Figure 5: Cracking and maximum principal hot spot stresses (Nagati 2012).

Complicated geometry and stresses in the web gap region made accurate comparisons between models a difficult task. A one-point hot spot stress (HSS) procedure was used as the basis for this comparison in which stresses were extracted at a set distance (half the web thickness, 3 mm [1/8 in.]) from the discontinuity, either a weld or crack. This procedure has

been found to be less sensitive to mesh density than extracting maximum stress from the models (Adams 2009). Two hot spot stress paths were chosen for consideration as shown in Figure 6.

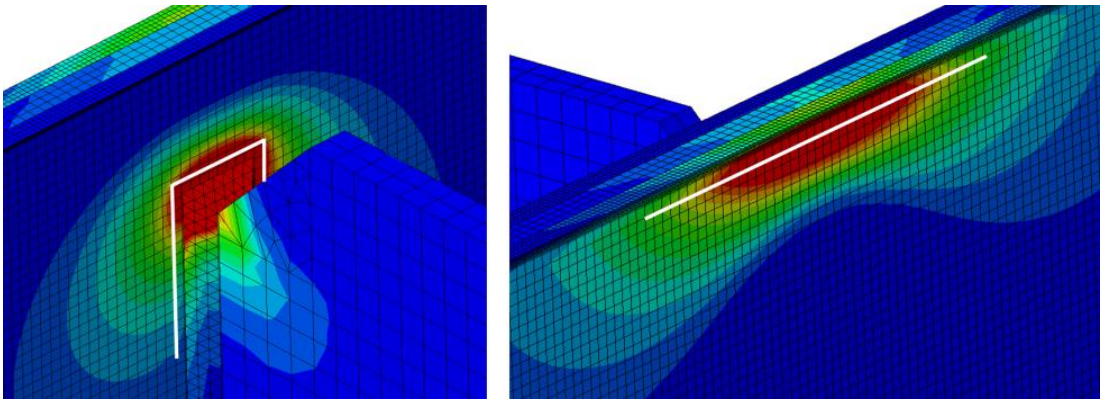

(a) **(b)**

Figure 6: Hot Spot Stress Paths for (a) interior connection plate side or connection plate-web weld, (b) exterior fascia side or flange-web weld.

DESCRIPTION OF RETROFITS

Three retrofit configurations were investigated in the computational simulations. First, an existing retrofit technique was explored in which positive attachment was provided between the connection plate and top flange using two angles oriented back-to-back. Next, a back-up stiffener technique was studied in which the web gap was stiffened by a secondary stiffener placed on the opposing web face. This retrofit can be applied using either a partial depth or full depth transverse stiffener; however, only a full depth stiffener was studied as it was expected to produce the best result, based upon findings from previous studies (Hassel et. al 2010). Back-up stiffeners were modeled using transverse stiffener dimensions and placed on the girder fascia side. Third, a retrofit in which attachment was provided between the connection plate and web through two angles and a back plate was explored. This last retrofit has been extensively investigated at the University of Kansas and has been termed the "angles-with-plate" technique (Alemdar et al. 2013a; 2013b). Several variations of the angles-with-backing plate retrofit were explored, in which the thickness of the angle and plate elements were varied (with retrofit-to-web ratios of 2 and 3), and one case in which the angles were modified to include internal stiffeners. Schematics of the retrofits studied are shown in Figure 7.

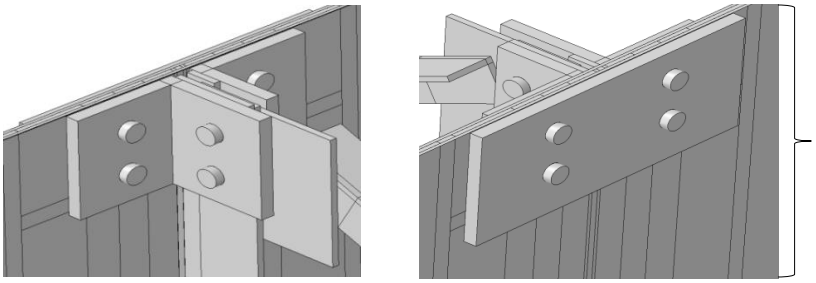

Angles:
L152x152 mm [L6x6 in.]
L127x152 mm [L5x6 in.]

Backing Plate:
457x457 mm [18x8 in.]

(a)

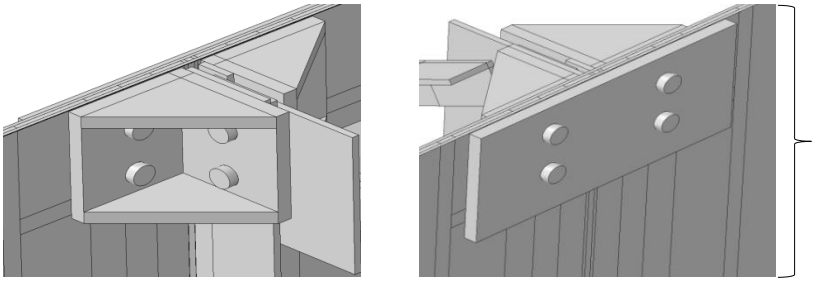

Angles:
L152x152 mm [L6x6 in.]
L127x152 mm [L5x6 in.]

Stiffeners:
133x133 mm [5.25x5.25 in.]
108x133 mm [4.25x5.25 in.]

Backing Plate:
457x457 mm [18x8 in.]

(b)

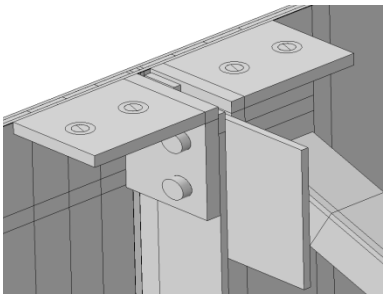

Angles:
L179x179mm [L7x7 in.]

(c)

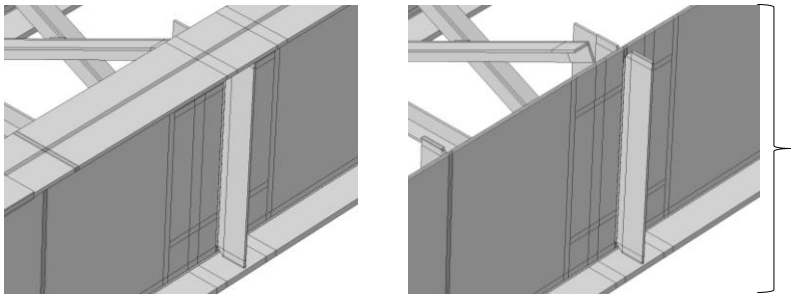

Back-up Stiffener:
9.5x127x876 mm [3/8x5x34-1/2 in.]
with 32x32 mm [1-1/4x1-1/4 in.]
clip

(d)

Figure 7: Views of various retrofits examined in finite element models: (a) angles-with- plate retrofit; (b) stiffened angles-with-plate retrofit; (c) positive attachment between transverse connection stiffener and top flange retrofit; and (d) full depth back-up stiffener bearing on top and bottom flanges.

RESULTS

All cracked and/or retrofitted models were normalized based on stress demands computed in the uncracked, unretrofitted finite element model. Although 45 models were analyzed, representative results have been presented in this paper. For the two hot spot stress paths considered, stresses at the connection plate-to-web weld and at the flange-to-web weld were found to be within 3% of one another in the uncracked, unretrofitted bridge model. Since all stresses presented have been normalized to hot spot stress demands from the uncracked, unretrofitted models, new stresses due to cracking and/or retrofitting have been approximately normalized to the same initial hot spot stress value due to this circumstance.

STRESS VS. CRACK LENGTH

For all horseshoe-shaped crack lengths studied, hot spot stress decreased or remained nearly constant as crack length increased for both retrofitted and unretrofitted conditions. The percentage of uncracked hot spot stress due to change in length of the horseshoe-shaped crack has been presented in Figure 8.

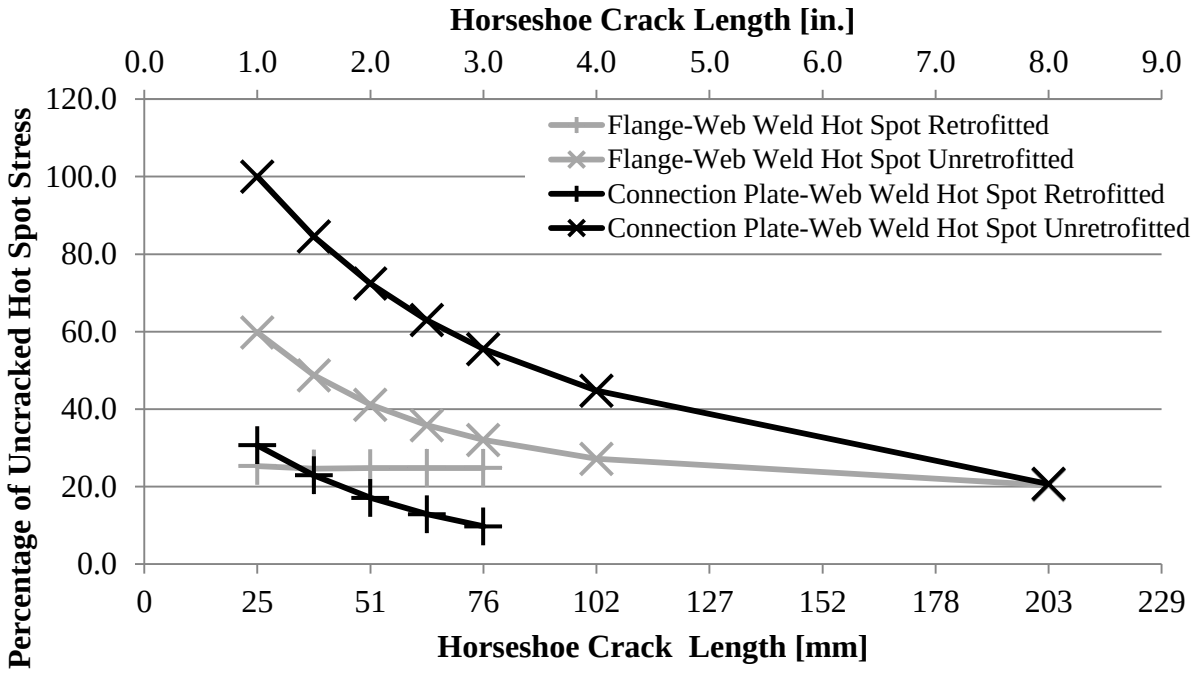

Figure 8: Percentage of uncracked hot spot stresses with change in horseshoe crack length for connection plate-web weld and flange-web weld.

Cracks were physically located at the connection plate-to-web weld toe on the web. For both the unretrofitted and retrofitted conditions, hot spot stress at the connection plate-to-web weld decreased as crack length was increased. At the flange-to-web weld in an unretrofitted state, the hot spot stress decreased as the horseshoe-shaped crack length was increased; however, for the retrofitted condition, hot spot stress remained nearly constant.

For the longitudinal flange-to-web crack lengths studied, hot spot stress behavior was found to be similar to that for the horseshoe-shaped cracks. As longitudinal crack length was increased, hot spot stresses for both the flange-to-web weld and connection plate-to-web weld decreased as shown in Figure 9. Initiation of a 25 mm [1 in.] longitudinal crack provided little reduction in flange-to-web hot spot stress demand, and increased stress demand at the connection plate-to-web weld by approximately 14%. Since both stresses were normalized to similar uncracked hot spot stresses (within 3% of each other), Figure 9 indicates that once a longitudinal crack initiated, a horseshoe-shaped crack is highly likely to initiate due to increased stresses at the connection plate-to-web weld.

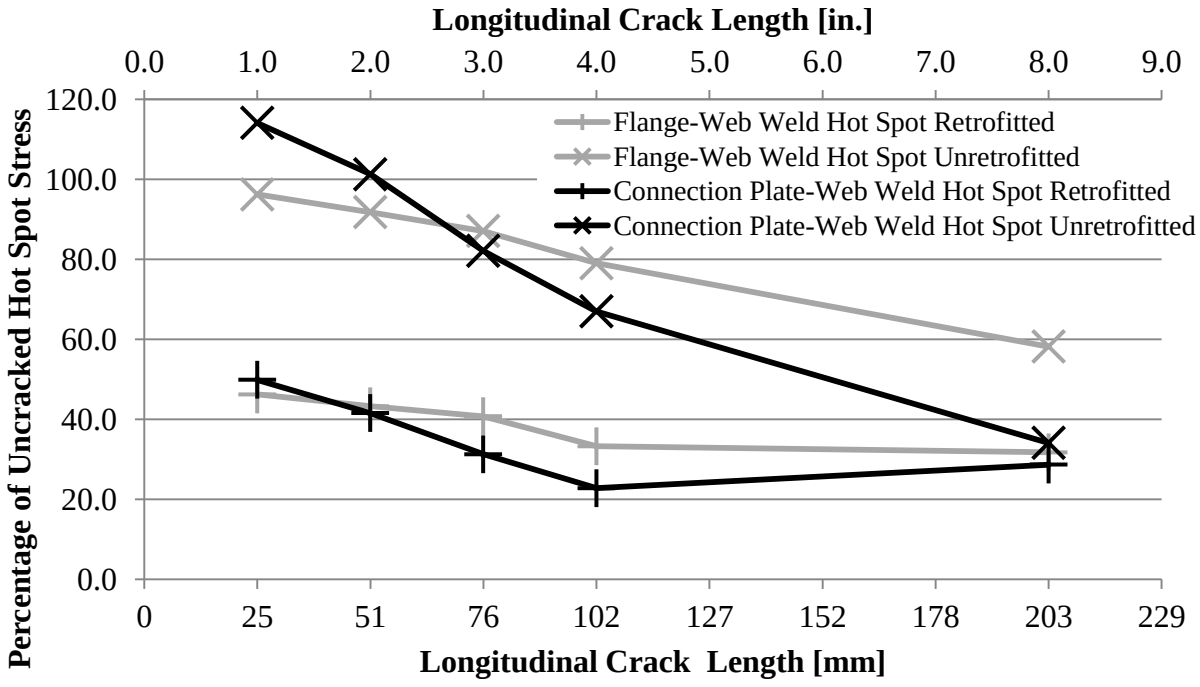

Figure 9: Percentage of uncracked hot spot stresses with change in longitudinal crack length for connection plate-web weld and flange-web weld.

Retrofit effectiveness in the presence of only a longitudinal crack was found to decrease significantly for the connection plate-to-web weld as crack length increased. The reduction in stress from cracked, unretrofitted to cracked, retrofitted for the connection plate-to-web weld was approximately 5% for a 203-mm [8-in.] longitudinal crack and 64% for a 25-mm [1-in.] crack. For the flange-to-web weld location, stress reduction due to retrofitting did not vary significantly with increasing crack length.

The reduction in hot spot stresses as crack length increased contradicts the findings inform the girder sub-assembly (2.8 m [9.3 ft.]) finite element modeling presented in Przywara (2013) and Alemdar et al. (2013a). For the models of the girder sub-assemblies, crack growth propensity increased as crack length increased. As explained in the introduction section, the girder sub-assemblies contained a flange (representing a top flange in a bridge) fixed to a concrete floor. This fixity with a corresponding lack of flange rotation as well as the complete lack of longitudinal bending within the girder, is hypothesized to be the primary cause of the significant differences in girder performance between the girder sub-assembly tests and the scaled bridge tests reported herein.

Effect of Reduced Deck Stiffness

Since cracking should be expected to occur in a concrete deck, reduced deck stiffness was applied to the model to determine the effect of deck stiffness on stress demand in the web gap region. For this condition, only a horseshoe-shaped crack was considered. In both hot spot locations in the top web gap, halving the concrete deck stiffness was found to increase stresses in the web gap region. This increase was approximately 20% of the hot spot stresses computed in a model with full deck stiffness with a horseshoe-shaped crack around the connection plate-to-web weld. Effect of reduced deck stiffness on south girder top web-gap stresses can be seen in Figure 10.

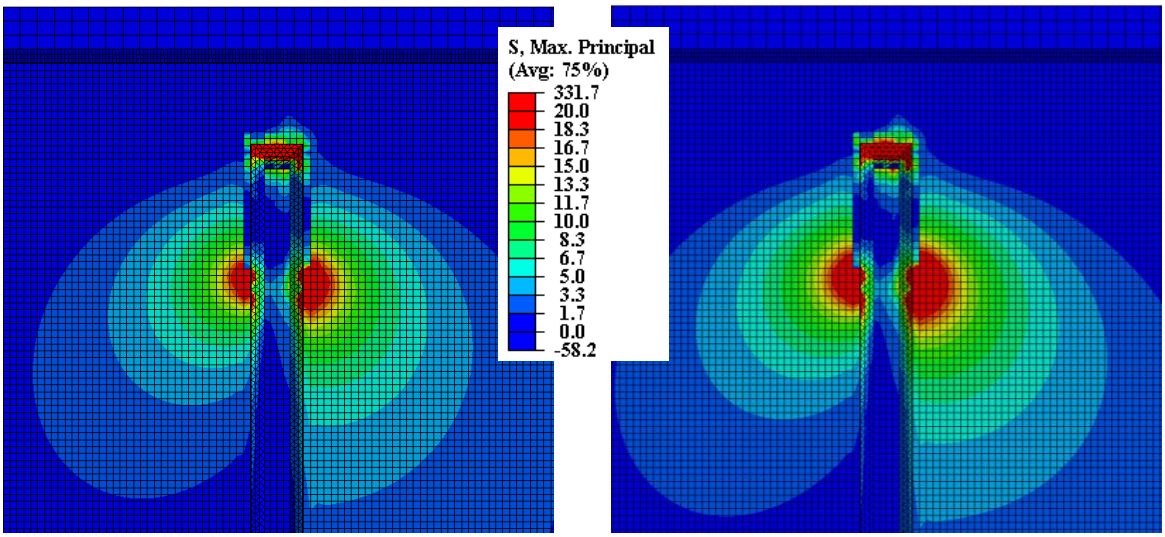

(a) **(b)**

Figure 10: Maximum principal stresses with scale from 0 MPa to 138 MPa [0 ksi to 20 ksi] for (a) unretrofitted model with normal deck stiffness and (b) unretrofitted model with reduced deck stiffness and a 51 mm [2 in.] crack. Legend stresses are in ksi.

EFFECT OF BROKEN CROSS FRAME

During experimental testing as outlined in the companion paper (Part 3), the north cross frame at mid-span experienced a fracture through the diagonal member framing into the top web-gap of the north girder. The effect of this failure on the bridge system was analyzed in a model of the bridge with a 25-mm [1-in.] horseshoe-shaped crack. In this finite element model, which directly modeled the severed cross frame member where it should have framed into the north girder top web-gap, hot spot stresses where the cross frame element previously framed into the girder decreased significantly. This reduction in stresses in the top web-gap of the north girder was approximately 77%. At the bottom web-gap of the same girder, hot spot stresses more than doubled. This correlated well with the computed maximum principal stress magnitudes in the cross frame members framing into the north girder, which saw a decrease in the broken member and an increase in the horizontal element framing into the bottom web-gap. In the south girder, away from the broken cross frame, maximum principal stresses in all cross frame elements decreased. Cross frame stresses can be seen in Table 2.

Table 2: Cross Frame Element Stresses with 25 mm [1 in.] Horseshoe Crack (MPa [ksi])

	Angles-and-Plate 19 mm [3/4 in.]			Angles-and-Plate 19 mm [3/4 in.] with Broken Cross Frame Element		
	Maximum Principal	**Horizontal**	**Vertical**	**Maximum Principal**	**Horizontal**	**Vertical**
Inclined Cross Frame Element Framing into North Girder Top Web-Gap	39 [5.7]	28 [4.1]	8 [1.1]	0 [0.0]	0 [0.0]	0 [0.0]
Inclined Cross Frame Element Framing into North Girder Bottom Web-Gap	0 [0.0]	-19 [-2.8]	-6 [-0.9]	0 [0.0]	-23 [-3.4]	-11 [-1.6]
Horizontal Cross Frame Element Framing into North Girder Bottom Web-Gap	29 [4.2]	30 [4.3]	0 [0.0]	41 [6.0]	38 [5.5]	0 [0.0]
Inclined Cross Frame Element Framing into South Girder Top Web-Gap	37 [5.3]	28 [4.1]	7 [1.0]	24 [3.5]	19 [2.7]	5.5 [0.8]
Inclined Cross Frame Element Framing into South Girder Bottom Web-Gap	0 [0.0]	-23 [-3.3]	-6 [-0.9]	0 [0.0]	-19 [-2.8]	-5.5 [-0.8]
Horizontal Cross Frame Element Framing into South Girder Bottom Web-Gap	29 [3.9]	29 [4.2]	0 [0.0]	24 [3.5]	24 [3.5]	0 [0.0]

Girder lateral deflections can be seen in Figure 11. Deflections show as if looking at the girder deflection profiles. The north girder bottom flange moves out toward the right (positive deflection in the plot) and the south girder bottom flange moves out toward the left (negative deflection in plot). The response of the north and south girders in the cracked, unretrofitted condition (25 mm [1 in.] horseshoe-shaped crack) and the response of the girders with the same crack geometry under the angles-with-plate retrofit were found to be symmetric. For the north girder (where the cross frame element was broken), lateral girder deflections were significantly decreased after the cross-frame member was severed, resulting in decreased girder rotation between top and bottom flanges. Additionally, top web-gap differential deflection was found to be nearly zero. Different behavior was found to define the south girder after the cross-frame was severed. In the south girder, top web-gap differential deflection was still decreased, but bottom

flange deflection increased significantly, resulting in larger girder rotation between top and bottom flanges.

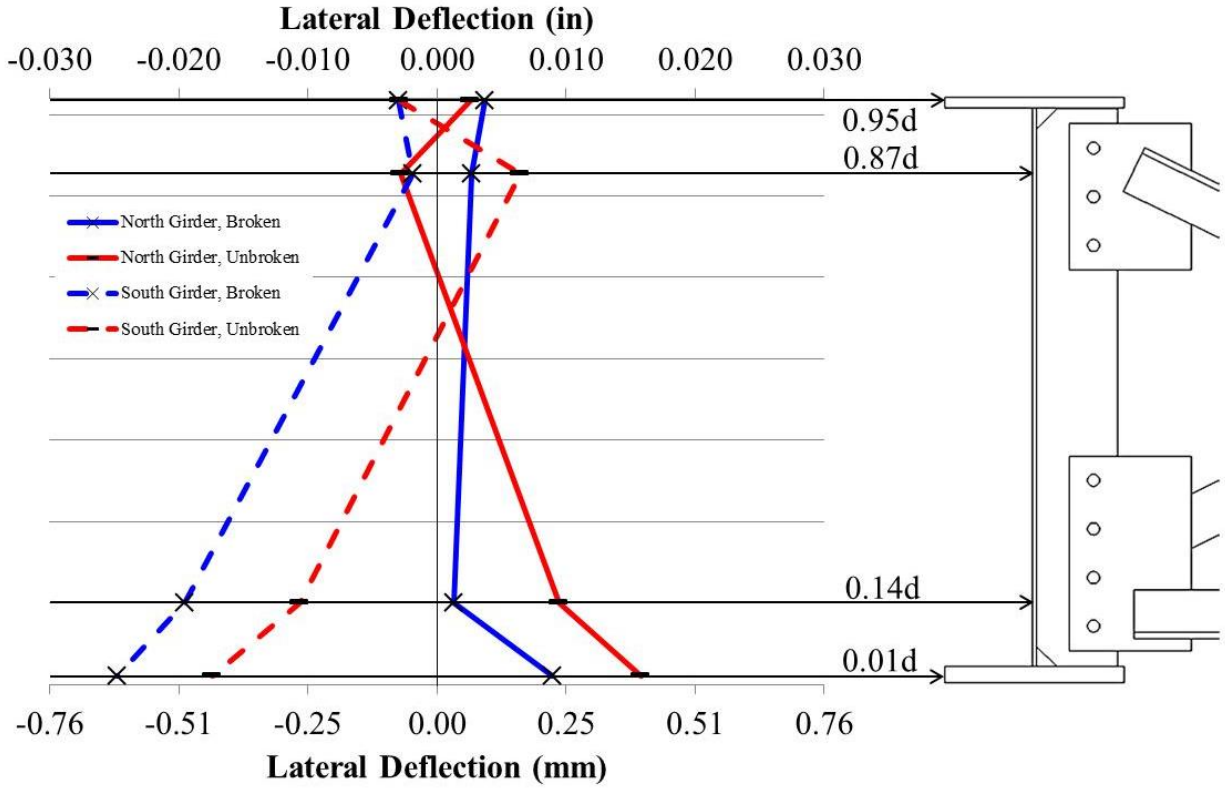

Figure 11: Girder lateral deflections with unbroken cross frame elements and broken cross frame element framing into the north girder top web-gap.

Cross section deflected shapes have been shown in Figure 12. These figures provide images for the results outlined in Figure 11. A localized stress concentration (hot spot) can be seen at the on the tab plate near the end of the inclined cross frame angle as shown in Figure 12(a). Once the cross frame element is broken, little force exists in the tab plate and therefore little out-of-plane forces are transferred into the north girder top web-gap as seen in Figure 12(b). Symmetric bending was found to occur while both cross frames were fully attached; however, deflections were asymmetric under the broken cross frame condition. For the north girder, slightly more flange rotation and less web rotation as shown in Figure 12.

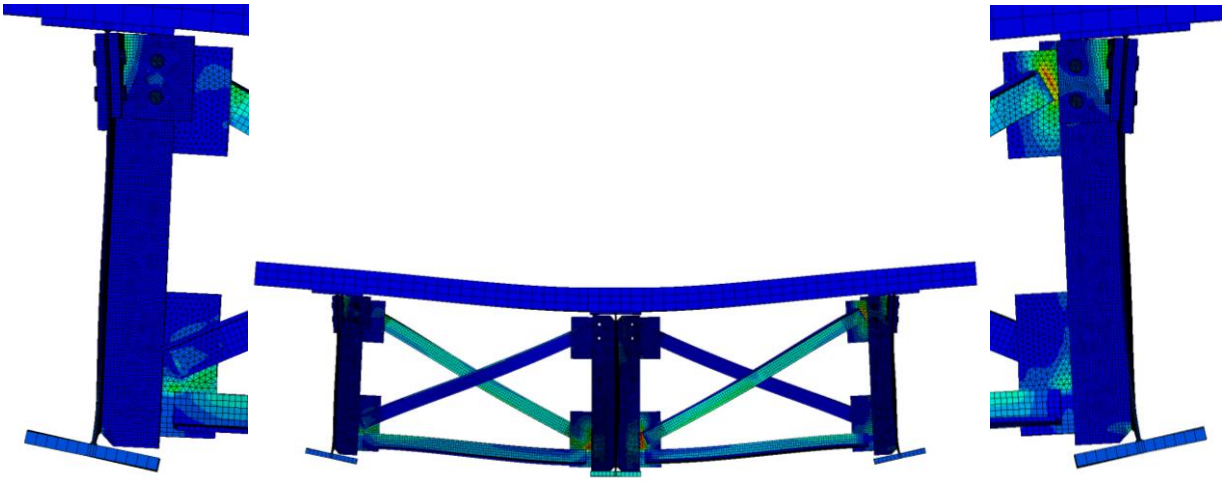

(a)

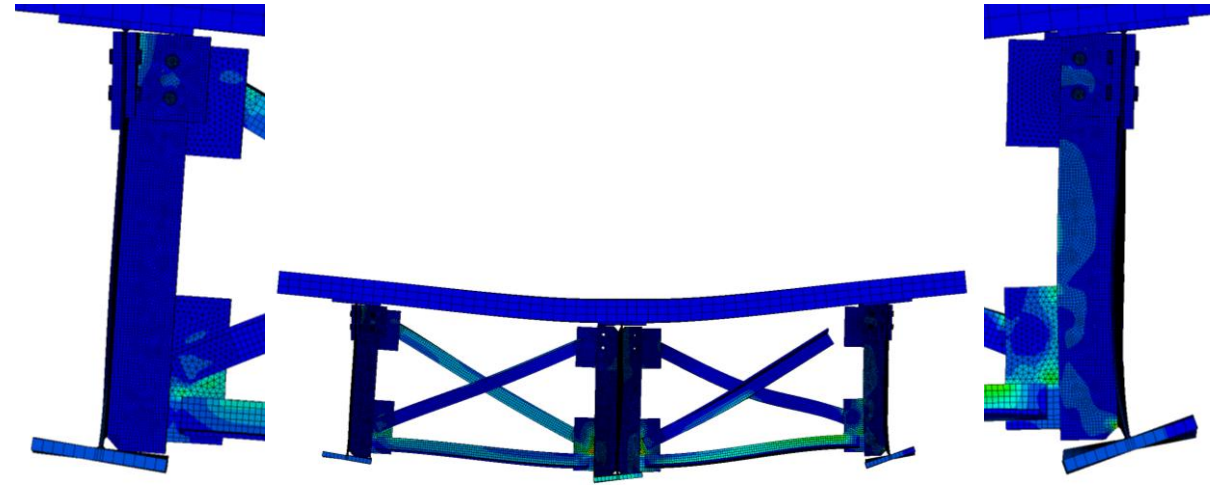

(b)

Figure 12: Girder deflection profiles for (a) 25 mm [1 in.] cracked and retrofitted model and (b) 25 mm [1 in.] cracked and retrofitted model with broken north cross frame element.

Hot spot stresses were influenced by the broken north cross frame element framing into the top web-gap. Stresses extracted from finite element models have been presented in Table 3. When the north girder cross frame element framing into the north girder top web-gap was severed, the hot spot stress at the north girder connection plate-to-web weld decreased by more than 50%. In the north girder bottom web-gap, connection plate-to-web weld stress more than doubled. South girder stresses were only slightly affected by the broken north cross frame.

Table 3: Maximum Principal Hot Spot Stresses with 25 mm [1 in.] Horseshoe Crack (MPa [ksi])

	Angles-and-Plate 19 mm [3/4 in.]	Angles-and-Plate 19 mm [3/4 in.] with Broken Cross Frame Element
North Girder Top Web-Gap Connection Plate-Web Weld	71 [10.3]	29 [4.2]
North Girder Top Web-Gap Flange-Web Weld	101 [14.6]	37 [5.4]
North Girder Bottom Web-Gap Connection Plate-Web Weld	92 [13.4]	191 [27.7]
North Girder Bottom Web-Gap Flange-Web Weld	38 [5.5]	77 [11.1]
South Girder Top Web-Gap Connection Plate-Web Weld	52 [7.6]	60 [8.7]
South Girder Top Web-Gap Flange-Web Weld	102 [14.8]	66 [9.6]
South Girder Bottom Web-Gap Connection Plate-Web Weld	97 [14.1]	56 [8.1]
South Girder Bottom Web-Gap Flange-Web Weld	41 [5.9]	25 [3.6]

RETROFIT COMPARISON

The relative effectiveness of the various retrofits investigated have been presented by showing the stress demands in the web gap region in the retrofitted condition as percentage of the stress demands from the uncracked, unretrofitted condition. All retrofits were analyzed and applied over a horseshoe-shaped crack only. The angles-with-plate retrofit was also analyzed with longitudinal cracks. The percent of uncracked stress in connection plate-to-web weld and flange-to-web weld for changing horseshoe-shaped crack lengths are shown in Figure 13(a) and 13(b), respectively. For all retrofits considered, the pattern of stress reduction was similar for all crack lengths studied. As crack length increased from 25 mm [1 in.] to 76 mm [3 in.], the percent reduction in hot spot stress decreased for both the connection plate-to-web weld and flange-to-web weld locations. As crack length increases, hot spot stresses decrease as shown in Figure 8 andFigure 9. As the retrofit was applied to larger cracks with lower initial stresses, the reduction in stress decreased. Additionally, at a crack length of 76 mm [3 in.], all retrofits provide a reduction in stress of more than 80%. Continuing to improve on this stress (which is already low) becomes inefficient.

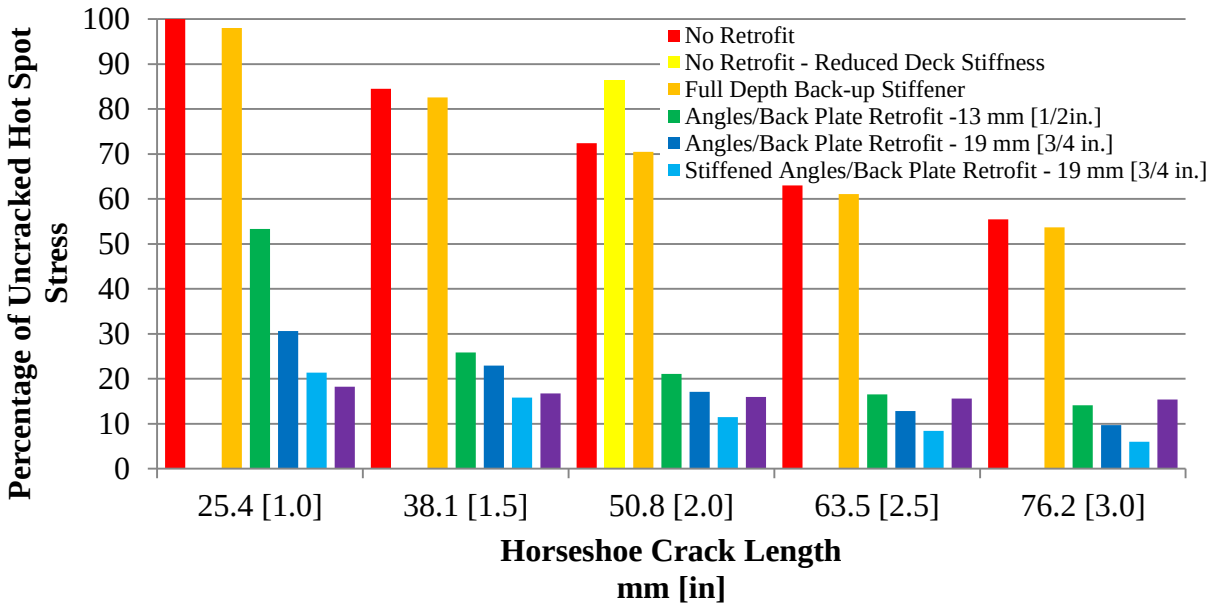

(a)

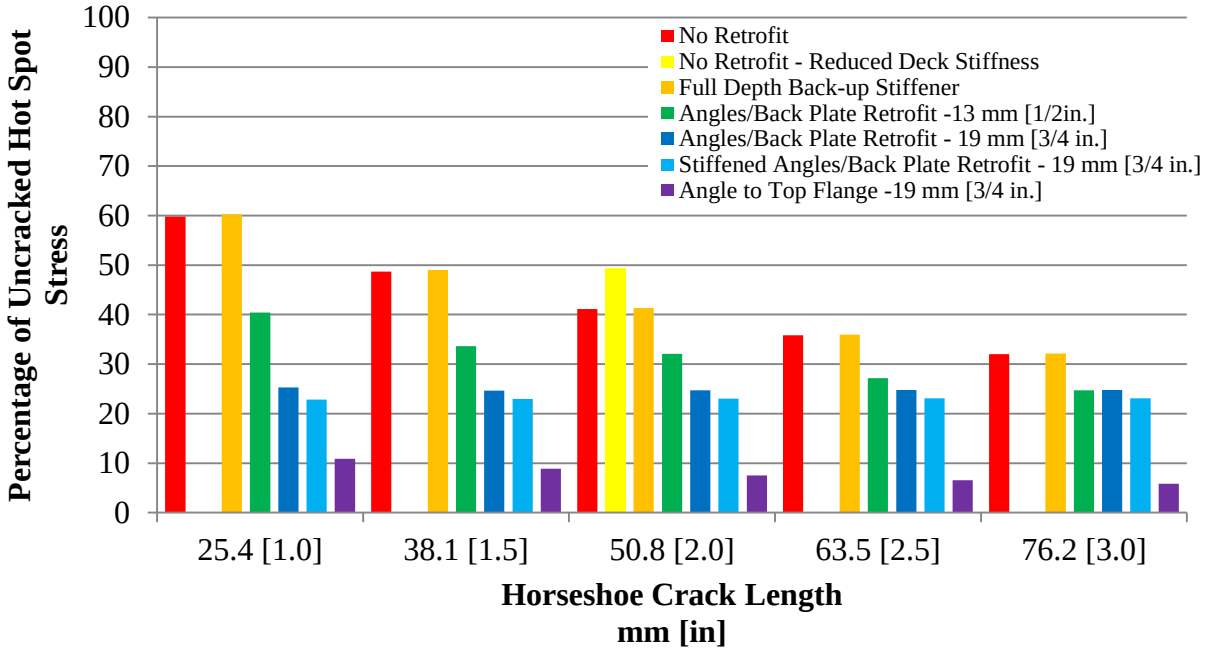

(b)

Figure 13: Percent of uncracked stress at (a) connection plate-web weld and (b) flange-web weld for various retrofit techniques and crack lengths.

Since similar patterns were found for each of the crack lengths investigated, results for a horseshoe-shaped crack length of 51 mm [2 in.] are shown in Figure 14.

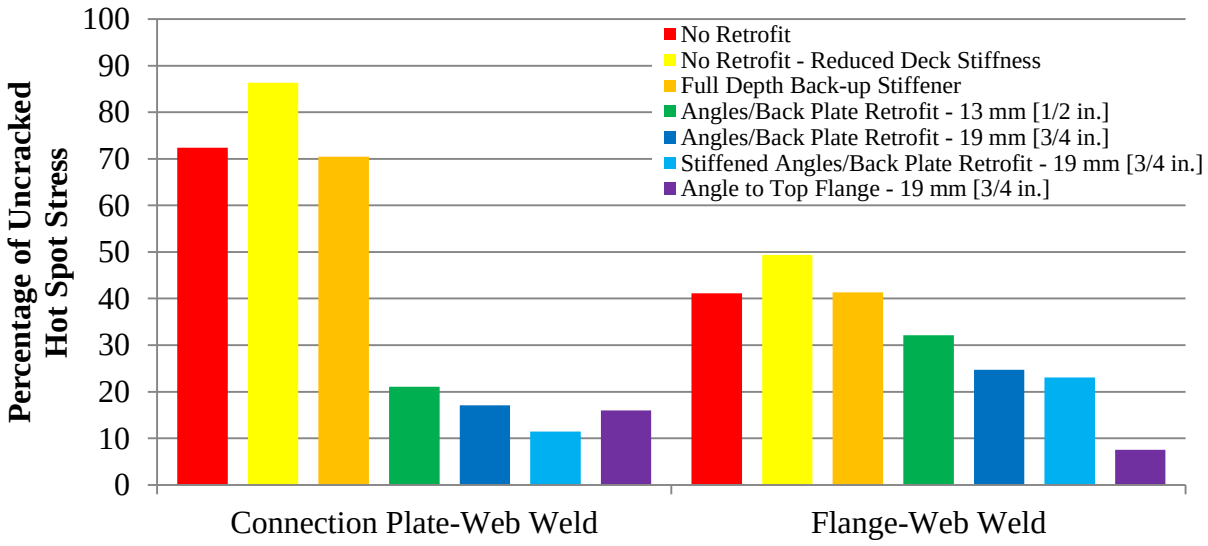

Figure 14: Percentage of uncracked hot spot stresses for connection plate-web weld and flange-web weld with various retrofit conditions and a 51 mm [2 in.] horseshoe crack.

As shown, an initial horseshoe-shaped crack length of 51 mm [2 in.] resulted in a connection plate-web weld hot spot stress of approximately 72% of the uncracked state while flange-web weld hot spot stress was approximately 41% of the uncracked state. Retrofit performance was based on additional reduction from the cracked state. As stated previously, initial uncracked hot spot stresses for each location were within 3% of each other. Therefore, all retrofitted hot spot stresses were normalized against a similar value and can be compared directly. In other words, because of this coincidence, a reduction of 10% in the connection plate-web weld is approximately the same as a 10% reduction in the flange-web weld.

Full depth back-up stiffeners provided minimal relief in hot spot stress for both welds of interest. Since the bridge studied was a non-skewed bridge with cross frames placed back-to-back, this corroborates previous findings (Hartman et. al 2010). Excluding back-up stiffeners, all other retrofits resulted in a reduction of stress demand.

Based on all models studied, the best retrofit for reduction of hot spot stress around the connection plate-web weld was found to be the stiffened angles-with-backing plate. For a 51 mm [2 in.] crack, stiffening the angles resulted in an additional reduction of over 5% when compared with the performance of the unstiffened retrofit; however, adding stiffeners did not

significantly improve the stress reduction for the flange-to-web weld. In this location, the additional reduction due to added stiffness was less than 2%.

For the angles-with-plate retrofit, changes in thickness impacted the hot spot stress demand at the two fatigue-susceptible welds. At the connection plate-to-web weld for a 51 mm [2 in.] horseshoe-shaped crack, a retrofit thickness of 13 mm [1/2 in.] provided a stress reduction of approximately 51%. Increasing the retrofit thickness to 19 mm [3/4 in.] provided an additional stress reduction of 4%. Similarly for the flange-to-web weld, a thickness of 13 mm [1/2 in.] decreased stresses by 9% while a thickness of 19 mm [3/4 in.] decreased stresses an additional 7%. Based on this data, it is estimated that increasing the angles and plate thicknesses would not continue to provide significant additional reduction in stress—there would be a point in which increasing thickness provides little or no additional benefit.

For the flange-to-web weld, it was found the best performing retrofit was the angles connected with the girder top flange. This retrofit minimized the differential rotation between the girder flange and web, forcing the elements to rotate together rather than separately. This retrofit was also found to perform slightly better than the 19-mm [3/4-in.] thick angles-with-backing plate retrofit for the connection plate-to-web weld. Although this traditional retrofit indicated good performance, these findings must be balanced against the required additional welding and/or deck removal with traffic disruption for field implementation.

CONCLUSIONS

Since many steel bridges built prior to 1985 are in need of repair, it is critical to develop effective retrofit techniques for many different bridge configurations. Finite element simulations can be used to evaluate retrofit effectiveness and can also provide meaningful insight into appropriate retrofit thickness and performance to complement laboratory and/or field implementation. In this study, several retrofits were considered including: full depth back-up stiffeners, angles-with-backing plate (several variations), and angles connected to the top flange. Additionally, the effect of a broken cross frame element and reduced deck stiffness due to cracking were analyzed. The following conclusions were found:

- Hot spot stresses at connection plate-to-web welds and flange-to-web welds decreased or remained constant as horseshoe-shaped crack length was increased in both unretrofitted models and angles-with-plate (19 mm [3/4 in.] thickness) retrofitted models.

- Hot spot stresses at connection plate-to-web welds and flange-to-web welds decreased as longitudinal crack length was increased in both unretrofitted models and angles-with-plate (19 mm [3/4 in.] thickness) retrofitted models. Initiation of a longitudinal crack increased hot spot stresses at the connection plate-to-web weld; therefore, horseshoe-shaped cracking would likely initiate soon after the formation of a longitudinal crack.
- When deck stiffness was halved, hot spot stresses in both the connection plate-to-web weld and flange-to-web weld increased 20%.
- Although the analysis of the cross frame failure did not provide any significant conclusions, changes in bridge response were evident. With the broken north cross frame, the south cross frame and girder did *not* pick up significantly more load in terms of web-gap stresses. In fact, web-gap stresses actually decreased in the top web-gap flange-web weld and the bottom web-gap flange-web weld and connection plate-web weld. In terms of stresses, the only location within the bridge that gathered more load was the north girder bottom web-gap and horizontal cross frame member in the north cross frame.
- Due to the cross frame failure, slight increases in flange rotation and decreases in web rotation were experienced by the north girder. South girder lateral deflections increased due to north cross frame failure while north girder lateral deflection decreased.
- For all crack lengths studied, the order of retrofit effectiveness remained constant. As crack lengths increased, initial hot spot stresses decreased, resulting in less stress reduction due to retrofitting.
- Both hot spot stresses experienced reduction due to retrofitting. Full depth back-up stiffeners provided minimal stress relief in the system due to bridge configuration.
- Retrofit performance listed in order from most reduction to least reduction was found to be as follows for the connection plate-to-web weld: stiffened angles-with-backing plate 19 mm [3/4 in.], angles to top flange 19 mm [3/4 in.], angles-with-backing plate 19 mm [3/4 in.], angles-with-backing plate 13 mm [1/2 in.], and full depth back-up stiffener.
- Retrofit performance listed in order from most reduction to least reduction was found to be as follows for the flange-web weld: angles to top flange 19 mm [3/4 in.], stiffened angles-with-backing plate 19 mm [3/4 in.], angles-with-backing plate 19 mm [3/4 in.], angles-with-backing plate 13 mm [1/2 in.], and full depth back-up stiffener.

- To improve angles-with-backing plate performance, addition of stiffeners to the angles may be a viable option. This may allow for reduction in thickness of angles and backing plate for field implementation.

Although significant modeling efforts have been performed at the University of Kansas in the past, the models and associated physical tests were aimed at girder sub-assemblies. These sub-assemblies only included out-of-plane effects and did not capture longitudinal bending effects.

In the analyses described in this study, a significant effort was placed in determining at appropriate retrofit technique for a 9.1 m [30 ft.] laboratory test bridge. These models were also used to explain bridge and retrofit behavior.

Based on this investigation, effective retrofits (primarily considering angles-with-plate variations) can be chosen for application on the test bridge. As such, the next retrofit selected for test bridge implementation is stiffened angles-with-plate. With laboratory test data to validate results, efforts will then be placed toward field implementation in which the angles-with-plate retrofit will provide an effective and inexpensive technique requiring little-to-no traffic closure.

REFERENCES

Adams, C. (2009). "Finite Element Study on Bridge Details Susceptible to Distortion-Induced Fatigue." Master's Thesis, University of Kansas.

Alemdar, F., Overman, T., Matamoros, A., Bennett, C., and Rolfe, S. (2013a). "Repairing Distortion-Induced Fatigue Cracks in Steel Bridge Girders using Angles-with-Plate Retrofit Technique, Part I: Physical Simulations." *Journal of Structural Engineering*, ASCE, In Press.

Alemdar, F., Nagati, D., Matamoros, A., Bennett, C., and Rolfe, S. (2013b). "Repairing Distortion-Induced Fatigue Cracks in Steel Bridge Girders using Angles-with-Plate Retrofit Technique, Part II: Computer Simulations." *Journal of Structural Engineering*, ASCE, In Press.

Hartman, A., Hassel, H., Adams, C., Bennett, C., Matamoros, A., and Rolfe, S. (2010). "Effects of Cross-Frame Placement and Skew on Distortion-Induced Fatigue in Steel Bridges." TRB: Journal of the Transportation Research Board. 2200 (1). 62-68.

Hassel, H., Hartman, A., Bennett, C., Matamoros, A., and Rolfe, S. (2010). "Distortion-Induced Fatigue in Steel Bridges: Causes, Parameters, and Fixes." *2010 ASCE/SEI Structures Congress Proceedings*. 471-483.

Nagati, D. (2012). "Repair of Steel Bridge Girders Damaged by Distortion-Induced Fatigue." Master's Thesis, University of Kansas.

Przywara, J. (2013). "Applications of the Extended Finite Element Method (XFEM) for the Analysis of Distortion-Induced Fatigue Cracking in Highway Bridge Girders." Master's Thesis, University of Kansas.

Richardson, T. (2012). "Analytical Investigation of Repair Methods for Fatigue Cracks in Steel Bridges." Master's Thesis, University of Kansas.

Part 5

INNOVATIVE RETROFIT TECHNIQUE FOR DISTORTION-INDUCED FATIGUE CRACKS IN STEEL GIRDER WEB GAPS

Amanda Hartman

Graduate Research Assistant, University of Kansas, CEAE Dept., 1530 W. 15th St., Lawrence, KS 66045, ahartman@ku.edu

Caroline Bennett

Associate Professor, University of Kansas, CEAE Dept., 1530 W. 15th St., Lawrence, KS 66045, crb@ku.edu

Adolfo Matamoros

Professor, University of Kansas, CEAE Dept., 1530 W. 15th St., Lawrence, KS 66045, abm@ku.edu

Stan Rolfe

A.P. Learned Distinguished Professor, University of Kansas, CEAE Dept., 1530 W. 15th St., Lawrence, KS 66045, srolfe@ku.edu

ABSTRACT**:** Cracking in web gaps of steel girder bridges is often difficult and expensive to repair, especially at the top web gap. A commonly-used retrofit technique involves creating new load path between a transverse connection plate and the top flange of the girder, by means of bolted angles on both sides of the transverse connection plate. This technique often requires removing portions of the bridge deck to create the bolted connection at the top flange, which is an approach that can incur significant expense and inconvenience to the traveling public. This study was aimed at evaluating the effectiveness of a newly-developed retrofit technique, in which connection is made between the transverse connection plate and the girder web, through use of bolted angles on both sides of the transverse connection plate and a backing plate on the opposing face of the girder web. The retrofit was evaluated through extensive structural testing and finite element modeling. Testing was performed on a 9.1-m [30-ft] long test bridge system, comprised of three 910-mm [36-in.] deep girders and a concrete deck. The system was loaded to produce distortion-induced fatigue cracking, and then the bridge was retrofitted with the newly-developed stiffener-to-web repair technique. Results of the testing were compared to findings from finite element analyses, as well as findings from structural tests performed on 2.7-m [9-ft.] long segments of similar girders tested under distortion-induced fatigue. Results have indicated that the newly-developed retrofit technique has significant potential for effectively controlling

distortion-induced fatigue cracking in web gaps of steel girder bridges without requiring disruption to the concrete deck.

1. INTRODUCTION

1.1 DISTORTION-INDUCED FATIGUE

Fatigue cracking due to distortion-induced fatigue is a significant problem faced by state departments of transportations, and is common in steel bridges built prior to the mid-1980s. As adjacent girders experience differential deflection under traffic loading, cross-frames carry secondary forces and impose stresses and deformations at the connection details. In many steel bridges constructed prior to the mid-1980s there exists a lack of connection between transverse connection plates and the adjacent flange. This detailing practice, which has since been eliminated, resulted in the presence of a web gap – a highly flexible, short length of web bounded at one end by the transverse connection plate and at the other by the girder flange. After cross-frame members transfer forces through the connection plate, the load path is such that out-of-plane forces must be transferred through the web gap region to the relatively laterally-stiff flange, and if the web gap is at the top flange, into the bridge deck (Fig. 1). Connor & Fisher (2006) have estimated that 90% of fatigue cracking in steel bridges is due to secondary stresses.

A commonly-used retrofit to repair distortion-induced fatigue is to provide attachment between transverse connection plates and flanges (Fisher et al. 1990) through use of connecting elements, such as angles. For the case in which the girder top flange is attached to a concrete deck, additional challenges must be faced to provide this attachment. Two angles can be used to provide positive connection; however, bolting the top leg of the angle to the flange often requires disturbance of the concrete deck, which is an expensive undertaking and can cause traffic disruption.

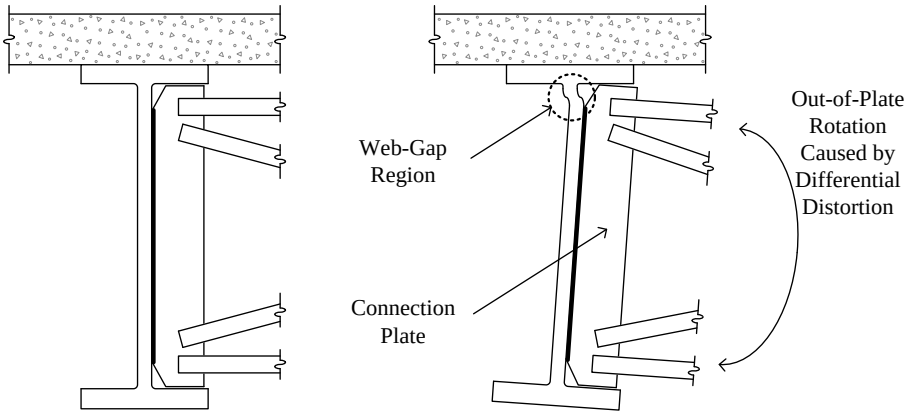

Figure 1: Schematic showing distortion-induced fatigue.

1.2 ANGLES-WITH-BACKING PLATE REPAIR

An extensive study has been performed at the University of Kansas, in which a new retrofit for distortion-induced fatigue was developed with the aim of eliminating the need for disturbing the concrete deck. This new retrofit involves using two segments of steel angle and a steel plate. The angles each are bolted to the transverse connection plate and the web of the steel girder (one angle on each face of the transverse connection plate); the steel plate, which is referred to as a "backing plate," is bolted to the opposite side of the web. This retrofit technique has been referred to as the "angles-with-backing plate" repair technique throughout this paper.

The advantage to this technique over the existing repair technique that connects the transverse connection plate to the adjacent flange is that the angles-with-backing plate repair does not require access to the top flange. Thus, this repair can be implemented completely from underneath a bridge without requiring lane closures or interferences with the concrete deck.

The angles-with-backing plate repair technique was developed for the case in which there is no stiffener on the opposite face of the web, which would often be the case in an exterior bridge girder or in a skewed bridge which utilizes cross-frames placed in a staggered layout. However, it is anticipated that the repair could be easily modified for cases in which there are stiffeners present on both sides of the web by using four steel angles rather than two angles and a plate.

2. OBJECTIVE & SCOPE

The primary objective of this study was to evaluate, both analytically and experimentally, the effectiveness of a new retrofit technique for steel bridges experiencing distortion-induced fatigue.

The effectiveness of the angles-with-backing plate repair technique has been investigated through a series of structural tests on component-level scaled girders, structural tests performed on a scaled bridge system, and a suite of finite element models. The performance of the retrofit is discussed in this paper, as examined through those three means.

3. COMPONENT-LEVEL TESTING

A series of structural tests aimed at exploring the performance of the angles-with-backing plate retrofit have been performed on 2.8-m [9-ft.] long girder segments. The retrofit applied to this type of girder specimen can be seen in Figure 2, and consisted of two angles, L152x152x19 mm [L6x6x3/4 in], providing a connection between the transverse connection plate and girder web with a backing plate, 457x457x19 mm [18x8x3/4 in], on the other girder face to distribute out-of-plane forces over a larger web area. Two specimens (Specimen 2 and Specimen 3) were tested with this retrofit in the laboratory, and a total of seven angles-with-backing plate retrofitted tests were performed on those two specimens. These tests are described in detail in Nagati (2012). It should be noted that in all trials, the retrofit was applied over sharp cracks without drilled crack-arrest holes; this was to ensure a demanding test procedure. A cumulative series of computational simulations were performed to augment the component-level testing; these are described in detail in Overman (2012) and Richardson et al. (2012).

The test set-up was such that the girder was flipped upside-down, with the top flange restrained against the strong floor. The fixity to the concrete strong floor was intended to capture the lateral restraint provided by the concrete deck in a real bridge system, although this is readily admitted to be a "boundary" scenario. Since the entire top flange was fixed to a strong floor, longitudinal bending of the girder segment was not permitted in this test set-up. Out-of-plane forces were induced by pulling upward on the cross-frame with a MTS 244.41 490 kN [110-kip] servo-controlled actuator, simulating downward adjacent girder deflection in a real bridge.

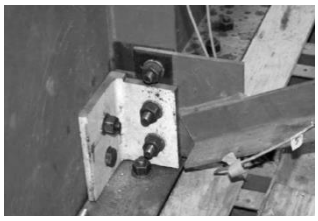

(b)

(a) **(c)**

Figure 2: New retrofit technique applied to component girder, where (a) displays the overall test set-up, (b) displays the angles on the cross-frame side (Overman 2012) and (c) displays the backing plate on the fascia side (Overman 2012).

Cracking observed in tests performed on the 2.7-m [9-ft] girder segments included two primary types: cracks at the flange-to-web weld and at the transverse connection plate-web weld. Transverse connection plate-web weld cracks consisted of vertical cracking along the weld toe and horizontal/spider cracking progressing into the web (referred to as "horseshoe" and "spider" crack types in Figures 3 and 4). Little crack growth was observed under the retrofit when the set-up was cycled between 3.6 kN [0.8 kip] and 20 kN [4.6 kip]. Each retrofit trial was loaded for 1.2 million cycles and no crack-arrest holes were drilled at crack tips underneath retrofits. Short periods of crack growth were permitted between test trials by removing the retrofit from the test. Therefore, the effectiveness of the angles-with-backing plate repair was tested over various crack lengths. Crack growth data for Specimen 3 has been presented in Figures 3 and 4.

Unlabeled regions in Figures 3 and 4 denote periods during testing in which the girder specimen was unretrofitted and cracks freely propagated. When the angles-with-backing plate retrofit was applied to the web gap near the artificial deck boundary condition, crack growth was halted under cyclic loading. Referring to the labels in Figures 3 and 4, Retrofit 1 was applied when the horizontal flange-to-web weld crack reached a length of 5 cm [2 in.]. After Retrofit 1 was loaded to 1.2 million cycles, cracks were allowed to grow in the unretrofitted condition until

the horizontal flange-web-weld crack length reached a length equal to 10 cm [4 in.]. Again the retrofit was applied and was loaded to 1.2 million cycles. This process was repeated for crack lengths of 15 cm [6 in.] and 20 cm [8 in.].

During the period of crack growth between applications of Retrofits 2 and 3, cracking also initiated in the other web gap of Specimen 3 at the free flange; however, this crack remained a constant length through remainder of testing and was not retrofitted.

Although crack propagation and retrofit performance is shown for Specimen 3, retrofitting performed comparably for Specimen 2, which is discussed in detail in Nagati (2012).

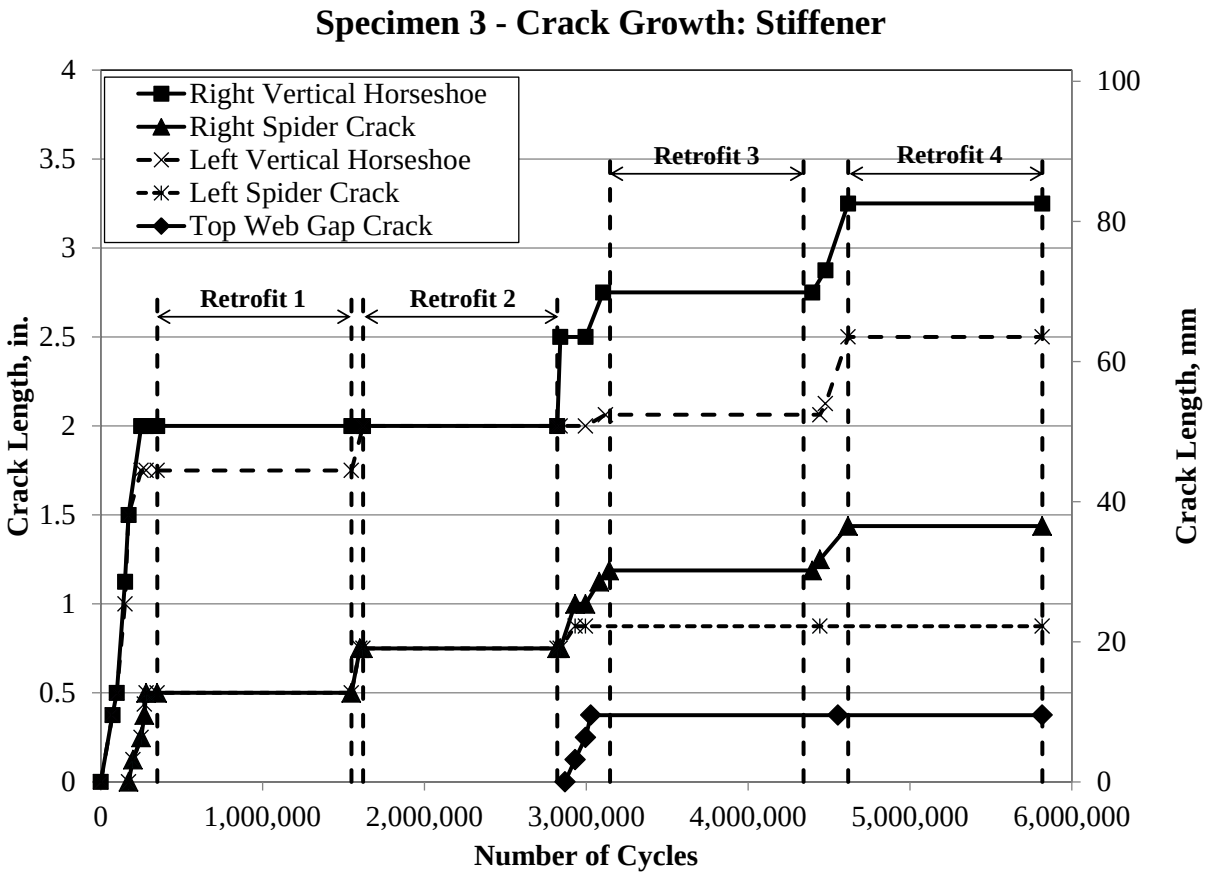

Figure 3: Crack growth plot for Specimen 3 – transverse connection plate-to-web crack (Nagati 2012).

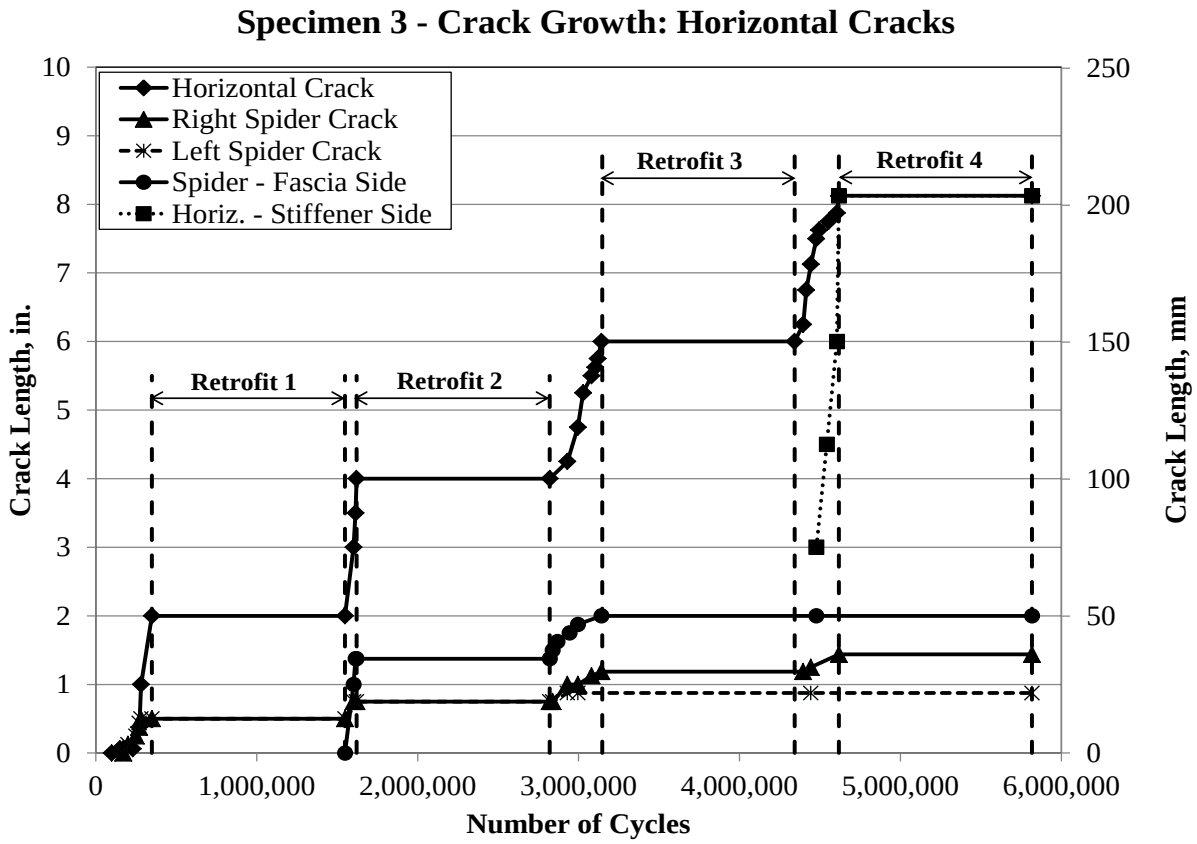

Figure 4: Crack growth plot for Specimen 3 – horizontal web-to-flange crack (Nagati 2012).

4. SCALED BRIDGE SYSTEM TESTING

A series of structural tests aimed at exploring the performance of the angles-with-backing plate retrofit were also performed using a scaled bridge test set-up. The test bridge included three 9.1-m [30-ft.] long girders spaced at 1.5 m [5 ft], with X-type cross-frames provided at supports and at midspan (Figure 5 (a)). Each girder was supported on a roller-type bearing to minimize the potential for axial forces to develop in the girders. Girder length and spacing were primarily dictated by laboratory constraints. The clear span for each girder between roller supports was 8.7 m [28.5 ft]. The girder cross-sections and the concrete deck were dimensioned to be half-scale of a typical highway overpass structure. Specifically, the cross-section dimensions were scaled from those presented in AISI Example 1: Simple-Span Composite I Girder (AISI 1997); dimensions of the test girders have been presented in Figure 5 (b) and (c).

Each of the three test girders was comprised of three segments connected with full moment splices. Since the details being tested were located at midspan, it was considered

desirable to be able to remove the interior third of each girder to allow for replacement of those girder segments after cracking became severe. The test trials described within this paper all focus on trials performed on one bridge set-up; in other words, the interior segments of the test girders were unchanged throughout this testing protocol.

The test bridge included a concrete deck that was fabricated at the KU Structures Laboratory. Five deck panels were cast and cured, and were fabricated with regularly-spaced voids in the deck to allow the deck to be bolted directly to the top flanges of the steel girders. After the concrete deck panels were bolted to the steel girders, the voids were filled with grout to allow the bolts to transfer the horizontal shear demands between the girders and deck.

Loads were applied to the bridge system at midspan, centered over the interior girder. Cyclic loading was delivered by a MTS 201.70 actuator (1470 kN [330 kips] capacity in compression) powered by MTS 505.90 90 GPM pump and controlled with a MTS FlexTest II CTC Controller. A steel plate was centered on the bridge deck, and was grouted in place under the footprint of the actuator. The purpose of the steel plate was to distribute the concentrated compressive force delivered by the actuator. The location of the actuator is shown in the schematics in Figure 5 (b) and (c). Loading was applied at rates varying between 1.5 – 2.0 Hz, depending on the load range being applied.

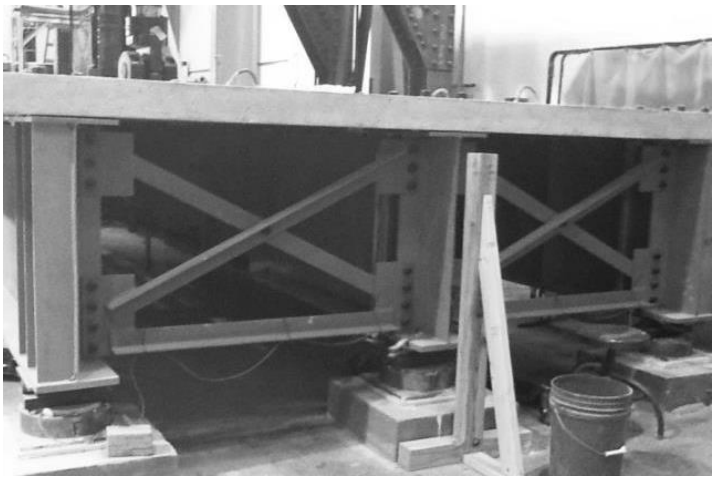

(a)

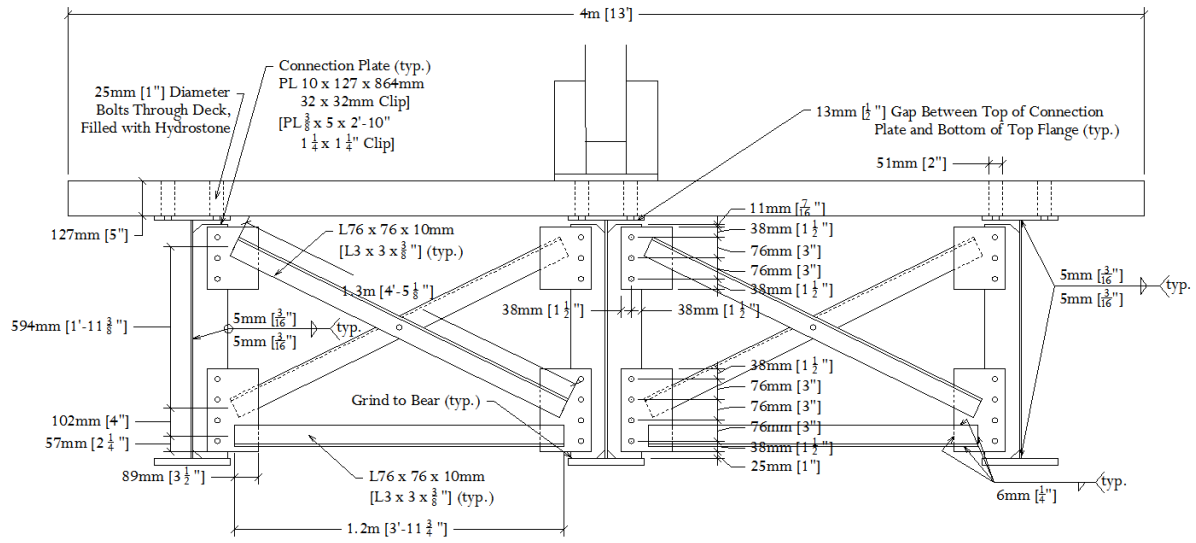

(b)

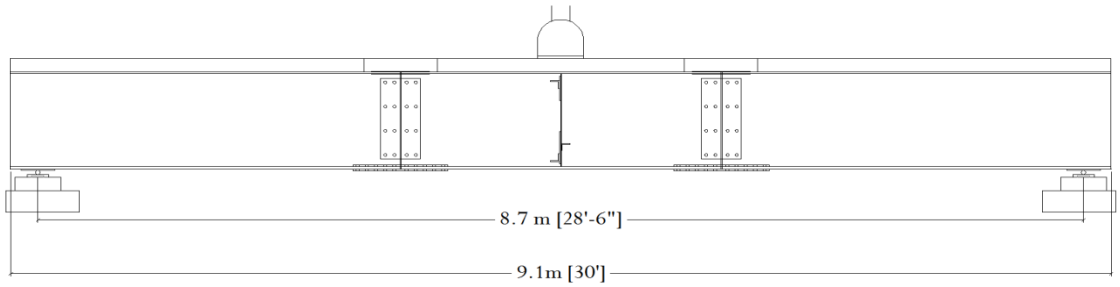

(c)

Figure 5: (a) Photograph of the test bridge supported on load cells, (b) schematic of the bridge cross-section, and (c) girder elevation.

Several forms of instrumentation were used to monitor the test bridge response. Load cells were manufactured and placed at each of the girder ends to measure load distribution. Reusable strain transducers manufactured by Bridge Diagnostics Inc. (BDI) were used to measure bending strains in each girder. Two BDI strain transducers were placed on each girder, one near the top flange and one near the bottom flange. Displacements were monitored using linear voltage displacement transducers (LVDTs) and string potentiometers. Initially, nine LVDTs were used to measure vertical girder displacements and lateral displacements of exterior girders. LVDTs monitoring lateral displacement were positioned at three girder heights—one at the top web gap region, one near mid height, and one at the bottom flange. After Trial 2 (first retrofit application), the six LVDTs on the exterior girders were replaced with eight string potentiometers. Each girder was then monitored with four string potentiometers—one at the top

flange, one below the top web gap, one above the bottom web gap, and one at the bottom flange. Strains in the web gap region were monitored using bondable strain gages (Micro-Measurements WK-06-250BG-350 gages); gage placements can be seen in Figure 6.

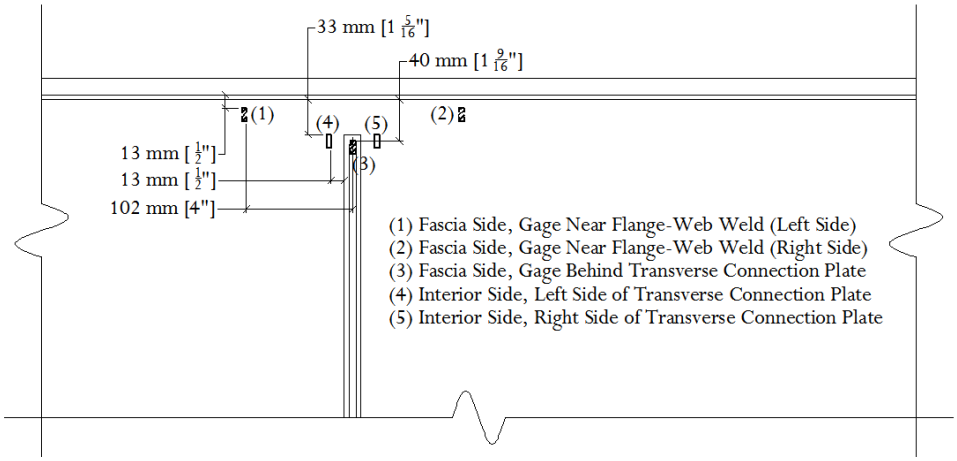

Figure 6: Bondable strain gage placements in web gap region.

A total of five test trials were conducted on the scaled bridge system, as summarized in Table 1. Trial 1 was aimed at initiating cracking in the bridge while in the unretrofitted condition. At 20,000 cycles, cracking initiated at the juncture of the transverse connection plate-to-web weld and transverse connection plate clip in the north exterior girder. After an additional 10,000 cycles, south girder cracking initiated in the same location as seen in the north girder. Once cracking initiated in the south exterior girder, nearly all crack propagation in the north girder halted. Since cracking in the south girder was more significant, only crack growth for the south girder is discussed herein.

Table 1: Test matrix for the scaled bridge system set-up

Test Trial	Description	Number of cycles for each test trial	Target Load Range *kN [kips]*
Trial 1	Bare Specimen; test bridge cycled in unretrofitted condition to develop cracking	150,000	267 – 270 [6 – 60]
Trial 2	Angles-with-backing plate retrofit applied to exterior girders of test bridge	1,200,000	27 – 270 [6 – 60]
Trial 3	Angles-with-backing plate retrofit applied to exterior girders of test bridge	1,200,000	36 – 360 [8 – 80]
Trial 4	Angles-with-backing plate retrofit applied with 6-mm [1/4-in.] crack-arrest holes to exterior girders of test bridge	1,061,097	45 – 450 [10 – 100]
Trial 5	Angles-with-backing plate retrofit applied with 13-mm [1/2-in.] crack-arrest holes to exterior girders of test bridge	1,200,000	45 – 450 [10 – 100]
		Sum = 4,811,097	

After initiation, cracks propagated diagonally downward through the stiffener-web weld toward the weld toe on the web. Once cracks propagated into the web, cracking followed two paths. First cracks progressed vertically down the weld toe. Next, secondary branching cracks (referred to as spider cracks) developed and propagated into the web. As the spider cracks developed and propagated, they progressed through the web thickness and developed as through-cracks on the fascia side of the girder.

Trial 2 involved the first application of the angles-with-backing plate retrofit to the bridge. The retrofit was applied to both the north and south exterior girders once one leg of the transverse connection plate-to-web weld crack reached a length of 25 mm [1 in.]. The geometry of the angles-with-backing plate retrofit was only slightly different for application on the scaled bridge system than it was when applied on the component-level test set-up. This retrofit consisted of two angles, L152x152x19 mm [L6x6x3/4 in] that were 178-mm [7-in.] long, and a backing plate with dimensions of 457x457x19 mm [18x8x3/4 in.]. Two A325 19-mm [3/4-in.] diameter structural bolts were used to connect the angles with the transverse connection plate and an additional four bolts provided attachment between the angles and backing plate and the web. All bolts were installed fully-tensioned using direct tension indicator washers. Figure 7 presents

the geometry of the retrofit installed on the scaled bridge test set-up. Figure 7 (a) and (b) show the angle geometry used on both sides of the interior transverse connection plate, while (c) shows the backing plate geometry used on the fascia side of the girder.

In Trial 3, the same retrofit was applied to the bridge; however, the load range was increased from 27 – 270 kN [6 – 60 kips] to 36 – 360 kN [8 – 80 kips] to produce a more demanding test of the retrofit's effectiveness.

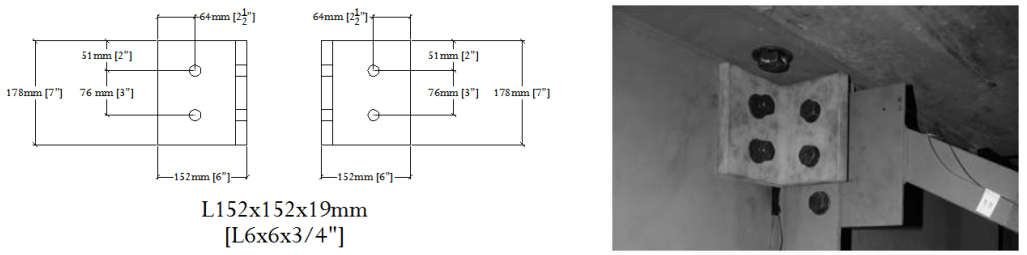

(a)

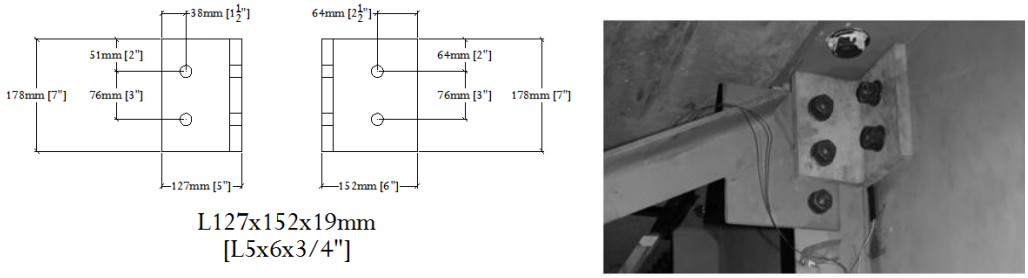

(b)

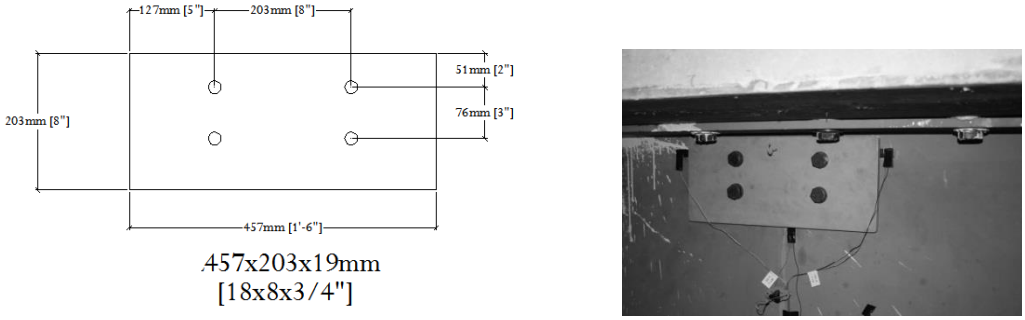

(c)

Figure 7: Angles-with-backing plate retrofit applied to the scaled bridge test set-up: (a)L152x152x19 [L6x6x3/4]; (b) L127x152x19 [L5x6x3/4]; (c) PL 457x203x19 mm [PL18x8x3/4]

During Trials 2 and 3, crack growth was significantly slowed but not halted. Crack length vs. number of fatigue cycles has been reported in Figure 8. The cracks grew less than 10 mm [3/8 in.] over 1,200,000 cycles.

At the outset of Trial 4, 6-mm [1/4-in.] diameter crack-arrest holes were drilled at the crack tips. New crack lengths were defined as the total crack length plus the diameters of the crack-arrest holes. Because of this, Figure 8 displays an instantaneous jump in crack length when crack stop holes were drilled at the start of Trial 4.

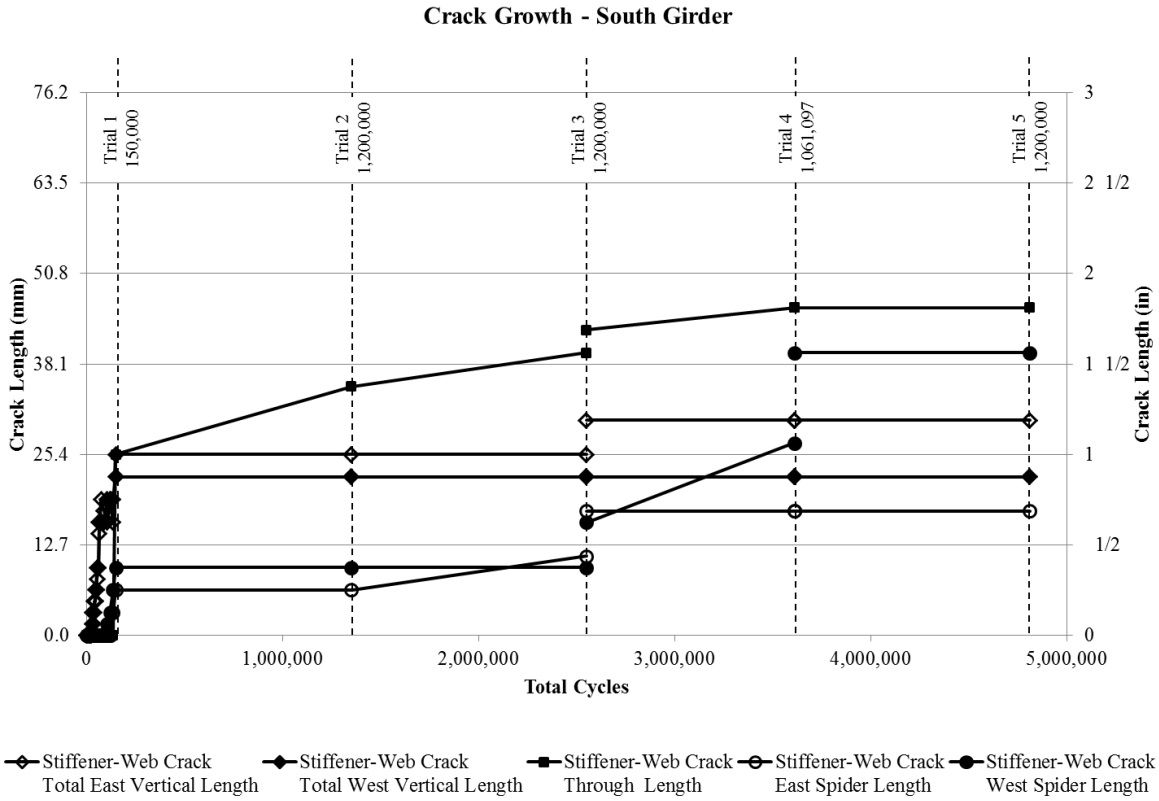

Figure 8: South girder crack growth.

The test bridge exhibited different behavior during Trial 4 while in the retrofitted condition. Approximately 650,000 cycles after the start of Trial 4, a faint clicking noise was noticed coming from the transverse connection plate in the north girder. After inspection, no change in bridge response was observed. While under inspection at 1.06 million cycles, the cross-frame between the north and middle girders was found to be cracked through as seen in

Figure 9. It is estimated that the crack started at the bottom corner of the weld toe where the angle frames into the plate.

Once the north girder cross-frame was no longer properly attached, a significant shift in loading occurred. Two cracks experienced growth during Trial 4, in which cracks reinitiated through the 6-mm [1/4-in.] diameter crack-arrest holes. This crack growth was thought to be caused, at least in part, by the failure of the north cross-frame which increased load distribution to the south girder. It was decided to drill a 13-mm [1/2-in.] diameter crack-arrest hole at the tips of those cracks which had exhibited propensity for propagation. Therefore, another instantaneous jump in crack length can be seen at the end of Trial 4 in Figure 8. Since Trial 4 did not reach 1.2 million cycles due to the cross-frame failure, Trial 5 utilized identical loading with a new, larger crack-arrest hole where growth occurred in Trial 4. No further crack growth was seen at the end of Trial 5.

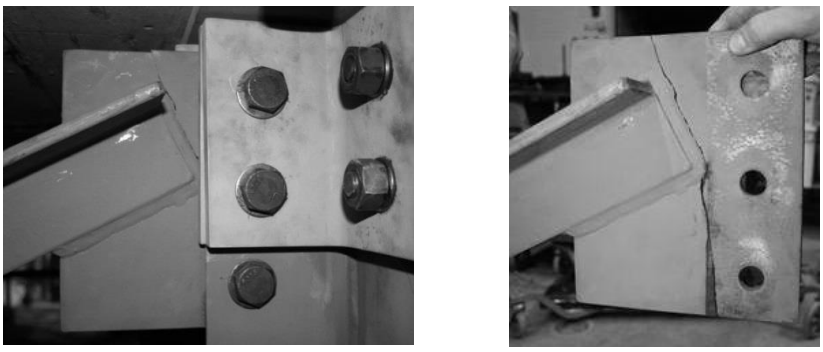

(a) **(b)**

Figure 9: North cross-frame failure: (a) View of cracked tab plate in the cross-frame assembly while the retrofit is in place on the bridge test set-up; (b) View of cracked tab plate in the cross-frame assembly after removal from the bridge test set-up.

5. COMPARISON OF RETROFIT PERFORMANCE BETWEEN COMPONENT-LEVEL AND SCALED BRIDGE TESTS

The angles-with-backing plate retrofit was found to perform well in both component-level and scaled bridge experimental tests. The component-level tests were a less expensive manner in which the retrofit variations were tested for proof-of-concept prior to application on the scaled bridge test set-up. For both component-level and scaled bridge testing, similar crack initiation

and propagation patterns occurred around the transverse connection plate-web weld. However, an important difference between the two set-ups was that a horizontal crack was found to consistently develop at the flange-to-web weld in the component-level tests. This is believed to be due to the fact that the component-level tests were subjected entirely to out-of-plane loading, including no interaction with strong-axis bending. Alternatively, the scaled bridge test set-up which included significant strong-axis bending effects did not produce horizontal web-to-flange cracking. This is an important distinction between the two test set-ups, and it is also important that the retrofit technique was tested in both scenarios. Many actual bridges susceptible to distortion-induced fatigue do not generate cracking at the web-to-flange weld, but many others do. Therefore, it was critical to test the effectiveness of this retrofit in situations that did and did not produce cracking at the web-to-flange weld in addition to the cracking that typically forms at the connection plate-to-web weld.

Despite differences in crack patterns between the two test set-ups, the angles-with-backing plate retrofit was successful in preventing crack propagation in steel bridge girders damaged by distortion-induced fatigue.

6. ANALYTICAL INVESTIGATION

6.1 MODELING METHODOLOGY

A detailed finite element model of the bridge test system was developed using ABAQUS v.6.10. The model was constructed using three-dimensional solid elements with linear-elastic material properties. Concrete was specified to have a modulus of elasticity of 25,000 MPa [3,605 ksi] and Poisson's ratio of 0.2. Material properties specified for steel included a modulus of elasticity of 200,000 MPa [29,000 ksi] and Poisson's ratio of 0.3.

The entire steel and concrete assembly was modeled in ABAQUS primarily using hexahedral (C3D8R) elements with varying mesh densities. Near region of interest, elements were sized as small as 2.5 mm [0.1 in.] while other areas contained element sizes as large as 25 mm [1 in.]. Transitions between these element sizes were made using tetrahedral (C3D4) elements. The element size used in the concrete deck was 64 mm [2-1/2 in.].

Parts, including welds, were built separately and then assembled using surface-to-surface ties. When parts were not welded in the actual scaled bridge test set-up, hard contacts with a

friction coefficient of 0.35 were used in place of ties in the simulations. The overall model geometry has been presented in Figure 10.

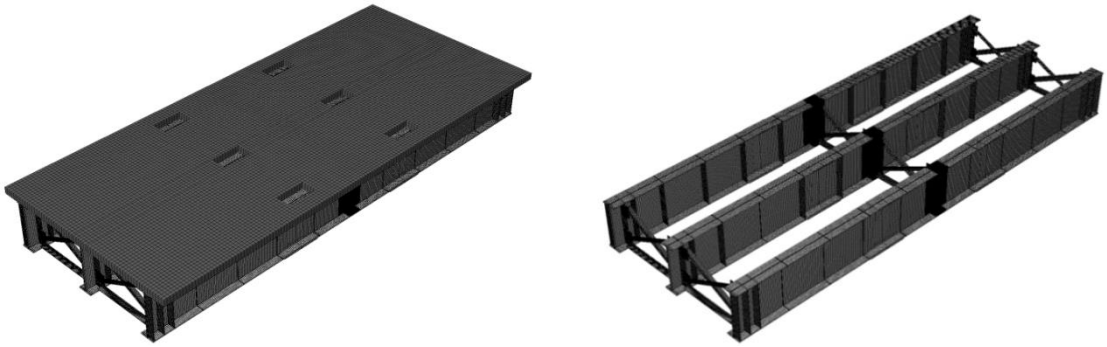

(a) **(b)**

Figure 10: View of finite element model: (a) entire model and (b) model shown without the concrete deck.

Maximum principal stresses were extracted from finite element models using a one-point hot spot stress (HSS) procedure in which stresses of interest were computed at a specific distance (half the web thickness) from a discontinuity as seen in Figure 11. Use of HSS to extract stresses decreases the sensitivity of stresses due to mesh location and size (Adams 2009, Hartman et al. 2010). Additionally, a convergence study was performed for web gap mesh size, leading to the minimum element size of 2.5 mm [0.1 in.] in that region.

As a basis for comparison between simulations, maximum principal stresses were extracted from the finite element models. Component-level testing at KU showed excellent correlation between maximum principal stresses and crack initiation/growth (Nagati 2012).

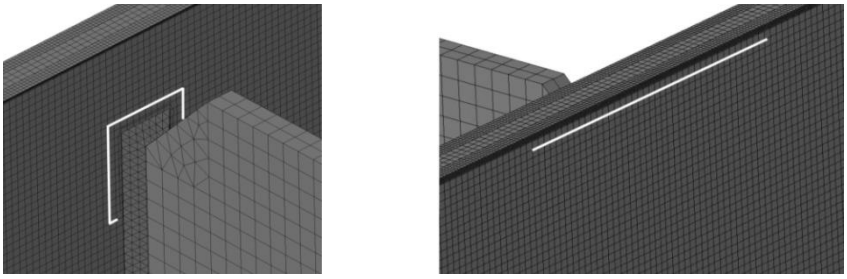

(a) **(b)**

Figure 11: Location of hot spot stress paths (shown in white) for (a) transverse connection plate side and (b) fascia side.

The load applied to the test bridge in the model consisted of a static 270-kN [60-kip] load placed over two areas of 400x114 mm [15-3/4 x 4-1/2 in.] to represent the application of the load through the two "feet" of the actuator's swivel end.

Cracks were modeled using the Extended Finite Element Method (XFEM) in ABAQUS. Using XFEM, cracks of various shapes can be easily modeled without affecting the mesh in the region of interest. Additionally, cracks can be placed anywhere within elements, as opposed to being restricted to placement of cracks at element boundaries. Cracking at the transverse connection plate-to-web weld was modeled by creating a U-shaped crack around the transverse connection plate weld. Cracks were modeled using three-dimensional planar XFEM elements with a depth larger than the girder web thickness of 6 mm [1/4 in.]. When crack lengths are reported herein for the transverse connection plate-to-web weld, the length refers to a single vertical leg of the "U"-shape, not the entire path of the crack.

A limitation to using XFEM is that only two crack tips can exist for one crack. In experimental testing, cracks often branch out into multiple cracks. This branching cannot be modeled using XFEM; however, even though branched cracks exist experimentally, it was found in prior testing that the vertical crack tended to progress while the branch crack growth slowed (Nagati 2012). Due to this, only vertical cracks lengths were modeled. Unretrofitted models contained several crack lengths from 25 mm [1 in.] to 76 mm [3 in.], varied in 13-mm [1/2-in.] increments. All models that included retrofits were created with one crack length, 38 mm [1-1/2 in.], for comparison.

Nine variations were considered in the computational simulations and are presented in Table 2. Two thicknesses were considered for the angles-with-backing plate retrofit: 19 mm [3/4 in.] and 13 mm [1/2 in.]; these are shown pictorially in Figure 12 (a). Angle thickness and backing plate thickness were only varied together, not separately. Figure 12 (b) shows a variation on the angles-with-backing plate technique in which stiffeners were included in the retrofit. This technique is referred to within this paper as the stiffened angles-with-backing plate retrofit. Finally, the repair technique in which angles connect the connection plate to the flange was also modeled (Fig. 12 (c)).

Table 2: Finite element modeling matrix

Model Description / Crack Length	No Crack	25 mm [1 in.]	38 mm [1-1/2 in.]	51 mm [2 in.]	64 mm [2-1/2 in.]	76 mm [3 in.]
Unretrofitted scaled test bridge	X	X	X	X	X	X
Angles-with-backing plate repair with 19-mm [3/4-in.] thicknesses applied to test bridge (Figure 12 (a))			X			
Angles-with-backing plate repair with 13-mm [1/2-in.] thicknesses applied to test bridge (Figure 12 (a))			X			
Stiffened angles-with-backing plate repair with 19-mm [3/4-in.] thicknesses applied to test bridge (Figure 12 (b))			X			
Traditional angles repair connected to flange with 19-mm [3/4-in.] thickness applied to test bridge (Figure 12 (c))			X			

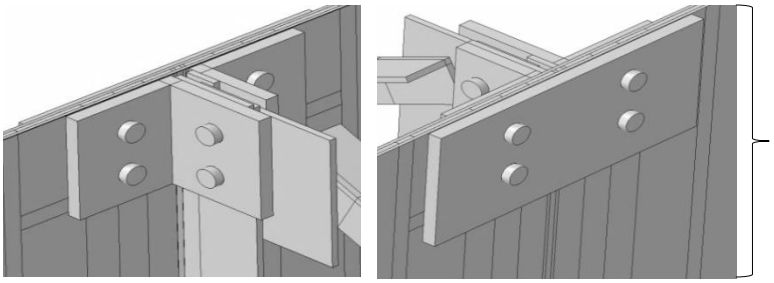

Angles:
L152x152 mm [L6x6 in.]
L127x152 mm [L5x6 in.]

Backing Plate:
457x457 mm [18x8 in.]

(a)

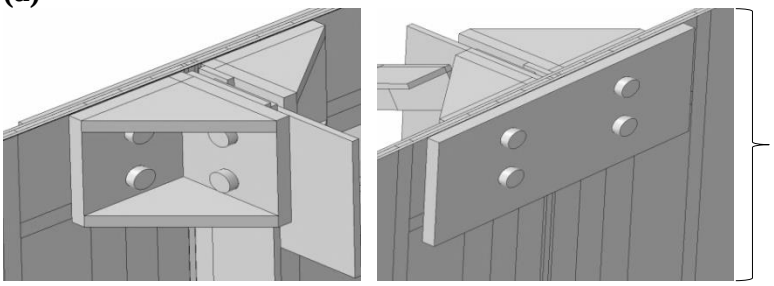

Angles:
L152x152 mm [L6x6 in.]
L127x152 mm [L5x6 in.]

Stiffeners:
133x133 mm [5.25x5.25 in.]
108x133 mm [4.25x5.25 in.]

Backing Plate:
457x457 mm [18x8 in.]

(b)

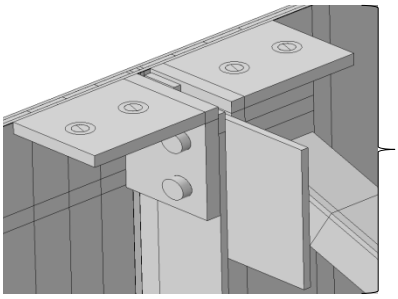

(c)

Figure 12: Views of various retrofits examined in finite element models: (a) Interior and fascia views of the test bridge model with angles-with-backing plate retrofit technique applied; (b) Interior and fascia views of the test bridge model with stiffener angles-with-backing plate retrofit technique applied; (c) Interior view of the test bridge model with retrofit technique in which the transverse connection stiffener is attached to the top flange of the girder with double angles.

6.2 WEB GAP STRAINS

Strains extracted from an uncracked finite element model of the girder specimen were compared with laboratory static strain data prior to cyclic testing, each under 267 kN [60 kip] loading. For comparison between analytical and experimental data, only strains in the vertical direction were extracted from the finite element models since experimental gages placed on the specimen were oriented vertically (capturing vertical strains). This comparison has been presented in Table 3. The computed strains were found to agree well with the measured strains.

Table 3: Experimental (0 Cycles) and analytical strain data for uncracked south girder

	Experimental Data [με]	Analytical Data	Percent Differenc	Absolute Difference in
Fascia Side, Gage Behind Transverse Connection Plate	-839	-858	2.3%	20
Interior Side, Left Side of Transverse Connection Plate	522	447	14.5%	75
Interior Side, Right Side of Transverse Connection Plate	558	458	17.8%	100

An unretrofitted model having a crack length of 25 mm [1 in.] was compared with structural measurements taken at 150,000 cycles, when maximum crack length reached 25 mm

[1 in.]. This comparison has been presented in Table 4. During structural testing, a crack developed behind the fascia side gage near the end of Trial 1, destroying that strain gage; therefore, no data is reported in Table 4 for that gage.

It was found that the percent difference between analytical and experimental data was significantly higher in the cracked configuration. A primary source for this difference is believed to be the crack pattern. Analytically, only vertical cracks were placed in the model and all cracking exists in the web, rather than passing through the weld. Experimentally, cracking begins in the weld but propagates into the web with vertical and spider cracking. Additionally, physical strain gage measurements are an average over the length of the gage, whereas strains are computed at a single finite point in the simulations. This can be a significant factor when examining regions with high strain gradients. Finally, both computed and measured strain magnitudes from the cracked configuration were significantly lower than the magnitudes for the uncracked configurations. The absolute difference in magnitudes between measured and computed values was found to be smaller, on average, for the cracked data than for the uncracked data. Based on these findings, it is believed that an appropriate level of agreement was observed between the computational simulations and the physical measurements.

Table 4: Experimental (150,000 Cycles) and analytical strain data for cracked south girder

	Experimental Data [με]	Analytical Data [με]	Percent Difference	Absolute Difference in
Fascia Side, Gage Behind Transverse Connection Plate	N/A	151	N/A	N/A
Interior Side, Left Side of Transverse Connection Plate	-52	-78	52.2%	26
Interior Side, Right Side of Transverse Connection Plate	-135	-90	33.3%	45

6.3 GIRDER LATERAL DEFLECTIONS

A comparison between measured and computed lateral girder deformations has been presented in Figure 13. It was found that excellent agreement was obtained between the deformation modes.

Lateral deformation behavior can be categorized into three distinct categories, as a function of girder height. The first category defines out-of-plane displacement experienced in the girder top web gap. For the unretrofitted condition, this displacement was found to be fairly large and contained displacement reversal. A highly-linear portion of the graph was located where the transverse connection plate was welded to the girder web. In this region, rotation was constant due to the high stiffness provided by the presence of the transverse connection plate. The last region was defined by rotation of the bottom web gap. As depicted in Figure 13, the amount of out-of-plane displacement experienced in this region was significantly lower than that observed in the top web gap. Small rotations in the bottom web gap may have contributed to the lack of fatigue cracking found experimentally in this region.

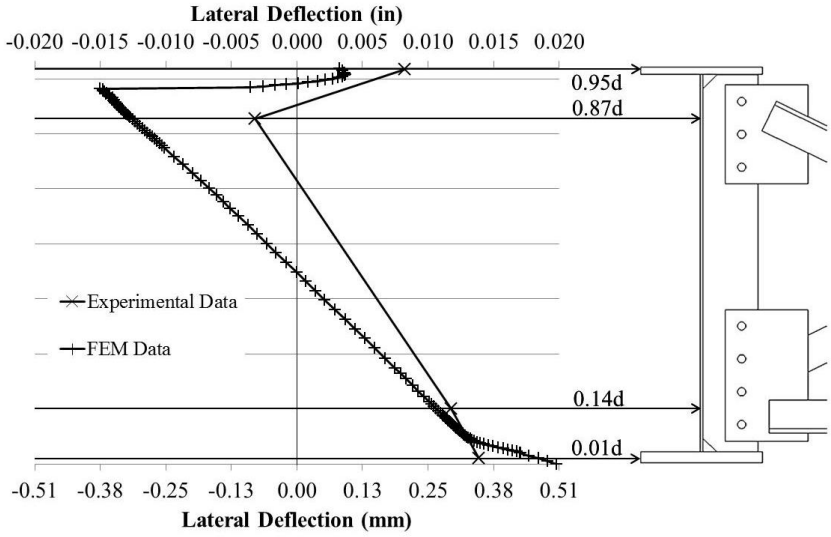

Figure 13:Comparison of lateral deflections obtained from structural test measurements and computational simulations.

6.4 ANALYTICAL RETROFIT COMPARISON

Each finite element model with cracks and/or retrofits was evaluated against the performance of an uncracked, unretrofitted model. Figure 14 shows the percentage of hot spot stress for each condition relative to that of a model of the uncracked, unretrofitted test bridge.

A 25-mm [1-in.] long crack resulted in similar stress magnitudes as was found for an uncracked specimen model. As crack length was increased by 13-mm [1/2-in.] increments,

percent reduction decreased, implying that the stress demand on larger cracks was lower than that for smaller cracks. Cracks 76-mm [3-in.] long experienced only approximately 55% of the stress experienced by a 25-mm [1-in.] long crack.

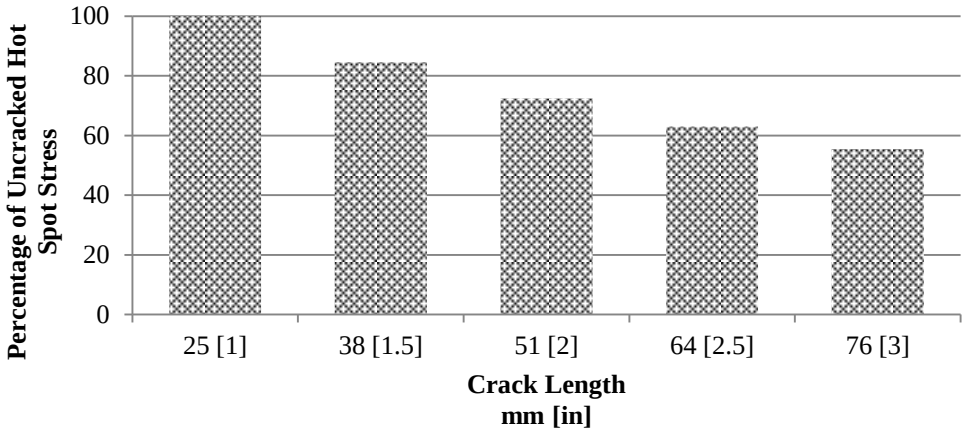

Figure 14: Analytical percent of uncracked HSS for various crack lengths.

A comparison of stress demand has been presented in Figure 15 for models containing a crack length of 38 mm [1-1/2 in.] retrofitted with the various techniques described. The first retrofit considered was the angles-with-backing plate technique, modeled with two different thicknesses for the angles and backing plate. Since the web was 6-mm [1/4-in.] thick, angle and backing plate thicknesses considered were double and triple the web thickness. Increasing angle and plate thickness was found to not significantly improve stress reduction.

The next retrofit considered was the stiffened angles-with-backing plate retrofit, which resulted in an additional stress reduction of approximately 7%. The stiffened angles-with-backing plate retrofit was found to also perform 4% better than the traditional retrofit used in which angles are used to provide positive attachment to the girder flange.

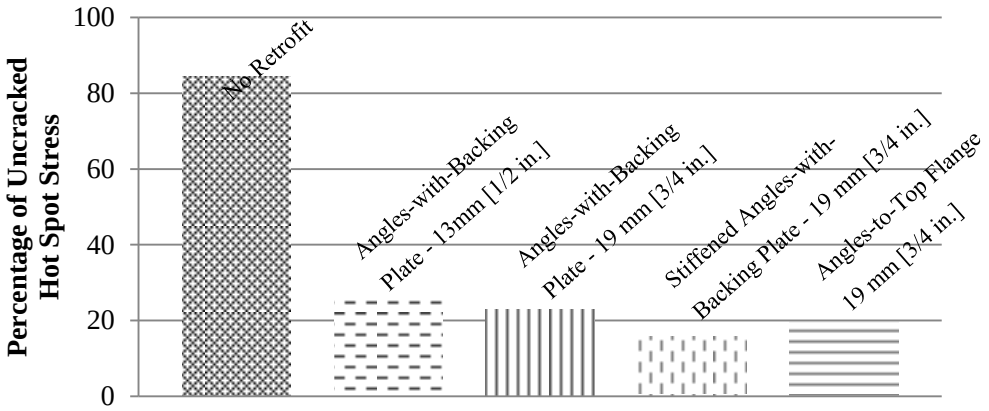

Figure 15: Analytical percent of uncracked HSS for 38 mm [1-1/2 in.] crack under unretrofitted and retrofitted conditions.

7. CONCLUSIONS

A study aimed at evaluating the effectiveness of a new retrofit technique for steel bridges experiencing distortion-induced fatigue was performed. This study was based on evidence collected by performing structural tests on component-level girders and on a scaled bridge system, as well as on complementing analytical studies. This study has resulted in the following conclusions:

- Computational simulations of the scaled bridge test set-up showed good correlation with the experimental testing performed in the scaled bridge test set-up. Vertical strains from modeling of an uncracked specimen were within 20% of experimental strains found using strain gages oriented vertically. Additionally, the mode of lateral deflection was observed to be similar for both the structural test and the simulations. Girder lateral deflections were categorized into three regions including top web gap, transverse connection plate, and bottom web gap. Out-of-plane displacements experienced in the top web gap region were found to be much larger than those found in the bottom web gap region.
- For both structural test set-ups, crack growth under the angles-with-backing plate retrofit was found to be significantly slowed when crack tips remained sharp.
- For the scaled bridge test set-up, crack growth was halted under the angles-with-backing plate retrofit when crack tips were smoothed with small diameter crack-arrest holes.
- Performance of the four retrofits that were considered analytically, presented in order of most effective stress reduction, were found to be as follows:
  1. Stiffened angles-with-backing plate with 19-mm [3/4-in.] thickness,

2. Angles to top flange with 19-mm [3/4-in.] thickness,
3. Angles-with-backing plate with 19-mm [3/4-in.] thickness, and
4. Angles-with-backing plate with 13-mm [1/2-in.] thickness.

- The stiffened angles-with-backing plate with 19-mm [3/4-in.] thicknesses was found to be the most effective retrofit technique examined analytically. The angles-with-backing plate retrofit technique (without stiffeners), examined in two experimental test set-ups and analytically, was found to also be highly effective in repairing distortion-induced fatigue cracking. These techniques have the potential to allow for highly effective retrofitting of distortion-induced fatigue cracks without generating the need for disturbing the bridge deck.

As bridge infrastructure ages, valuable resources will be needed to repair bridges and extend their useful life. There exist several repair techniques for distortion-induced fatigue cracking; however, these repairs can induce significant strain on valuable resources. The angles-with-backing plate retrofit technique developed at the University of Kansas in which two angles in combination with a backing plate provide additional positive connection between a transverse connection plate and girder web has potential for field use.

This new retrofit has been shown to slow crack growth under demanding laboratory testing with sharp crack tips. When combined with small diameter crack-arrest holes, this retrofit has halted crack growth. Since attaching angles to a transverse connection plate and web does not require deck removal, this technique produces a significant time savings and minimizes traffic disruption. All of these factors make this new retrofit technique a viable and valuable option for retrofitting distortion-induced fatigue.

8. REFERENCES

Adams, C. (2009). “Finite Element Study on Bridge Details Susceptible to Distortion-Induced Fatigue.” Master’s Thesis, University of Kansas.

American Iron and Steel Institute (AISI) Example 1: Simple-Span Composite I Girder (1997). *American Iron and Steel Institute.*

Connor, R. and Fisher, J. (2006). “Identifying Effective and Ineffective Retrofits for Distortion Fatigue Cracking in Steel Bridges Using Field Instrumentation.” *Journal of Bridge Engineering,* 11(6), 745-752.

Fisher, J., Jian, J., Wagner, D., and Yen, B. (1990). “Distortion-Induced

Fatigue Cracking in Steel Bridges.” *National Cooperative Highway Research Program Report #336,* Transportation Research Board, National Research Council, Washington, D. C.

Hartman, A., Hassel, H., Adams, C., Bennett, C., Matamoros, A., and Rolfe, S. (2010). “Effects of Cross-Frame Placement and Skew on Distortion-Induced Fatigue in Steel Bridges.” TRB: Journal of the Transportation Research Board. 2200 (1). 62-68.

Nagati, D. (2012). “Repair of Steel Bridge Girders Damaged by Distortion-Induced Fatigue.” Master’s Thesis, University of Kansas.

Overman, T. (2012). “Analytical Investigation of Repair Methods for Fatigue Cracks in Steel Bridges.” Master’s Thesis, University of Kansas.

Richardson, T., Alemdar, F., Bennett, C., Matamoros, A., and Rolfe, S. (2012). "Evaluation of the performance of retrofit measures for distortion-induced fatigue using finite element analysis," *Proc., National Steel Bridge Alliance (NSBA) World Steel Bridge Symposium (WSBS),* NSBA, Chicago, IL.

Appendices

APPENDIX A: TEST SPECIMEN SPECIFICATIONS

GIRDERS

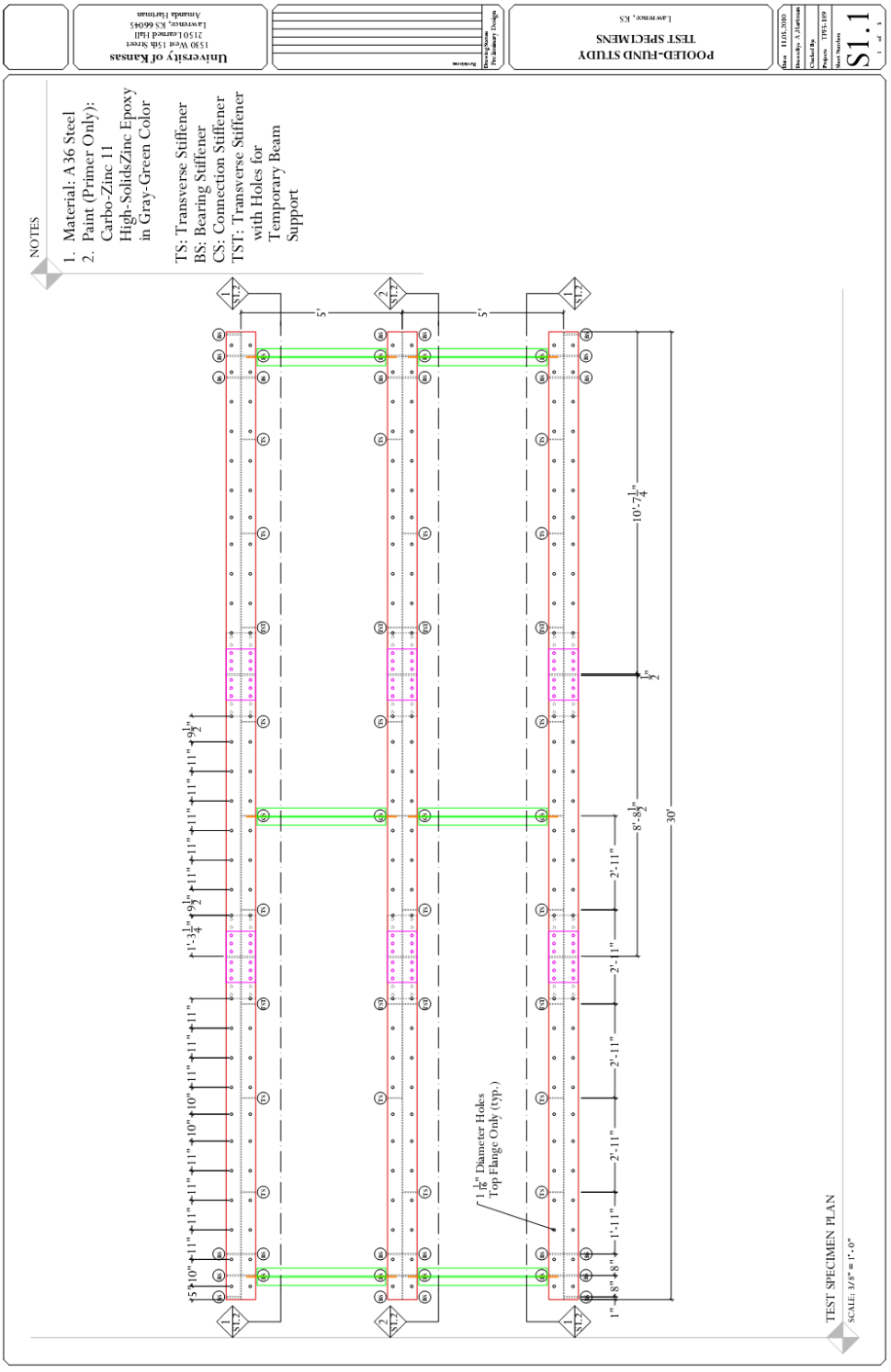

Figure A. 1: Specimen plan.

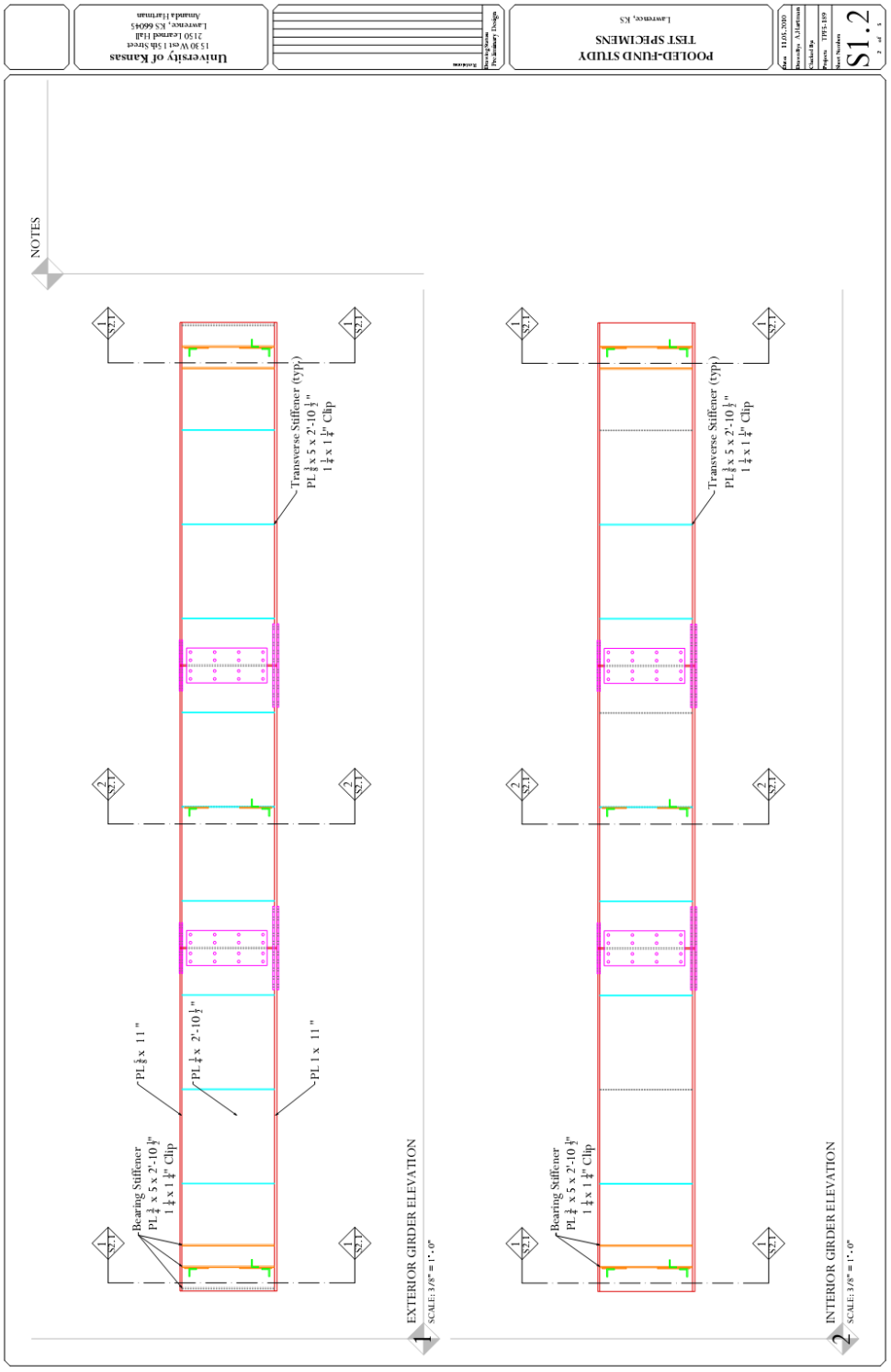

Figure A. 2: Specimen girder elevations.

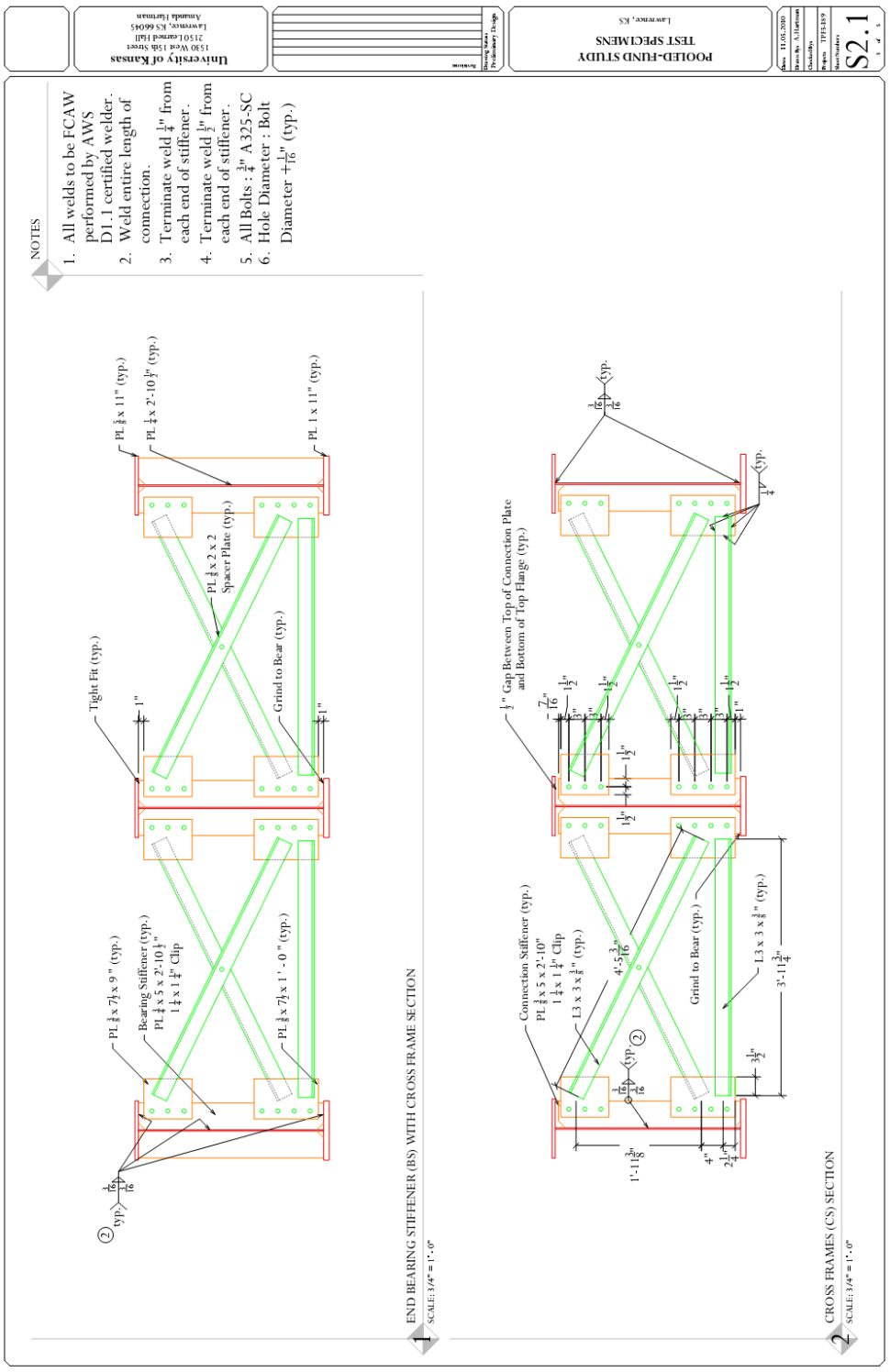

Figure A. 3: Specimen cross frame elevations.

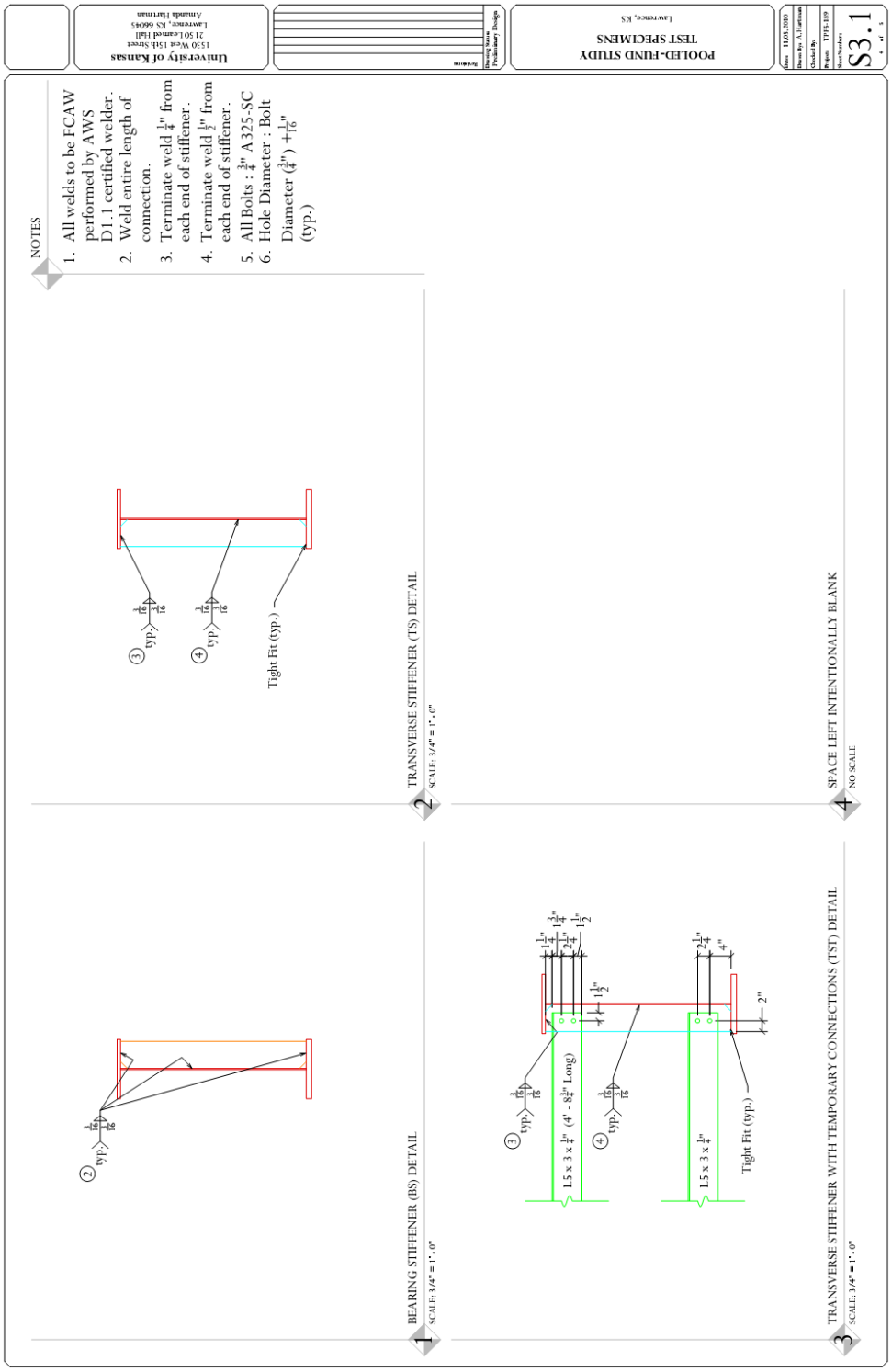

Figure A. 4: Specimen stiffener details.

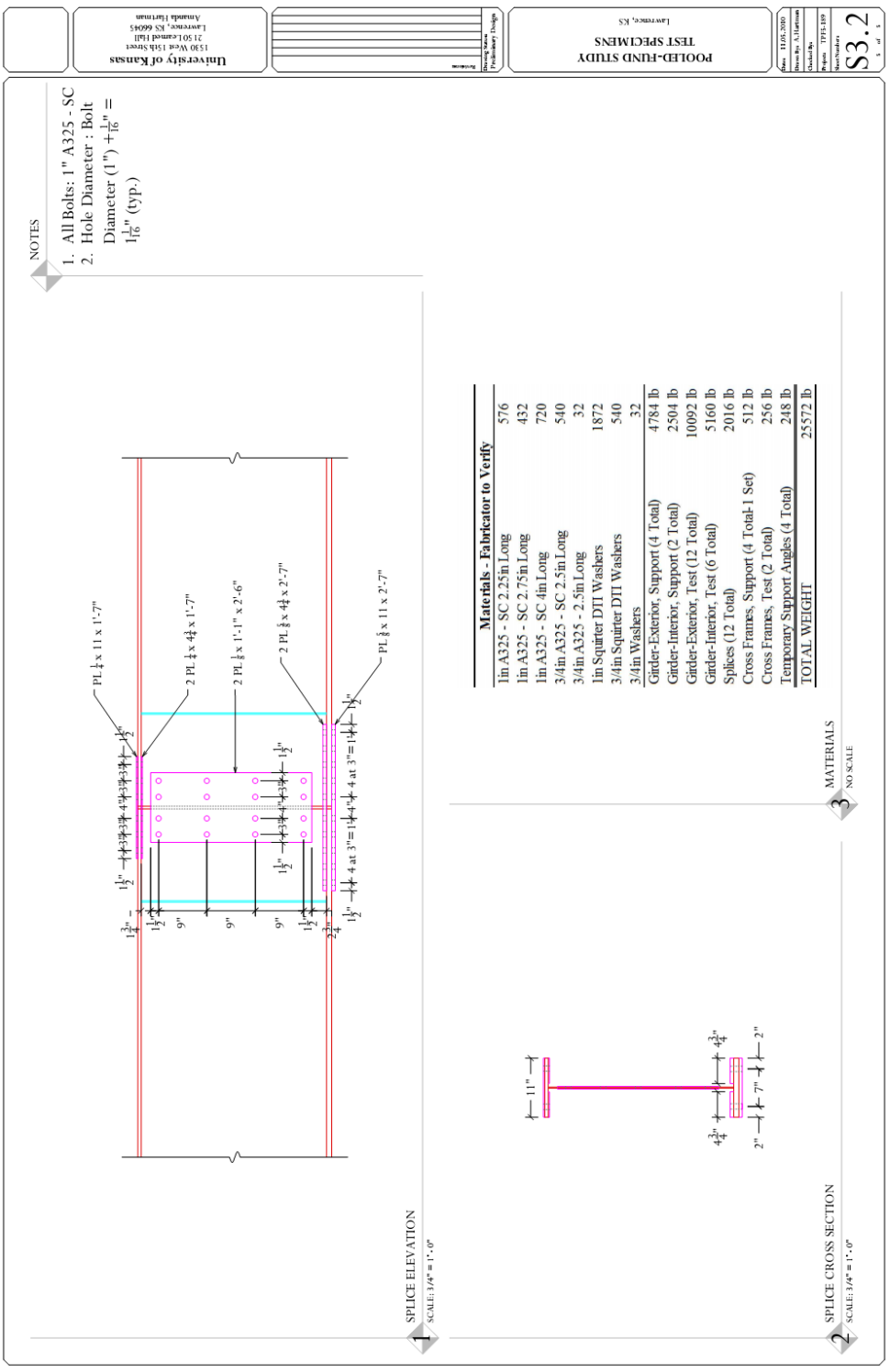

Figure A. 5: Specimen splice details.

RETROFIT

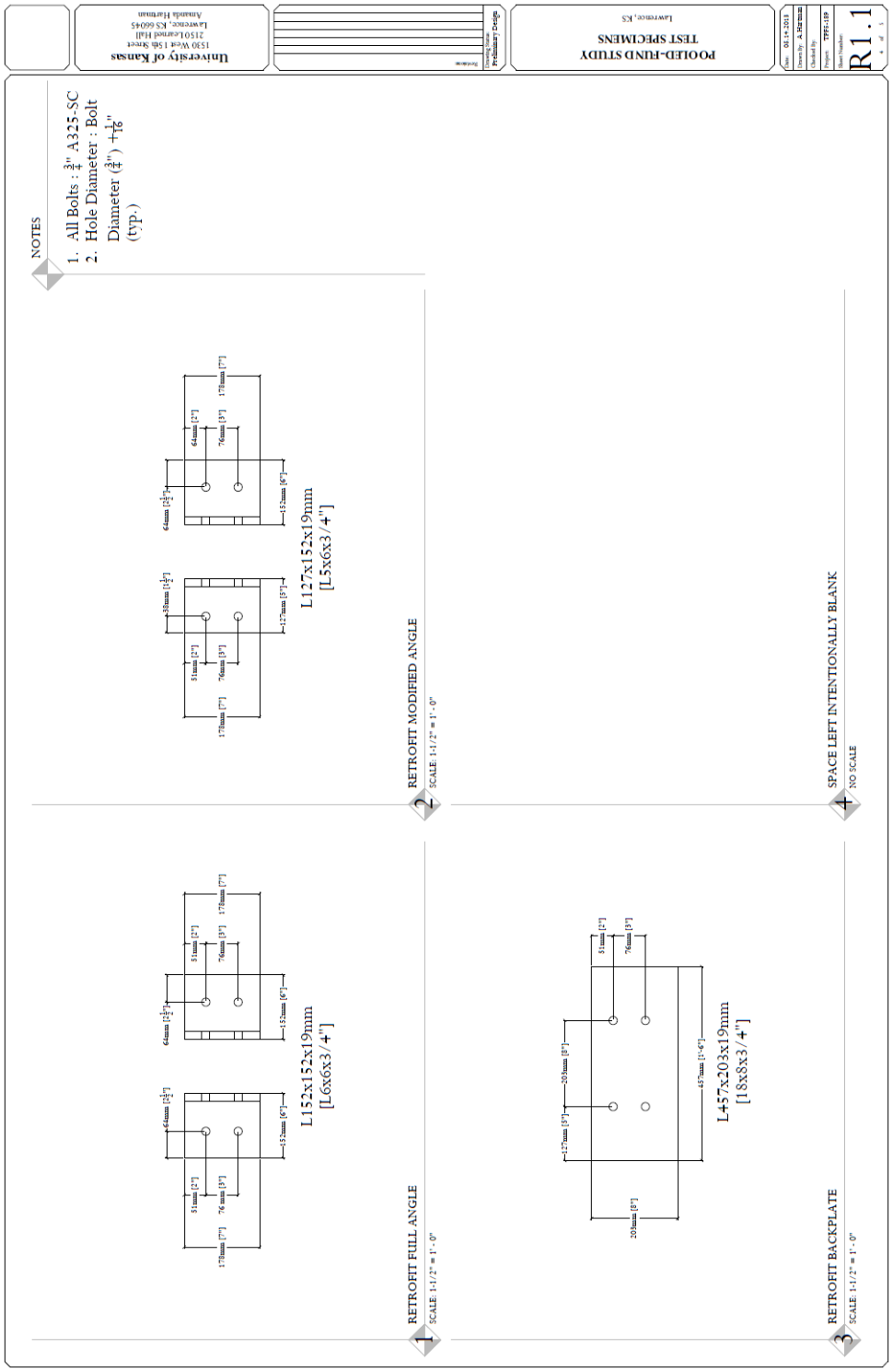

Figure A. 6: ¾ in. Retrofit Dimensions.

LOAD CELLS

Load cells were designed by Daniel Nagati. All information on load cells can be found in his master's thesis (Nagati 2012).

CONCRETE DECK

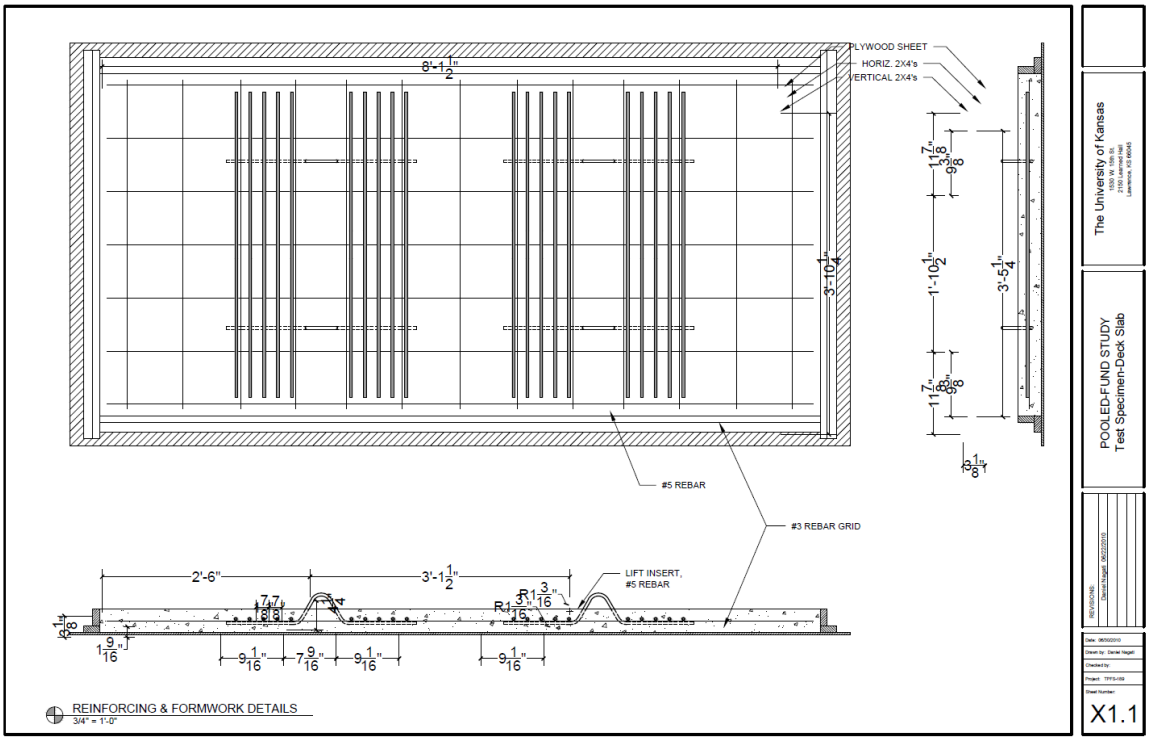

Figure A. 7: Deck reinforcement.

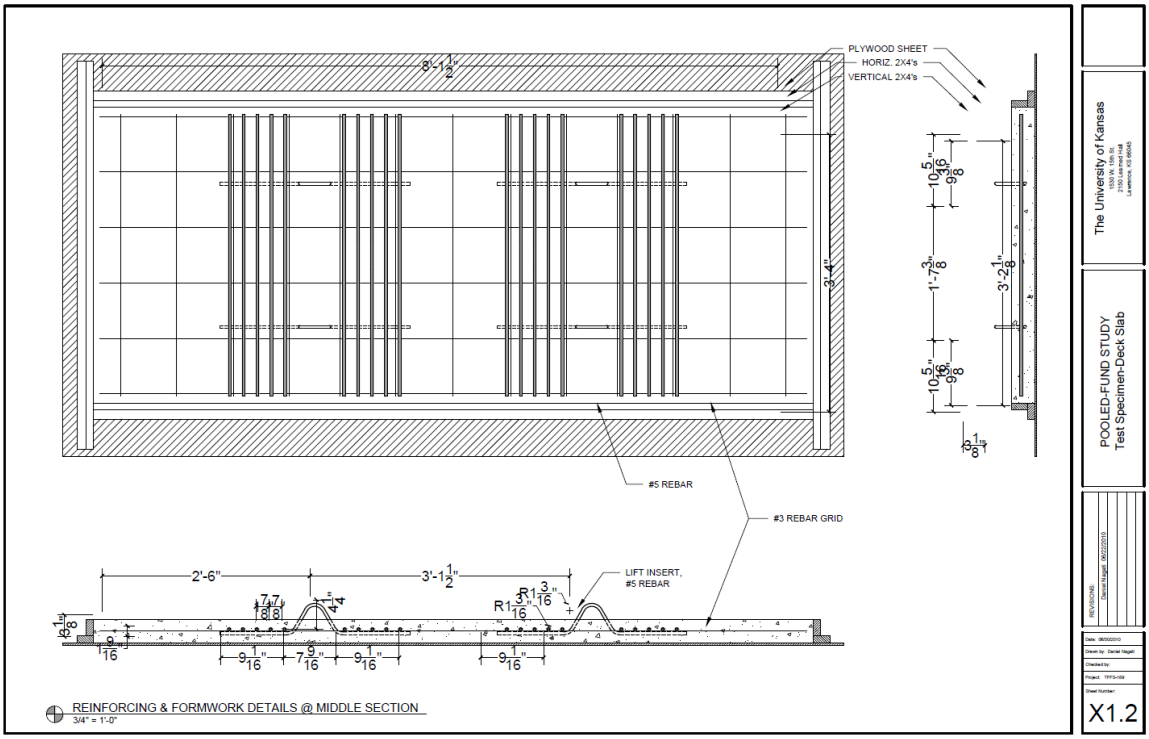

Figure A. 8: Deck reinforcement for center panel.

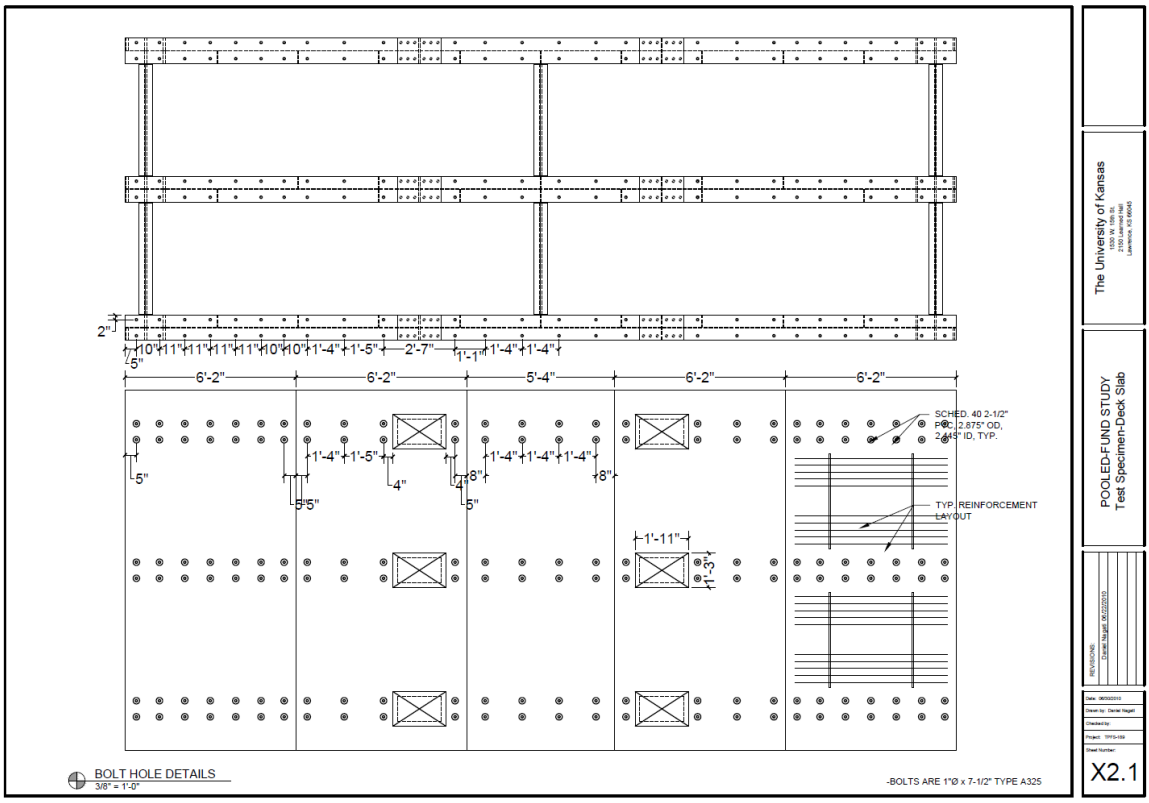

Figure A. 9: Deck panel and hole layout.

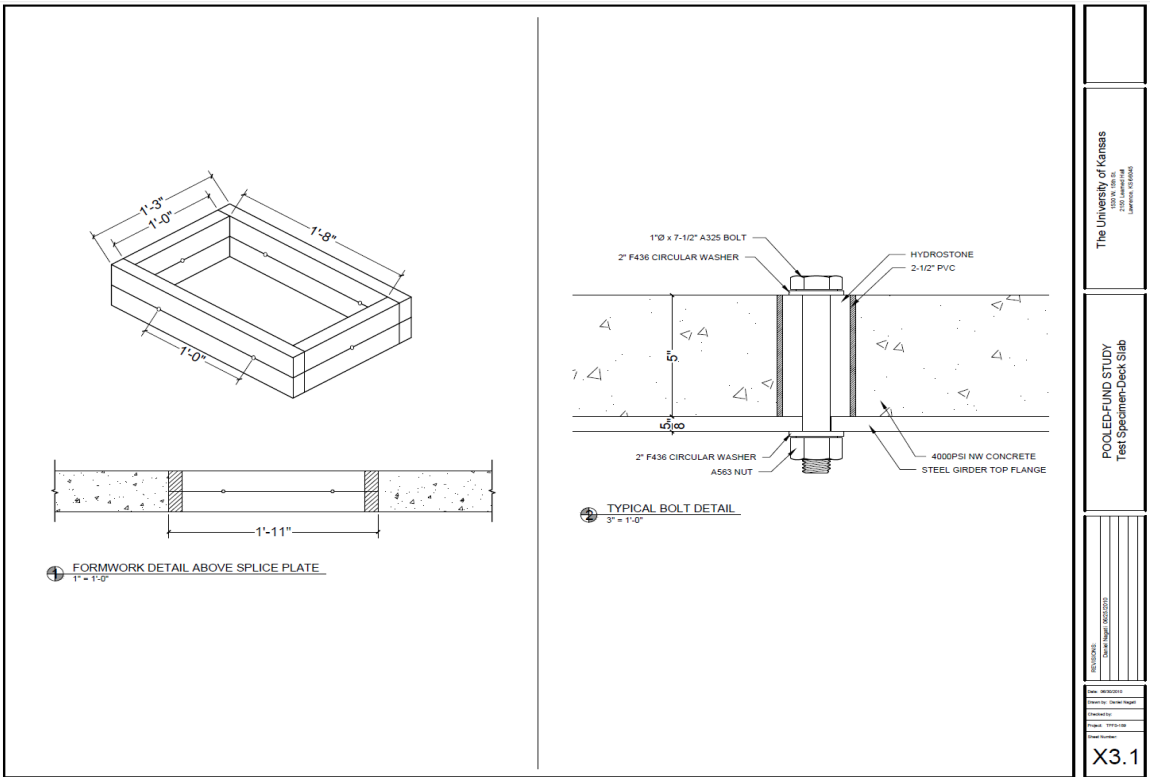

Figure A. 10: Details for deck framing and attachment to girder flanges.

GAGE PLACEMENT

Static data was recorded throughout testing. Due to the significant number of gages and length of testing, continuous data was not recorded. During collection of static data, load was slowly increased on the bridge to capture gage data at defined loading increments. At the beginning of testing, a 2.5 kip load increment was used for loads up to 80 kip. Once bridge loading exceeded 80 kip, a larger increment of 5 kip was used up to a load of 100 kip. Once loading exceeded 100 kip, static data was recorded up to 120 kip.

LATERAL GIRDER DEFLECTIONS – LVDTS OR STRING POTENTIOMETERS

Initially LVDTs were placed at three heights along the girder as shown in Figure A. 11(a). Initial gage locations matched closely with previous 9 ft. girder testing at the University of Kansas (Nagati 2012). At 1.35 million cycles when LVDTs were not reliable under loading, the switch was made to string potentiometers. Additionally, data collection locations were changed to isolate displacements occurring in the web gaps as shown in Figure A. 11(b).

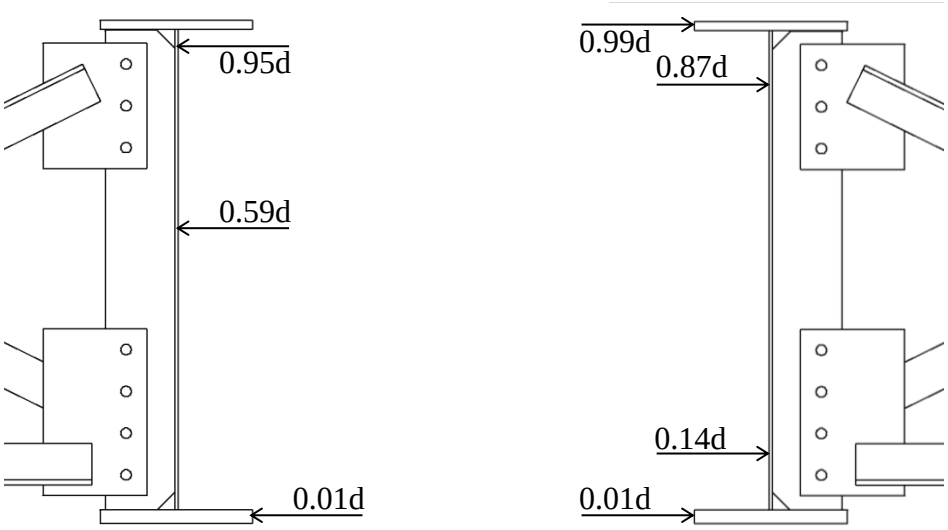

Figure A. 11: Lateral deflection monitoring for (a) LVDT placement and (b) String Potentiometer placement.

VERTICAL GIRDER DEFLECTIONS – LVDTS

LVDTs were placed at the center of each girder on the bottom flange to measure maximum girder deflection.

STRAIN GAGES

Strain gages were placed in web gaps of all girders. Placements can be seen in Figure A. 12.

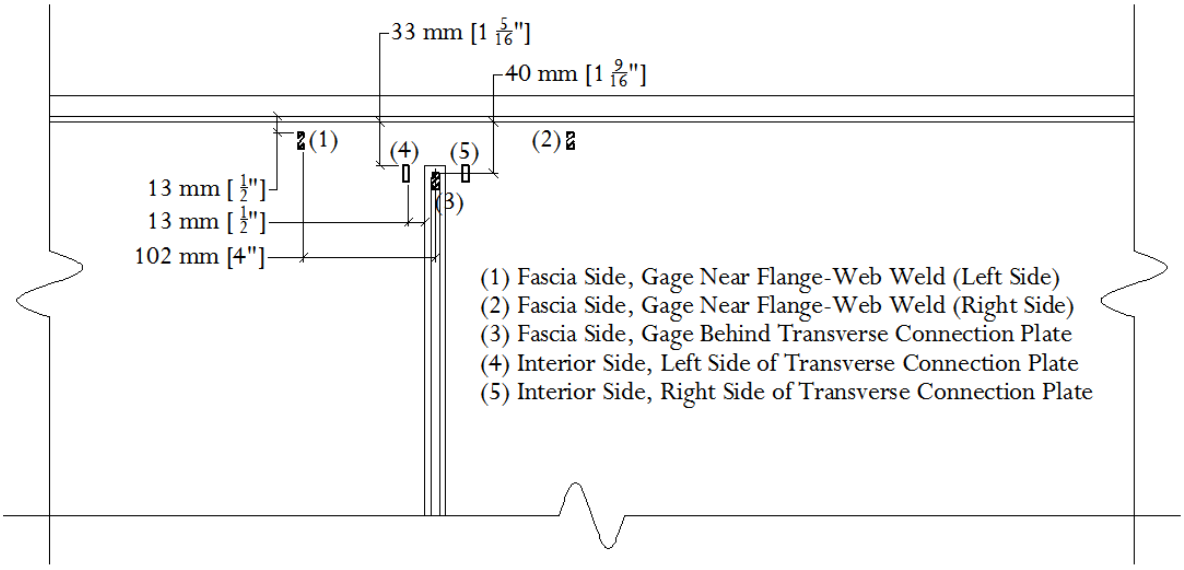

Figure A. 12: Web gap strain gage placements.

On the fascia side of exterior girders, in the top web gap only, gages (1) and (2) were placed. These gages were intended to capture high stresses near the flange-web weld. Gage (3) is placed on the fascia side of exterior girders in both the top and bottom web gaps. Since gage (3) was placed directly behind the connection plate, it was an indicator of initial cracking. All top and bottom web gaps of each girder were instrumented with gages (4) and (5). These gages are intended to capture high stresses around the connection plate-web weld. After the first retrofit application, all gages in the top web gaps of the exterior girders were destroyed and no longer recorded data.

Strain gages were placed on all cross frame element located in the test region. Each gage was oriented along the axis of the element. On the horizontal angle of the cross frame, the gage was placed mid-span. For the diagonal members which were bolted at mid-span, the gages were placed at the quarter-point of the span nearest the exterior girder.

STRAIN TRANSDUCERS

Bridge Diagnostics Inc. (BDI) strain transducers were placed on each girder to monitor bending. One BDI was placed 2 in. down from the top flange and one was placed 2 in. up from the bottom

flange. These BDIs were placed away from the connection plate to minimize localized effects. This separation distance was 2’-1 3/4" as shown in Figure A. 13.

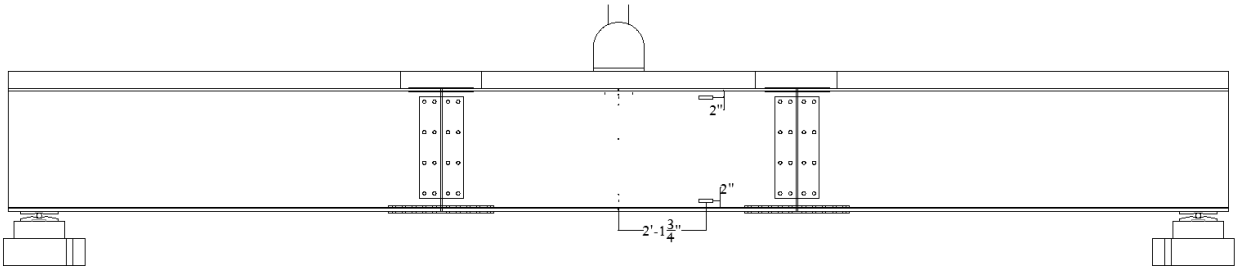

Figure A. 13: BDI placements.

GAGE LABELING

All gages were labeled in a consistent pattern. Table A. 1defined the gage labeling used for data collection.

Table A. 1: Labeling Definition for Data Acquisition

Gage Label	Description
Girder Labeling Scheme	
GN-N	North Girder, North Face of Web
GN-S	North Girder, South Face of Web
GM-N	Middle Girder, North Face of Web
GM-S	Middle Girder, South Face of Web
GS-N	South Girder, North Face of Web
GS-S	South Girder, South Face of Web
Cross Frame Labeling Scheme	
XN AT	Inclined Cross Frame Angle Framing into North Girder Top Web-Gap
XN AB	Inclined Cross Frame Angle Framing into North Girder Bottom Web-Gap
XN HB	Horizontal Cross Frame Angle Framing into North Girder Bottom Web-Gap
XS AT	Inclined Cross Frame Angle Framing into South Girder Top Web-Gap
XS AB	Inclined Cross Frame Angle Framing into South Girder Bottom Web-Gap
XS HB	Horizontal Cross Frame Angle Framing into South Girder Bottom Web-Gap
Strain Gage Labeling Scheme	
B-SC	Bottom Web-Gap, Gage (3) – Behind Stiffener
T-SC	Top Web-Gap, Gage (3) – Behind Stiffener
T-LE	Top Web-Gap, Gage (1/2) – Longitudinal East of Stiffener
T-LW	Top Web-Gap, Gage (1/2) – Longitudinal West of Stiffener
B-UE	Bottom Web-Gap, Gage (4/5) – Horseshoe East of Stiffener
B-UW	Bottom Web-Gap, Gage (4/5) – Horseshoe West of Stiffener
T-UE	Top Web-Gap, Gage (4/5) – Horseshoe East of Stiffener

T-UW	Top Web-Gap, Gage (4/5) – Horseshoe West of Stiffener
BDI Labeling Scheme	
GN-N T	North Face of North Girder near Top Flange
GN-N B	North Face of North Girder near Bottom Flange
GM-N T	North Face of Middle Girder near Top Flange
GM-N B	North Face of Middle Girder near Bottom Flange
GS-S T	South Face of South Girder near Top Flange
GS-S B	South Face of South Girder near Bottom Flange
Load Cell Labeling Scheme	
WN LCA	Load Cell under West Support of North Girder
WM LCB	Load Cell under West Support of Middle Girder
WS LCC	Load Cell under West Support of South Girder
EN LCD	Load Cell under East Support of North Girder
EM LCE	Load Cell under East Support of Middle Girder
ES LCF	Load Cell under East Support of South Girder
LVDT Labeling Scheme	
GS-S T LVDT1	South Face of South Girder near Top Web-Gap
GS-S M LVDT2	South Face of South Girder near Mid-Height
GS-S B LVDT3	South Face of South Girder at Bottom Flange
GN-N T LVDT4	North Face of North Girder near Top Web-Gap
GN-N M LVDT5	North Face of North Girder near Mid-Height
GN-N B LVDT6	North Face of North Girder at Bottom Flange
GS LVDT7	South Girder Vertical Deflection at Mid-Span
GM LVDT8	Middle Girder Vertical Deflection at Mid-Span
GN LVDT9	North Girder Vertical Deflection at Mid-Span
String Potentiometer Labeling Scheme	
GS-S T SP1	South Face of South Girder at Top Flange
GS-S M SP2	South Face of South Girder below Top Web-Gap
GS-S B SP3	South Face of South Girder above Bottom Web-Gap
SPA	South Face of South Girder at Bottom Flange
GN-N T SP4	North Face of North Girder at Top Flange
GN-N M SP5	North Face of North Girder below Top Web-Gap
GN-N B SP6	North Face of North Girder above Bottom Web-Gap
SPB	North Face of North Girder at Bottom Flange

APPENDIX B: CALIBRATION CONSTANTS

STRAIN TRANSDUCERS FROM BRIDGE DIAGNOSTICS INC. (BDI)

Calibrations are provided by Bridge Diagnostics Inc. but must be modified based on supplied voltage. A supply voltage of 5 V was applied to each strain transducer.

$$\text{Calibration Constant} = \frac{\text{General Factor } \mu\varepsilon/mV/\text{V} \cdot 1000\, mV/V}{\text{Input Voltage } V}$$

These modified constants for the strain transducers can be found in Table B. 1.

Table B. 1: Calibration Constants for Strain Transducers

Strain Transducer Label	General Factor	Calibration Constant (5V)
BDI 1269	503.9 με/mV/V	100,780 με/V
BDI 1270	497.0 με/mV/V	99,400 με/V
BDI 1271	503.5 με/mV/V	100,700 με/V
BDI 1272	496.7 με/mV/V	99,340 με/V
BDI 1273	493.6 με/mV/V	98,720 με/V
BDI 1274	502.4 με/mV/V	100,480 με/V

LINEAR VARIABLE DIFFERENTIAL TRANSFORMER (LVDT)

Linear variable differential transformers were calibrated using a Pratt & Whitney Machine. LVDTs were supplied with a 15 V power source from Micro Measurements. Calibration constants for LVDTs can be found in Table B. 2.

Table B. 2: Calibration Constants for LVDTs

LVDT Label	Calibration Constant
LVDT 1	0.099386 in./V
LVDT 2	0.100298 in./V
LVDT 3	0.100361 in./V
LVDT 4	0.099289 in./V

LVDT 5	0.099631 in./V
LVDT 6	0.101083 in./V
LVDT 7	0.393128 in./V
LVDT 8	0.399862 in./V
LVDT 9	0.400382 in./V

All LVDTS were from Measurement Specialties—LVDT 1-6 were model number 500 DC-SE with 0.5 in. range and LVDT 7-9 were model number 2000 DC-SE with 2.0 in range.

LVDT 1-6 (measuring lateral displacement of North and South girders) were replaced with string potentiometers.

STRING POTENTIOMETERS

All string potentiometers were P510-5 with 004 option ordered from UniMeasure, Inc. String potentiometers were calibrated using the Baldwin. String potentiometers were supplied with the same 15 V power supply for LVDTs. Table B. 3 displays the calibration constants for string potentiometers used for testing.

Table B. 3: Calibration Constants for String Potentiometers

String Potentiometer Label	Calibration Constant
SP 1	0.500994 in./V
SP 2	0.497380 in./V
SP 3	0.498466 in./V
SP 4	0.498820 in./V
SP 5	0.497397 in./V
SP 6	0.496723 in./V
SP A	0.502021 in./V
SP B	0.499675 in./V

LOAD CELLS

Load cells were calibrated using a 6.55V power supply. Table B. 4 contains calibration constants for load cells.

Table B. 4: Calibration Constants for Load Cells

Load Cell Label	Calibration Constant
LC A	10237.4 kip/V
LC B	10052.8 kip/V
LC C	10713.9 kip/V
LC D	10280.4 kip/V
LC E	10111.9 kip/V
LC F	10155.1 kip/V

APPENDIX C: LOADING PROCEDURE

PUMP PROTOCOL

TURNING THE PUMP ON FOR 90 GPM PUMP

1. On the touch screen control panel, press the lower middle of the screen to access options. Once pressed, the screen should light up.
2. Before turning on any pumps, check the number of hours each pump has ran. To do this, select HPU. Number of hours for each pump will be displayed. Note which two pumps have the fewest hours. For testing using the 330 kip actuator, two pumps must be active.
3. Return to the main menu. Push and hold the enabled button for one of the pumps having the least number of hours. It will take a few seconds to activate.
4. To turn on the first pump, press and hold low pressure. This will turn the pump on to low pressure. Monitor the pressure readout on the screen.
5. Once the pressure reads around 300 psi, press and hold high pressure.
6. Once the pressure stabilizes around 3000 psi, the other pump can be enabled. To do this, press and hold the enable button for the pump containing the second-least number of hours.
7. If all three pumps are needed, repeat step 6 with the final pump.

TURNING THE PUMP OFF FOR 90 GPM PUMP

1. If the touch screen is not active, press the lower middle of the screen to access options.
2. At least two pumps should be on high pressure. Turn the first pump off by pressing and holding the disable button for that pump. Wait a few seconds before proceeding.
3. If all three pumps were on, press and hold the disable button for the second pump. This will leave only one pump remaining.
4. With only one pump running, press and hold high pressure. This will turn high pressure off. Monitor the pressure readout and wait to proceed until the pressure drops to around 300 psi.
5. Once pressure drops to 300 psi, press and hold low pressure turning off the remaining pump. The final pump will automatically return to disabled.

ACTUATOR WARM-UP

1. Activate the Function Generator in Station Manager.
2. On the Manual Command, check the box to Enable Manual Command. At this point, set the offsets; however, offsets will need re-zeroed (re-offset) for load before running a program.
3. Turn on the hydraulic fluid.
4. Change the Control Mode to Displacement and force the actuator to 15 kips.
5. Change the Control Mode to Force.
6. In the Function Generator, the Target Setpoint should be 15 kips and the Amplitude should be 5 kips.
7. On the Manual Command, uncheck the Enable Manual Command box.
8. Push Play in the Function Generator.
9. Display the Scope box to monitor the amplitude.

TUNING

1. In the Function Generator, change the dropdown menu to Tuning.
2. When prompted, enter the password, "Tuning."
3. Go to Station Setup.
4. Under Channels, adjust Force and Displacement using the Tuning Fork button.

NEW PROGRAM

1. Open Applications dropdown menu. Select Multipurpose Testware (Edit Only). Click OK when default warning pops up.
2. Open an existing procedure and save as a new procedure.
3. Ramp to absolute end level load (mean of stress range)
4. Set Absolute End Level 1 to low end of stress range
5. Set Absolute End Level 2 to high end of stress range
6. Save before closing.

TESTING

1. Once the system is warmed up testing can begin. On the Manual Command, check the box to Enable Manual Command. Check interlock controls.
2. Change the Control Mode to Displacement and take the actuator to the desired load (mean of stress range).
3. Activate MPT.
4. Open the new procedure.
5. Create new specimen and change the name in the dropdown menu.
6. Turn on ‘Scope’ to see command and output.
7. On the Manual Command, uncheck the Enable Manual Command box.
8. Return to Function Generator.
9. Push play.
10. Be prepared to hit pause or stop in case something goes wrong.

APPENDIX D: FINITE ELEMENT MODELING DATA

MODIFIABLE HOT SPOT STRESS PATH IMAGES

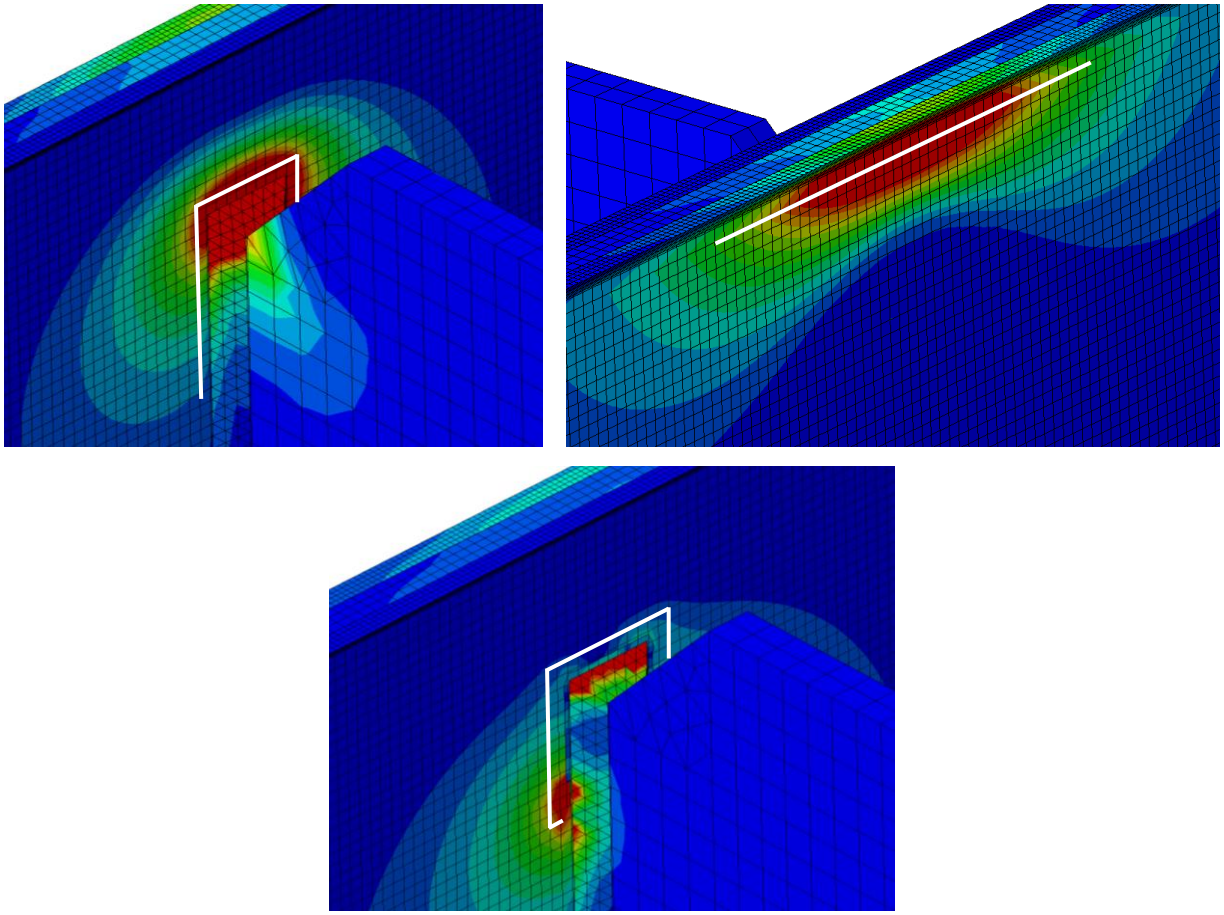

Figure D. 1: Modifiable hot spot stress path images.

MODEL FILE NAMES AND DESCRIPTIONS

Table D. 1: Model Naming and Descriptions

ODB File Name/Model Name	CAE File Name	Description
BaseModelNoCracks-60k	Specimen Model 12.14.2012	No Cracks
BaseModelUCracks1in-60k*	Specimen Model with 1 in Cracks 12.14.2012	1 in Horseshoe Cracks
BaseModelUCracks1point5in-60k	Specimen Model with 1.5 in Cracks 01.07.2013	1.5 in Horseshoe Cracks
BaseModelUCracks2in-60k	Specimen Model with 2 in Cracks 01.07.2013	2 in Horseshoe Cracks
BaseModelUCracks2point5in-60k	Specimen Model with 2.5 in Cracks 01.08.2013	2.5 in Horseshoe Cracks
BaseModelUCracks3in-60k	Specimen Model with 3 in Cracks 01.08.2013	3 in Horseshoe Cracks
BaseModelUCracks4in-60k	Specimen Model with 4 in Cracks 03.26.2013	4 in Horseshoe Cracks
BaseModelUCracks8in-60k	Specimen Model with 8 in Cracks 03.26.2013	8 in Horseshoe Cracks
BaseModelUCracks1in-60k*		
BaseModelUCracks1inRet1Tied-60k		
BaseModelUCracks1inRet1Bolts-60kTrial		
BaseModelUCracks1inRet1Bolts-60kRelSol		
BaseModelUCracks1inRet1BoltsNoHC-60kRS	Specimen Model with 1 in Cracks and Retrofit 01.03.2013	1 in Horseshoe Cracks with 3/4" Angles-with-Plate Retrofit
BaseModelUCracks1p5inRet1Bolts-60k	Specimen Model with 1.5 in Cracks and Retrofit 01.18.2013	1.5 in Horseshoe Cracks with 3/4" Angles-with-Plate Retrofit
BaseModelUCracks2inRet1Bolts-60k	Specimen Model with 2 in Cracks and Retrofit 01.18.2013	2 in Horseshoe Cracks with 3/4" Angles-with-Plate Retrofit
BaseModelUCracks2p5inRet1Bolts-60k	Specimen Model with 2.5 in Cracks and Retrofit 01.18.2013	2.5 in Horseshoe Cracks with 3/4" Angles-with-Plate Retrofit
BaseModelUCracks3inRet1Bolts-60k	Specimen Model with 3 in Cracks and Retrofit 01.18.2013	3 in Horseshoe Cracks with 3/4" Angles-with-Plate Retrofit
UCracks1inRet1-pt5-Bolts-60k	Specimen Model with 1 in Cracks and Retrofit 0.5inT 01.30.2013	1 in Horseshoe Cracks with 1/2" Angles-with-Plate Retrofit
UCracks1point5inRet1-pt5-Bolts-60k	Specimen Model with 1.5 in Cracks and Retrofit 0.5inT 01.30.2013	1.5 in Horseshoe Cracks with 1/2" Angles-with-Plate Retrofit
UCracks2inRet1-pt5-Bolts-60k	Specimen Model with 2 in Cracks and Retrofit 0.5inT 01.30.2013	2 in Horseshoe Cracks with 1/2" Angles-with-Plate Retrofit
UCracks2point5inRet1-pt5-Bolts-60k	Specimen Model with 2.5 in Cracks and Retrofit 0.5inT 01.30.2013	2.5 in Horseshoe Cracks with 1/2" Angles-with-Plate Retrofit
UCracks3inRet1-pt5-Bolts-60k	Specimen Model with 3 in Cracks and Retrofit 0.5inT 01.30.2013	3 in Horseshoe Cracks with 1/2" Angles-with-Plate Retrofit
UCracks1inRet1Stiffeners-60k	Specimen Model with 1 in. Cracks and Retrofit with Angle Stiffeners 02.15.2013	1 in Horseshoe Cracks with 3/4" Angles-with-Plate Retrofit with Stiffeners
UCracks1point5inRet1Stiffeners-60k	Specimen Model with 1.5 in. Cracks and Retrofit with Angle Stiffeners 02.15.2013	1.5 in Horseshoe Cracks with 3/4" Angles-with-Plate Retrofit with Stiffeners
UCracks2inRet1Stiffeners-60k	Specimen Model with 2 in. Cracks and Retrofit with Angle Stiffeners 02.15.2013	2 in Horseshoe Cracks with 3/4" Angles-with-Plate Retrofit with Stiffeners
UCracks2point5inRet1Stiffeners-60k	Specimen Model with 2.5 in. Cracks and Retrofit with Angle Stiffeners 02.15.2013	2.5 in Horseshoe Cracks with 3/4" Angles-with-Plate Retrofit with Stiffeners
UCracks3inRet1Stiffeners-60k	Specimen Model with 3 in. Cracks and Retrofit with Angle Stiffeners 02.15.2013	3 in Horseshoe Cracks with 3/4" Angles-with-Plate Retrofit with Stiffeners
UCracks1inFullBackupStiff-60k	Specimen Model with 1 in. Cracks with Backup Stiffener 03.19.2013	1 in Horseshoe Cracks with Full Depth Back-up Stiffener
UCracks1point5inFullBackupStiff-60k	Specimen Model with 1.5 in. Cracks with Backup Stiffener 03.19.2013	1.5 in Horseshoe Cracks with Full Depth Back-up Stiffener
UCracks2inFullBackupStiff-60k	Specimen Model with 2 in. Cracks with Backup Stiffener 03.19.2013	2 in Horseshoe Cracks with Full Depth Back-up Stiffener
UCracks2point5inFullBackupStiff-60k	Specimen Model with 2.5 in. Cracks with Backup Stiffener 03.19.2013	2.5 in Horseshoe Cracks with Full Depth Back-up Stiffener
UCracks3inFullBackupStiff-60k	Specimen Model with 3 in. Cracks with Backup Stiffener 03.19.2013	3 in Horseshoe Cracks with Full Depth Back-up Stiffener
UCracks1inRet2TFTension-60k	Specimen Model with 1 in Cracks and Retrofit Top Flange Tensioned 04.10.2013	1 in Horseshoe Cracks with 3/4" Angles Attached to Top Flange with Tensioned Bolts
UCracks1point5inRet2TFTension-60k	Specimen Model with 1.5 in Cracks and Retrofit Top Flange Tensioned 04.10.2013	1.5 in Horseshoe Cracks with 3/4" Angles Attached to Top Flange with Tensioned Bolts
UCracks2inRet2TFTension-60k	Specimen Model with 2 in Cracks and Retrofit Top Flange Tensioned 04.10.2013	2 in Horseshoe Cracks with 3/4" Angles Attached to Top Flange with Tensioned Bolts
UCracks2point5inRet2TFTension-60k	Specimen Model with 2.5 in Cracks and Retrofit Top Flange Tensioned 04.10.2013	2.5 in Horseshoe Cracks with 3/4" Angles Attached to Top Flange with Tensioned Bolts
UCracks3inRet2TFTension-60k	Specimen Model with 3 in Cracks and Retrofit Top Flange Tensioned 04.10.2013	3 in Horseshoe Cracks with 3/4" Angles Attached to Top Flange with Tensioned Bolts
UCracks1inRet1BoltsBrokenXF2-60k	Specimen Model with 1 in Cracks and Retrofit and Broken Cross Frame 04.22.2013	1 in Horseshoe Cracks with 3/4" Angles-with-Plate Retrofit and North Cross Frame (AT) Broken
UCracks2inRedDeckStiff-60k	Specimen Model with 2 in Cracks 04.30.2013	2 in Horseshoe Cracks with 3/4" Angles-with-Plate Retrofit and Half Deck Stiffness
LCracks1inRet1Bolts-60k*	Specimen Model with 1 in Cracks and Retrofit 05.03.2013	1 in Longitudinal Cracks with 3/4" Angles-with-Plate Retrofit
LCracks2inRet1Bolts-60k	Specimen Model with 2 in Cracks and Retrofit 05.03.2013	2 in Longitudinal Cracks with 3/4" Angles-with-Plate Retrofit
LCracks3inRet1Bolts-60k	Specimen Model with 3 in Cracks and Retrofit 05.03.2013	3 in Longitudinal Cracks with 3/4" Angles-with-Plate Retrofit
LCracks4inRet1Bolts-60k	Specimen Model with 4 in Cracks and Retrofit 05.10.2013	4 in Longitudinal Cracks with 3/4" Angles-with-Plate Retrofit
LCracks8inRet1Bolts-60k	Specimen Model with 8 in Cracks and Retrofit 05.10.2013	8 in Longitudinal Cracks with 3/4" Angles-with-Plate Retrofit
LCracks1in-60k*	Specimen Model with 1 in Cracks 05.03.2013	1 in Longitudinal Cracks
LCracks2in-60k	Specimen Model with 2 in Cracks 05.03.2013	2 in Longitudinal Cracks
LCracks3in-60k	Specimen Model with 3 in Cracks 05.03.2013	3 in Longitudinal Cracks
LCracks4in-60k	Specimen Model with 4 in Cracks 05.10.2013	4 in Longitudinal Cracks
LCracks8in-60k	Specimen Model with 8 in Cracks 05.10.2013	8 in Longitudinal Cracks

*Needs ran again, cannot find ODB and DAT but INP file exists

COMPLETE TABLE OF DATA FOR MODELS

Complete data set from all models can be found in Table D. 2.

Table D. 2: Complete data from models

	North Girder									Middle Girder					South Girder								
Model Name	Horseshoe Top [ksi]	Horseshoe Bottom [ksi]	Longitudinal Top [ksi]	Longitudinal Bottom [ksi]	Vertical Deflection [in.]	Top Flange Deflection [in.]	Top Web-Gap Deflection [in.]	Bottom Web-Gap Deflection [in.]	Bottom Flange Deflection [in.]	Horseshoe South Top [ksi]	Horseshoe South Bottom [ksi]	Horseshoe North Top [ksi]	Horseshoe North Bottom [ksi]	Vertical Deflection [in.]	Horseshoe Top [ksi]	Horseshoe Bottom [ksi]	Longitudinal Top [ksi]	Longitudinal Bottom [ksi]	Vertical Deflection [in.]	Top Flange Deflection [in.]	Top Web-Gap Deflection [in.]	Bottom Web-Gap Deflection [in.]	Bottom Flange Deflection [in.]
BaseModelNoCracks-60k	60.3	14.3	58.9	6.1	-0.037	0.003	-0.008	0.010	0.017	0.3	8.7	3.5	8.9	-0.080	56.4	14.9	55.3	6.5	-0.037	-0.003	0.008	-0.010	-0.017
BaseModelUCracks1in-60k	60.3	15.3	35.2	6.6	-0.036	0.003	-0.012	0.010	0.018	0.3	9.4	2.7	9.2	-0.082	43.6	14.9	32.9	6.5	-0.037	-0.003	0.011	-0.011	-0.019
BaseModelUCracks1point5in-60k	51.0	15.5	28.7	6.7	-0.036	0.004	-0.013	0.011	0.019	1.0	9.5	2.3	9.2	-0.082	35.9	14.9	26.7	6.5	-0.037	-0.003	0.012	-0.011	-0.019
BaseModelUCracks2in-60k	43.7	15.7	24.2	6.8	-0.036	0.004	-0.013	0.011	0.020	1.0	9.6	2.6	9.3	-0.082	30.2	14.9	22.5	6.5	-0.036	-0.003	0.013	-0.012	-0.020
BaseModelUCracks2point5in-60k	38.0	15.8	21.1	6.8	-0.036	0.004	-0.013	0.011	0.019	1.1	9.7	2.5	9.3	-0.082	25.8	15.0	19.6	6.6	-0.036	-0.003	0.013	-0.012	-0.020
BaseModelUCracks3in-60k	33.5	15.7	18.9	6.9	-0.036	0.004	-0.014	0.011	0.020	1.1	9.7	2.5	9.3	-0.082	22.3	15.0	17.5	6.6	-0.036	-0.004	0.013	-0.012	-0.020
BaseModelUCracks4in-60k	27.0	16.0	16.0	6.9	-0.035	0.004	-0.014	0.011	0.019	1.1	9.7	2.0	9.3	-0.082	17.4	15.0	14.8	6.6	-0.036	-0.004	0.014	-0.012	-0.020
BaseModelUCracks8in-60k	12.5	16.2	12.0	7.0	-0.035	0.004	-0.014	0.011	0.019	1.1	9.8	1.9	9.3	-0.083	10.8	15.1	11.0	6.6	-0.036	-0.004	0.014	-0.012	-0.020
BaseModelUCracks1inRet1BoltsNoHC-60kRS	18.5	13.4	14.9	5.4	-0.038	0.003	-0.003	0.009	0.016	2.0	7.6	4.6	7.9	-0.077	14.4	14.1	14.4	5.9	-0.038	-0.002	0.003	-0.009	-0.015
BaseModelUCracks1p5inRet1Bolts-60k	13.8	13.4	14.5	5.5	-0.038	0.003	-0.003	0.009	0.016	2.0	7.9	4.5	7.6	-0.077	10.3	14.1	14.8	5.9	-0.038	-0.003	0.003	-0.010	-0.015
BaseModelUCracks2inRet1Bolts-60k	10.3	13.4	14.6	5.5	-0.038	0.003	-0.003	0.009	0.016	2.0	7.9	4.5	7.6	-0.077	7.6	14.1	14.8	5.9	-0.038	-0.003	0.003	-0.009	-0.015
BaseModelUCracks2p5inRet1Bolts-60k	7.8	13.4	14.6	5.5	-0.038	0.003	-0.003	0.009	0.016	2.0	7.6	4.5	7.9	-0.077	5.7	14.1	14.8	5.9	-0.038	-0.003	0.003	-0.010	-0.015
BaseModelUCracks3inRet1Bolts-60k	5.9	13.4	14.6	5.5	-0.038	0.003	-0.003	0.010	0.016	2.0	7.6	4.5	7.9	-0.077	4.8	14.1	14.9	5.9	-0.038	-0.003	0.003	-0.009	-0.015
UCracks1inRet1-pt5-Bolts-60k	32.2	14.6	23.8	6.1	-0.034	0.003	-0.007	0.010	0.017	1.3	8.3	3.0	8.4	-0.077	26.5	14.8	23.0	6.3	-0.035	-0.003	0.006	-0.011	-0.017
UCracks1point5inRet1-pt5-Bolts-60k	15.6	17.1	19.8	7.0	-0.014	0.003	-0.003	0.011	0.018	2.6	7.1	6.2	7.5	-0.061	11.4	17.6	19.5	7.4	-0.015	-0.003	0.003	-0.011	-0.018
UCracks2inRet1-pt5-Bolts-60k	12.7	15.7	18.9	6.5	-0.019	0.003	-0.004	0.010	0.017	2.2	7.2	5.1	7.1	-0.062	9.5	16.2	18.7	6.8	-0.019	-0.003	0.004	-0.010	-0.017
UCracks2point5inRet1-pt5-Bolts-60k	10.0	12.7	16.0	5.3	-0.021	0.003	-0.005	0.008	0.014	1.6	5.5	3.3	5.6	-0.057	7.8	12.9	16.1	5.5	-0.022	-0.002	0.004	-0.009	-0.014
UCracks3inRet1-pt5-Bolts-60k	8.5	11.1	14.6	4.6	-0.025	0.002	-0.005	0.008	0.013	1.3	5.9	2.6	5.9	-0.058	6.9	11.2	14.9	4.8	-0.025	-0.013	0.005	-0.008	-0.002
UCracks1inRet1Stiffeners-60k	12.9	12.9	13.5	5.2	-0.038	0.002	-0.001	0.009	0.015	2.4	7.1	5.5	7.6	-0.076	9.6	14.0	14.1	5.9	-0.039	-0.002	0.001	-0.009	-0.014
UCracks1point5inRet1Stiffeners-60k	9.5	12.9	13.5	5.2	-0.038	0.002	-0.001	0.009	0.014	2.4	7.2	5.5	7.6	-0.076	7.1	14.0	14.2	5.9	-0.039	-0.002	0.001	-0.009	-0.014
UCracks2inRet1Stiffeners-60k	6.9	12.9	13.6	5.2	-0.038	0.002	-0.001	0.009	0.015	2.4	7.2	5.5	7.6	-0.076	5.2	14.0	14.2	5.9	-0.039	-0.002	0.001	-0.009	-0.015
UCracks2point5inRet1Stiffeners-60k	5.1	12.9	13.6	5.2	-0.038	0.002	-0.001	0.009	0.015	2.4	7.1	5.5	7.5	-0.076	3.7	14.1	14.3	5.9	-0.038	-0.002	0.001	-0.009	-0.015
UCracks3inRet1Stiffeners-60k	3.6	12.9	13.6	5.2	-0.038	0.002	-0.001	0.009	0.015	2.4	7.2	5.5	7.6	-0.076	3.0	14.0	14.3	5.9	-0.039	-0.002	0.001	-0.009	-0.015
UCracks1inFullBackupStiff-60k	59.1	8.6	35.5	8.8	-0.036	0.003	-0.012	0.011	0.016	0.9	9.3	1.6	9.1	-0.081	43.1	8.1	33.3	8.7	-0.037	-0.003	0.011	-0.012	-0.017
UCracks1point5inFullBackupStiff-60k	49.8	7.9	28.9	8.9	-0.036	0.004	-0.013	0.011	0.016	1.0	9.5	1.8	9.2	-0.082	35.3	8.0	27.0	8.7	-0.036	-0.003	0.012	-0.012	-0.017
UCracks2inFullBackupStiff-60k	42.5	8.8	24.4	8.8	-0.036	0.004	-0.013	0.011	0.016	1.0	9.6	1.9	9.2	-0.082	29.6	8.0	22.7	8.7	-0.036	-0.003	0.013	-0.012	-0.017
UCracks2point5inFullBackupStiff-60k	36.9	6.5	21.2	9.1	-0.036	0.004	-0.013	0.011	0.016	1.1	9.6	1.9	9.2	-0.082	25.2	8.0	19.8	8.8	-0.036	-0.003	0.013	-0.012	-0.017
UCracks3inFullBackupStiff-60k	32.4	8.1	18.9	9.1	-0.036	0.004	-0.014	0.011	0.016	1.1	9.7	2.0	9.3	-0.082	21.8	8.0	17.6	8.8	-0.036	-0.003	0.013	-0.012	-0.018
UCracks1inRet2TFTension-60k	11.0	11.2	6.4	4.5	-0.039	0.002	0.001	0.009	0.014	3.1	6.9	6.9	7.3	-0.075	9.8	12.7	5.3	5.3	-0.039	-0.002	-0.002	-0.009	-0.014
UCracks1point5inRet2TFTension-60k	10.1	11.2	5.2	4.5	-0.039	0.002	0.001	0.009	0.014	3.1	6.9	6.9	7.3	-0.075	9.1	12.7	4.4	5.3	-0.039	-0.002	-0.002	-0.009	-0.014
UCracks2inRet2TFTension-60k	9.6	11.2	4.4	4.5	-0.039	0.002	0.001	0.009	0.014	3.1	6.9	6.9	7.3	-0.075	8.7	12.7	3.8	5.3	-0.039	-0.002	-0.002	-0.009	-0.014
UCracks2point5inRet2TFTension-60k	9.4	11.2	3.9	4.5	-0.039	0.002	0.001	0.009	0.014	3.1	6.9	6.9	7.3	-0.075	8.4	12.7	3.3	5.3	-0.039	-0.002	-0.002	-0.009	-0.014
UCracks3inRet2TFTension-60k	9.3	11.2	3.4	4.5	-0.039	0.002	0.001	0.009	0.014	3.1	6.9	6.9	7.3	-0.075	8.2	12.7	3.0	5.3	-0.039	-0.002	-0.002	-0.009	-0.014
UCracks1inRet1BoltsBrokenXF2-60k	4.2	27.7	5.4	11.1	-0.035	0.004	0.003	0.001	0.009	18.5	12.5		6.9	-0.037	8.7	8.1	9.6	3.6	-0.037	-0.003	-0.002	-0.020	-0.025
UCracks2inRedDeckStiff-60k	52.1	15.5	29.1	7.0	-0.041	0.005	-0.016	0.013	0.022	0.7	10.8	1.1	10.4	-0.097	35.8	15.0	27.0	6.7	-0.041	-0.004	0.015	-0.013	-0.023
LCracks1inRet1Bolts-60k	30.1	13.3	27.2	5.4	-0.038	0.003	-0.002	0.009	0.015	2.2	7.5	4.8	7.8	-0.077	28.9	14.1	30.1	5.9	-0.038	-0.002	0.002	-0.009	-0.015
LCracks2inRet1Bolts-60k	25.1	13.3	25.5	5.4	-0.038	0.025	-0.003	0.009	0.015	2.1	7.6	4.7	7.8	-0.077	24.0	14.1	29.8	5.9	-0.038	-0.002	0.002	-0.009	-0.015
LCracks3inRet1Bolts-60k	18.9	13.4	24.0	5.5	-0.038	0.003	-0.003	0.009	0.015	2.1	7.6	4.6	7.9	-0.078	17.9	14.2	28.0	6.0	-0.038	-0.002	0.002	-0.009	-0.015
LCracks4inRet1Bolts-60k	13.8	13.5	19.6	5.5	-0.038	0.003	-0.003	0.009	0.015	2.0	7.6	4.5	7.9	-0.077	13.0	14.2	19.1	6.0	-0.038	-0.003	0.003	-0.009	-0.015
LCracks8inRet1Bolts-60k	17.3	13.7	18.7	5.6	-0.037	0.003	-0.004	0.010	0.016	1.8	7.8	3.9	8.0	-0.077	19.8	14.2	18.1	6.0	-0.038	-0.003	0.004	-0.010	-0.016
LCracks1in-60k	68.8	14.5	56.7	6.2	-0.037	0.003	-0.009	0.010	0.017	1.2	8.8	2.9	8.9	-0.080	64.3	14.9	55.0	6.5	-0.037	-0.003	0.008	-0.011	-0.018
LCracks2in-60k	61.1	14.8	54.1	6.3	-0.036	0.003	-0.010	0.010	0.018	1.0	9.0	2.4	9.0	-0.081	56.7	14.9	52.9	6.5	-0.037	-0.003	0.009	-0.011	-0.018
LCracks3in-60k	49.6	15.1	51.3	6.5	-0.036	0.003	-0.010	0.010	0.018	0.9	9.2	2.0	9.1	-0.081	45.4	15.0	49.5	6.5	-0.037	-0.003	0.010	-0.011	-0.019
LCracks4in-60k	40.4	15.4	46.6	6.6	-0.004	0.004	-0.012	0.010	0.018	0.9	9.4	1.5	9.2	-0.082	34.9	15.0	44.0	6.5	-0.037	-0.034	0.012	-0.011	-0.019
LCracks8in-60k	20.6	16.0	34.3	7.0	-0.035	0.004	-0.014	0.011	0.019	1.3	9.8	2.0	9.3	-0.083	14.2	15.0	30.4	6.6	-0.036	-0.004	0.014	-0.012	-0.020

DATA CHARTS

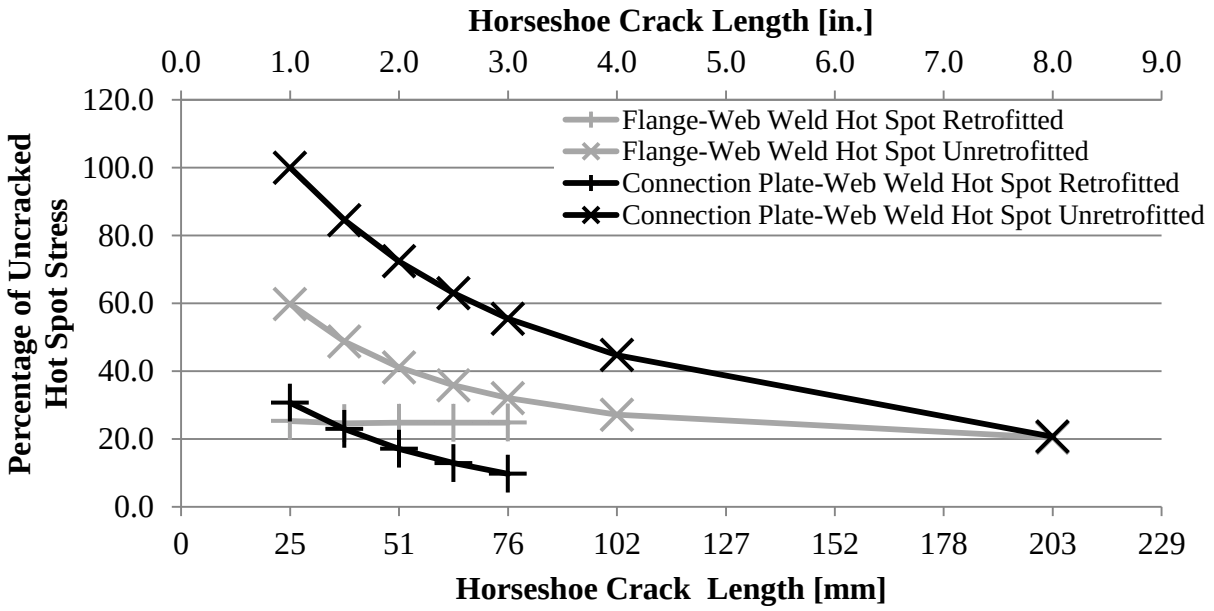

Figure D. 2: Effect of horseshoe crack length on hot spot stresses in flange-web welds and connection plate-web welds.

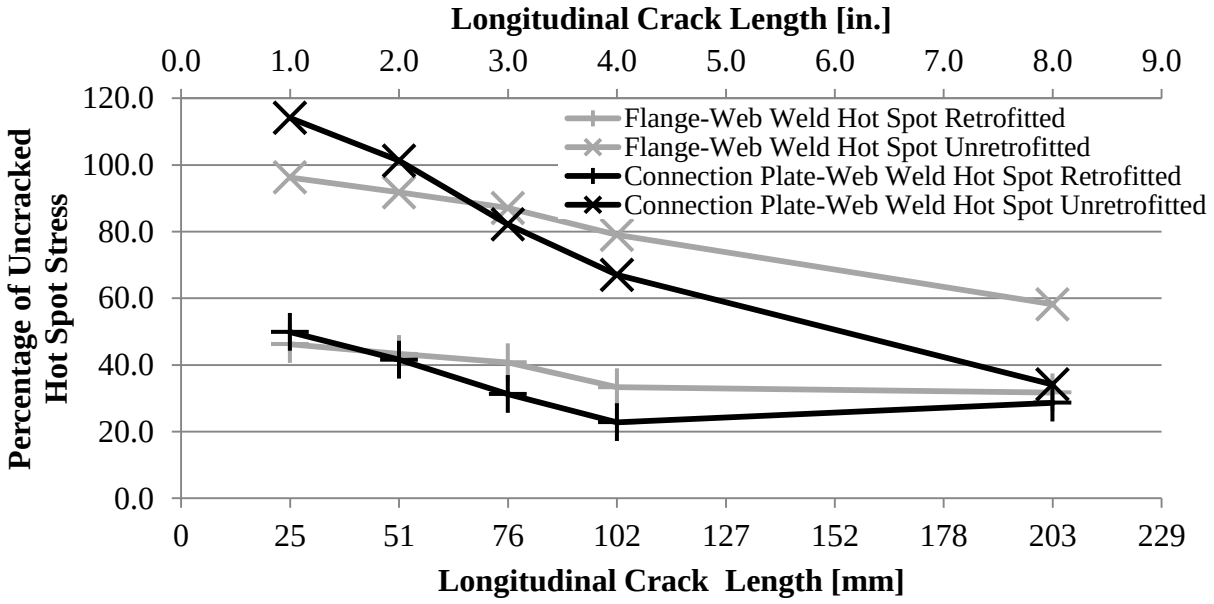

Figure D. 3: Effect of longitudinal crack length on hot spot stresses in flange-web welds and connection plate-web welds.

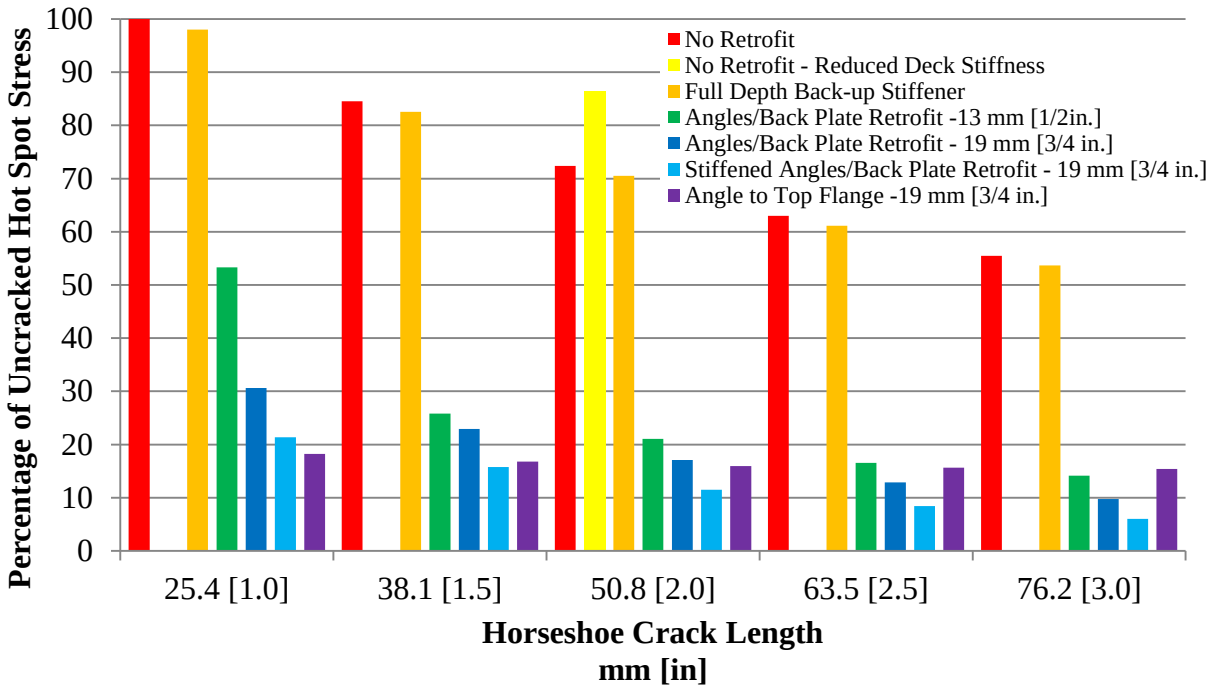

Figure D. 4: Retrofit performance at connection plate-web weld based on percentage of uncracked hot spot stress due to change in horseshoe crack length in the North Girder.

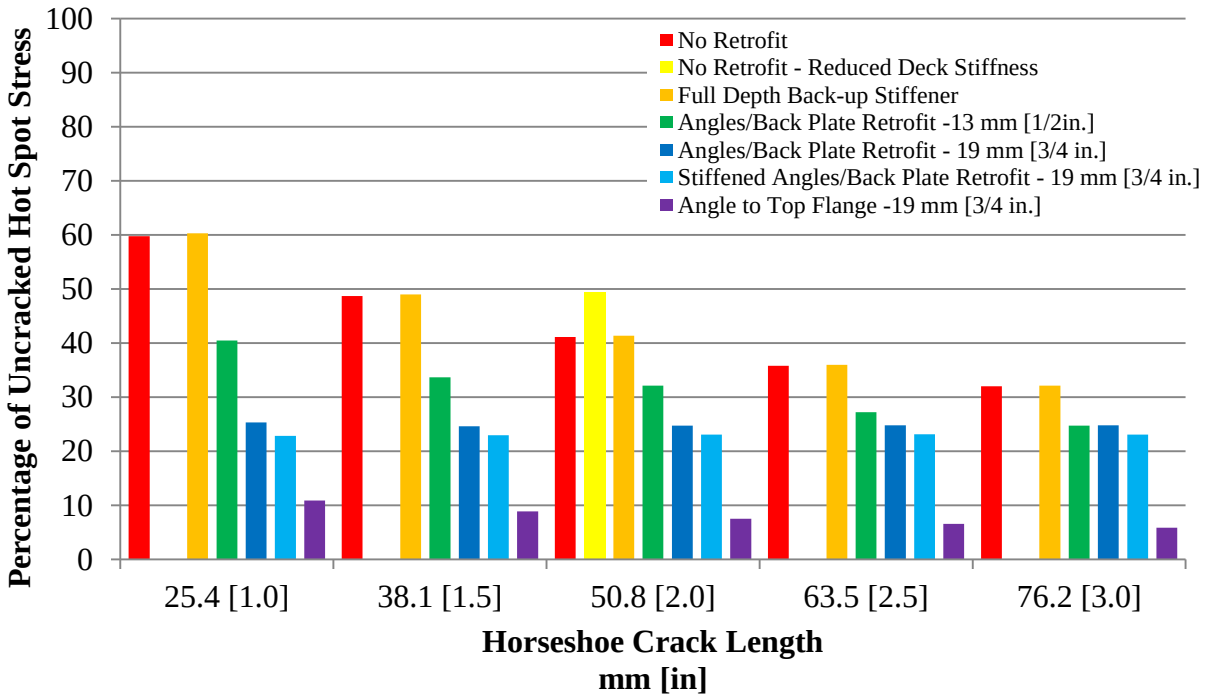

Figure D. 5: Retrofit performance at flange-web weld based on percentage of uncracked hot spot stress due to change in horseshoe crack length in the North Girder.

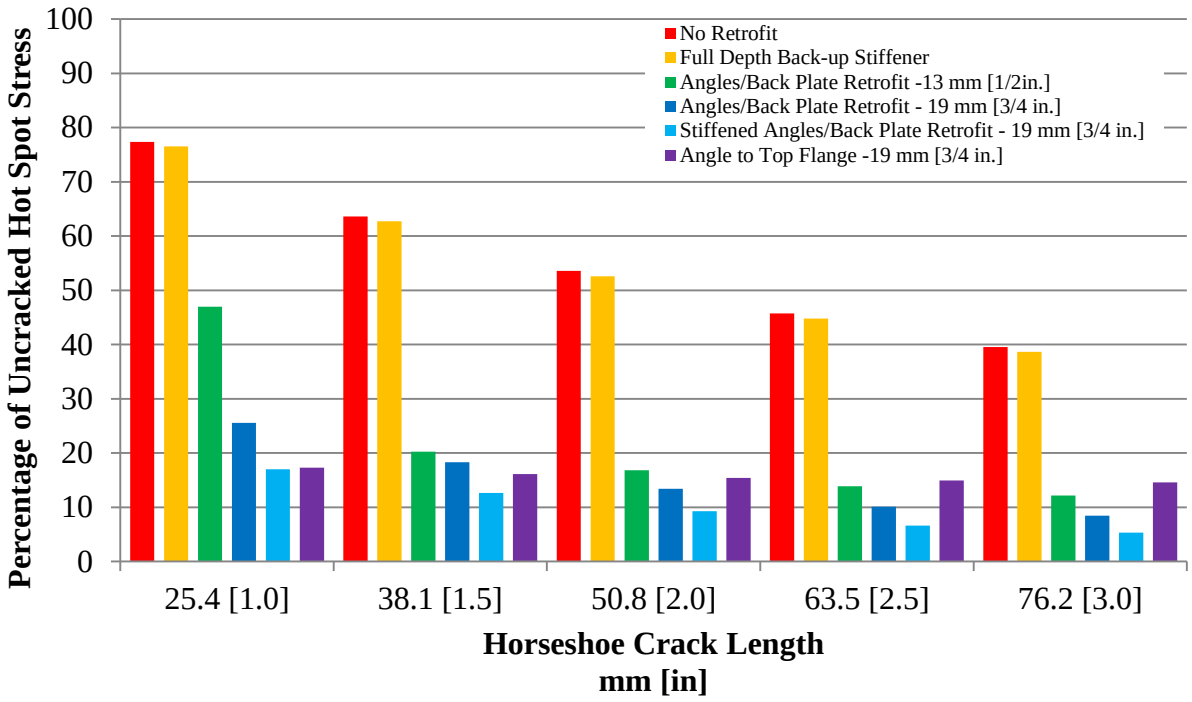

Figure D. 6: Retrofit performance at connection plate-web weld based on percentage of uncracked hot spot stress due to change in horseshoe crack length in the South Girder.

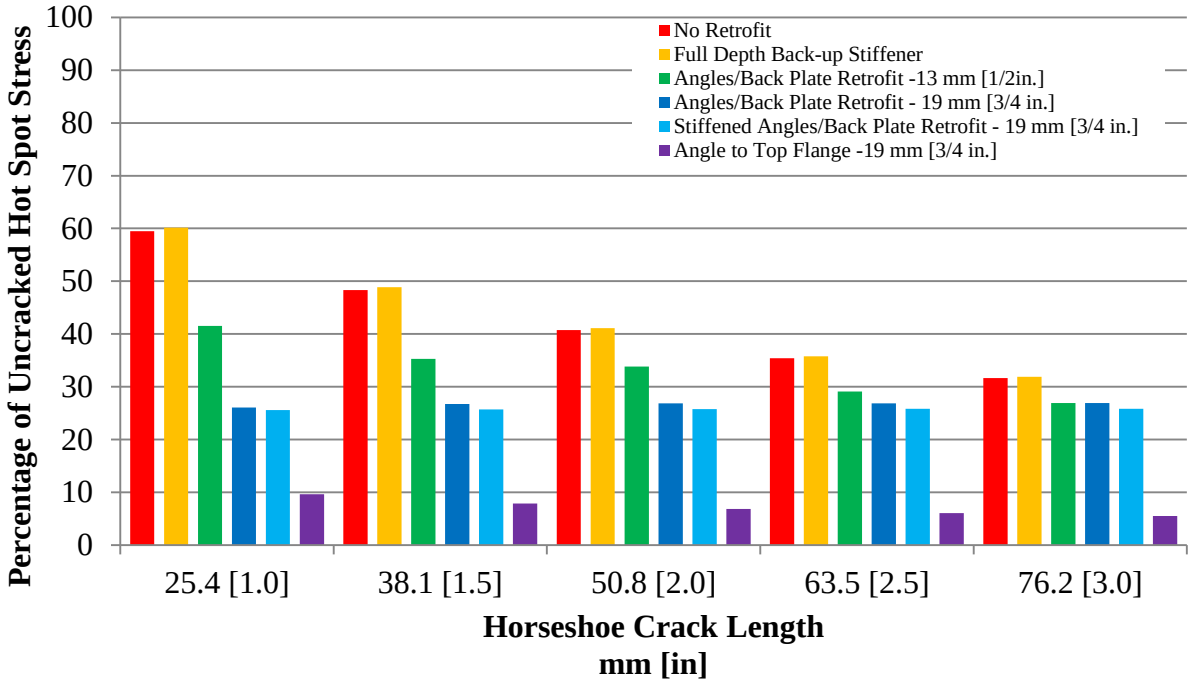

Figure D. 7: Retrofit performance at flange-web weld based on percentage of uncracked hot spot stress due to change in horseshoe crack length in the South Girder.

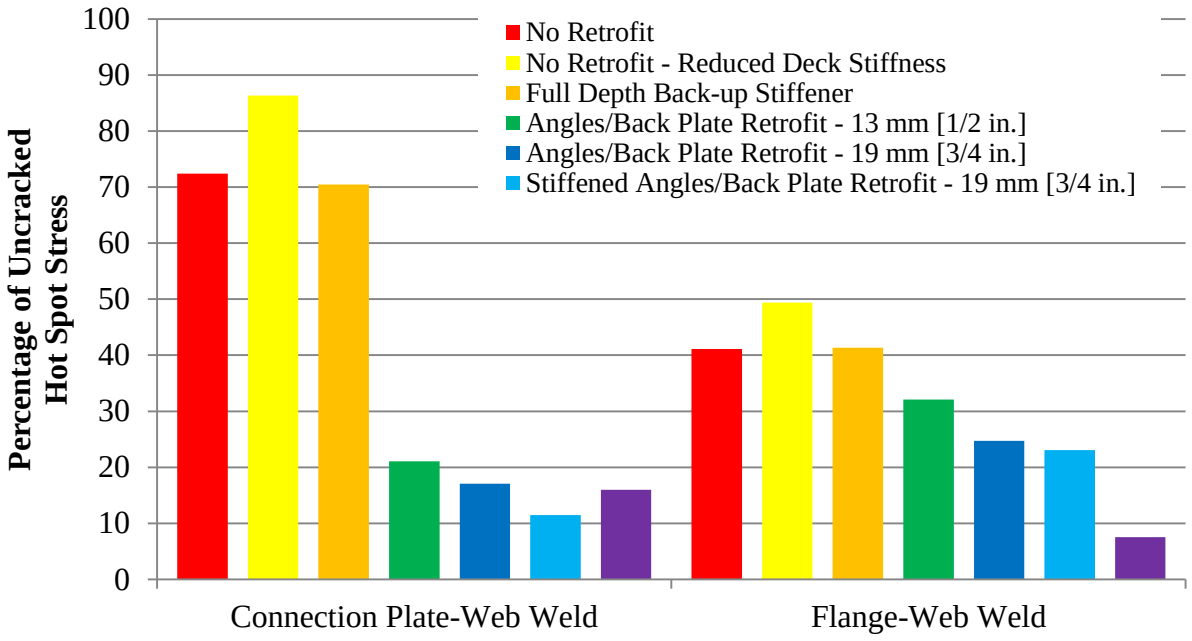

Figure D. 8: Effect of reduced deck thickness and retrofit performance based on percentage of uncracked hot spot stress in North Girder for 51 mm [2 in.] horseshoe crack length.

BROKEN CROSS FRAME MODEL

When the cross frame element framing into the top web-gap of the north girder broke, significant finite element analysis was performed and the following data was determined:

Table D. 3: Cross Frame Element Data

	Angles-and-Plate 19 mm [3/4 in.]			Angles-and-Plate 19 mm [3/4 in.] with Broken Cross Frame Element		
	Maximum Principal	**Horizontal**	**Vertical**	**Maximum Principal**	**Horizontal**	**Vertical**
Inclined Cross Frame Element Framing into North Girder Top Web-Gap	39 [5.7]	28 [4.1]	8 [1.1]	0 [0.0]	0 [0.0]	0 [0.0]
Inclined Cross Frame Element Framing into North Girder Bottom Web-Gap	0 [0.0]	-19 [-2.8]	-6 [-0.9]	0 [0.0]	-23 [-3.4]	-11 [-1.6]
Horizontal Cross Frame Element Framing into North Girder Bottom Web-Gap	29 [4.2]	30 [4.3]	0 [0.0]	41 [6.0]	38 [5.5]	0 [0.0]
Inclined Cross Frame Element Framing into South Girder Top Web-Gap	37 [5.3]	28 [4.1]	7 [1.0]	24 [3.5]	19 [2.7]	5.5 [0.8]
Inclined Cross Frame Element Framing into South Girder Bottom Web-Gap	0 [0.0]	-23 [-3.3]	-6 [-0.9]	0 [0.0]	-19 [-2.8]	-5.5 [-0.8]
Horizontal Cross Frame Element Framing into South Girder Bottom Web-Gap	29 [3.9]	29 [4.2]	0 [0.0]	24 [3.5]	24 [3.5]	0 [0.0]

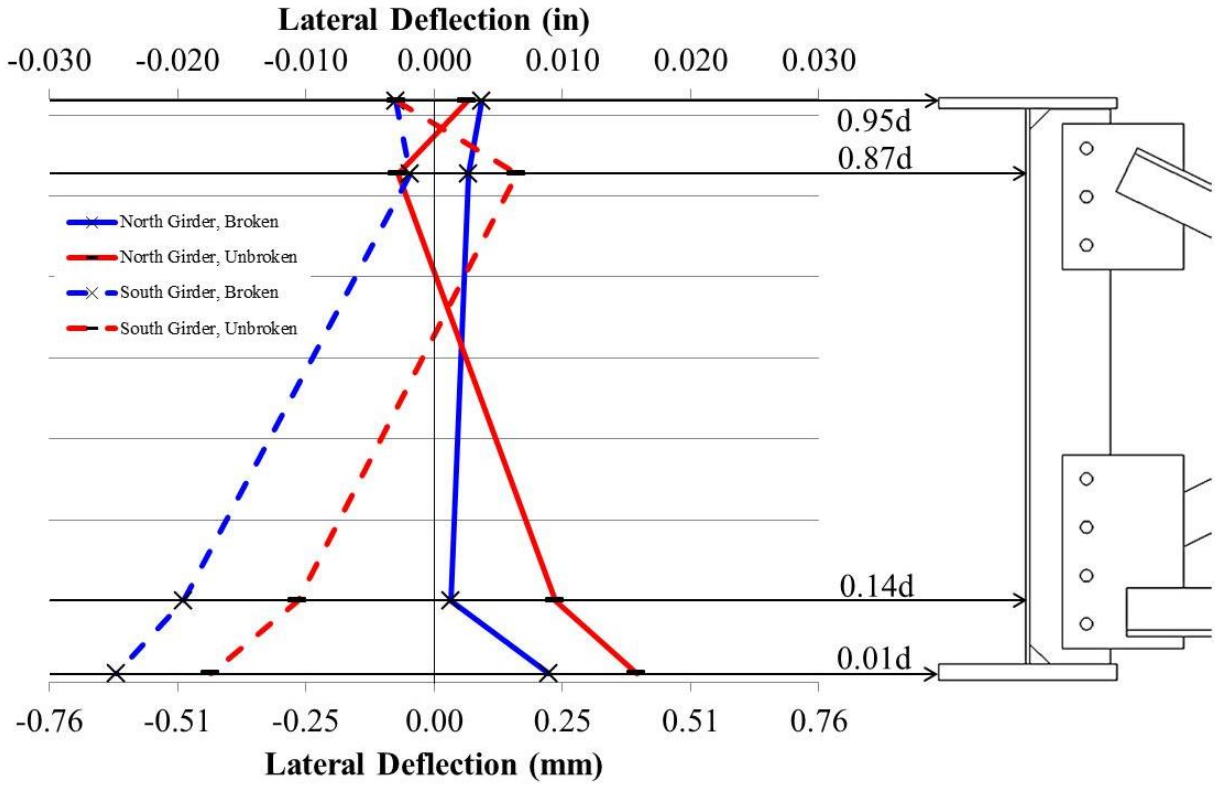

Figure D. 9: Lateral girder deflection with and without broken cross frame element

Table D. 4: Hot Spot Stresses for Unbroken and Broken Cross Frame Models

	Angles-and-Plate 19 mm [3/4 in.]	Angles-and-Plate 19 mm [3/4 in.] with Broken Cross Frame Element
North Girder Top Web-Gap Connection Plate-Web Weld	71 [10.3]	29 [4.2]
North Girder Top Web-Gap Flange-Web Weld	101 [14.6]	37 [5.4]
North Girder Bottom Web-Gap Connection Plate-Web Weld	92 [13.4]	191 [27.7]
North Girder Bottom Web-Gap Flange-Web Weld	38 [5.5]	77 [11.1]
South Girder Top Web-Gap Connection Plate-Web Weld	52 [7.6]	60 [8.7]
South Girder Top Web-Gap Flange-Web Weld	102 [14.8]	66 [9.6]
South Girder Bottom Web-Gap Connection Plate-Web Weld	97 [14.1]	56 [8.1]
South Girder Bottom Web-Gap Flange-Web Weld	41 [5.9]	25 [3.6]

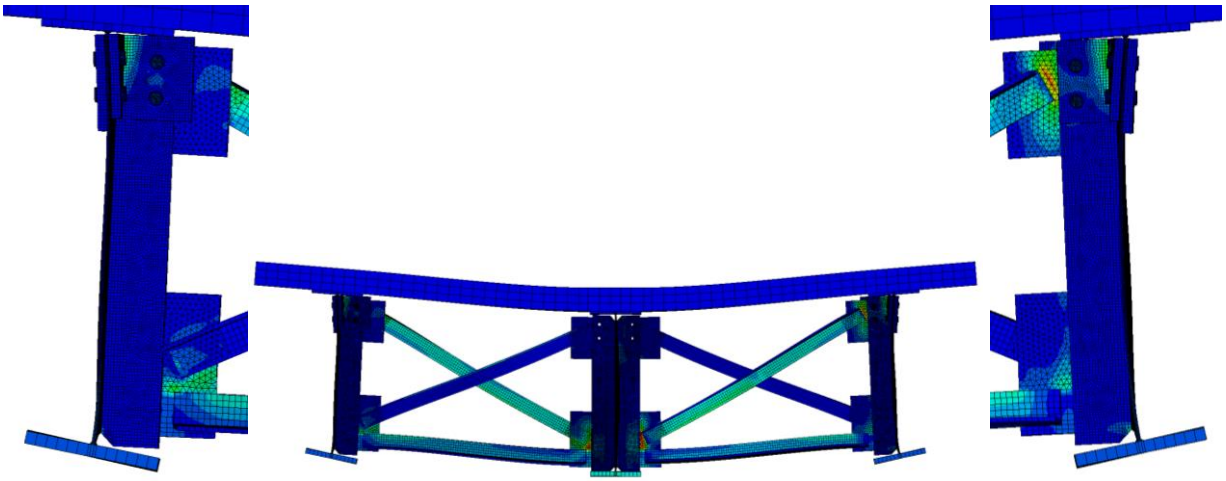

(a)

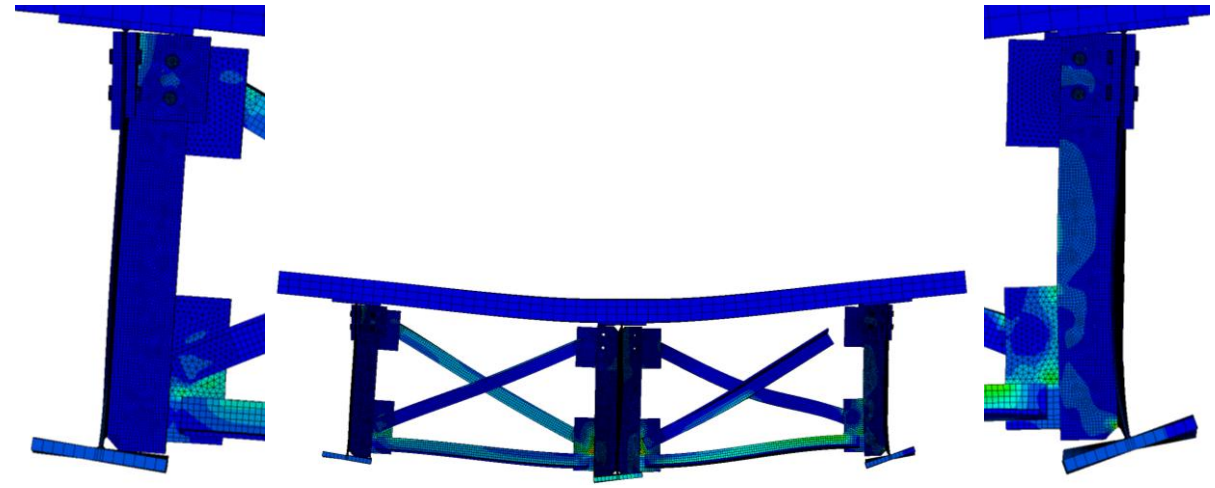

(b)

Figure D. 10: Deflected shapes for unbroken and broken cross frame models.

SCREEN SHOTS

Table D. 5: Uncracked, Unretrofitted Model

BaseModelNoCracks-60k		
	Interior	**Fascia**
South Girder	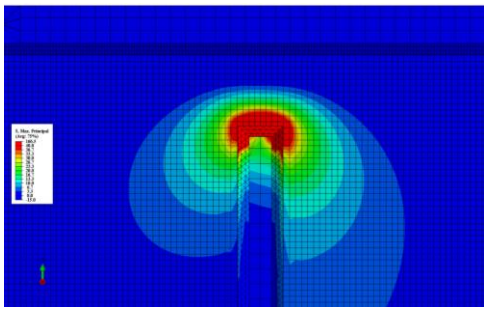	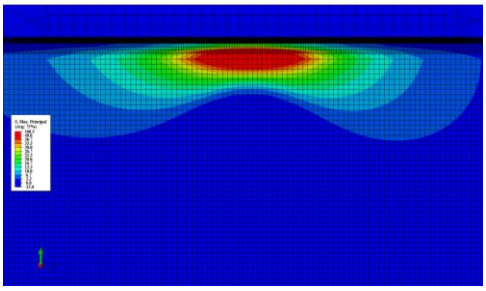
	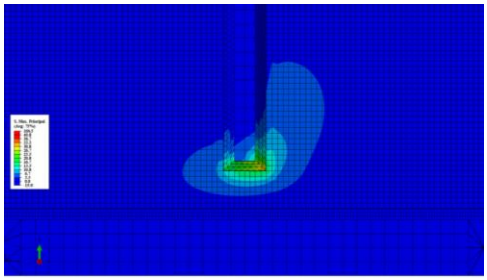	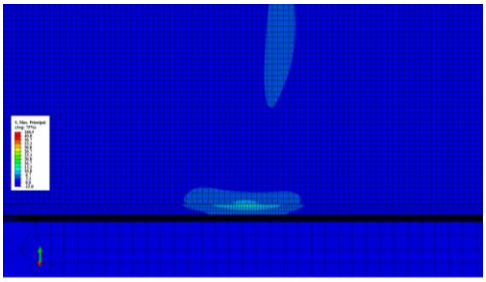
North Girder	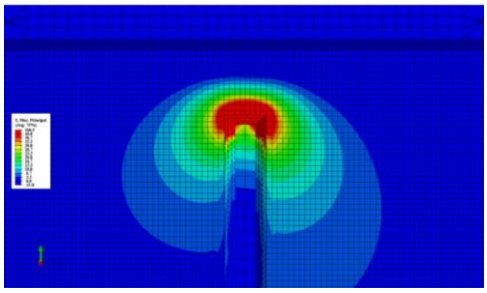	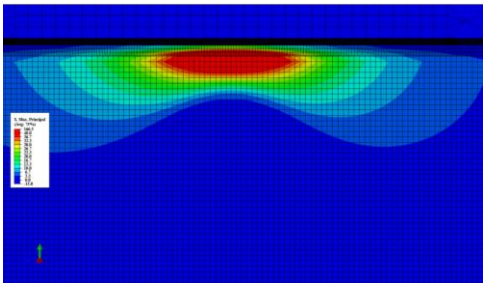
	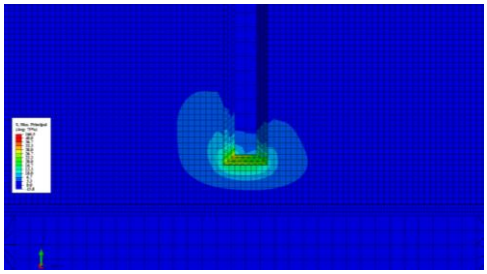	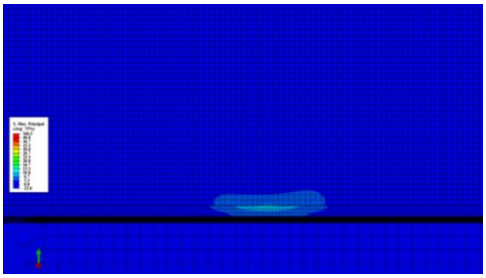

Table D. 6: 1 in. Horseshoe Crack, Unretrofitted Model

	BaseModelUCracks1in-60k	
	Interior	**Fascia**
South Girder	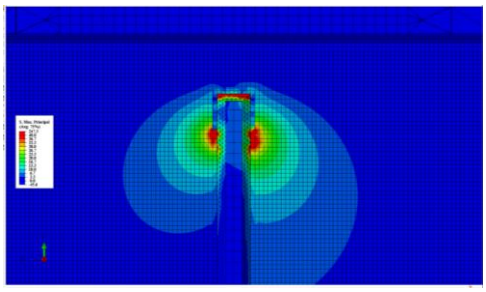	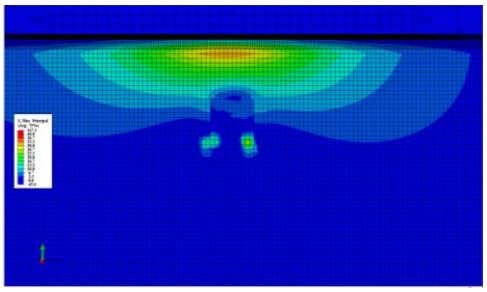
	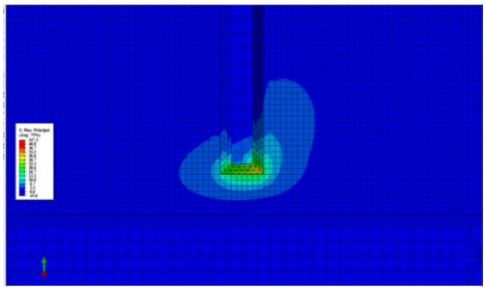	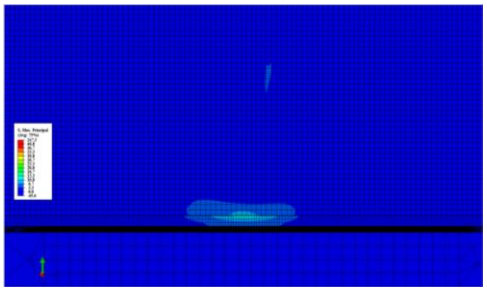
North Girder	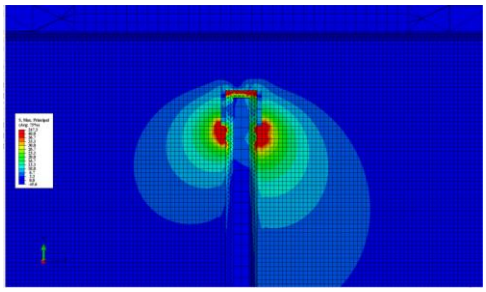	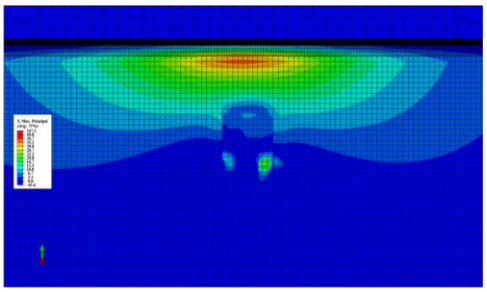
	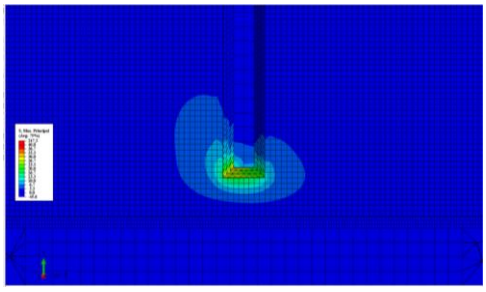	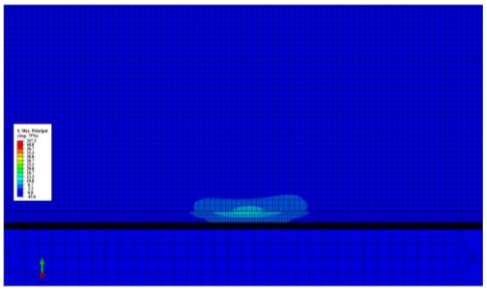

Table D. 7: 1.5 in. Horseshoe Crack, Unretrofitted Model

BaseModelUCracks1point5in-60k		
	Interior	**Fascia**
South Girder	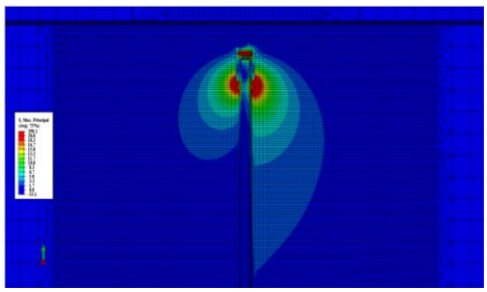	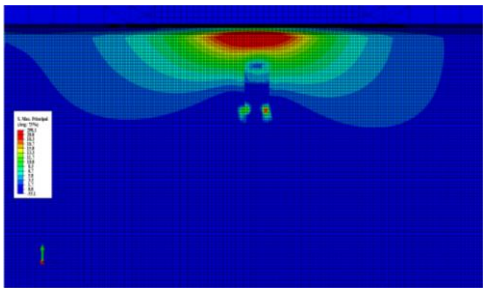
	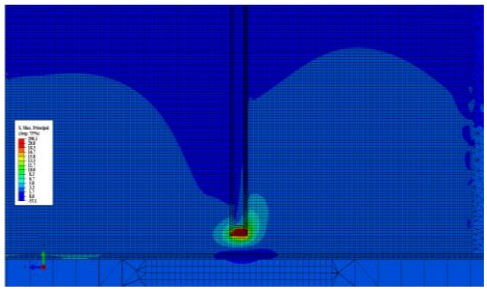	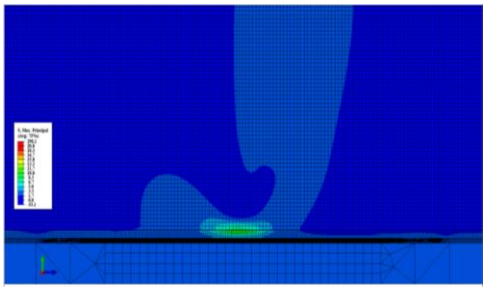
North Girder	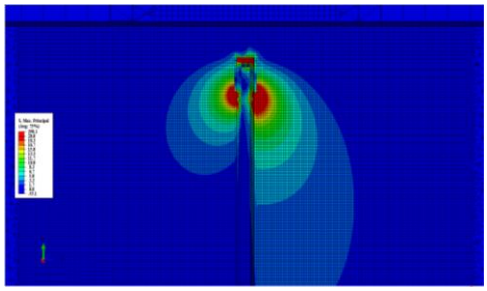	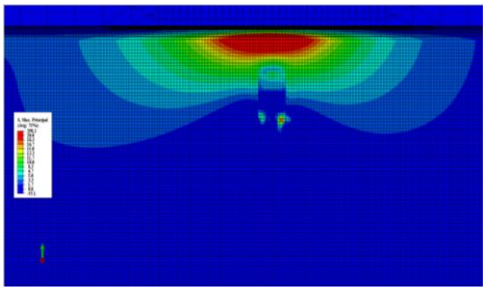
	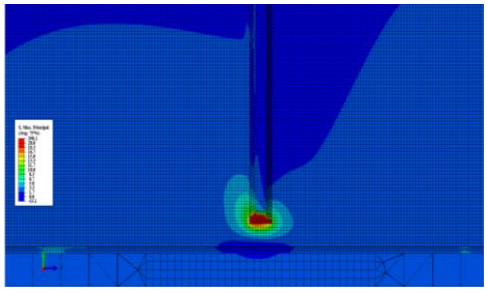	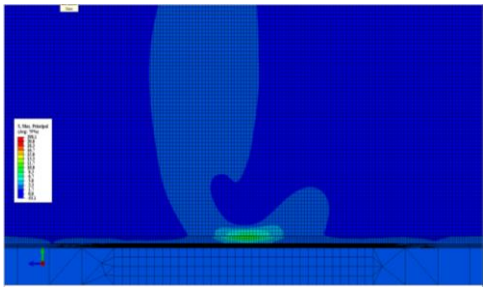

Table D. 8: 2 in. Horseshoe Crack, Unretrofitted Model

	BaseModelUCracks2in-60k	
	Interior	**Fascia**
South Girder	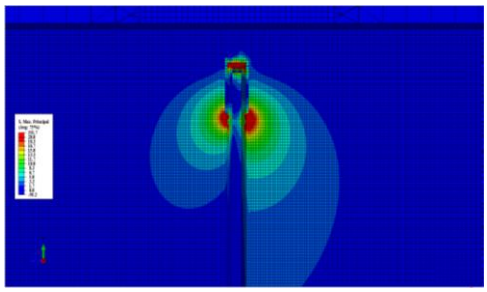	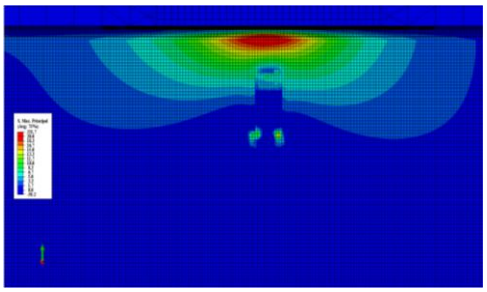
	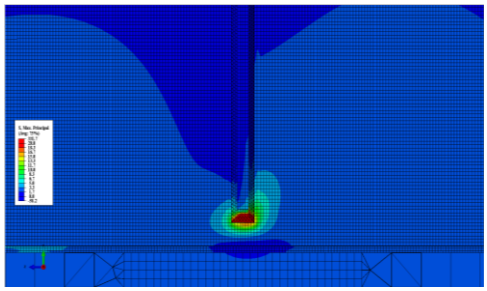	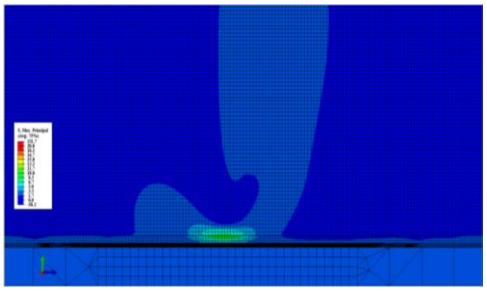
North Girder	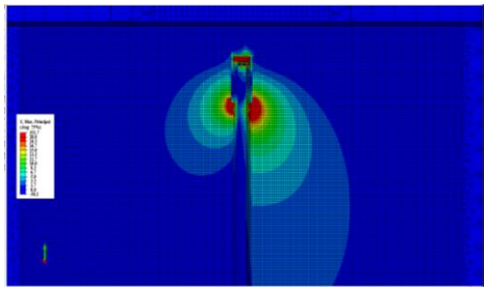	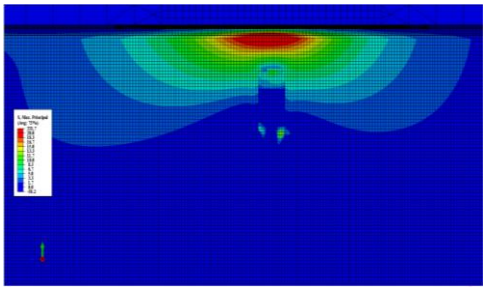
	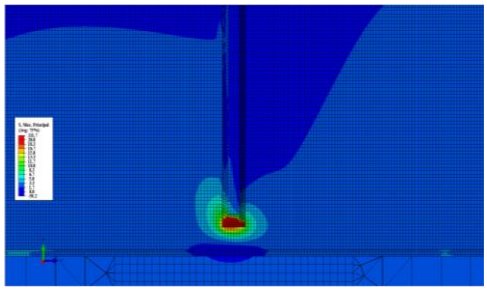	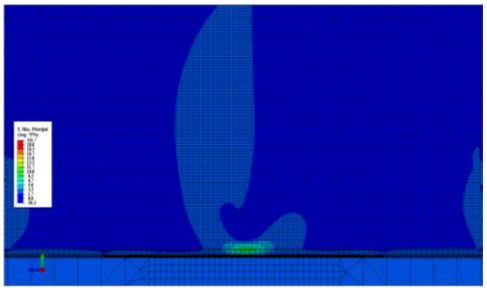

Table D. 9: 2.5 in. Horseshoe Crack, Unretrofitted Model

BaseModelUCracks2point5in-60k		
	Interior	**Fascia**
South Girder	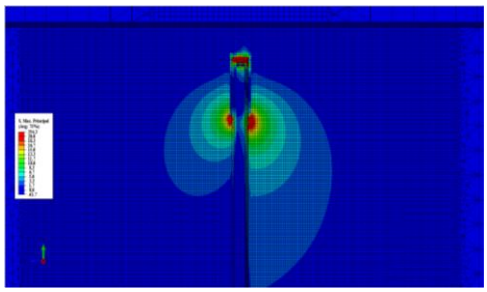	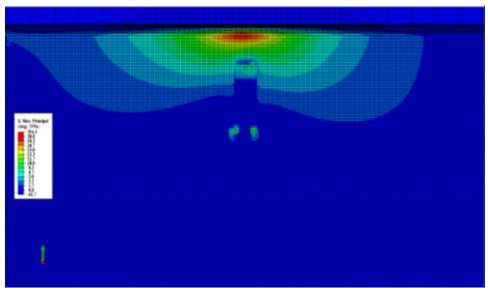
	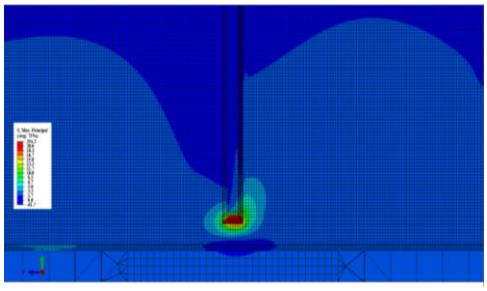	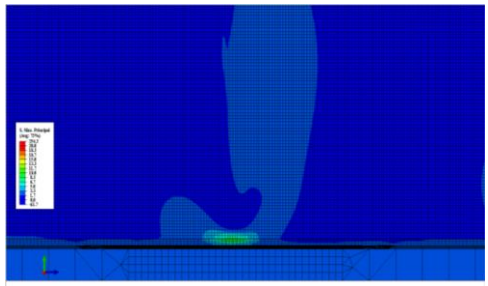
North Girder	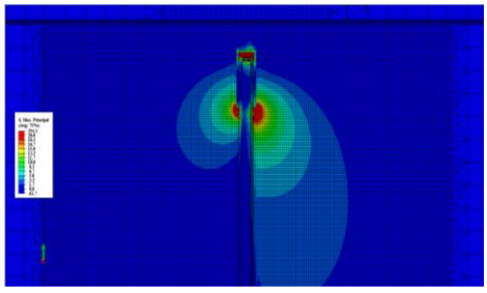	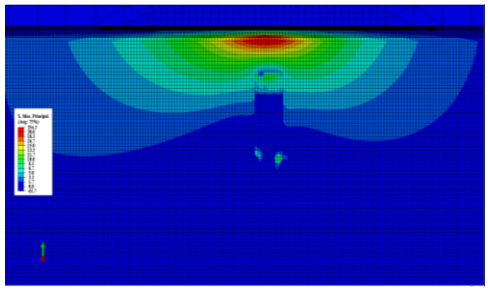
	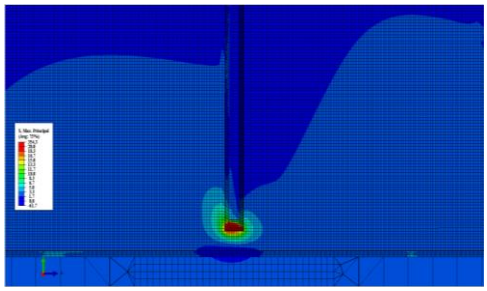	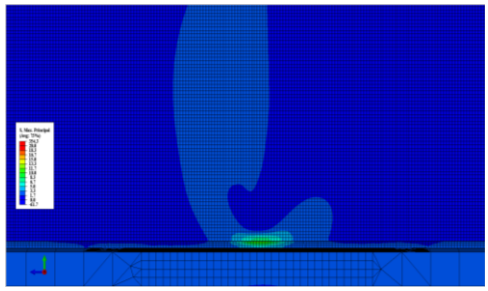

Table D. 10: 3 in. Horseshoe Crack, Unretrofitted Model

	BaseModelUCracks3in-60k	
	Interior	**Fascia**
South Girder	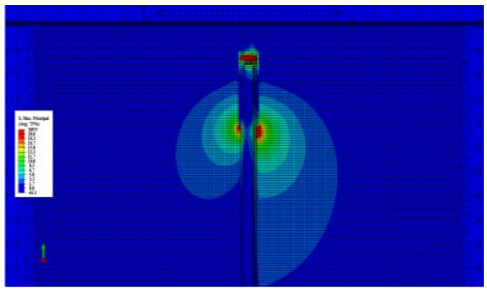	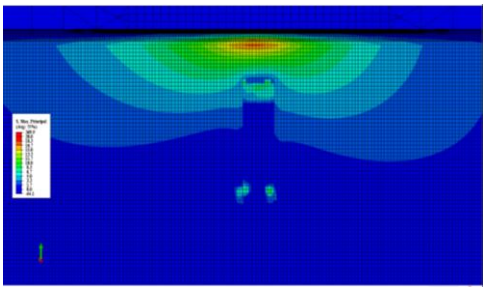
	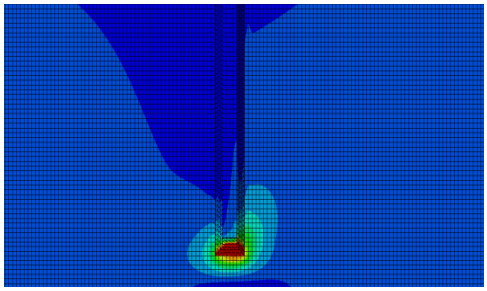	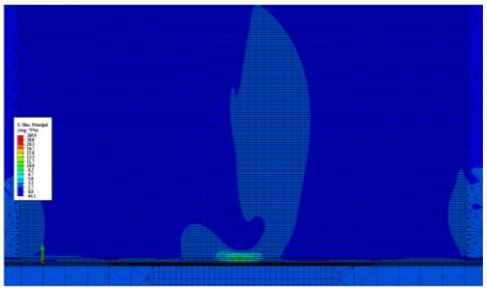
North Girder	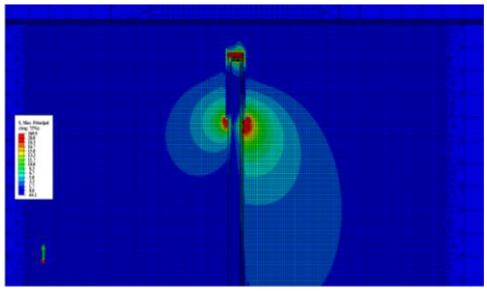	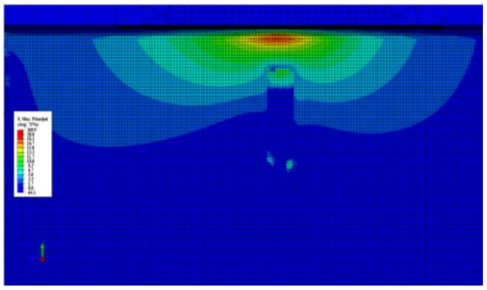
	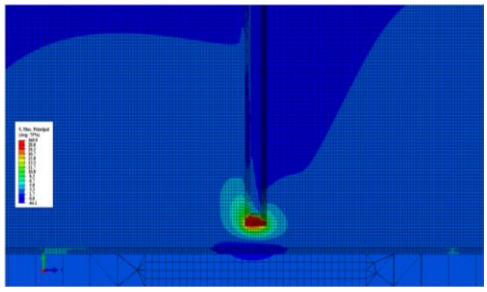	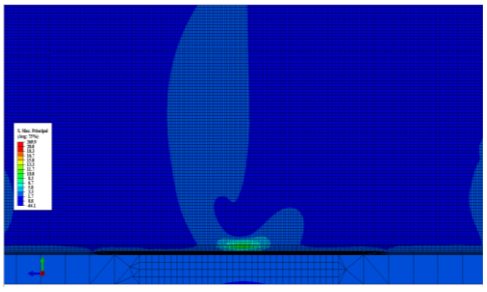

Table D. 11: 4 in. Horseshoe Crack, Unretrofitted Model

	BaseModelUCracks4in-60k	
	Interior	**Fascia**
South Girder	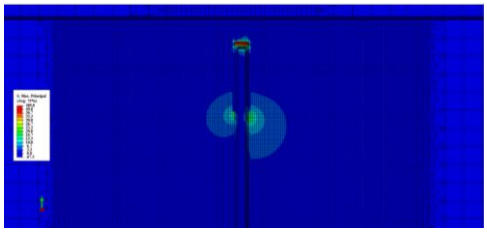	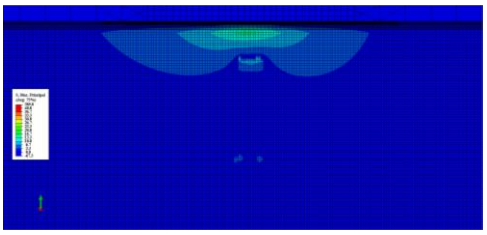
	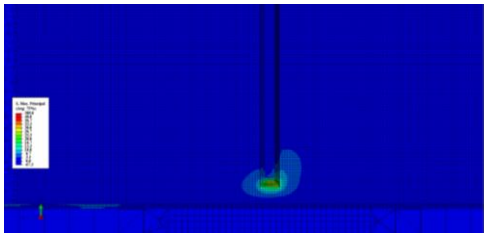	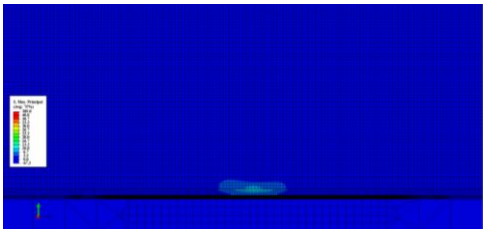
North Girder	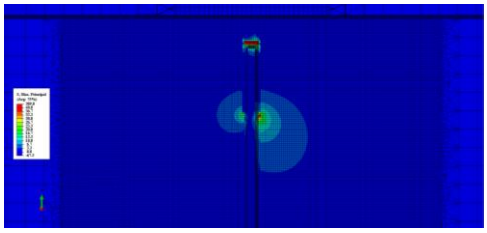	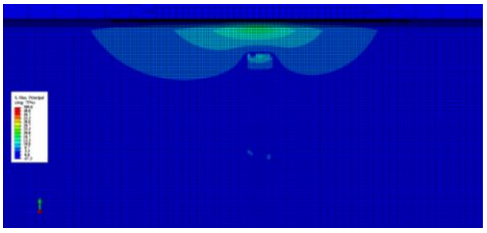
	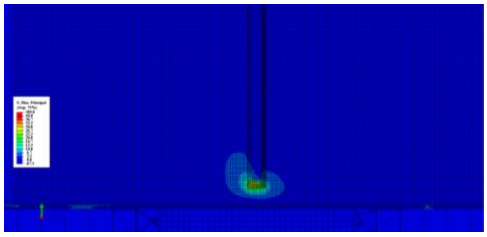	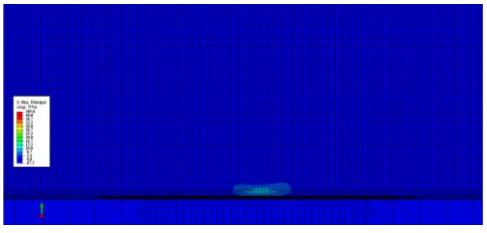

Table D. 12: 8 in. Horseshoe Crack, Unretrofitted Model

	BaseModelUCracks8in-60k	
	Interior	**Fascia**
South Girder	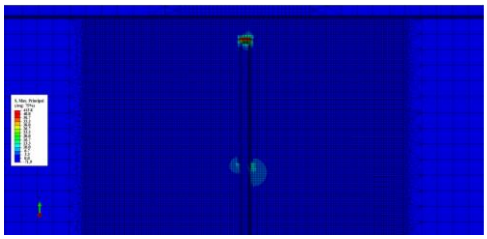	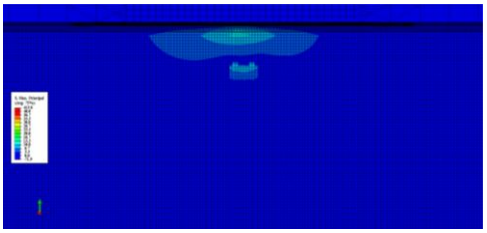
	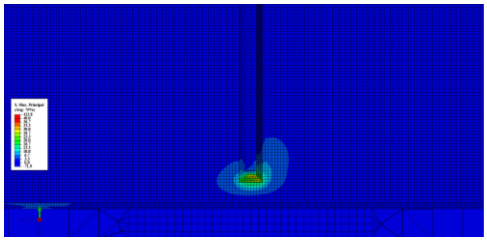	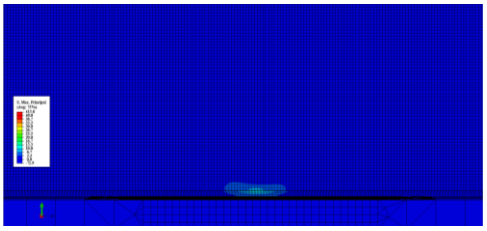
North Girder	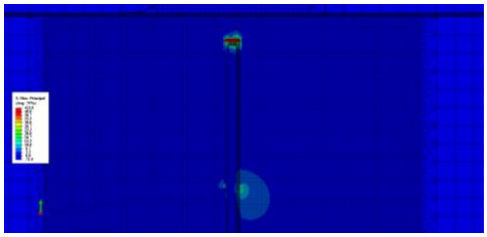	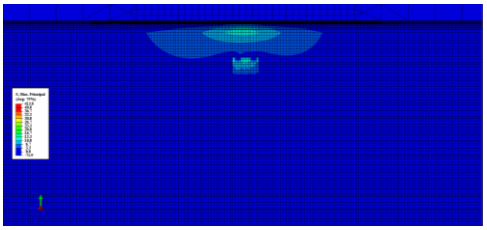
	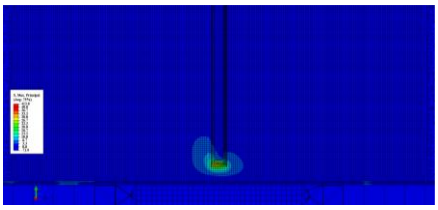	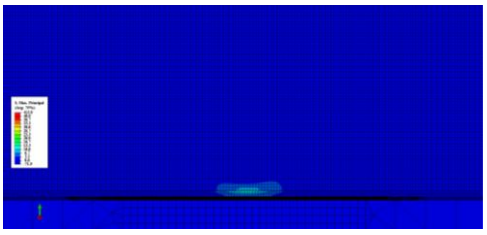

Table D. 13: 1 in. Horseshoe Crack, Retrofit1 Model

BaseModelUCracks1inRet1BoltsNoHC-60kRS		
	Interior	**Fascia**
South Girder	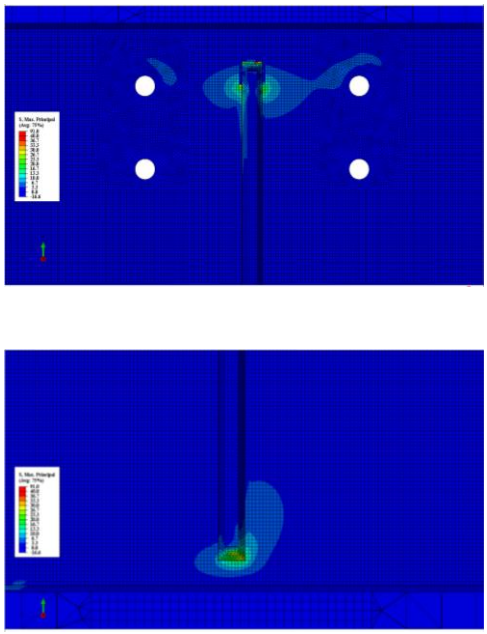	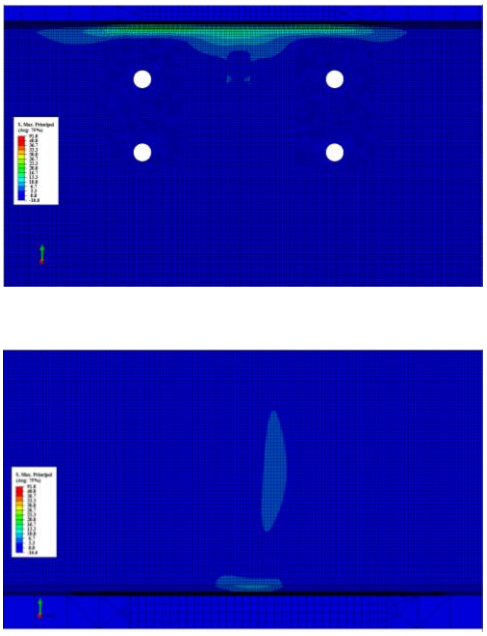
North Girder	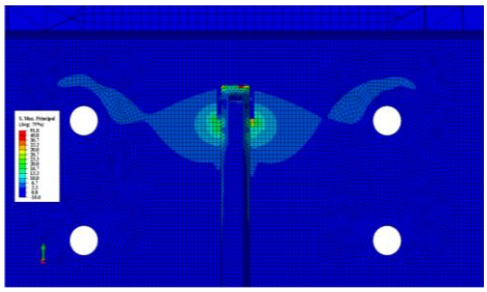	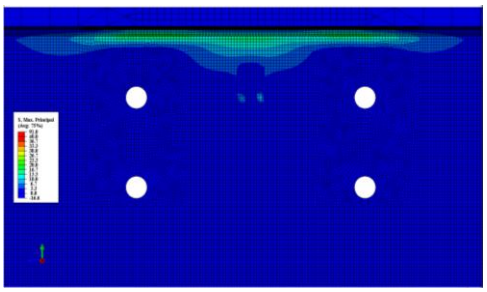
	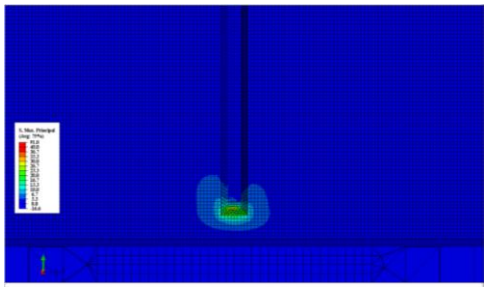	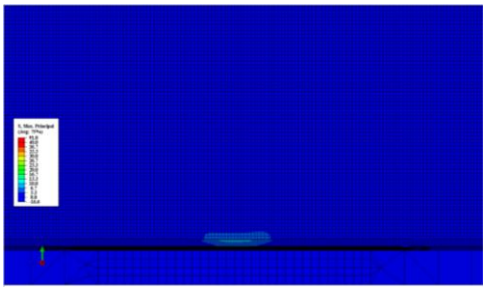

Table D. 14: 1.5 in. Horseshoe Crack, Retrofit1 Model

BaseModelUCracks1p5inRet1Bolts-60k		
	Interior	**Fascia**
South Girder	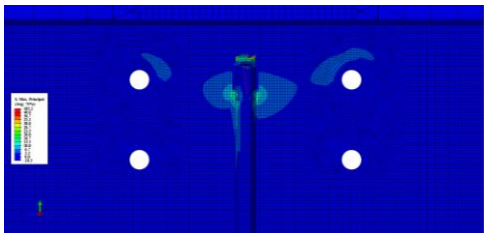	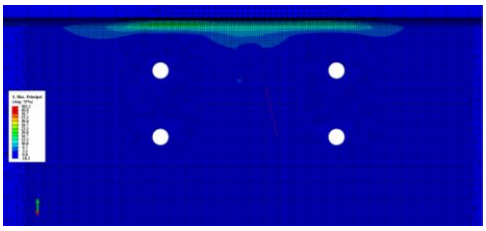
	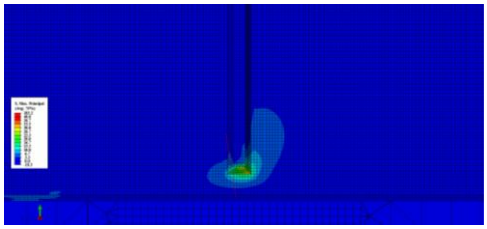	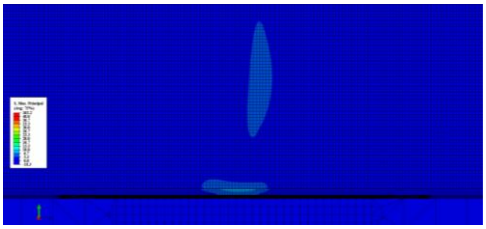
North Girder	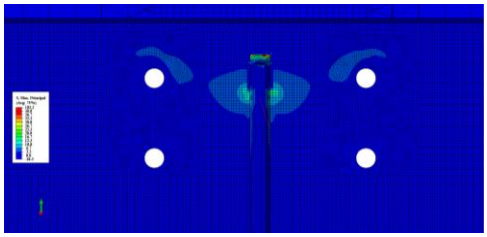	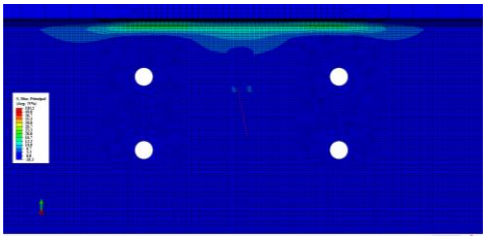
	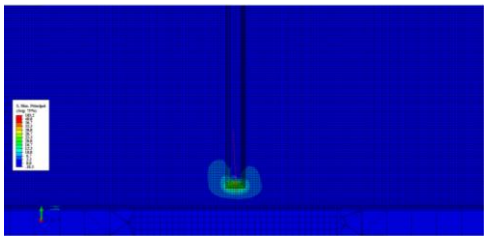	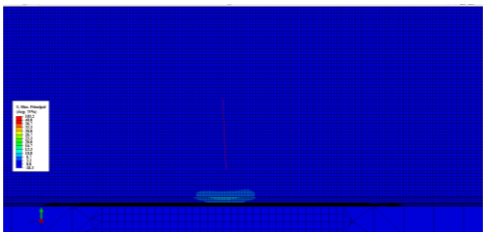

Table D. 15: 2 in. Horseshoe Crack, Retrofit1 Model

	BaseModelUCracks2inRet1Bolts-60k	
	Interior	**Fascia**
South Girder	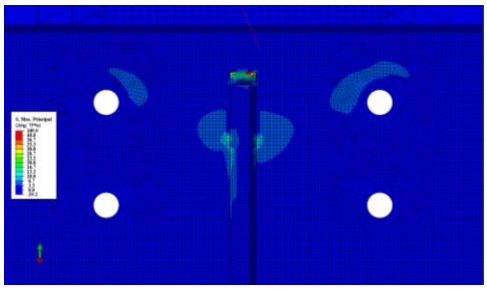	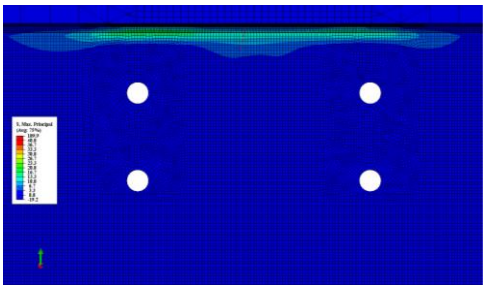
	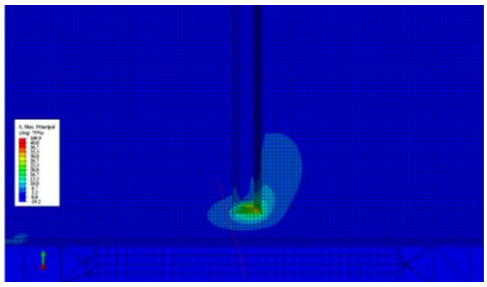	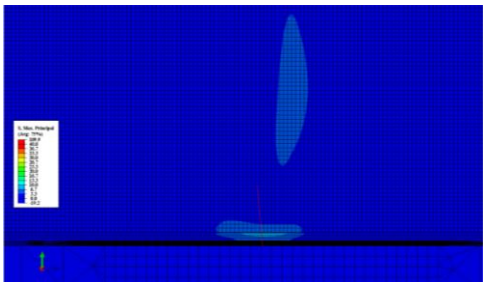
North Girder	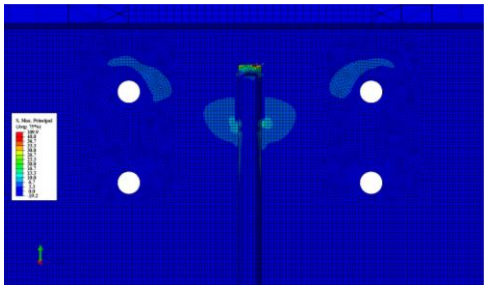	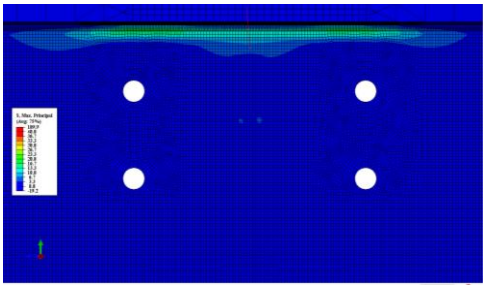
	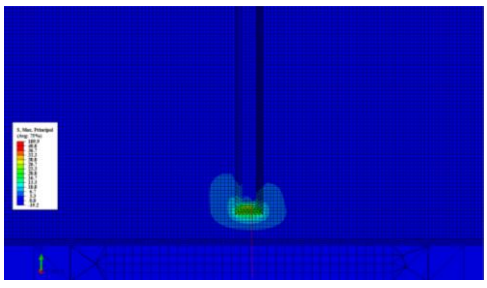	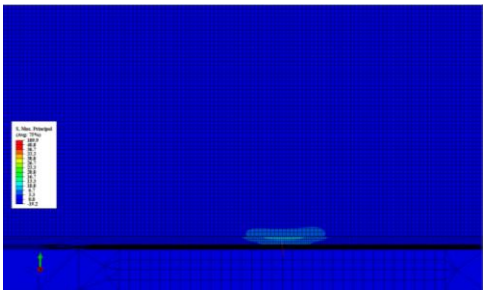

Table D. 16: 2.5 in. Horseshoe Crack, Retrofit1 Model

BaseModelUCracks2p5inRet1Bolts-60k		
	Interior	**Fascia**
South Girder	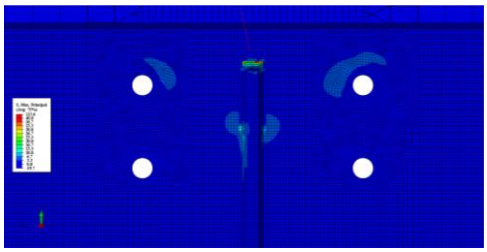	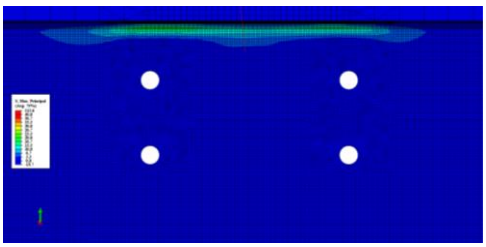
	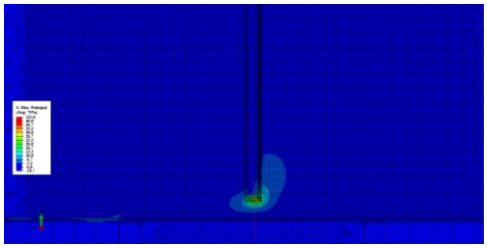	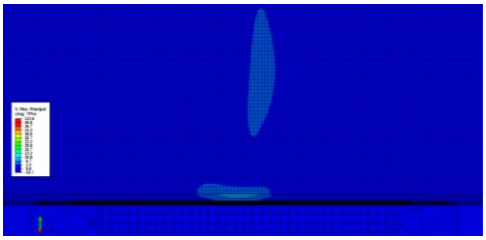
North Girder	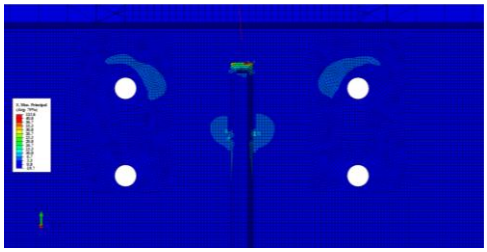	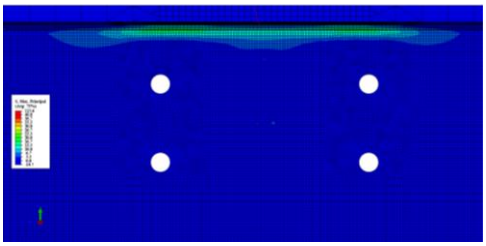
	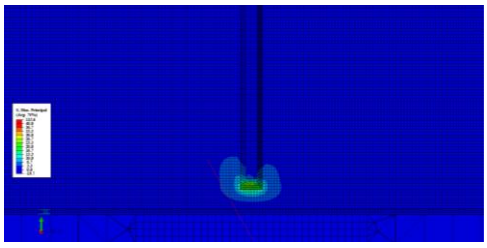	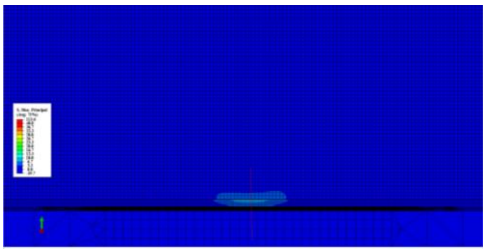

Table D. 17: 3 in. Horseshoe Crack, Retrofit1 Model

BaseModelUCracks3inRet1Bolts-60k		
	Interior	**Fascia**
South Girder	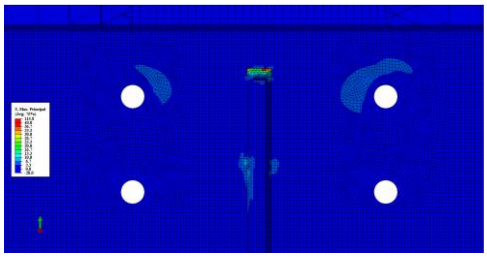	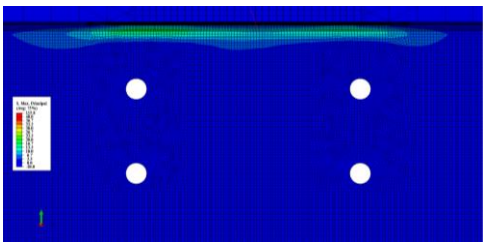
	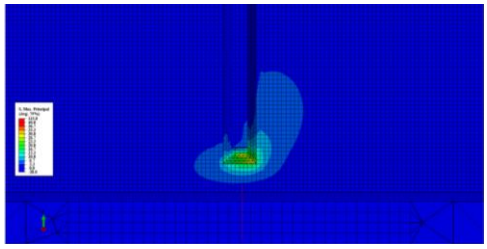	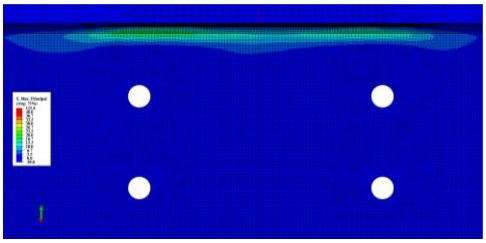
North Girder	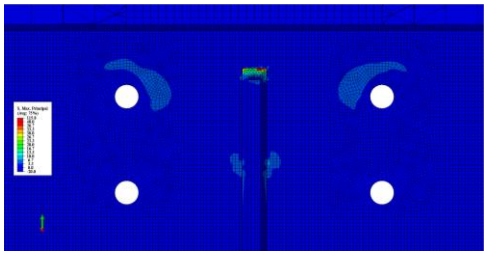	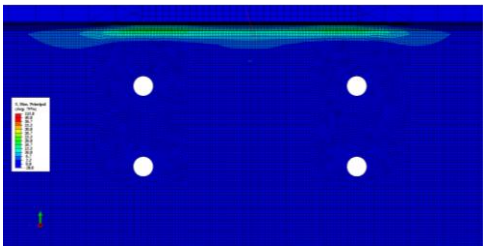
	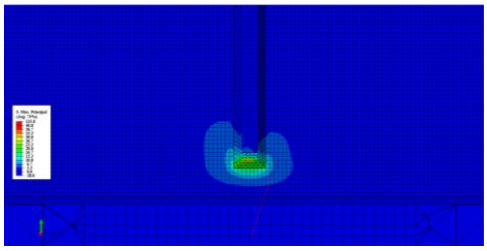	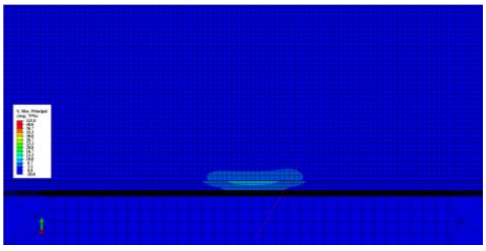

Table D. 18: 1 in. Horseshoe Crack, Retrofit1 Model ½' Thickness

UCracks1inRet1-pt5-Bolts-60k		
	Interior	**Fascia**
South Girder	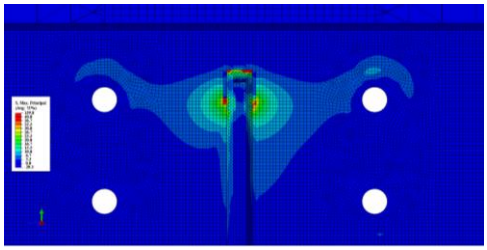	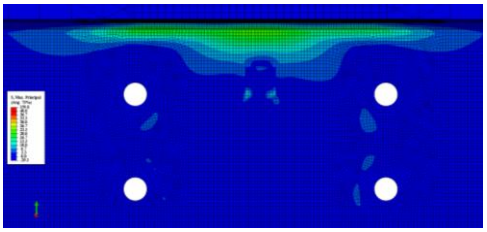
	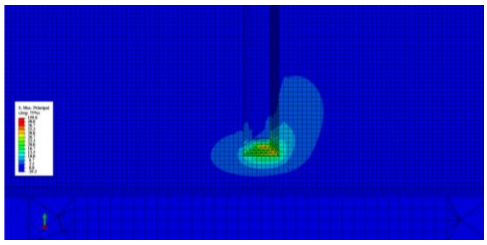	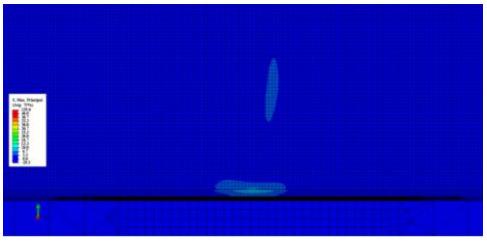
North Girder	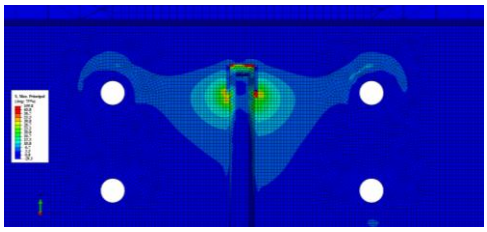	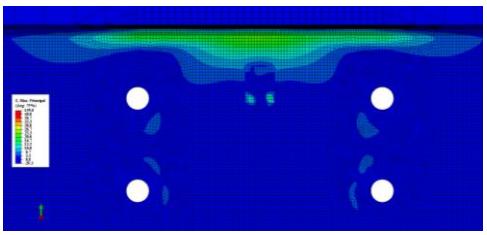
	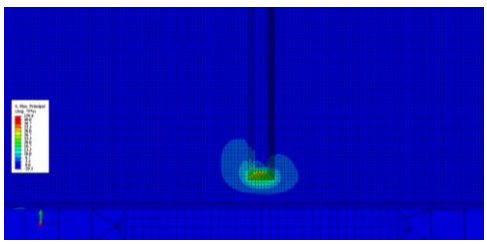	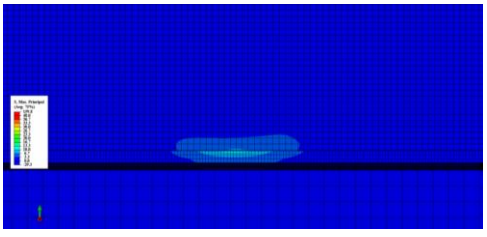

Table D. 19: 1.5 in. Horseshoe Crack, Retrofit1 Model ½' Thickness

UCracks1point5inRet1-pt5-Bolts-60k		
	Interior	**Fascia**
South Girder	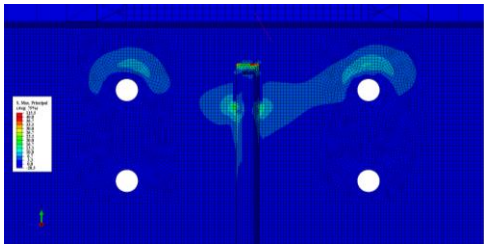	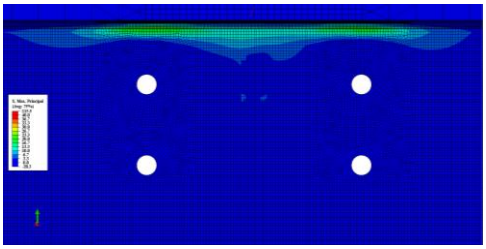
	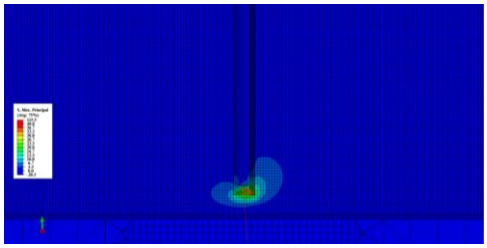	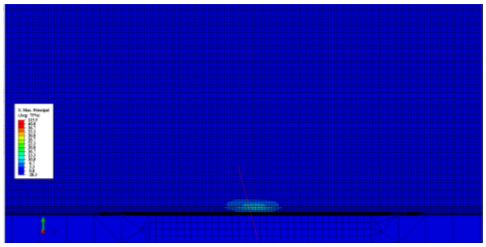
North Girder	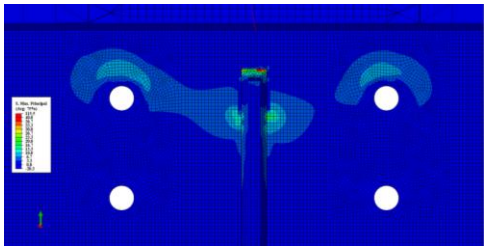	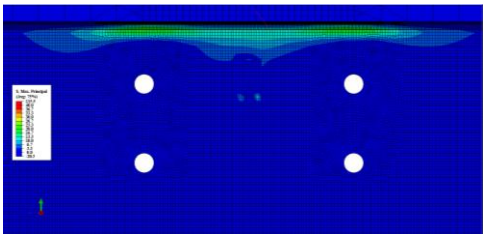
	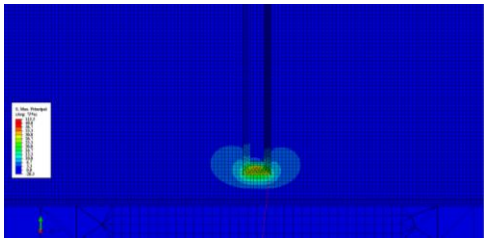	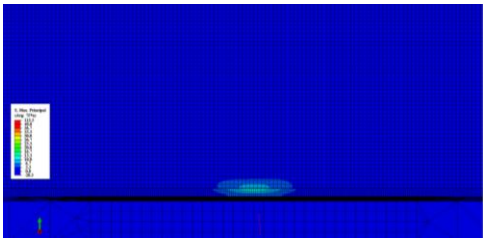

Table D. 20: 2 in. Horseshoe Crack, Retrofit1 Model ½' Thickness

UCracks2inRet1-pt5-Bolts-60k		
	Interior	**Fascia**
South Girder	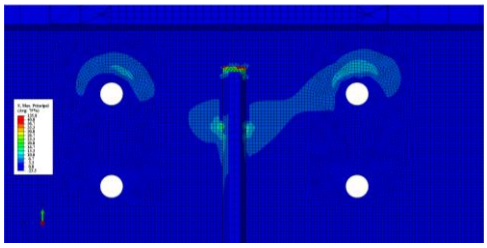	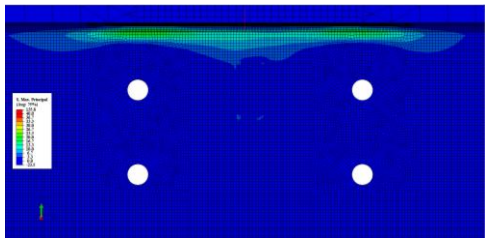
	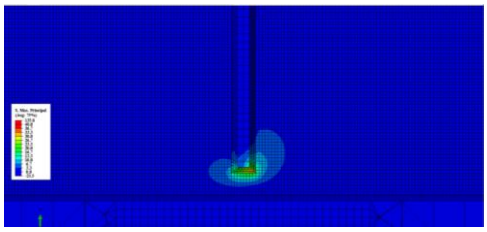	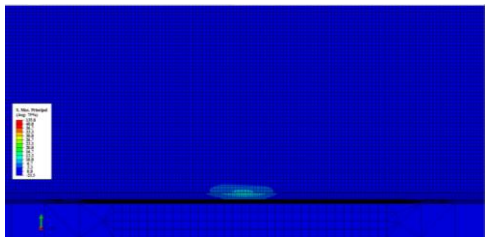
North Girder	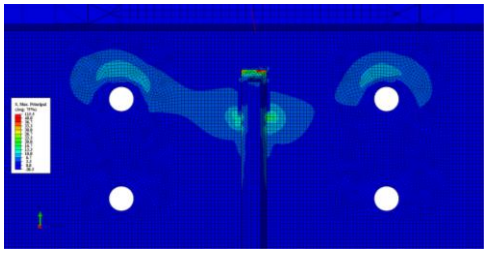	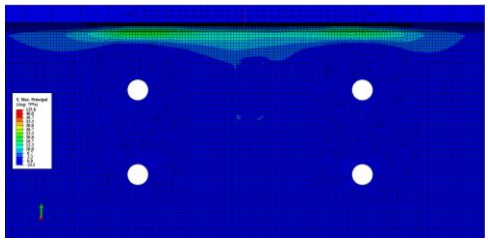
	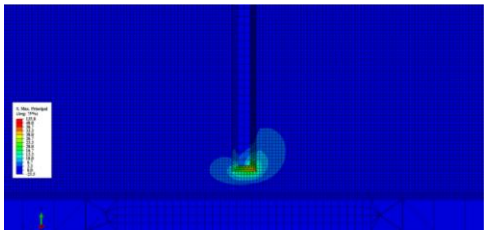	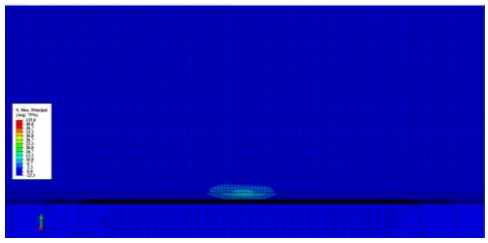

Table D. 21: 2.5 in. Horseshoe Crack, Retrofit1 Model ½' Thickness

UCracks2point5inRet1-pt5-Bolts-60k		
	Interior	**Fascia**
South Girder	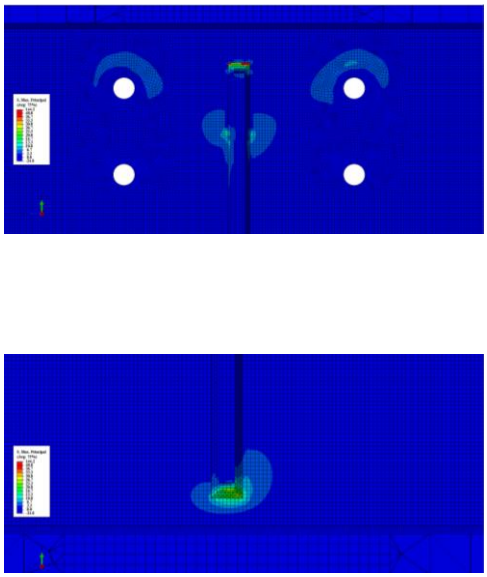	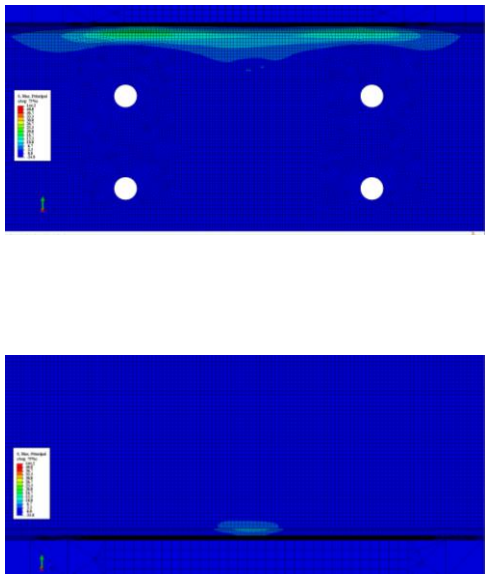
North Girder	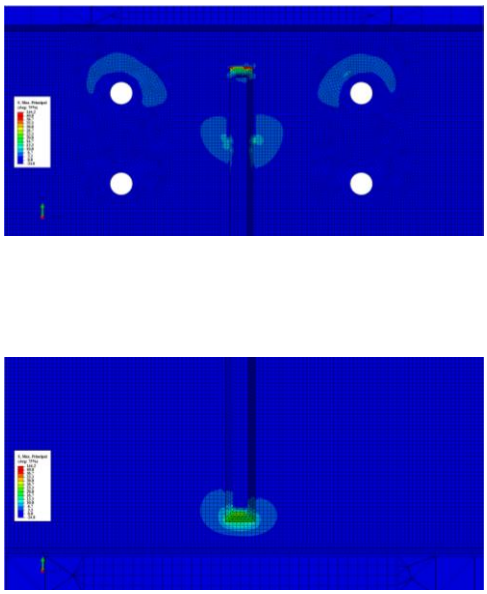	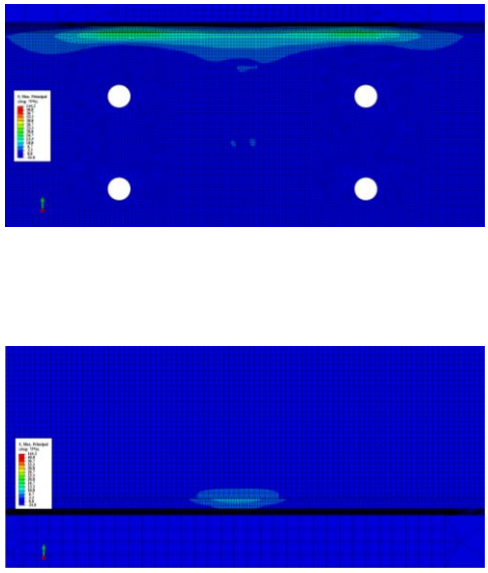

Table D. 22: 3 in. Horseshoe Crack, Retrofit1 Model ½' Thickness

Uncracked, Unretrofitted Model (UCracks3inRet1-pt5-Bolts-60k)		
	Interior	**Fascia**
South Girder	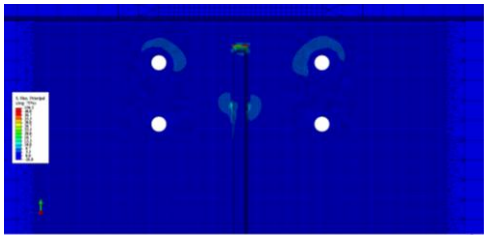	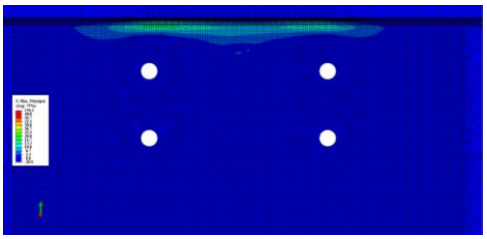
	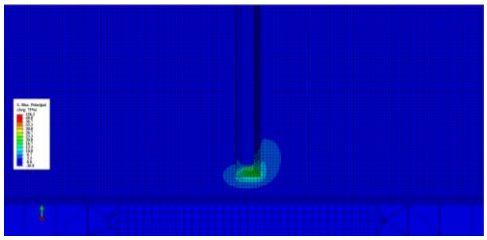	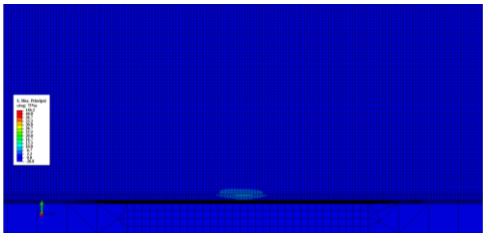
North Girder	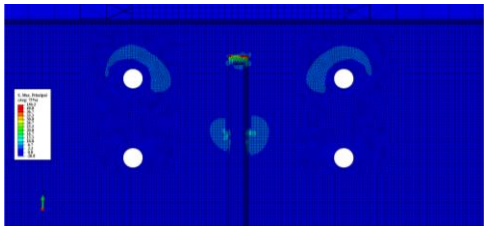	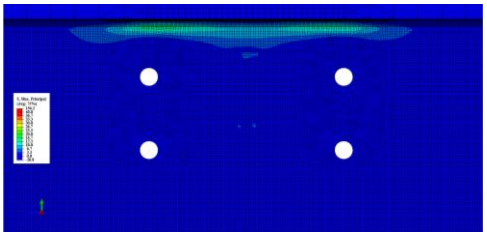
	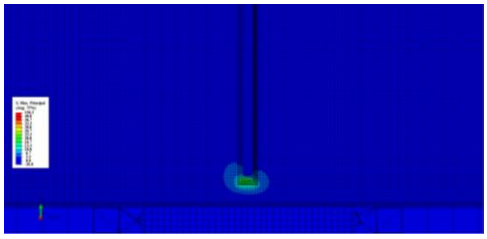	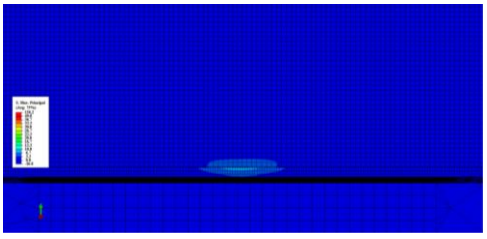

Table D. 23: 1 in. Horseshoe Crack, Retrofit1 Model with Stiffened Angles

UCracks1inRet1Stiffeners-60k		
	Interior	**Fascia**
South Girder	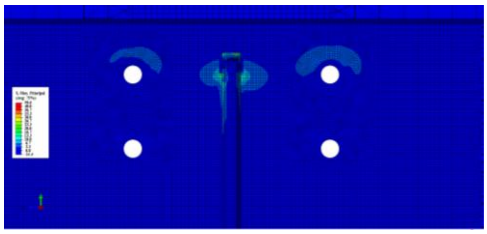	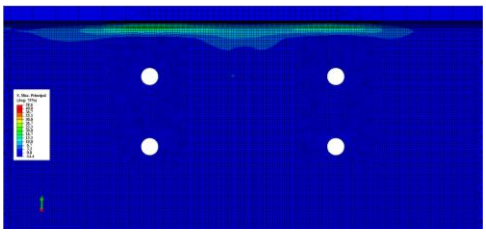
	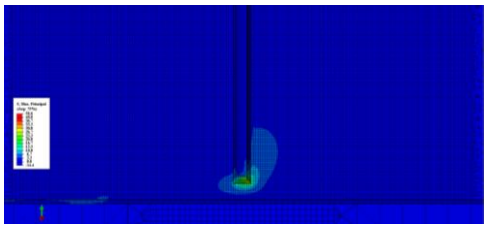	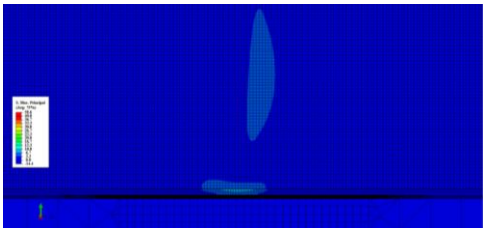
North Girder	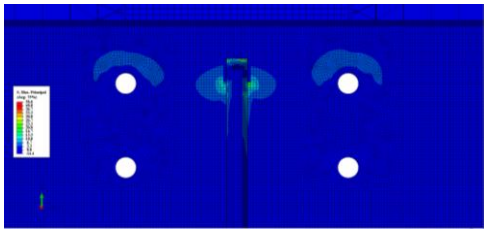	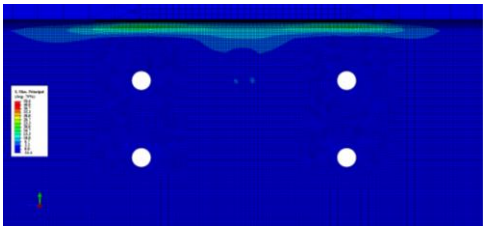
	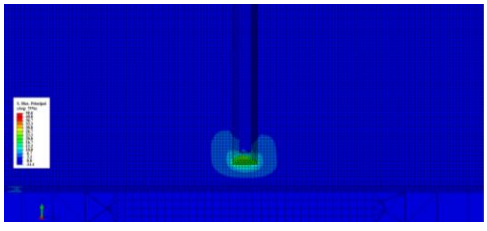	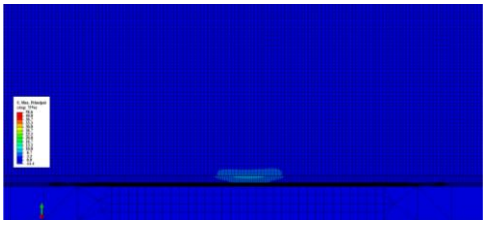

Table D. 24: 1.5 in. Horseshoe Crack, Retrofit1 Model with Stiffened Angles

UCracks1point5inRet1Stiffeners-60k		
	Interior	**Fascia**
South Girder	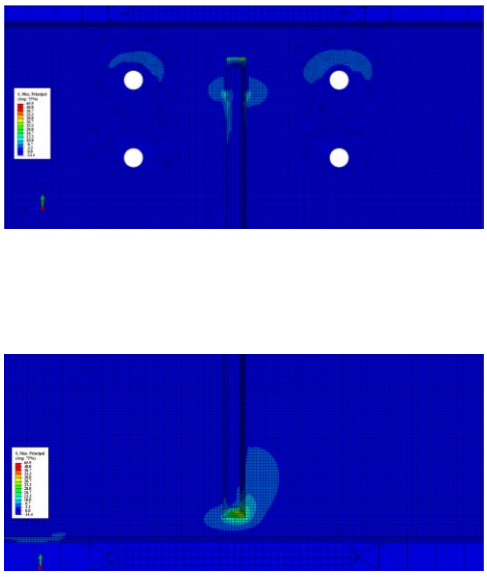	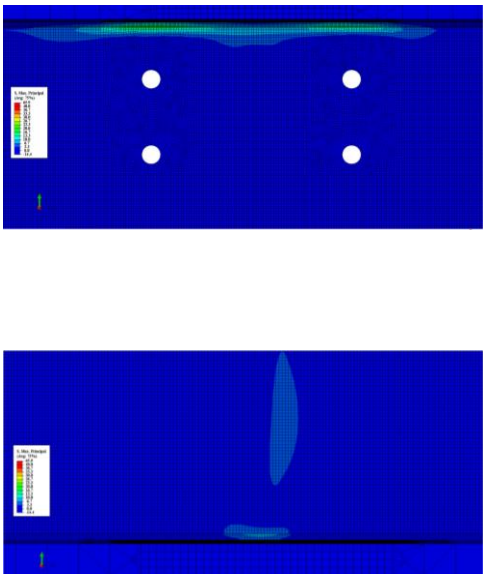
North Girder	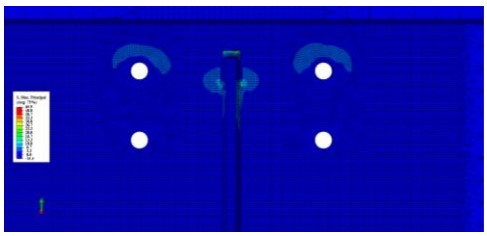	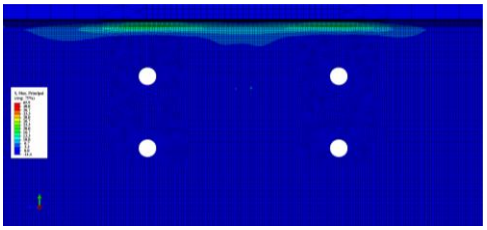
	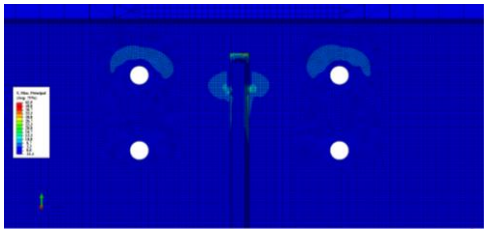	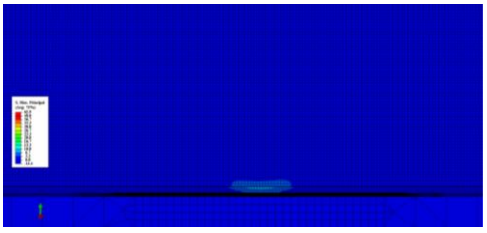

Table D. 25: 2 in. Horseshoe Crack, Retrofit1 Model with Stiffened Angles

UCracks2inRet1Stiffeners-60k		
	Interior	**Fascia**
South Girder	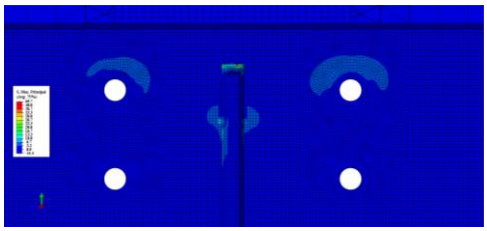	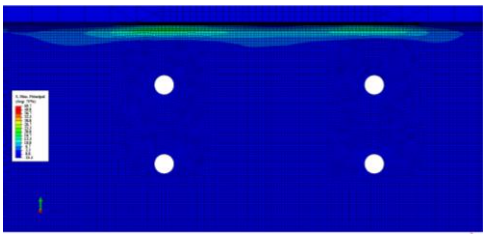
	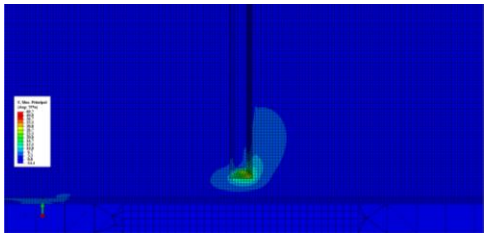	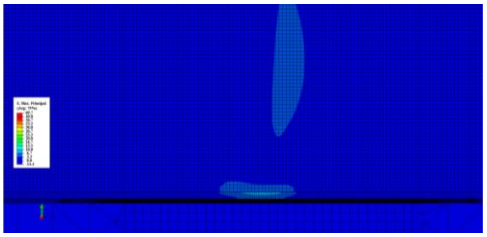
North Girder	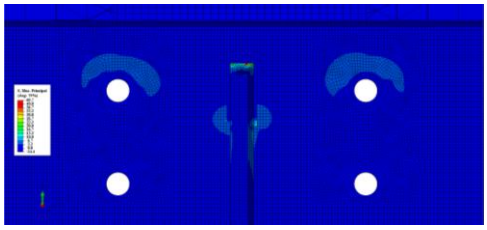	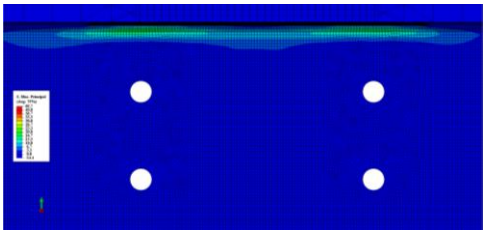
	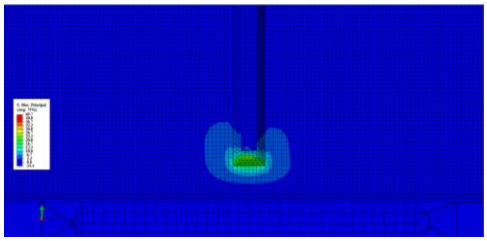	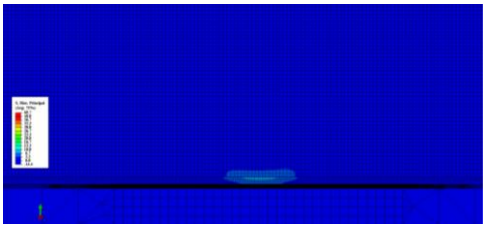

Table D. 26: 2.5 in. Horseshoe Crack, Retrofit1 Model with Stiffened Angles

UCracks2point5inRet1Stiffeners-60k		
	Interior	**Fascia**
South Girder	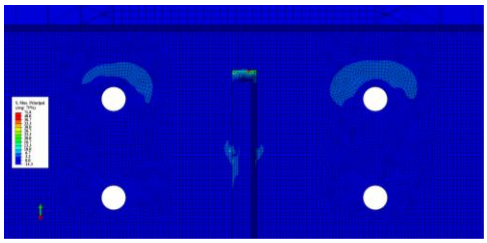	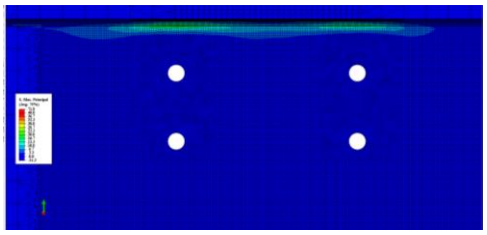
	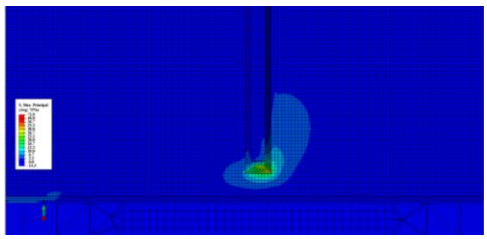	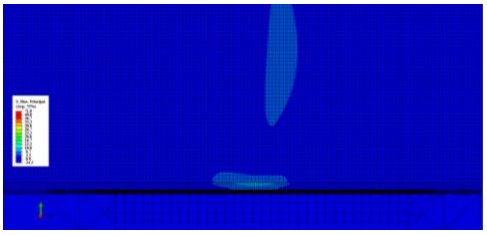
North Girder	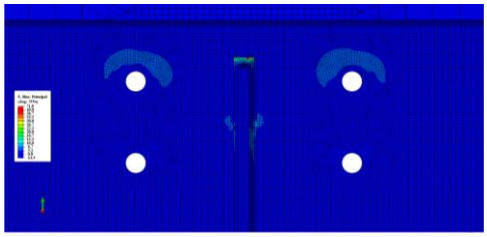	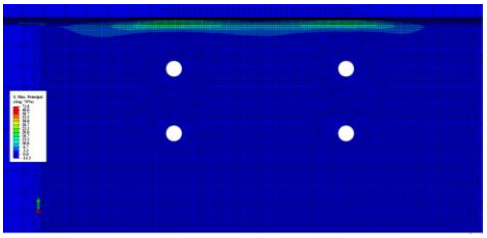
	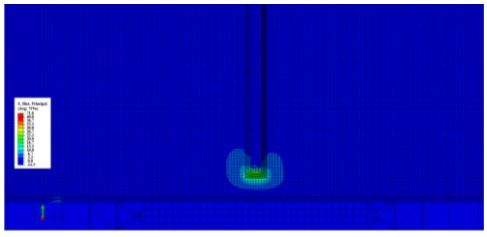	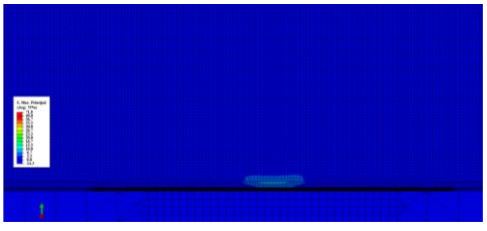

Table D. 27: 3 in. Horseshoe Crack, Retrofit1 Model with Stiffened Angles

UCracks3inRet1Stiffeners-60k		
	Interior	**Fascia**
South Girder	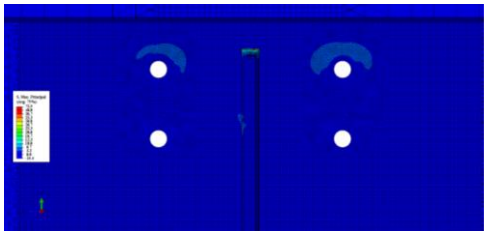	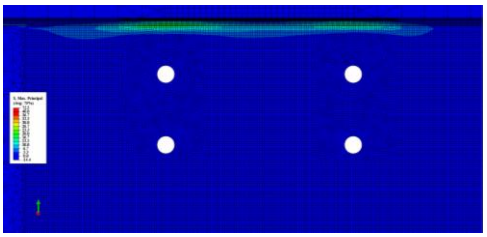
	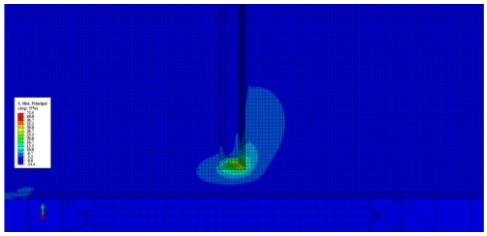	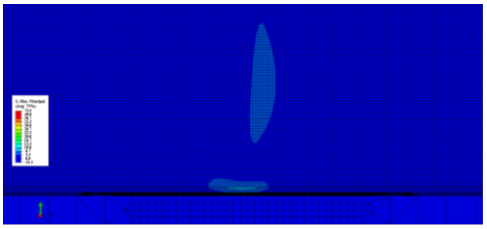
North Girder	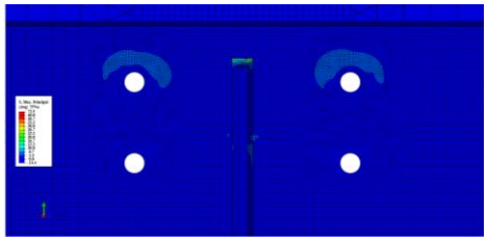	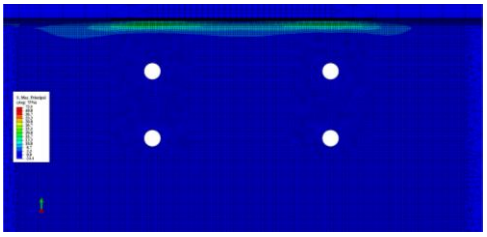
	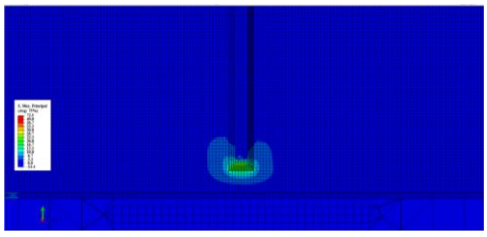	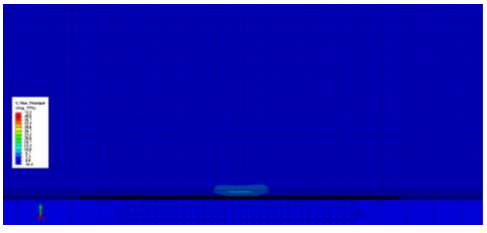

Table D. 28: 1 in. Horseshoe Crack, Full Depth Back-up Stiffener Model

UCracks1inFullBackupStiff-60k		
	Interior	**Fascia**
South Girder	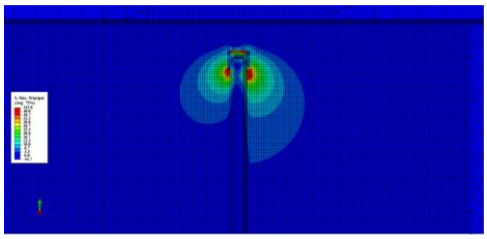	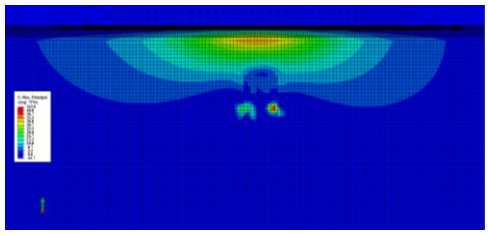
	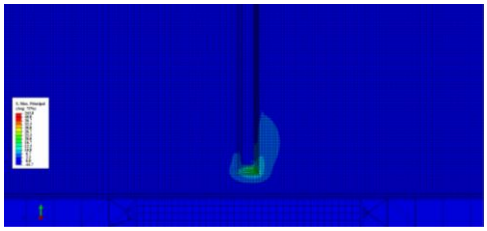	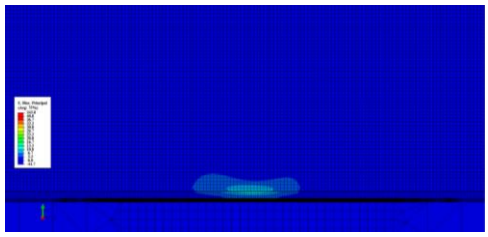
North Girder	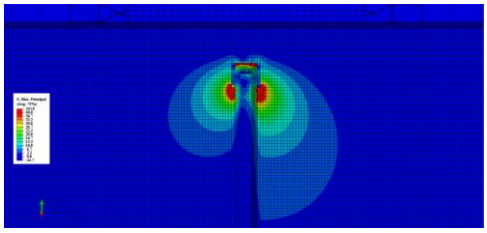	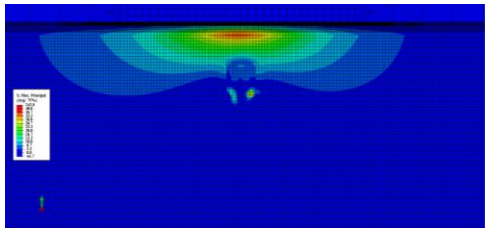
	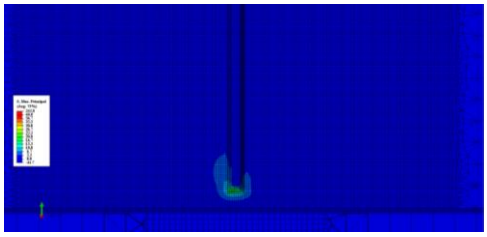	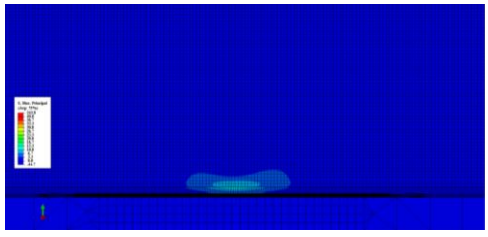

Table D. 29: 1.5 in. Horseshoe Crack, Full Depth Back-up Stiffener Model

	UCracks1point5inFullBackupStiff-60k	
	Interior	**Fascia**
South Girder	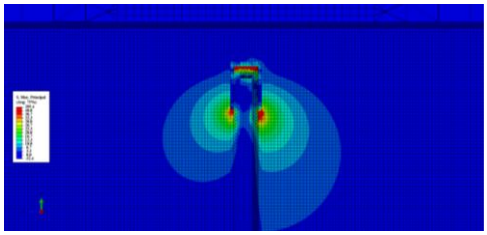	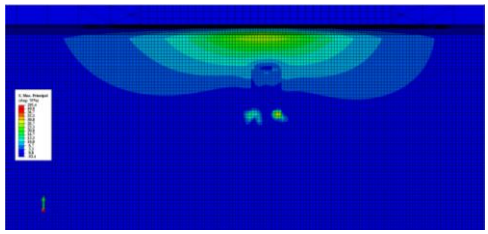
	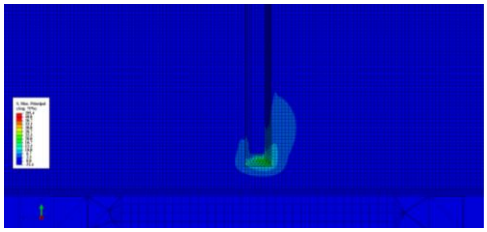	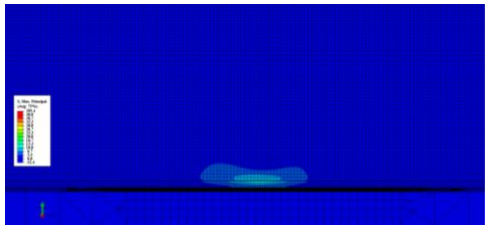
North Girder	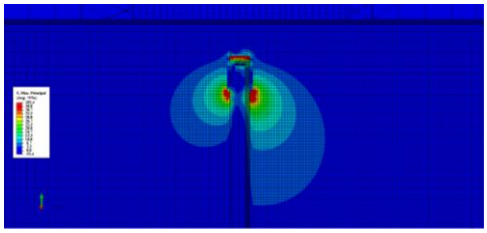	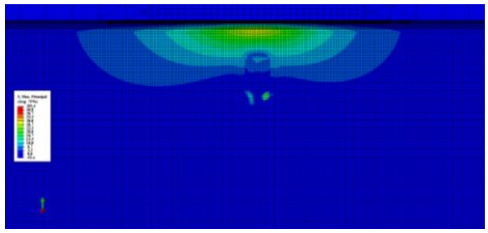
	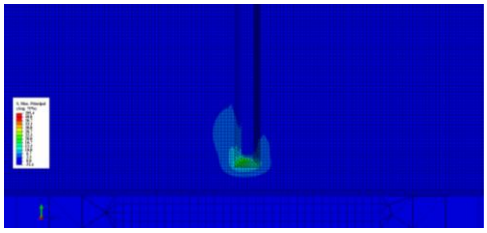	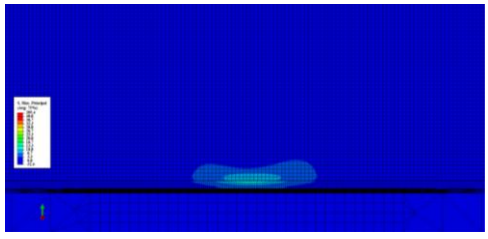

Table D. 30: 2 in. Horseshoe Crack, Full Depth Back-up Stiffener Model

UCracks2inFullBackupStiff-60k		
	Interior	**Fascia**
South Girder	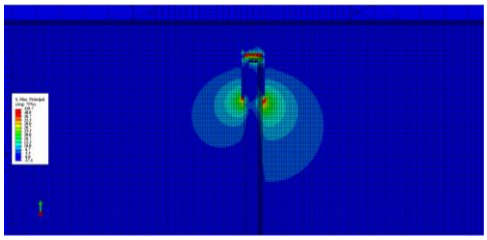	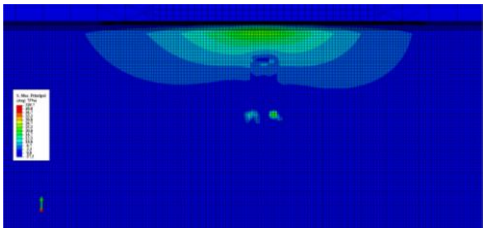
	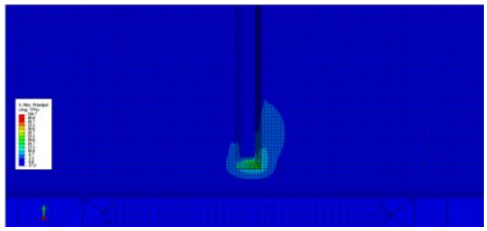	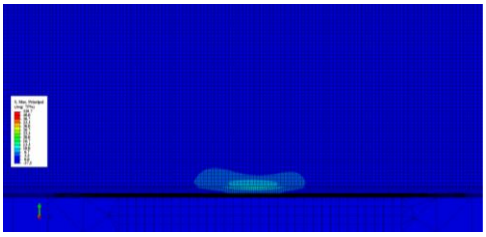
North Girder	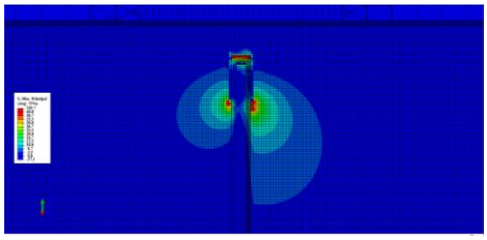	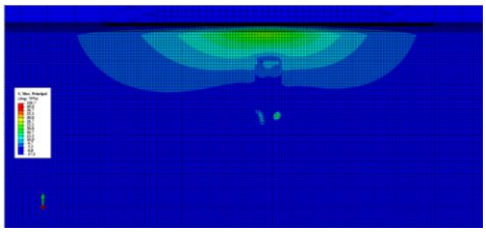
	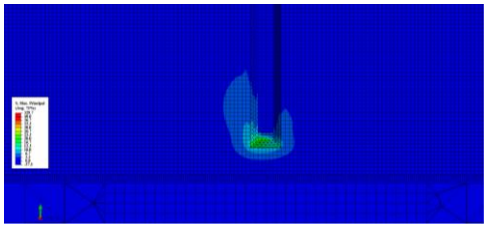	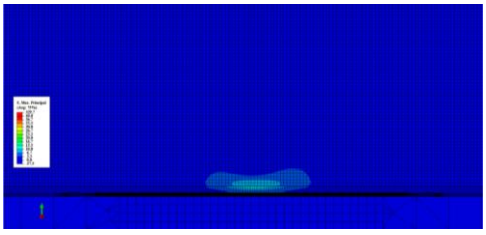

Table D. 31: 2.5 in. Horseshoe Crack, Full Depth Back-up Stiffener Model

UCracks2point5inFullBackupStiff-60k		
	Interior	**Fascia**
South Girder	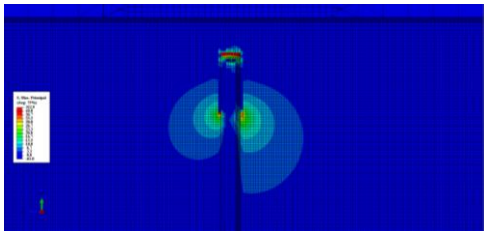	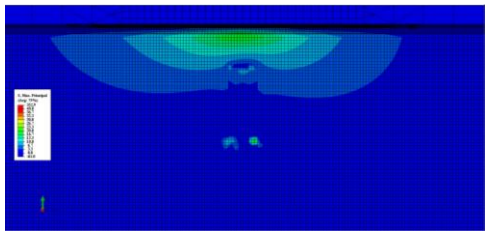
	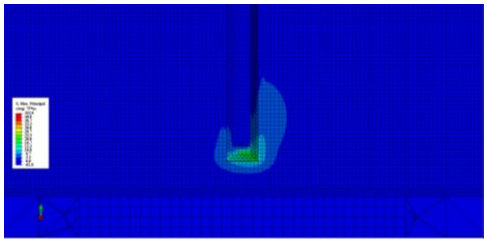	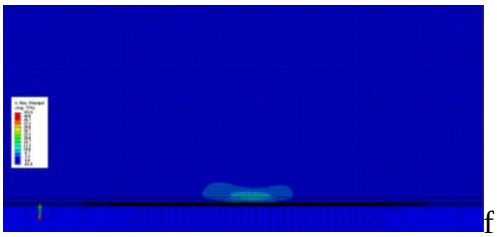
North Girder	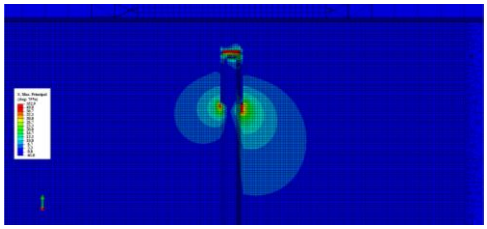	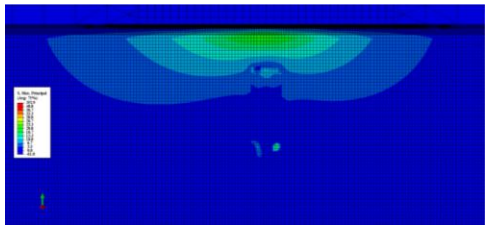
	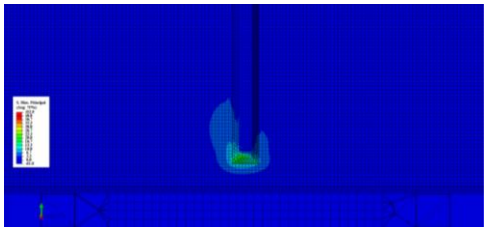	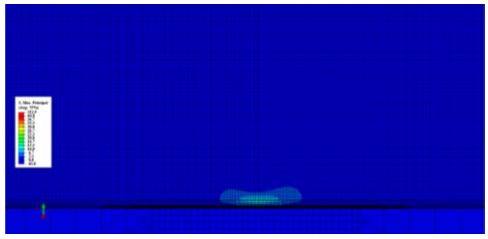

f

Table D. 32: 3 in. Horseshoe Crack, Full Depth Back-up Stiffener Model

UCracks3inFullBackupStiff-60k		
	Interior	**Fascia**
South Girder	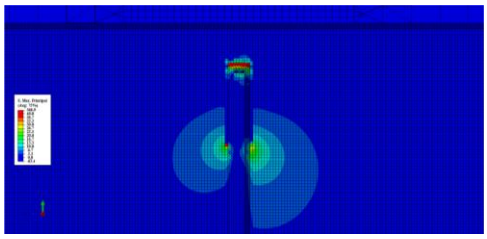	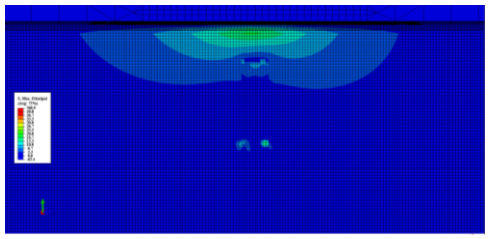
	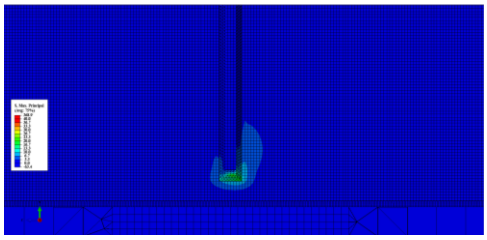	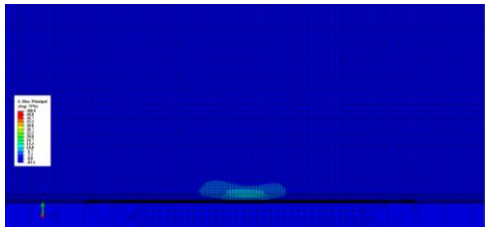
North Girder	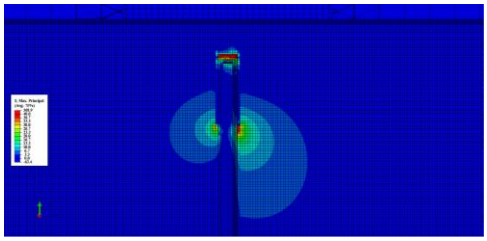	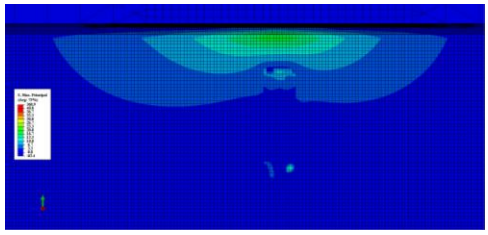
	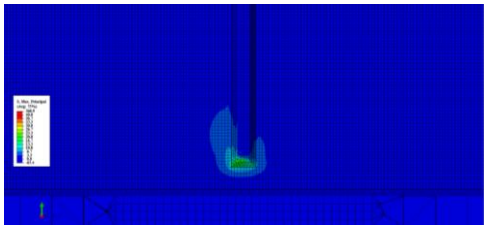	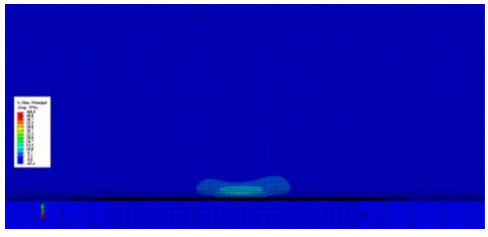

Table D. 33: 1 in. Horseshoe Crack, Angles to Top Flange with Tension Model

UCracks1inRet2TFTension-60k		
	Interior	**Fascia**
South Girder	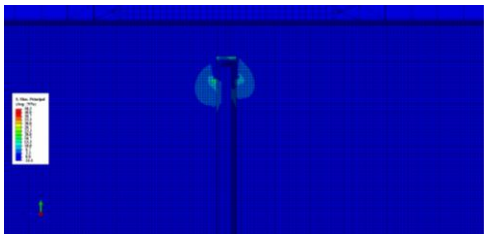	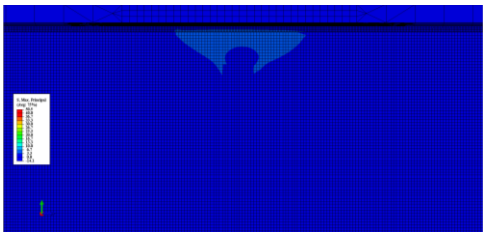
	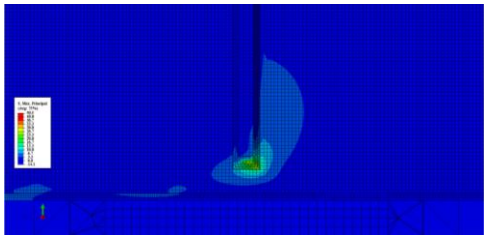	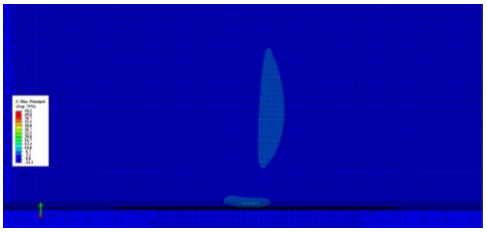
North Girder	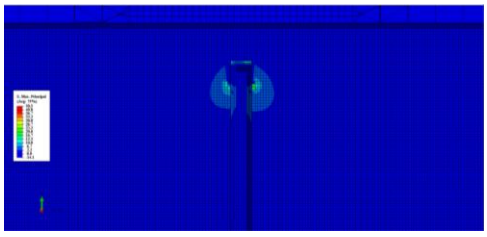	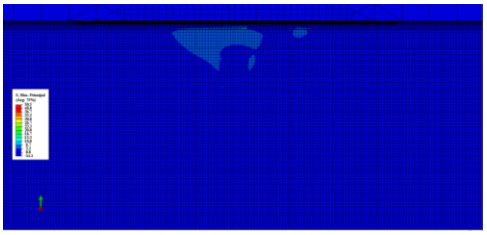
	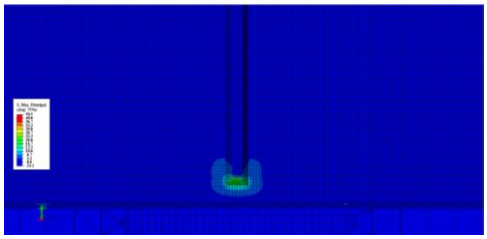	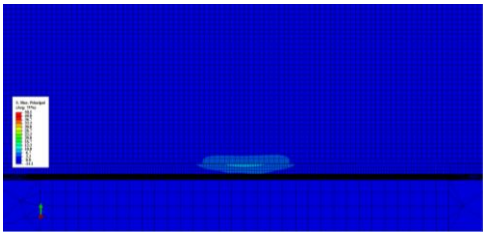

Table D. 34: 1.5 in. Horseshoe Crack, Angles to Top Flange with Tension Model

UCracks1point5inRet2TopFlange-60k		
	Interior	**Fascia**
South Girder	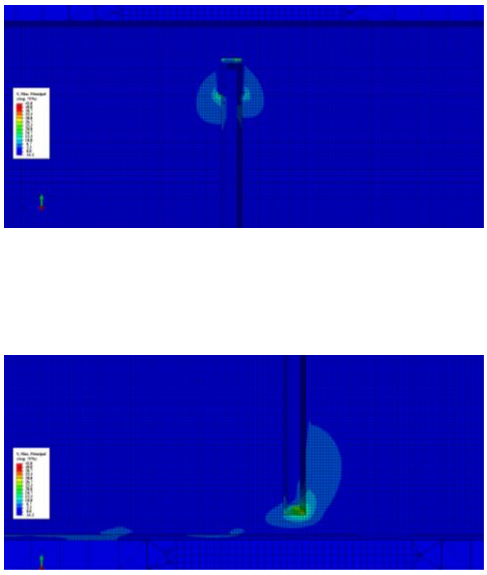	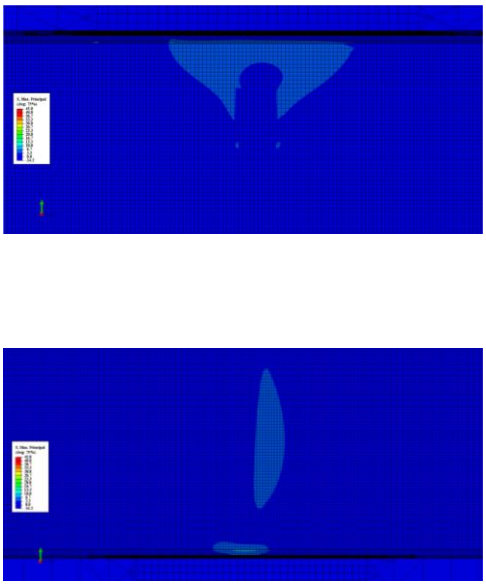
North Girder	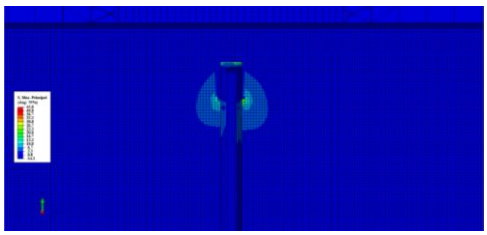	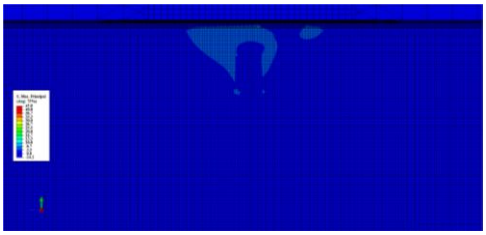
	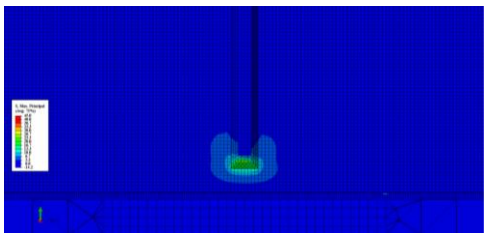	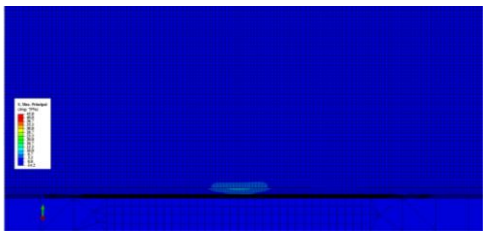

Table D. 35: 2 in. Horseshoe Crack, Angles to Top Flange with Tension Model

UCracks2inRet2TopFlange-60k		
	Interior	**Fascia**
South Girder	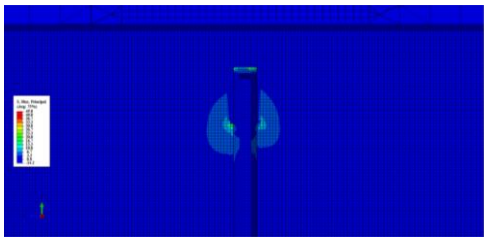	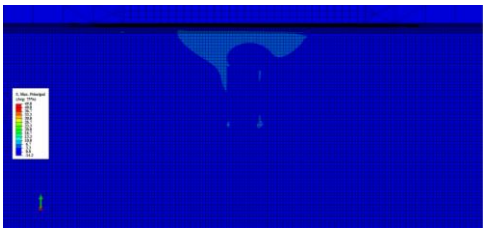
	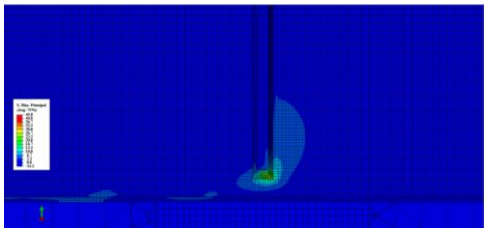	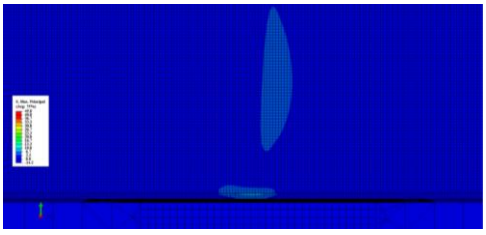
North Girder	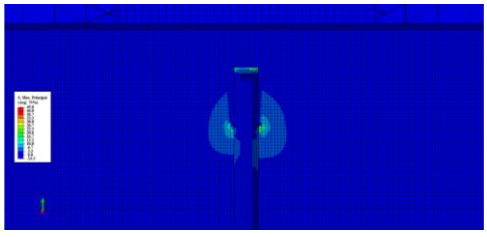	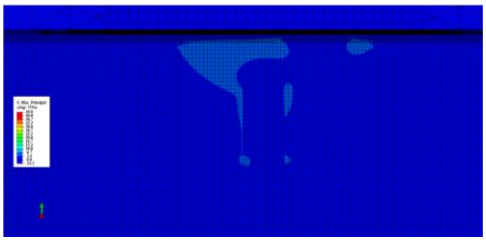
	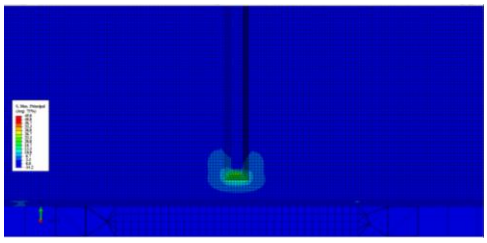	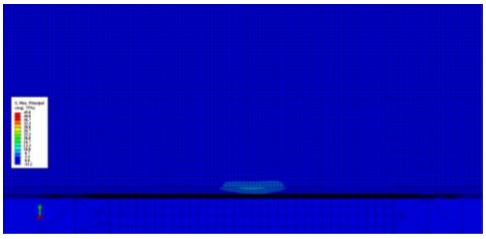

Table D. 36: 2.5 in. Horseshoe Crack, Angles to Top Flange with Tension Model

UCracks2point5inRet2TopFlange-60k		
	Interior	**Fascia**
South Girder	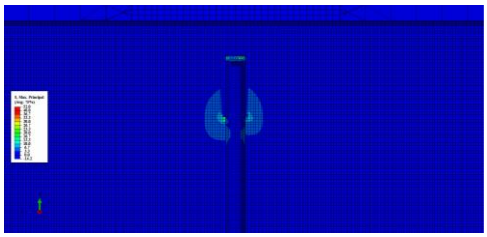	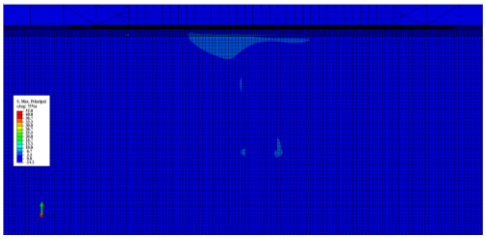
	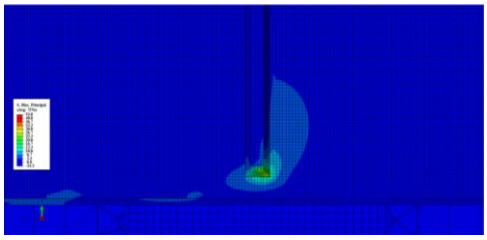	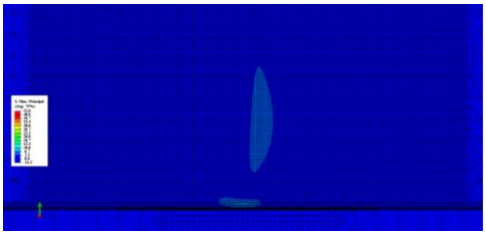
North Girder	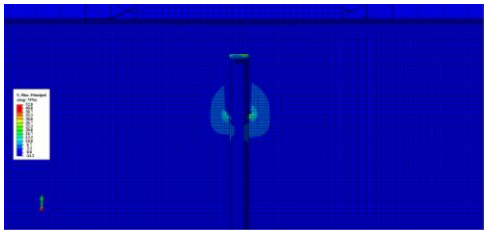	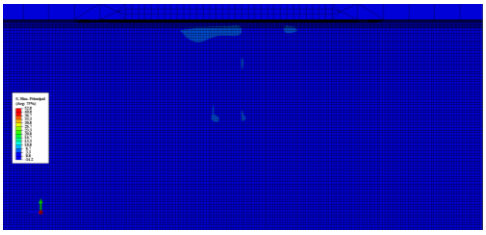
	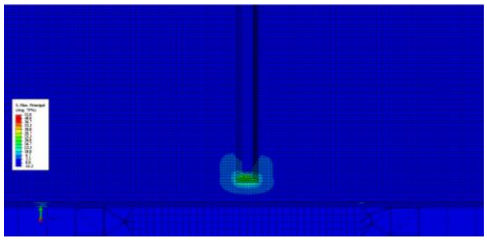	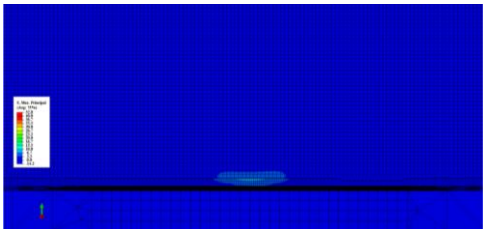

Table D. 37: 3 in. Horseshoe Crack, Angles to Top Flange with Tension Model

UCracks3inRet2TopFlange-60k		
	Interior	**Fascia**
South Girder	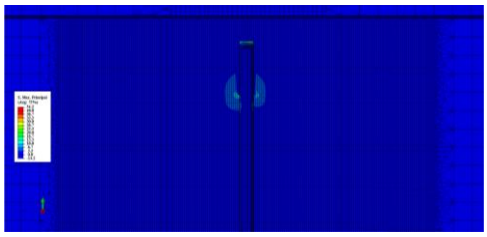	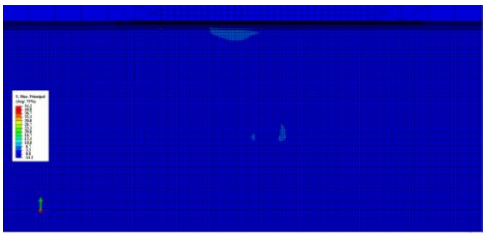
	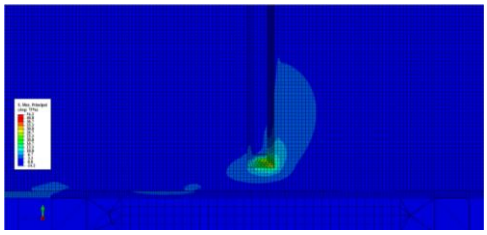	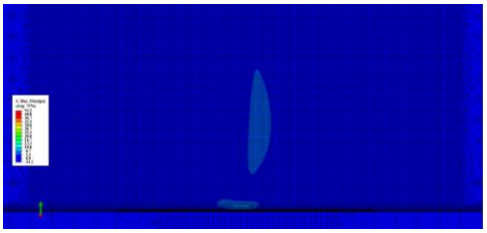
North Girder	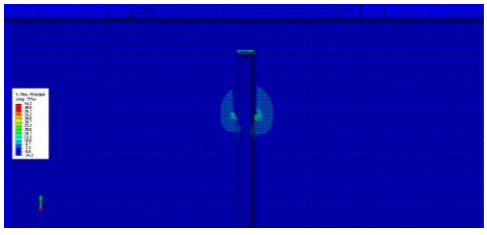	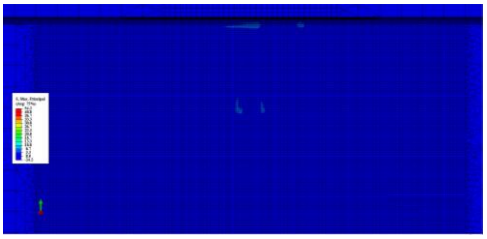
	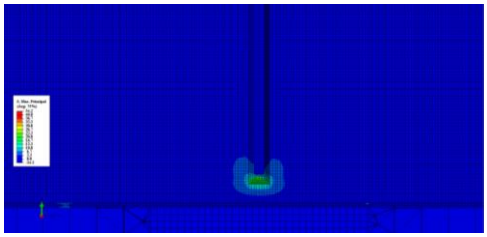	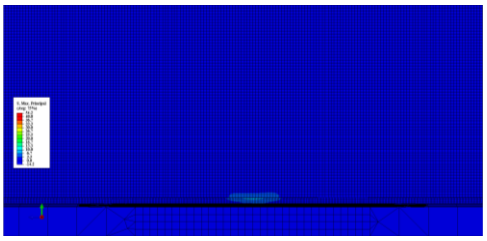

Table D. 38: 1 in. Horseshoe Crack, North Cross Frame Broken, Retrofit1 Model

UCracks1inRet1BoltsBrokenXF2-60k		
	Interior	**Fascia**
South Girder	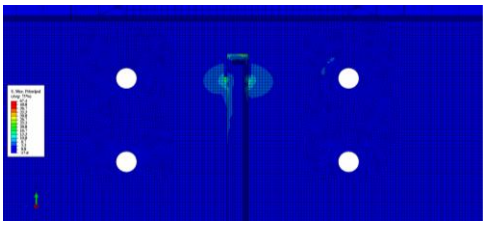	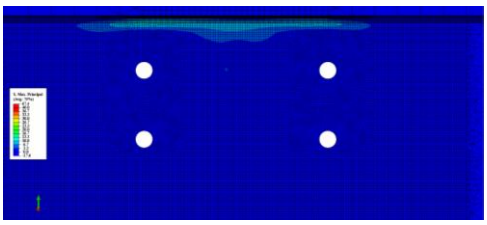
	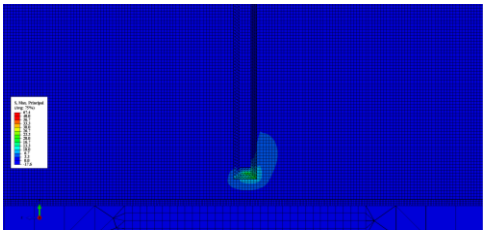	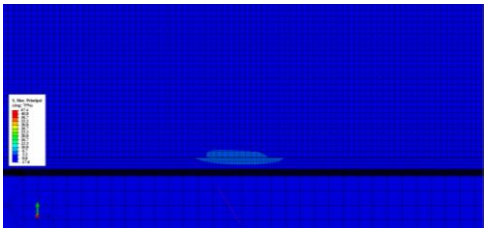
North Girder	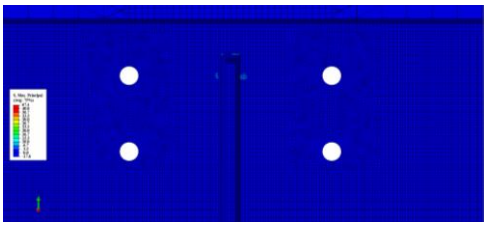	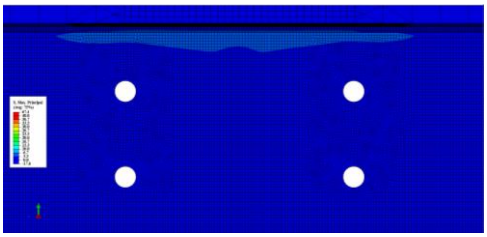
	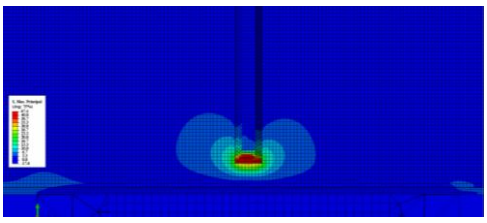	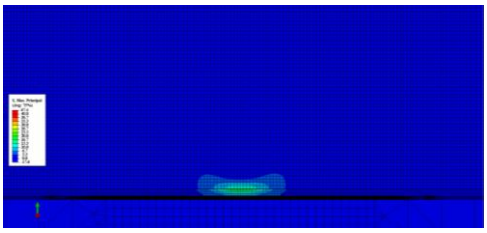

Table D. 39: 2 in. Horseshoe Crack, Reduced Deck Stiffness Model

UCracks2inRedDeckStiff-60k		
	Interior	**Fascia**
South Girder	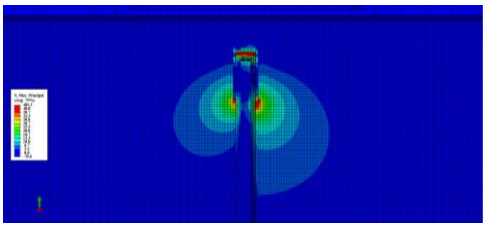	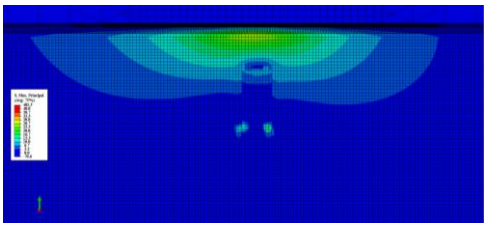
	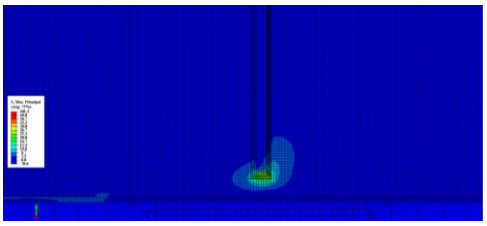	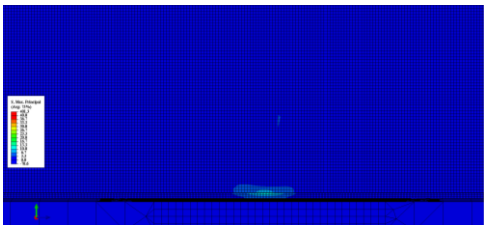
North Girder	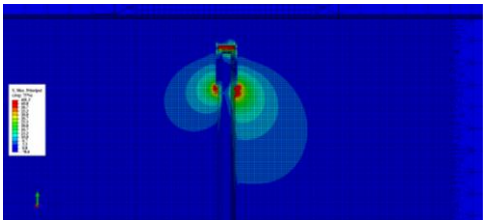	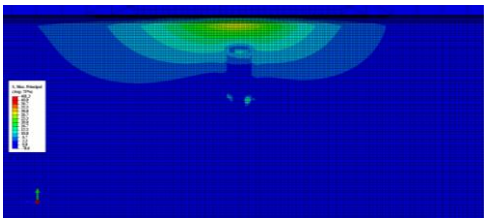
	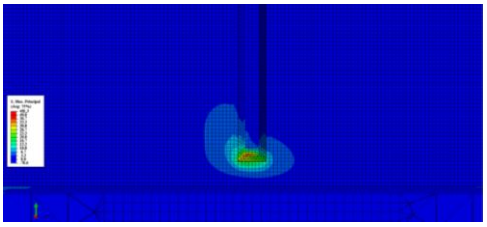	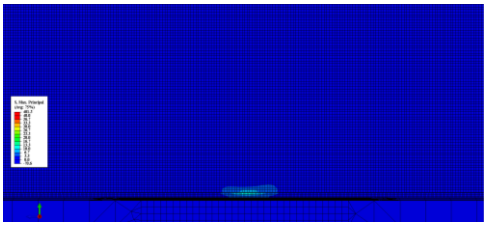

Table D. 40: 1 in. Longitudinal Crack, Retrofit1 Model

	LCracks1inRet1Bolts-60k	
	Interior	**Fascia**
South Girder	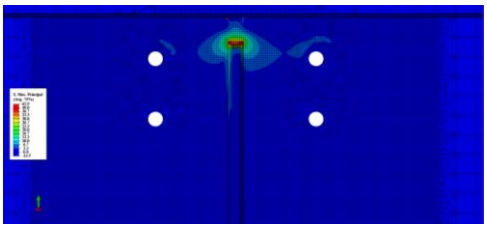	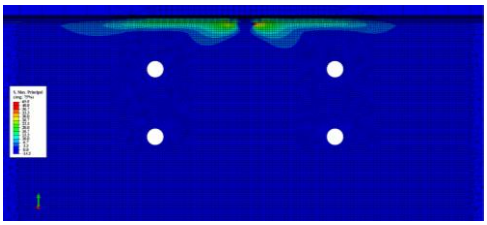
	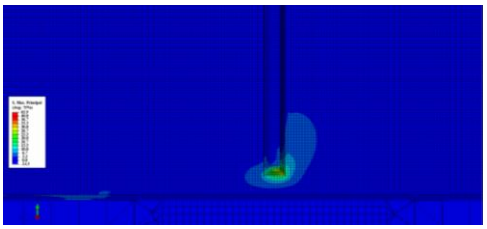	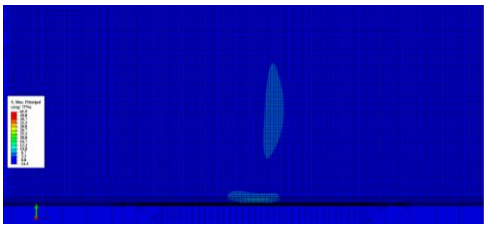
North Girder	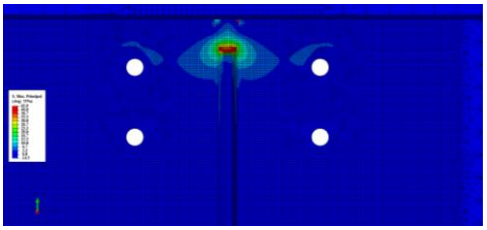	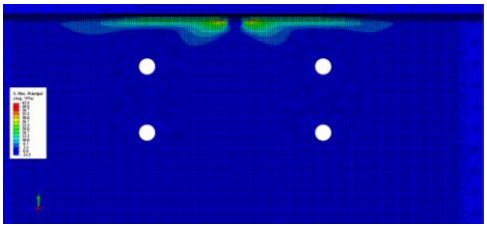
	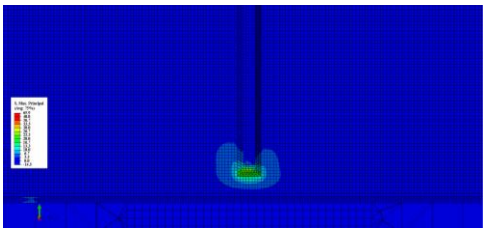	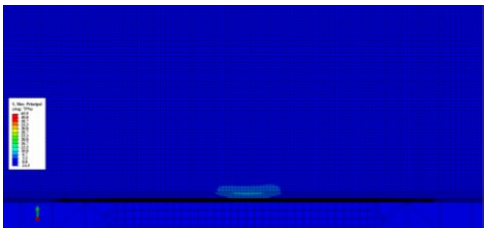

Table D. 41: 2 in. Longitudinal Crack, Retrofit1 Model

LCracks2inRet1Bolts-60k		
	Interior	**Fascia**
South Girder	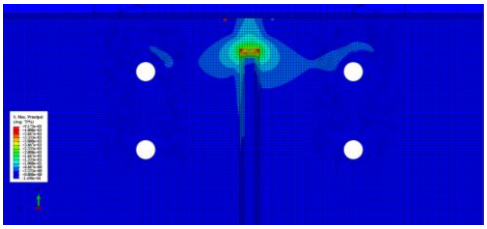	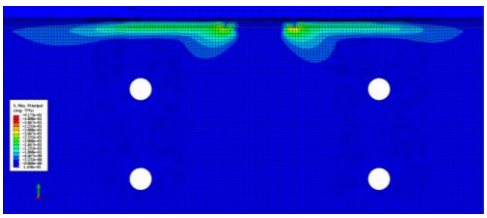
	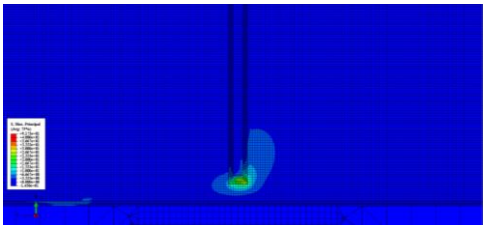	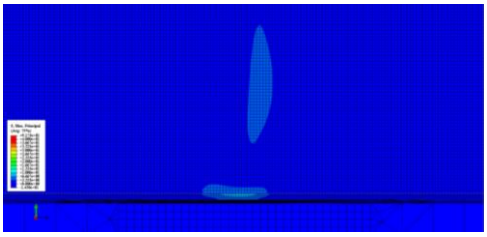
North Girder	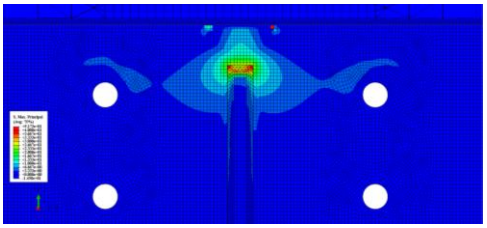	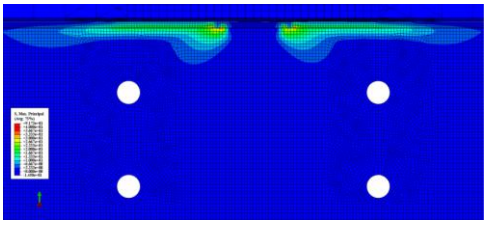
	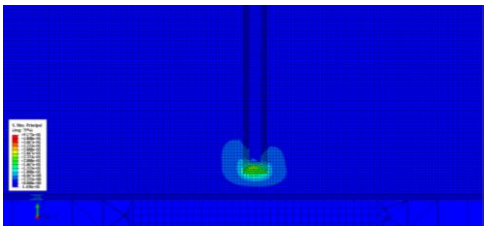	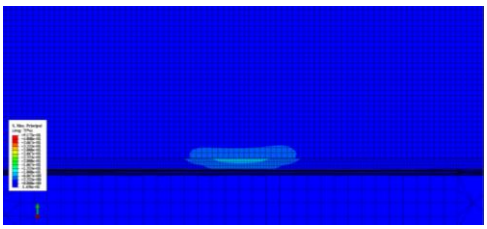

Table D. 42: 3 in. Longitudinal Crack, Retrofit1 Model

	LCracks3inRet1Bolts-60k	
	Interior	**Fascia**
South Girder	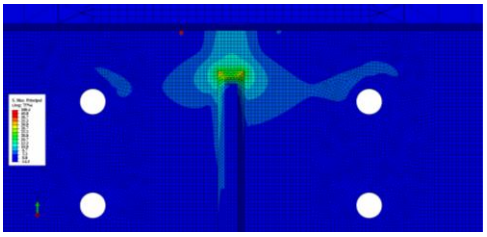	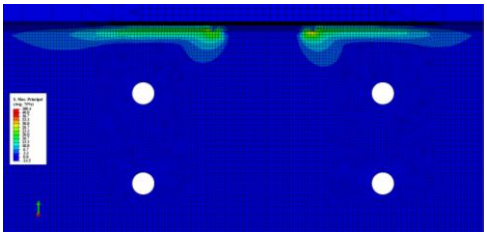
	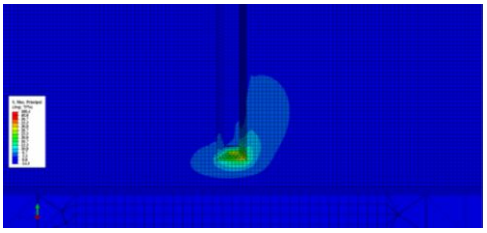	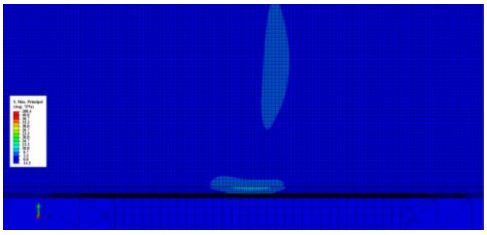
North Girder	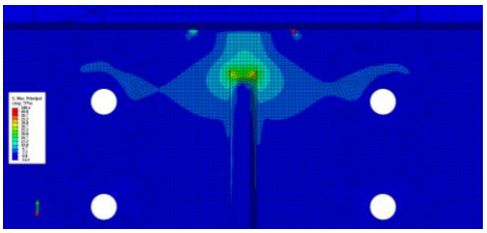	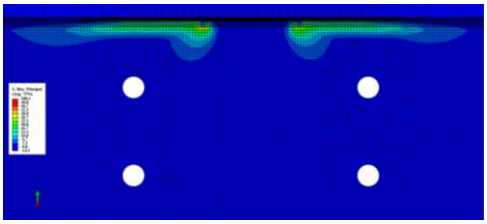
	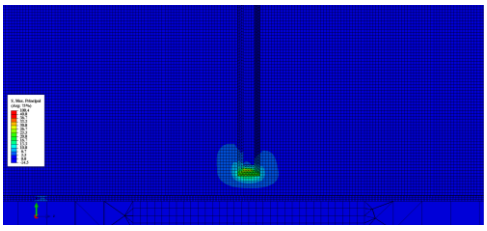	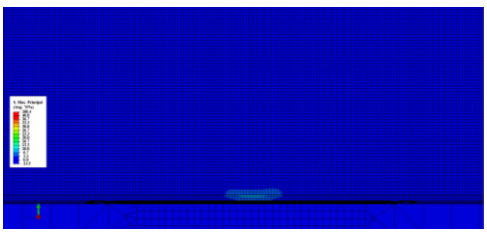

Table D. 43: 4 in. Longitudinal Crack, Retrofit1 Model

	LCracks4inRet1Bolts-60k	
	Interior	**Fascia**
South Girder	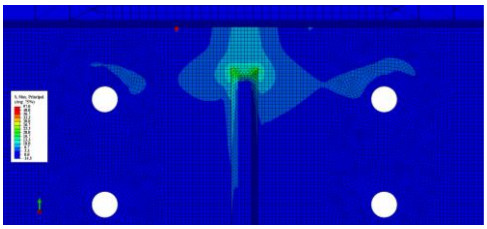	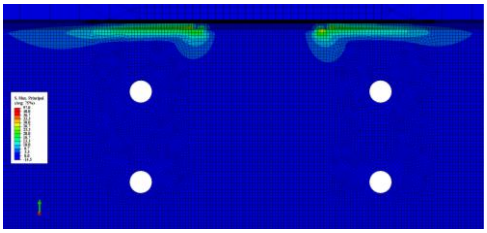
	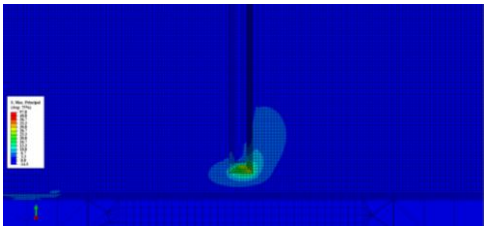	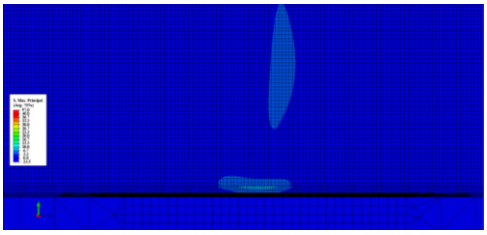
North Girder	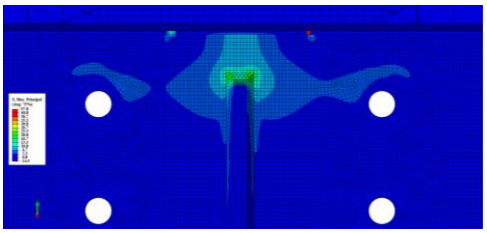	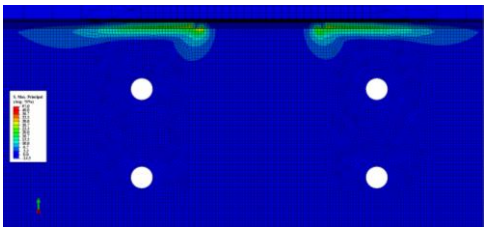
	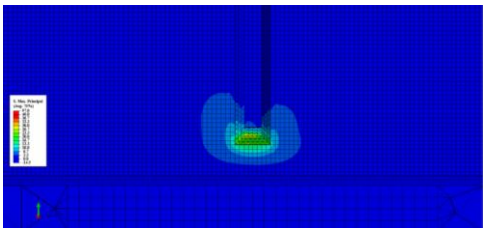	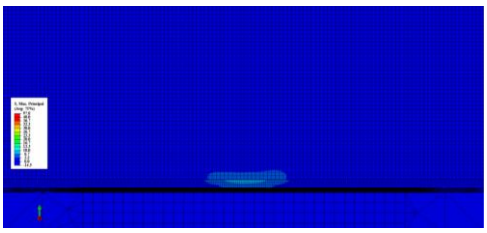

Table D. 44: 8 in. Longitudinal Crack, Retrofit1 Model

	LCracks8inRet1Bolts-60k	
	Interior	**Fascia**
South Girder	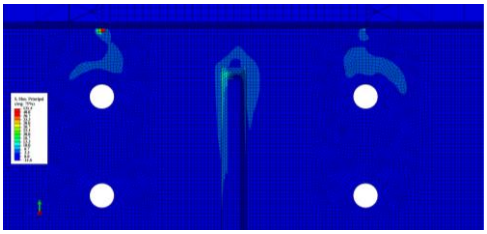	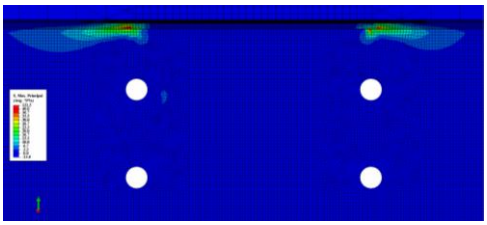
	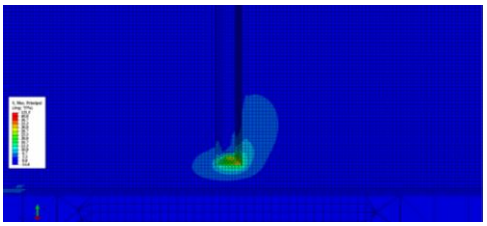	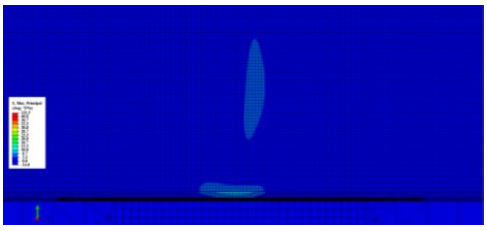
North Girder	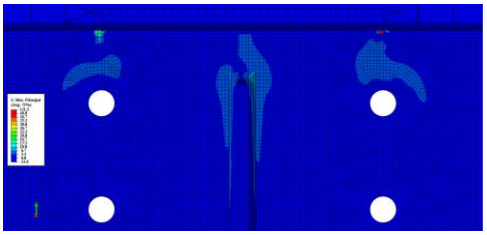	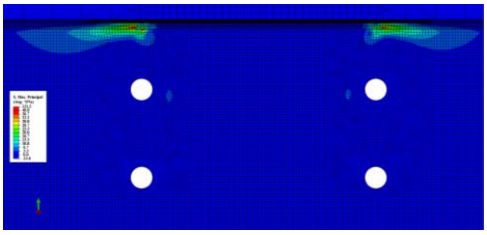
	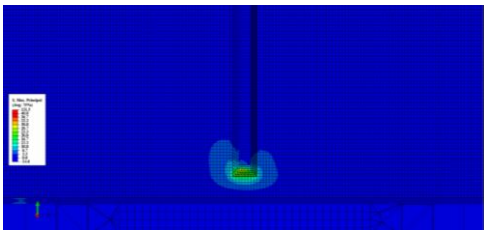	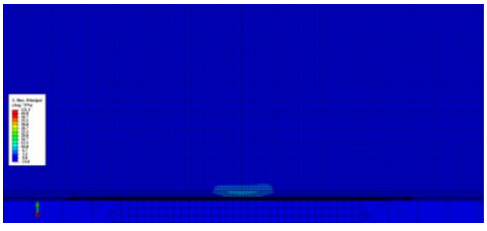

Table D. 45: 1 in. Longitudinal Crack Model

	LCracks1in-60k	
	Interior	**Fascia**
South Girder	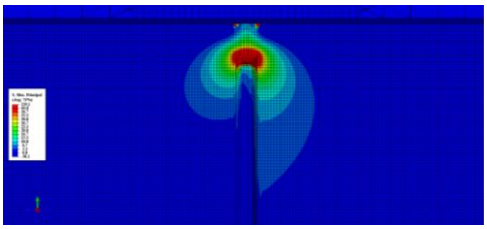	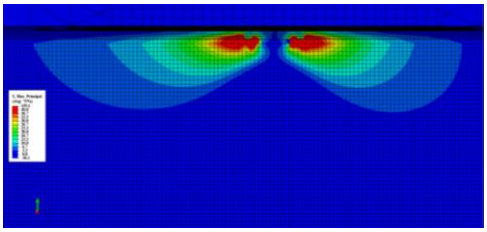
	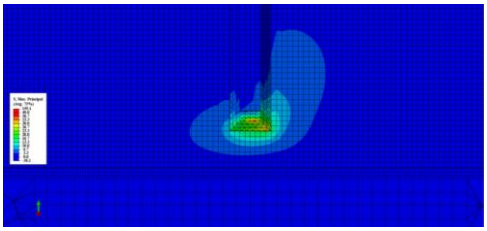	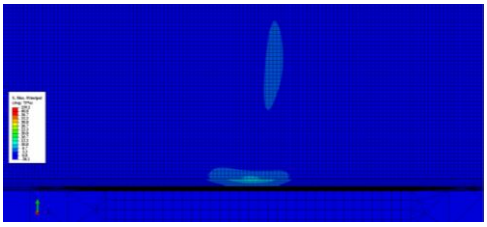
North Girder	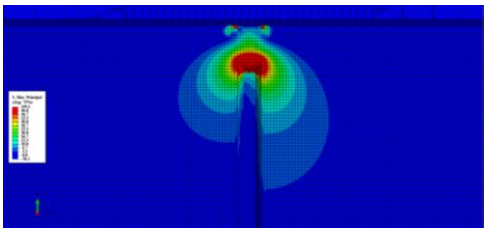	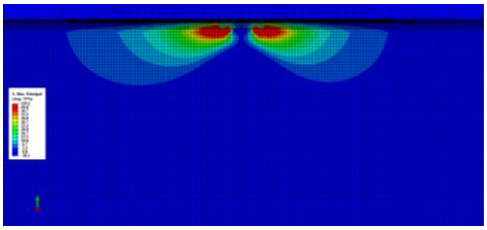
	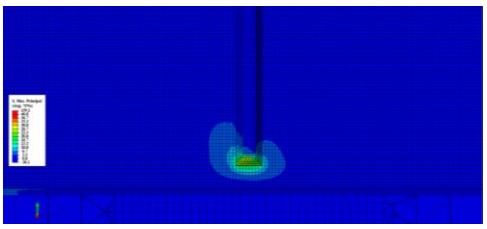	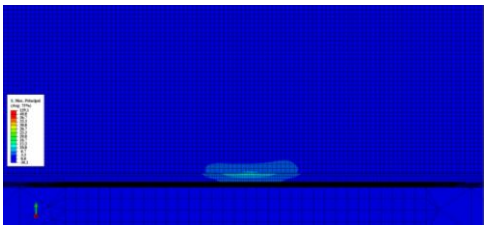

Table D. 46: 2 in. Longitudinal Crack Model

	LCracks2in-60k	
	Interior	**Fascia**
South Girder	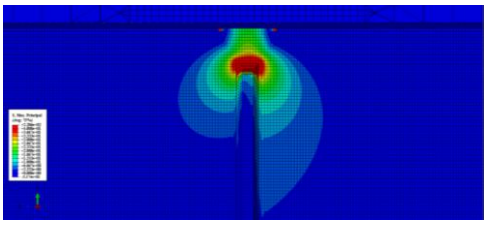	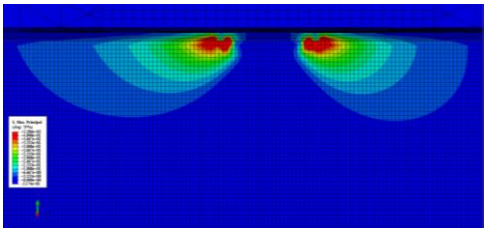
	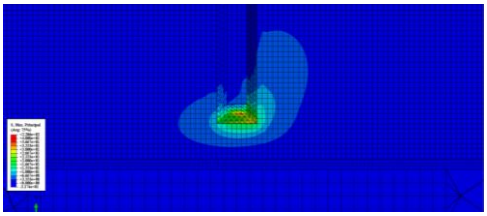	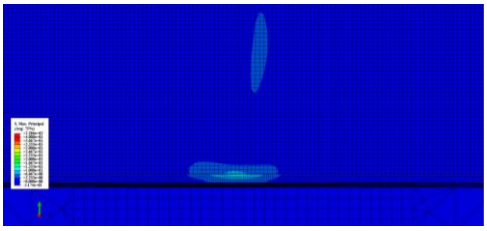
North Girder	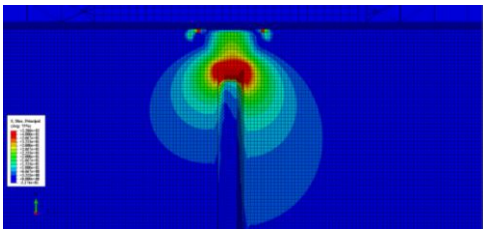	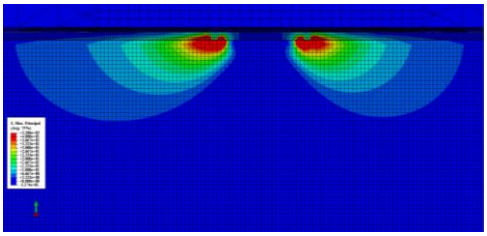
	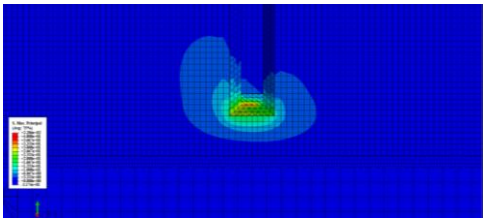	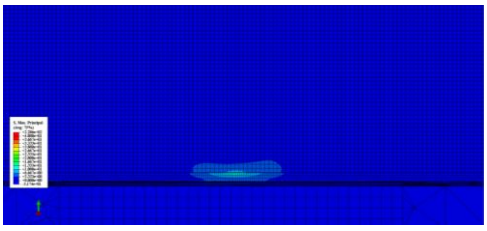

Table D. 47: 3 in. Longitudinal Crack Model

	LCracks3in-60k	
	Interior	**Fascia**
South Girder	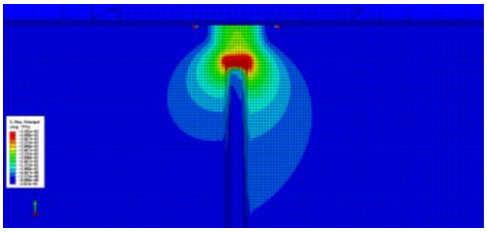	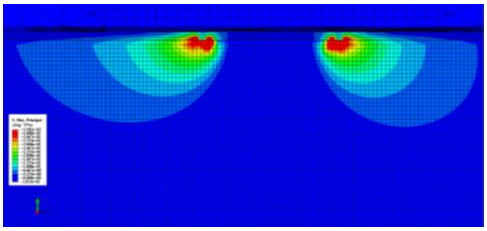
	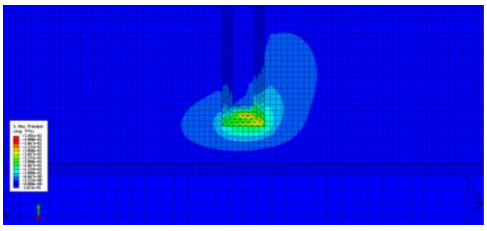	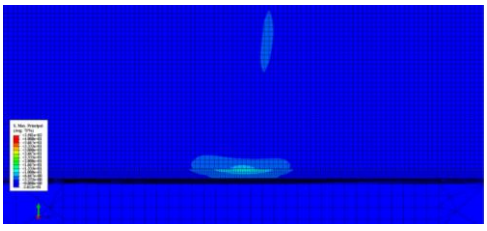
North Girder	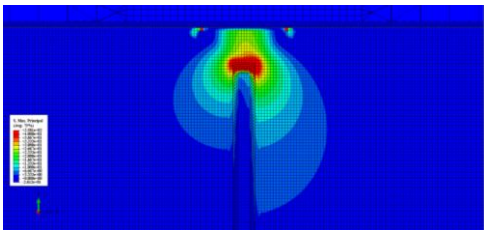	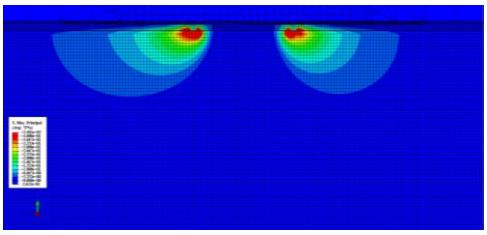
	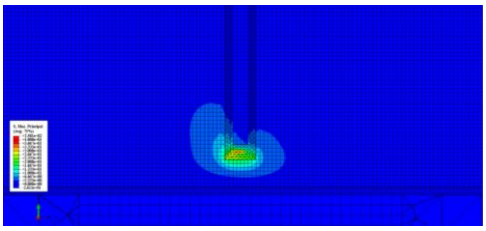	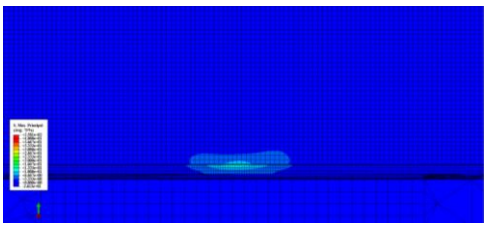

Table D. 48: 4 in. Longitudinal Crack Model

	LCracks4in-60k	
	Interior	**Fascia**
South Girder	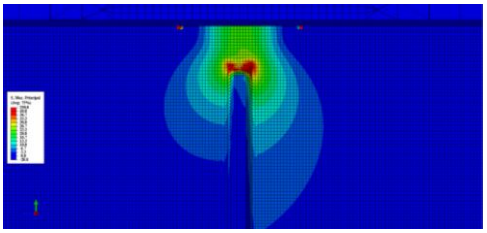	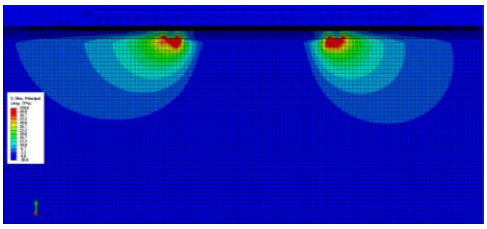
	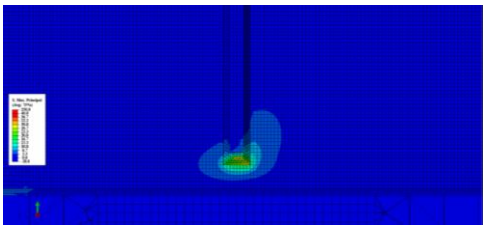	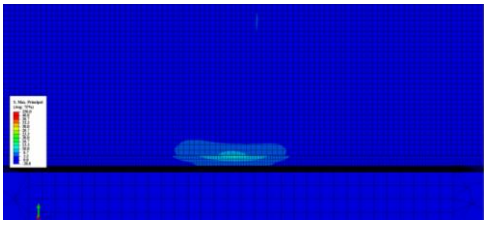
North Girder	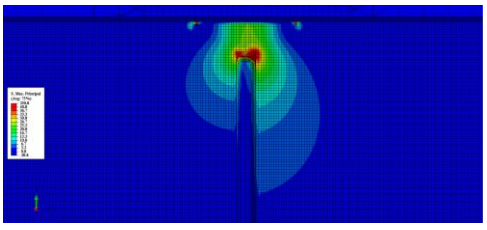	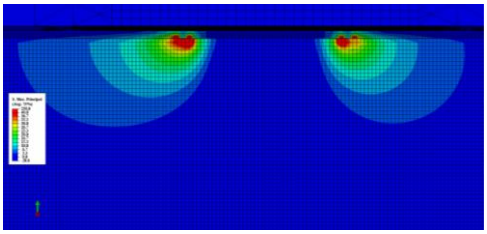
	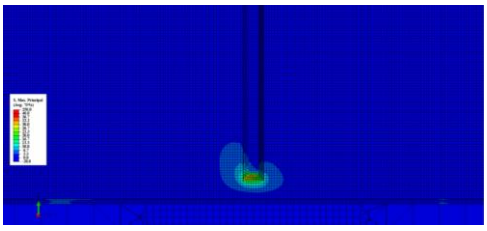	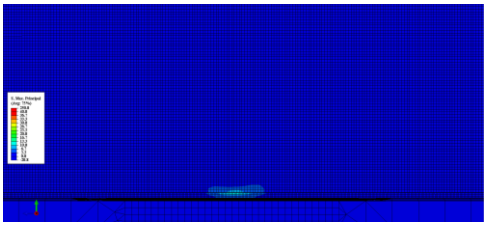

Table D. 49: 8 in. Longitudinal Crack Model

	LCracks8in-60k	
	Interior	**Fascia**
South Girder	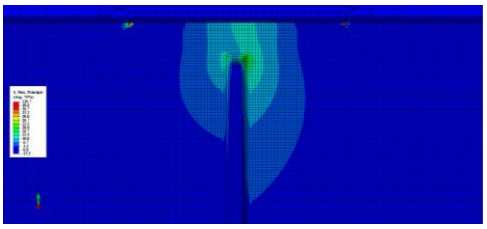	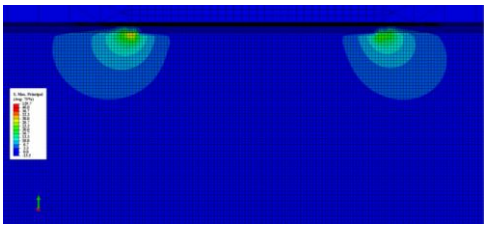
	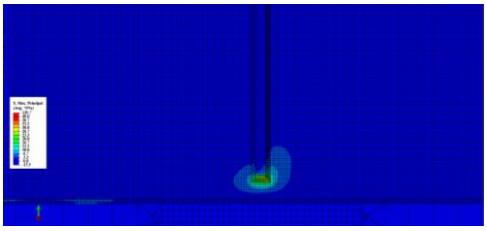	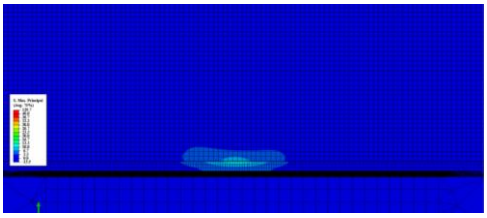
North Girder	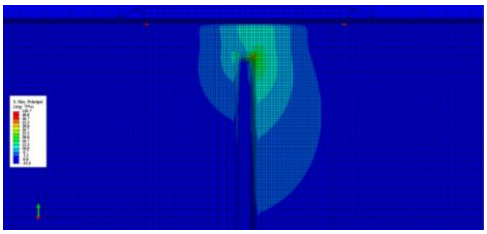	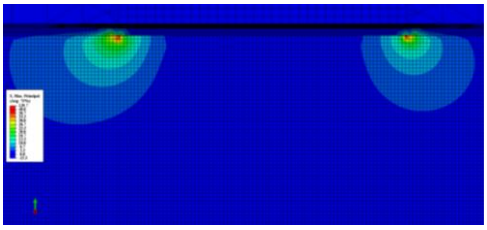
	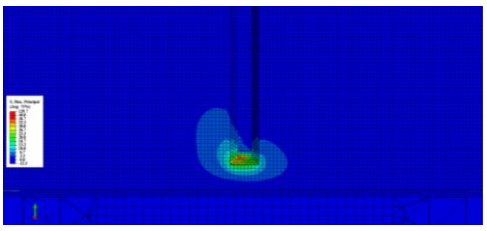	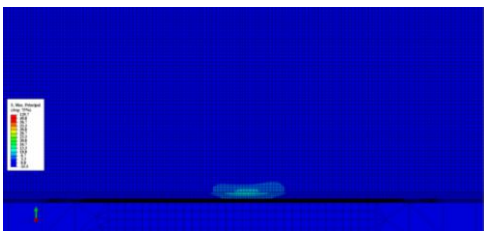

APPENDIX E: EXPERIMENTAL DATA

CONCRETE MATERIAL PROPERTIES

Table E. 1: Concrete Compressive Strengths in psi

Slab	Pour	7-day	Strength	14-day	Strength	21-day	Strength	28-day	Strength	56-day	Strength
#1	7/9/2010	7/16/2010	3270	7/23/2010	4030			8/6/2010	4014	9/3/2010	4916
#2 MCM	7/28/2010							8/25/2010	4173	9/22/2010	4244
#2 KU	7/28/2010									9/22/2010	5712
#3	8/20/2010	8/27/2010	3714	9/3/2010	4686			9/17/2010	4863	10/15/2010	5270
#4	9/10/2010	9/17/2010	3484	9/24/2010	4209			10/8/2010	3979	11/5/2010	4668
#5	10/1/2010	10/8/2010	3395	10/15/2010	4244			10/29/2010	4757	11/26/2010	
Base Block	2/15/2011					3/8/2011	7445	3/15/2011	8842		

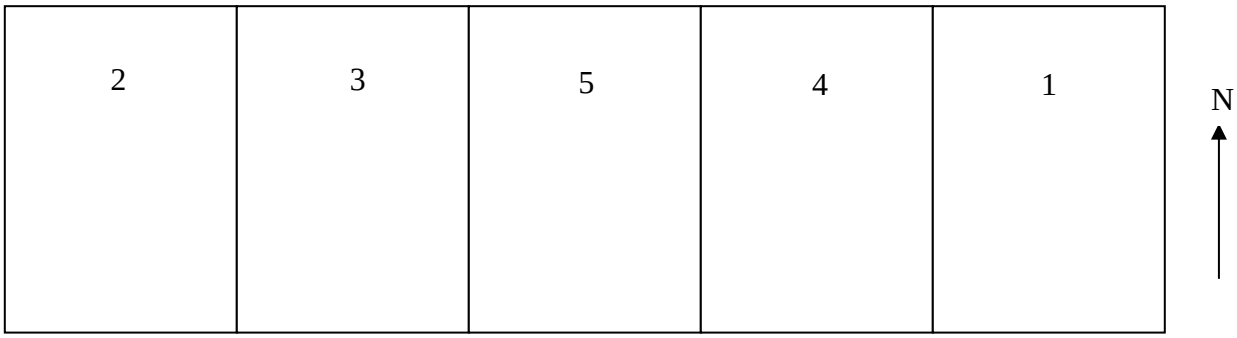

Figure E. 1: Deck Layout and Labeling

CRACK GROWTH

NORTH GIRDER

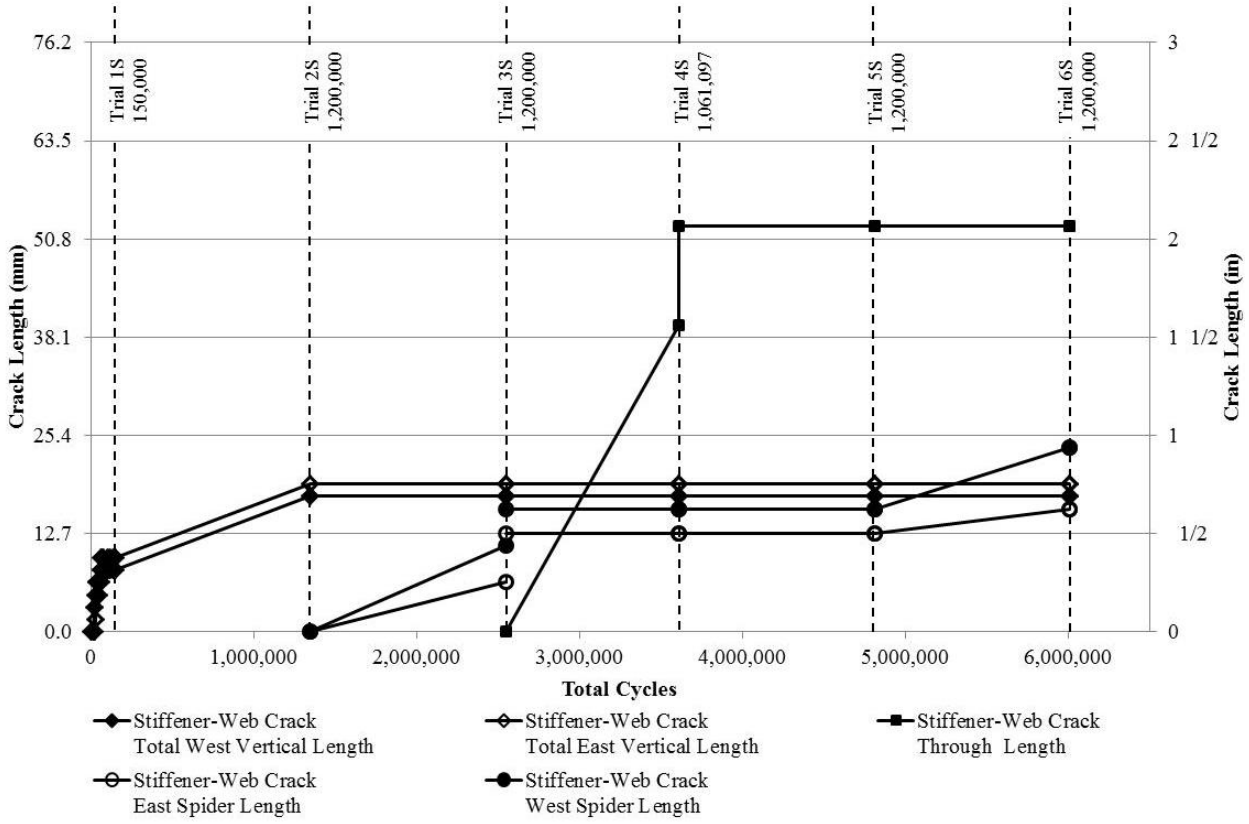

Figure E. 2: North girder crack growth

Table E. 2: North Girder Crack Figures

Trail	West of Stiffener	East of Stiffener	Fascia
1	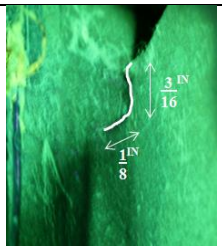	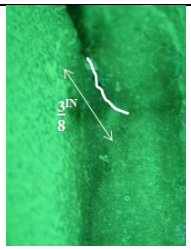	

2

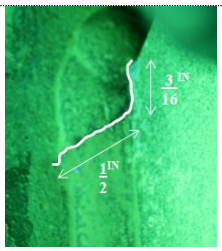
3/16 IN
1/2 IN

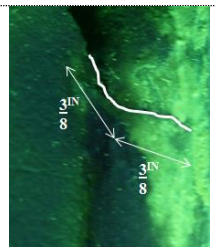
3/8 IN
3/8 IN

3

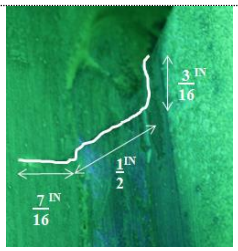
3/16 IN
1/2 IN
7/16 IN

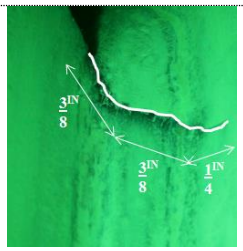
3/8 IN
3/8 IN
1/4 IN

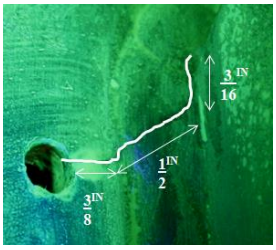
3/16 IN
1/2 IN
3/8 IN

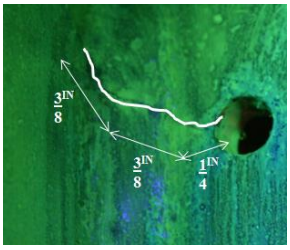
3/8 IN
3/8 IN
1/4 IN

4

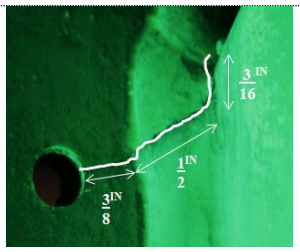
3/16 IN
1/2 IN
3/8 IN

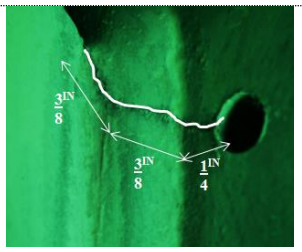
3/8 IN
3/8 IN
1/4 IN

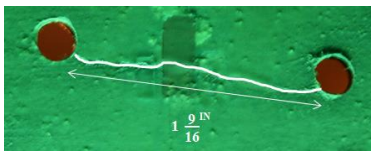
1 9/16 IN

5

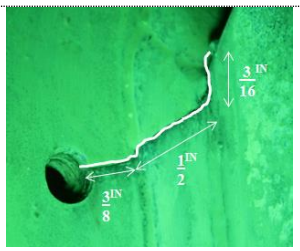
3/16 IN
1/2 IN
3/8 IN

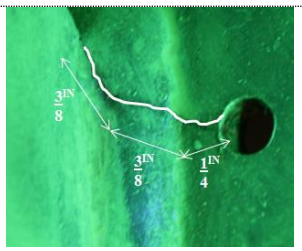
3/8 IN
3/8 IN
1/4 IN

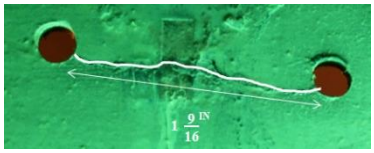
1 9/16 IN

6

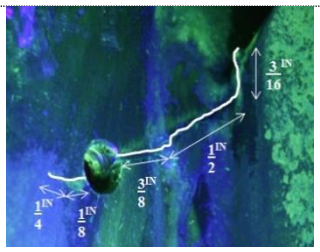
3/16 IN
1/2 IN
3/8 IN
1/4 IN
1/8 IN

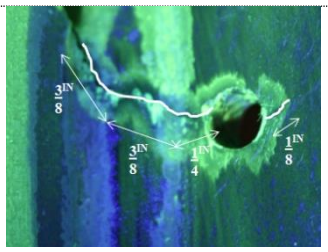
3/8 IN
3/8 IN
1/4 IN
1/8 IN

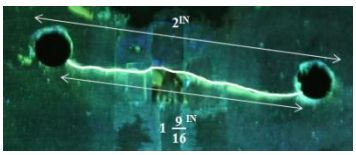
2 IN
1 9/16 IN

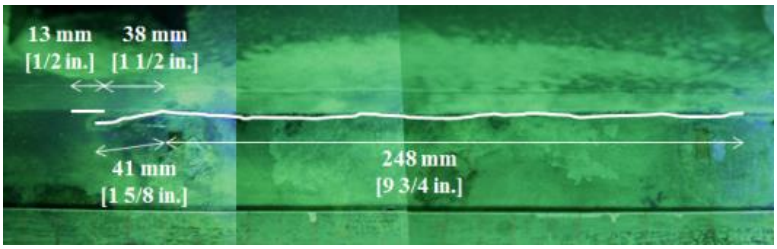

SOUTH GIRDER

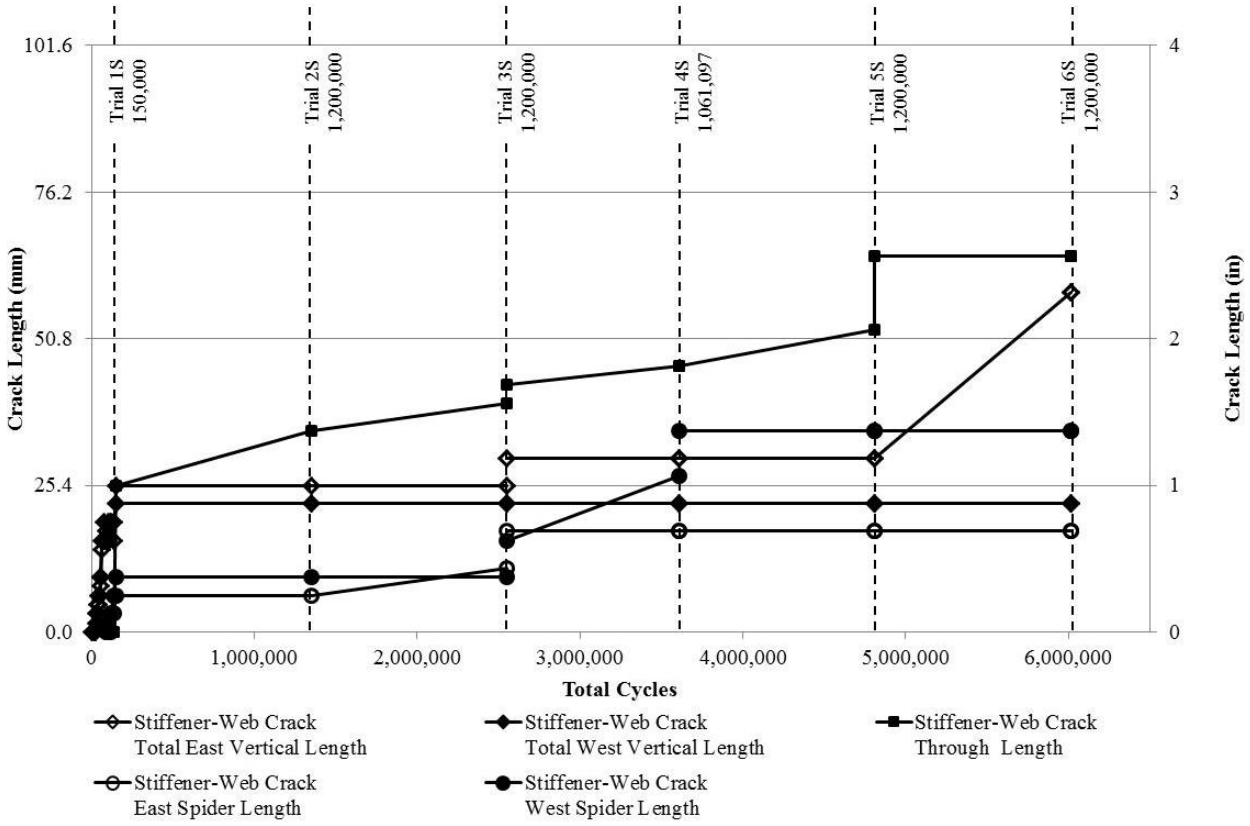

Figure E. 3: South girder crack growth

Table E. 3: South Girder Crack Figures

Trail	East of Stiffener	West of Stiffener	Fascia
1	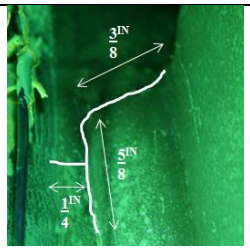	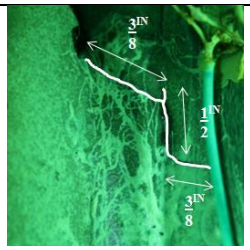	
2	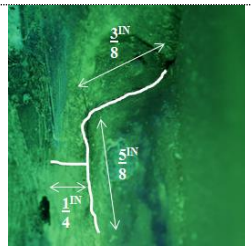	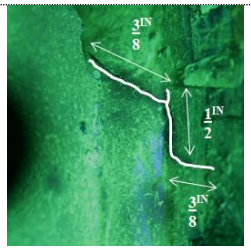	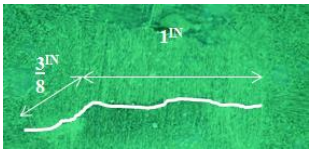
3	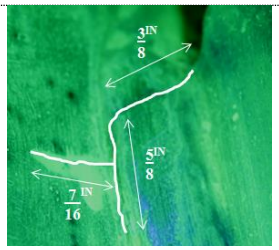	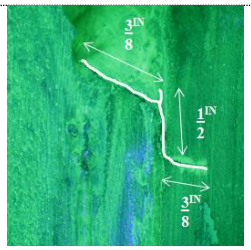	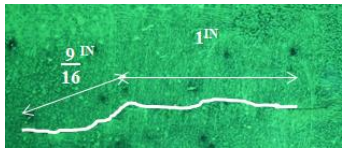
	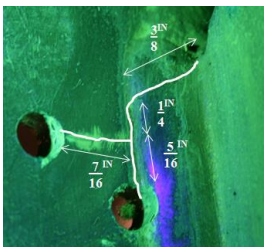	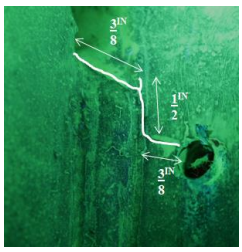	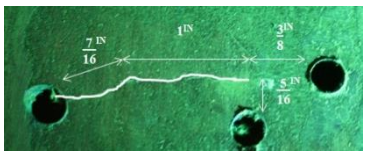
4	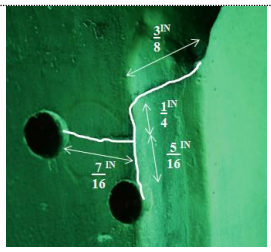	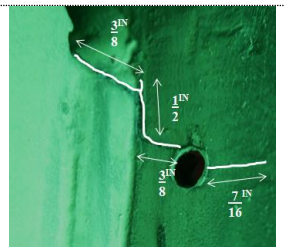	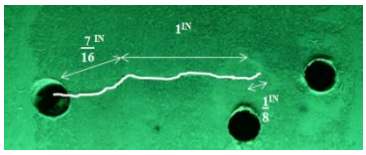
	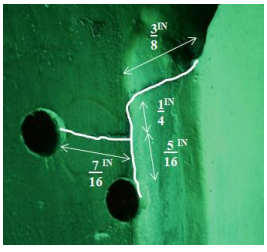	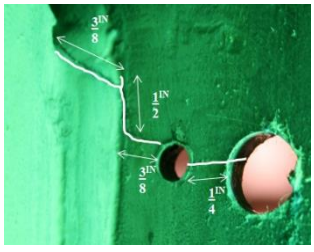	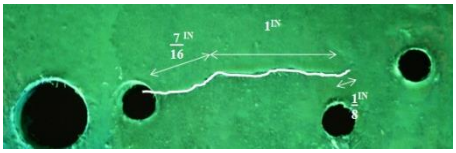

5	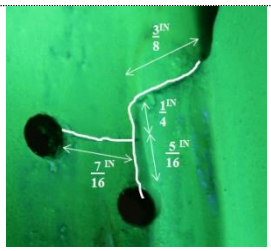	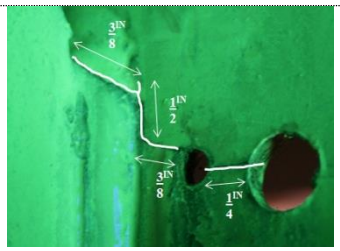	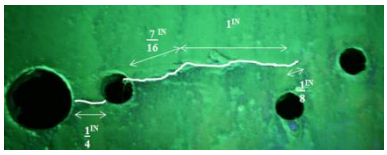
6		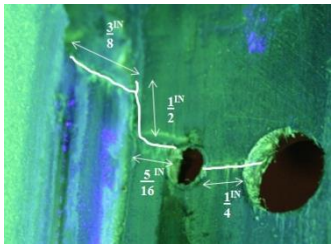	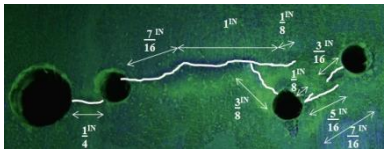
	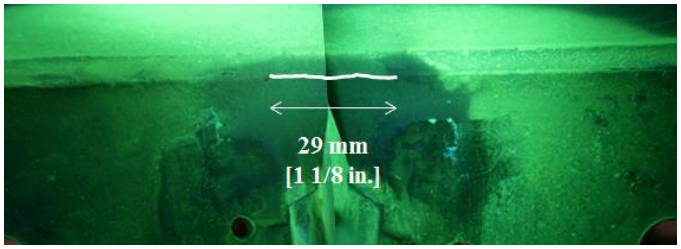		

LOAD DISTRIBUTION

Near the beginning of testing, load cells monitored load at each girder end. From this data, load distribution can be determined. For each set of static data, the average percentage of total load for each girder end was determined. Table E. 4 shows these results for 0 cycles and 150,000 cycles both without and with the angles-and-plate retrofit.

Table E. 4: Load Distribution from Load Cells

Load Cell\Cycles	0	150,000 w/o Retrofit	150,000 w/ Retrofit
WN LCA	10%	11%	11%
WM LCB	28%	No Data	No Data
WS LCC	11%	11%	12%

EN LCD	12%	12%	13%
EM LCE	28%	30%	28%
ES LCF	11%	10%	11%

In general, exterior girders (north and south) take approximately 21-24% of the total load on the bridge. The interior girder supports the remaining load (52-58%). As cracking occurs between 0 and 150,000 cycles, minimal changes in load distribution can be seen. Retrofitting the system slightly increases load supported by exterior girders when compared with the unretrofitted state at 150,000 cycles. Retrofitting results in similar load distribution to an uncracked specimen at 0 cycles.

EXPERIMENTAL DATA PLOTS

Table E. 5: Legend for Strain Plots

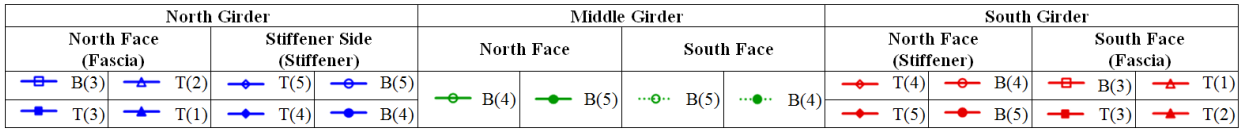

Figure E. 4: Static (0 Cycles) 5.24.2012

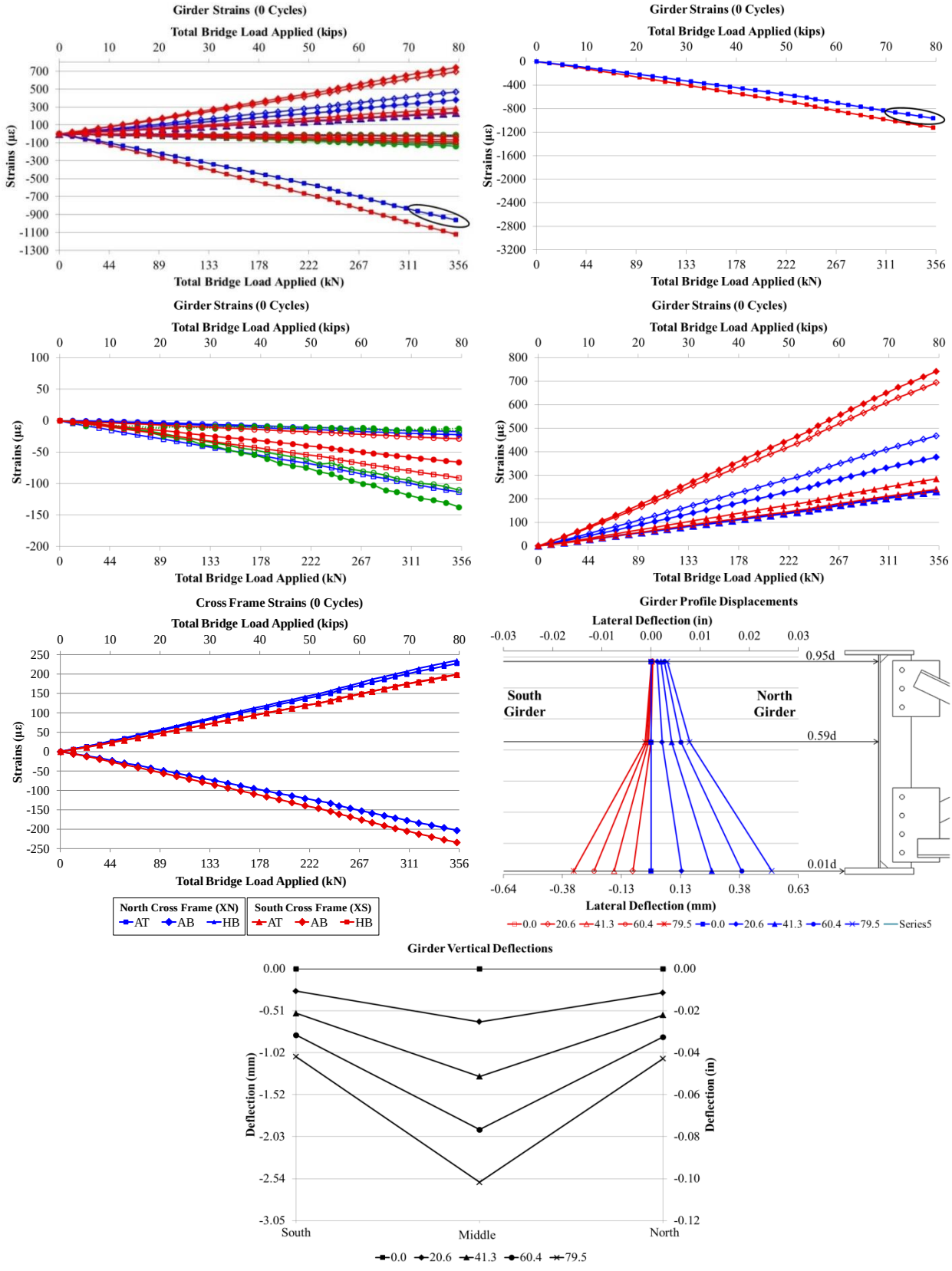

Figure E. 5: Static (15000 Cycles) 5.24.2012

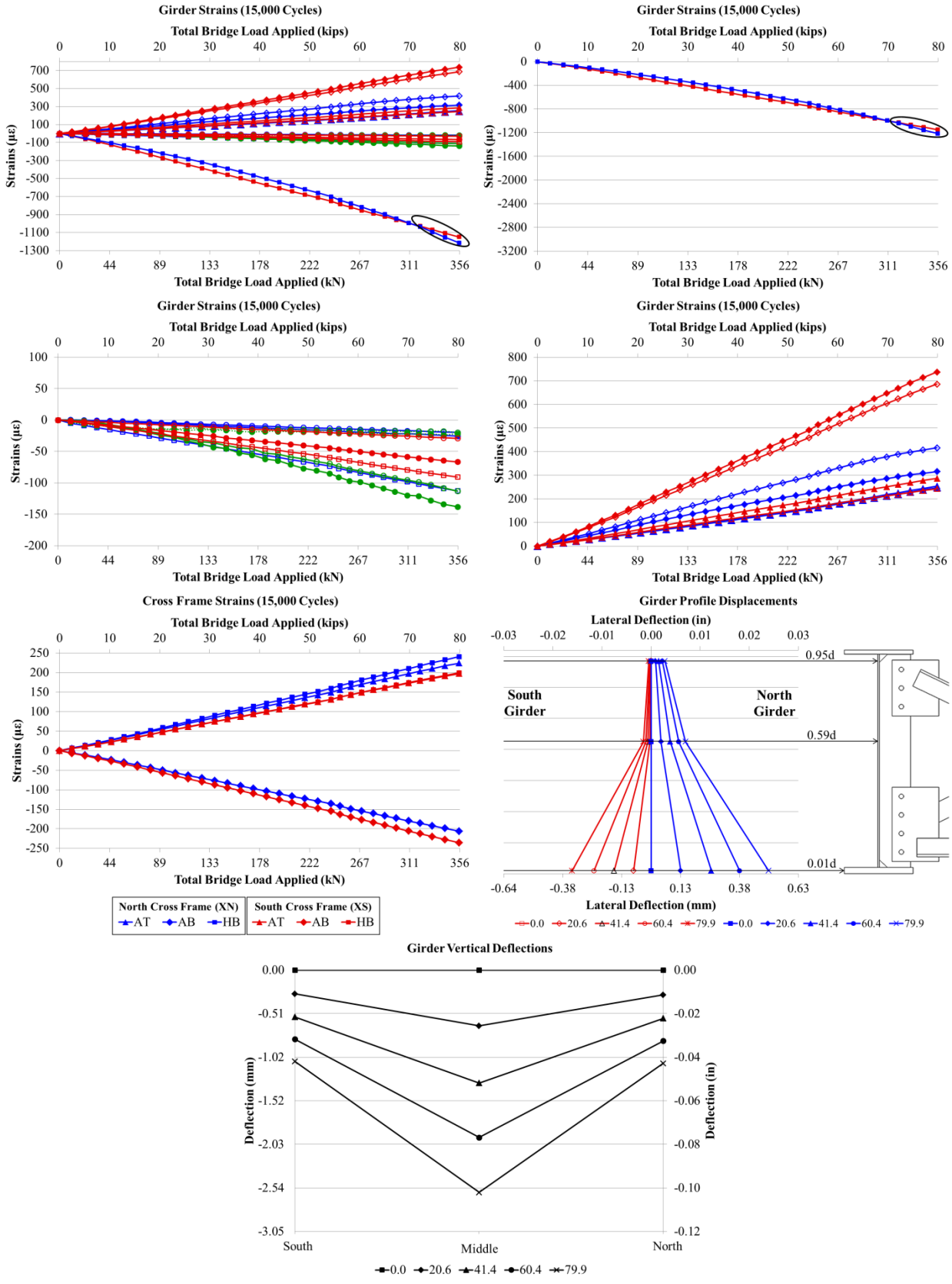

Figure E. 6: Static (20000 Cycles) 5.25.2012

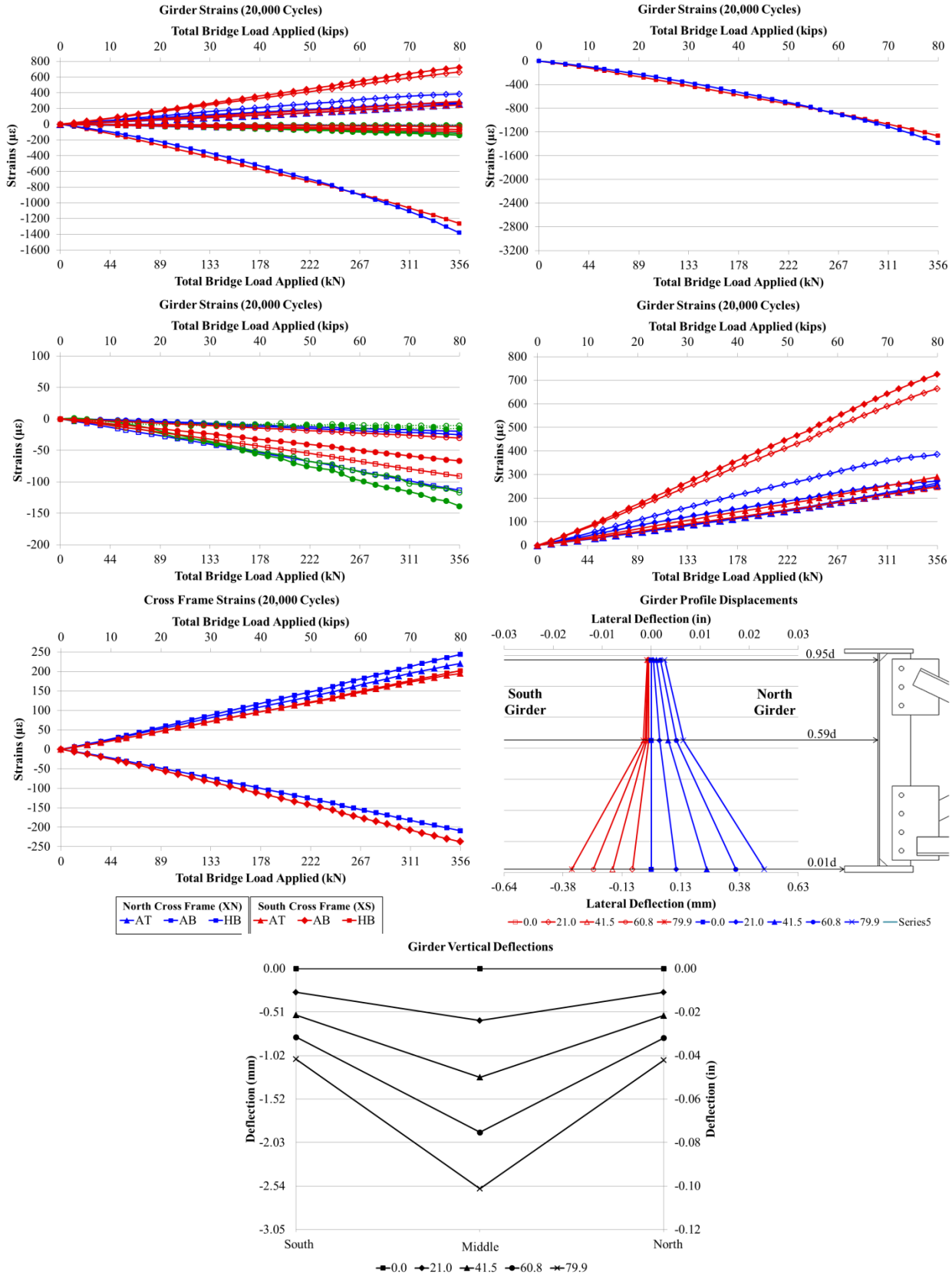

Figure E. 7: Static (30000 Cycles) 5.29.2012

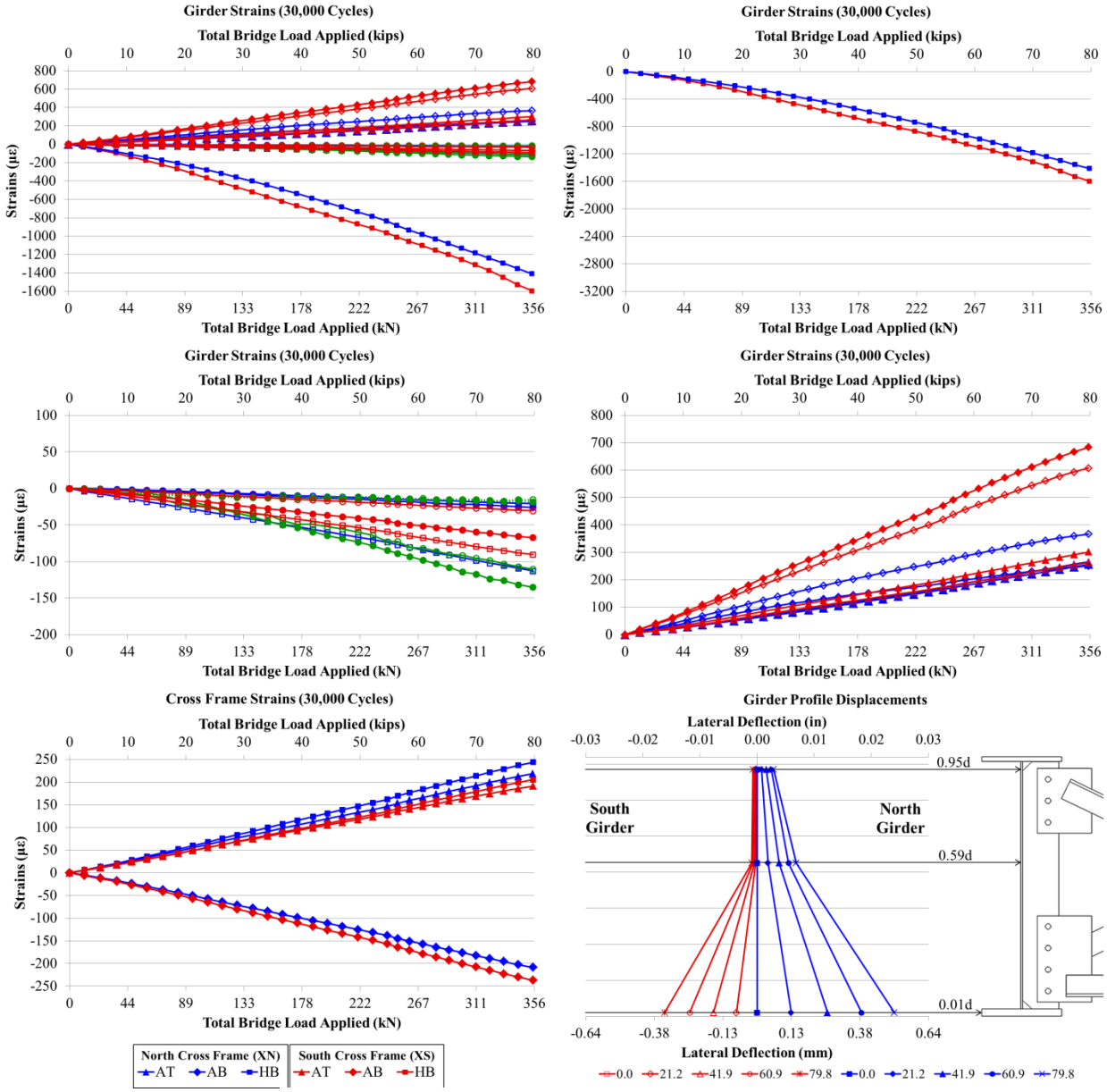

Figure E. 8: Static (45000 Cycles) 5.31.2012

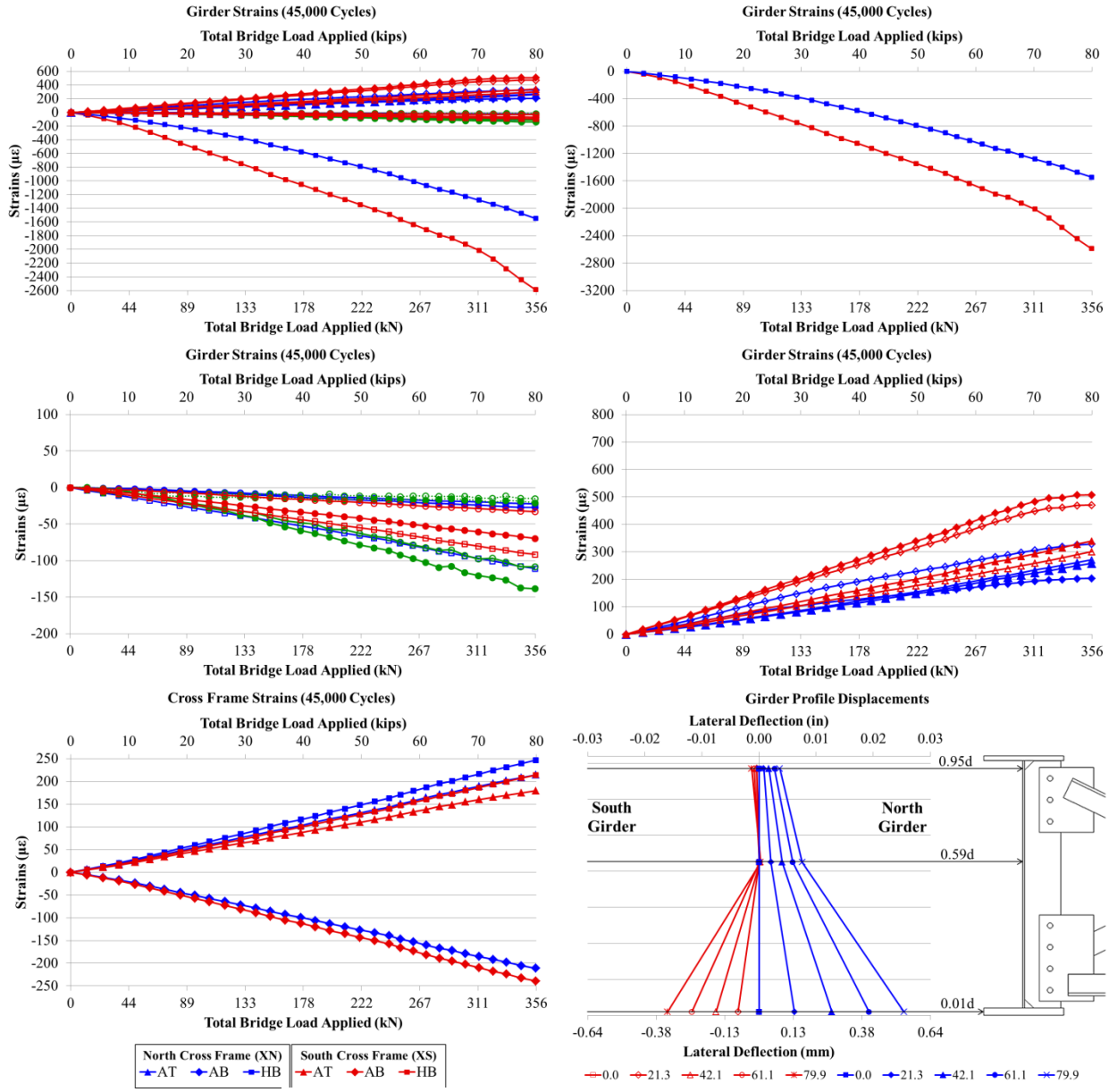

Figure E. 9: Static (60000 Cycles) 5.31.2012

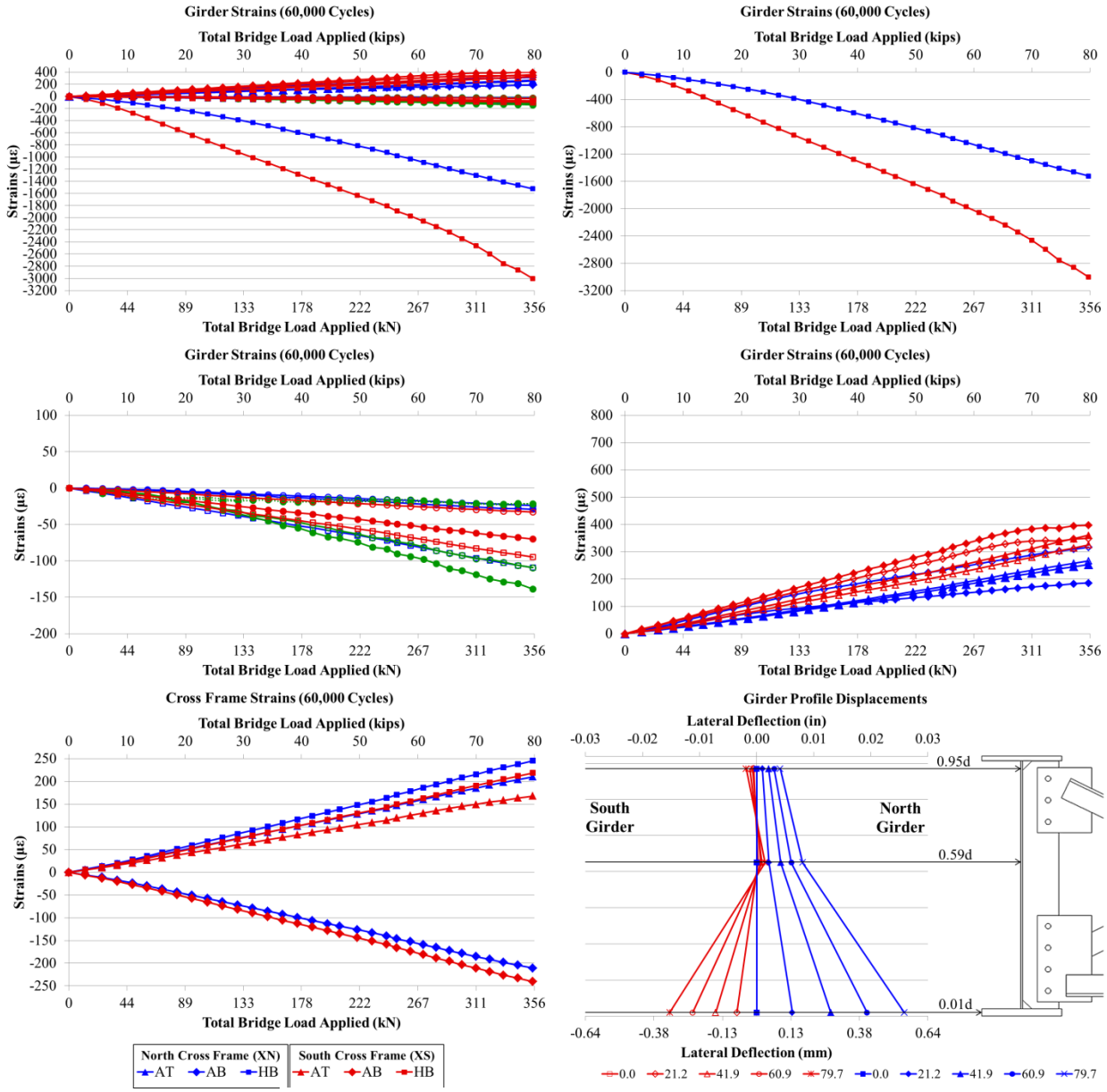

Figure E. 10: Static (75000 Cycles) 6.01.2012

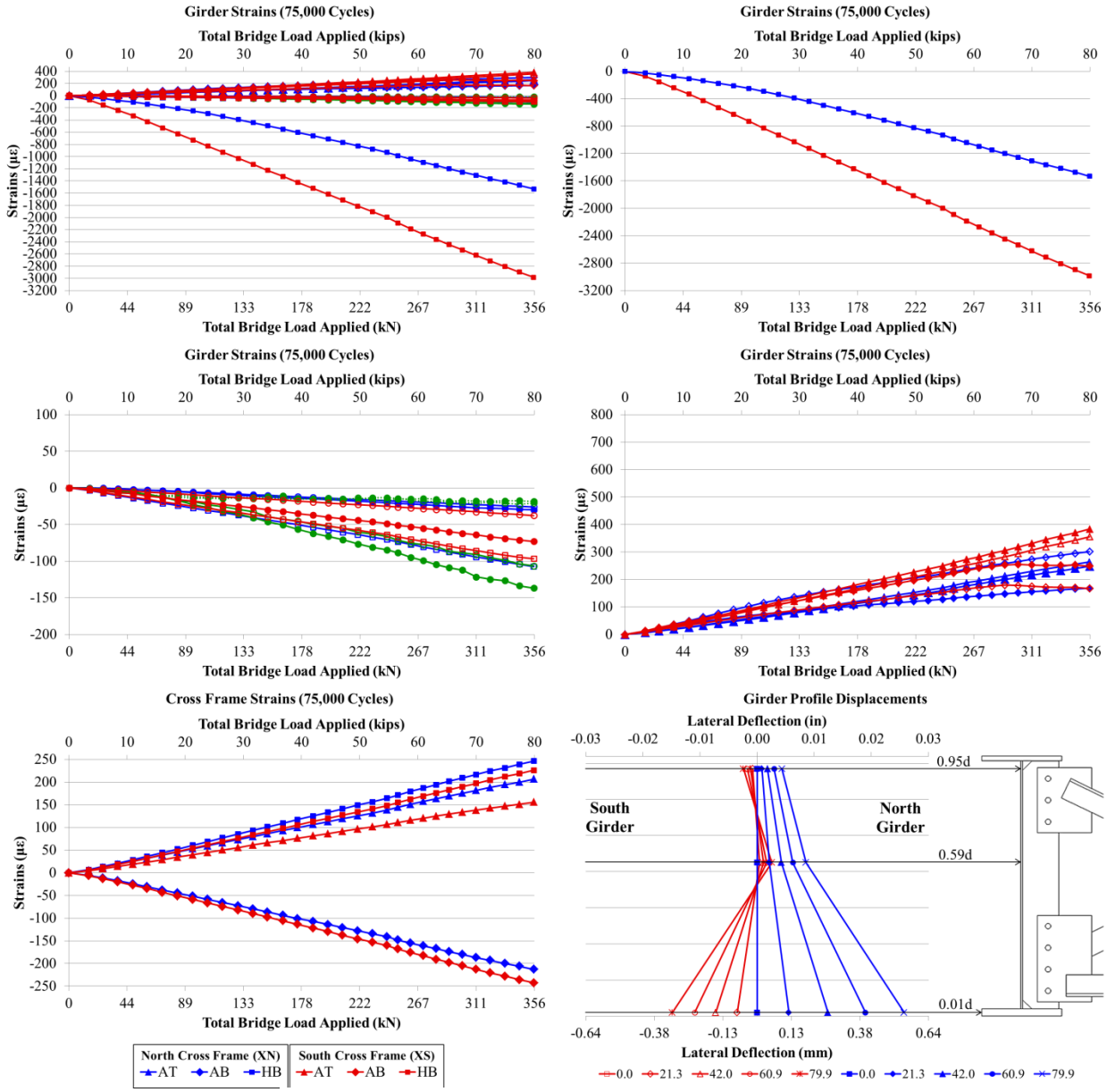

Figure E. 11: Static (90000 Cycles) 6.04.2012

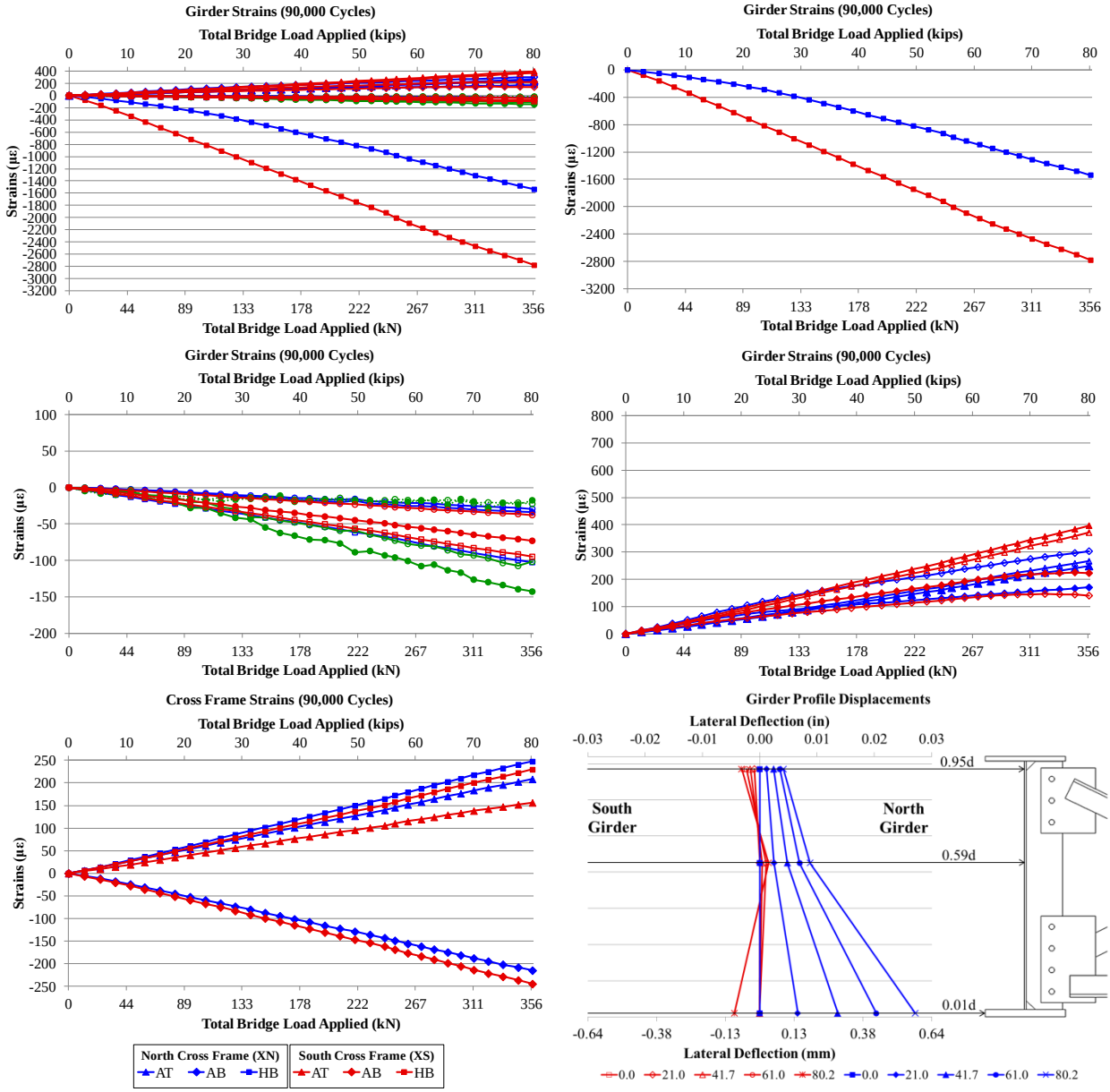

Figure E. 12: Static (105000 Cycles) 6.05.2012

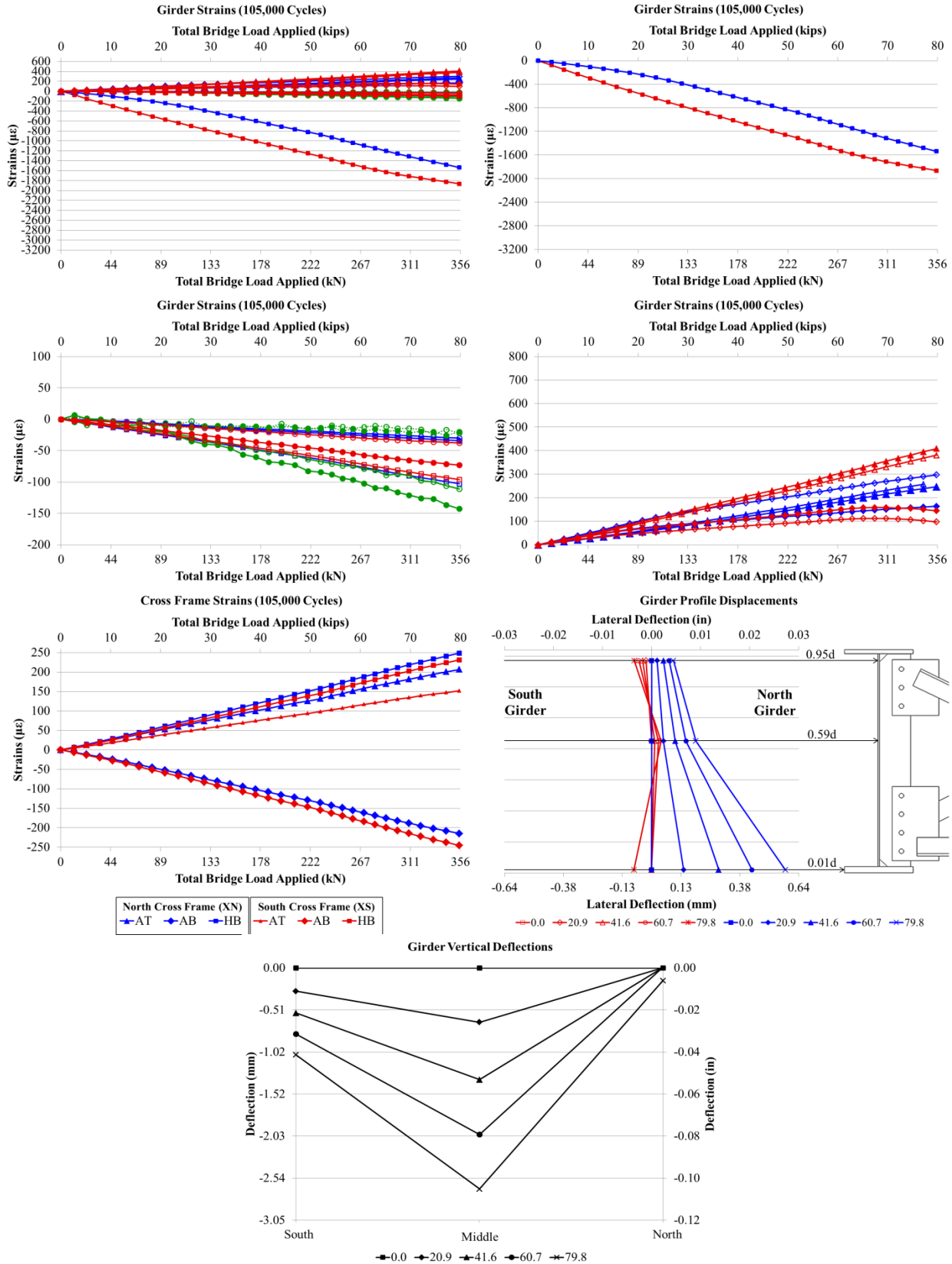

Figure E. 13: Static (120000 Cycles) 6.06.2012

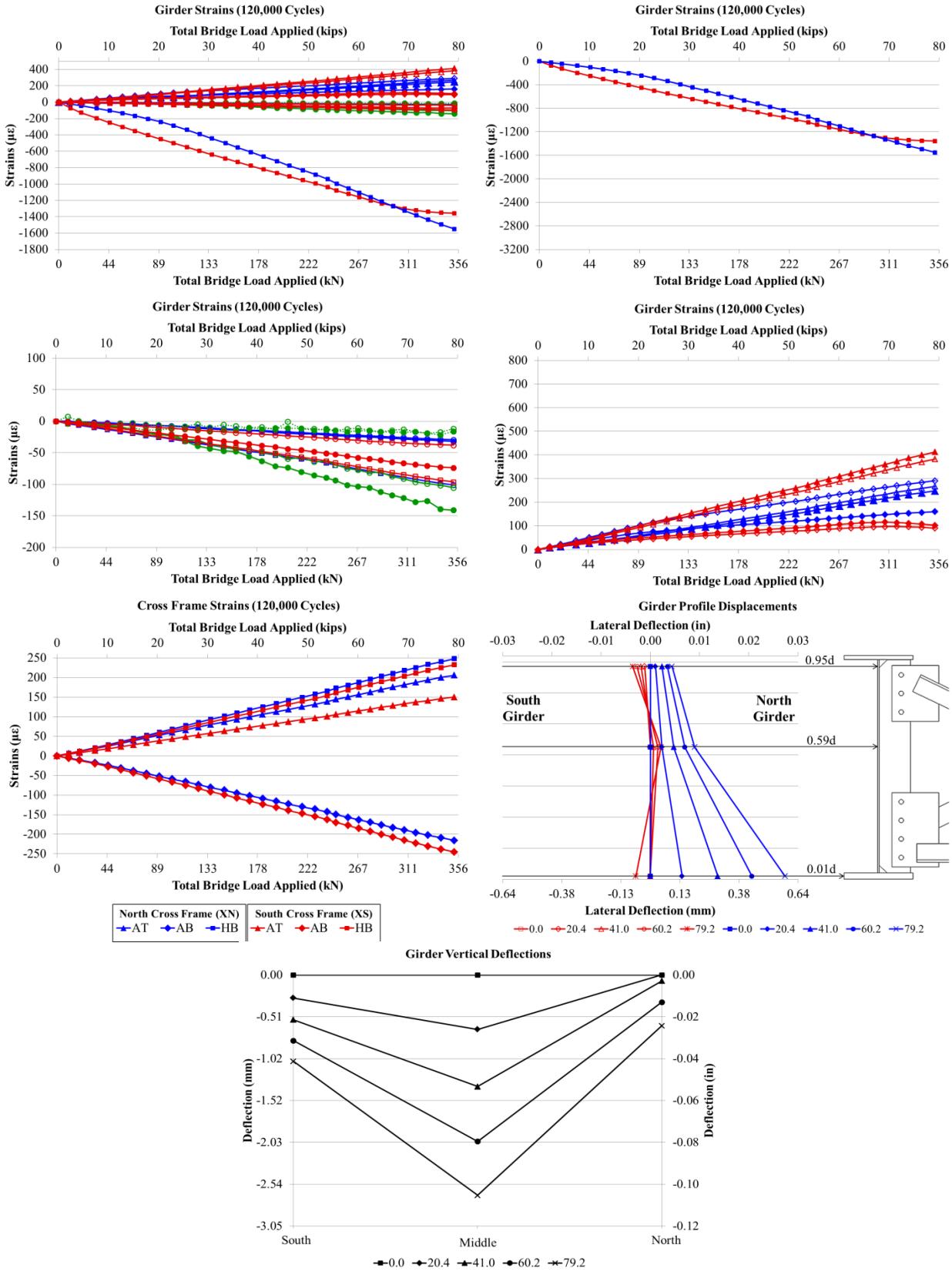

Figure E. 14: Static (135000 Cycles) 6.06.2012

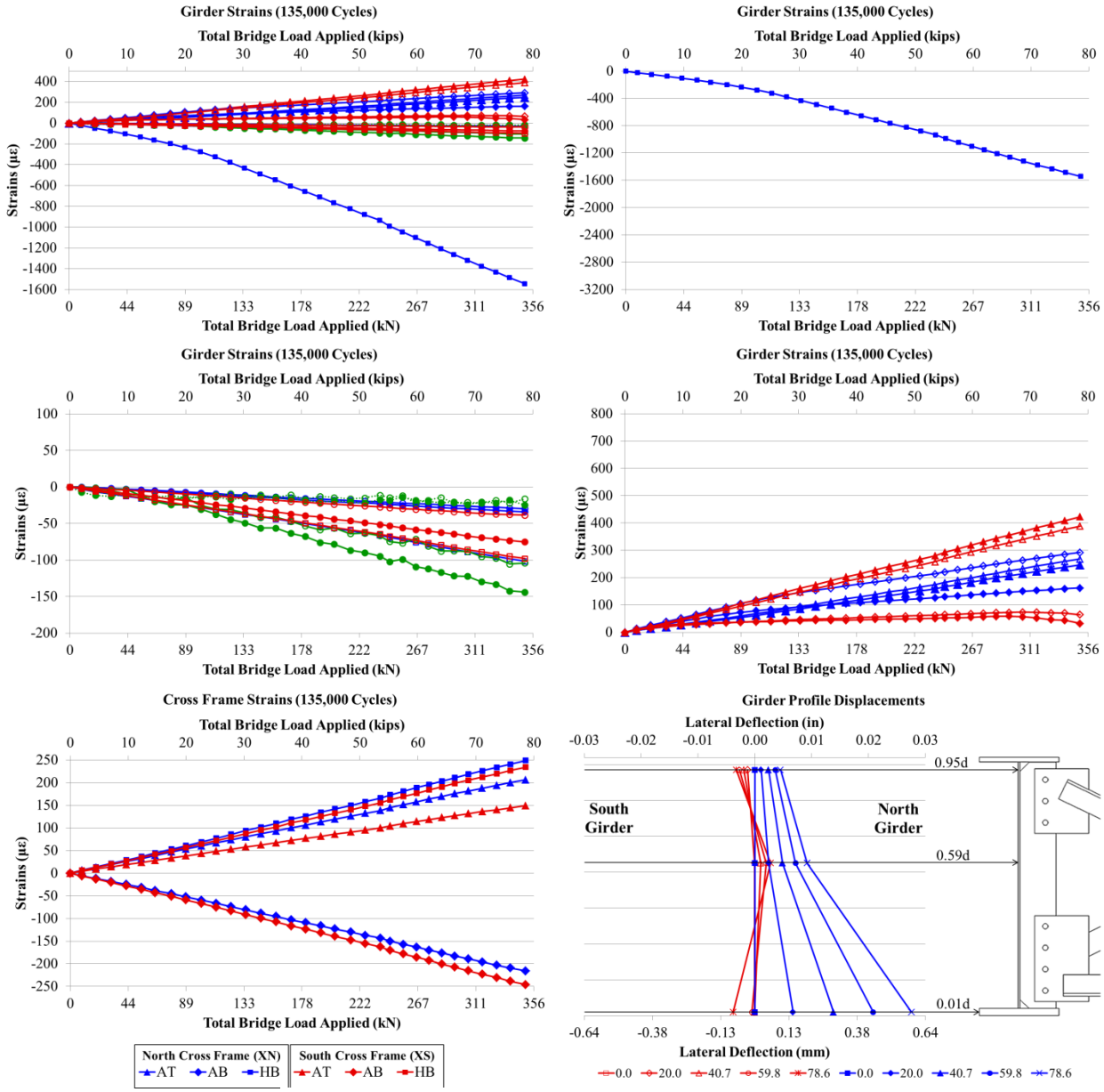

Figure E. 15: Static (150000 Cycles) 6.07.2012

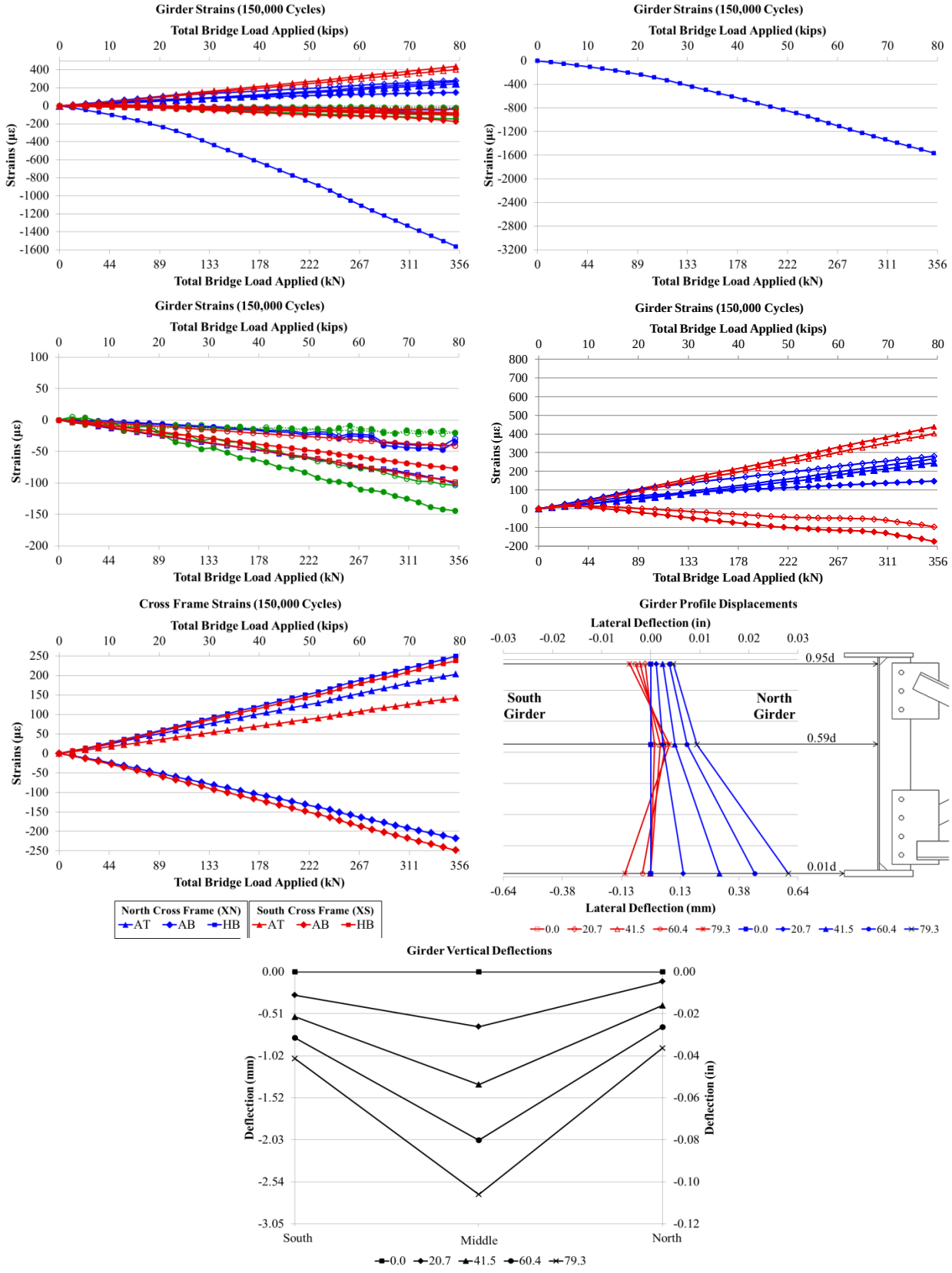

Figure E. 16: Static (150000 Cycles) 7.24.2012

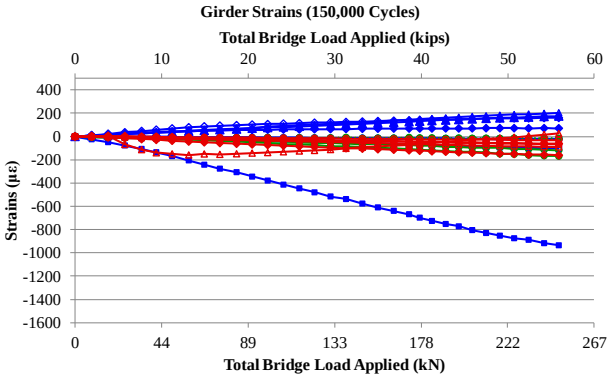

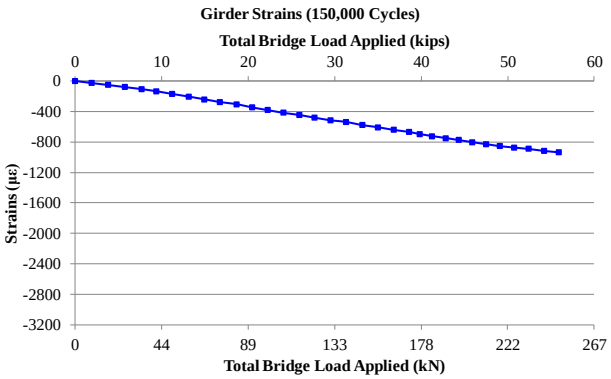

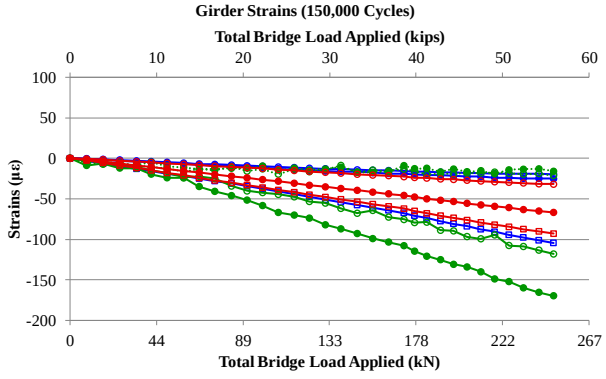

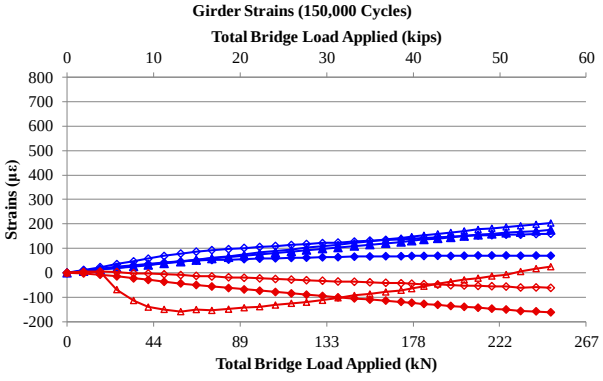

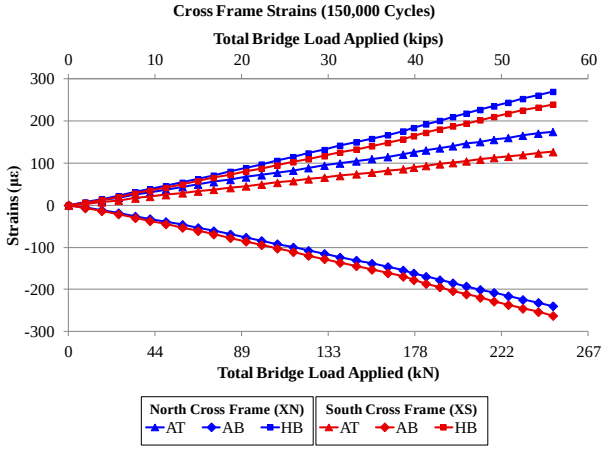

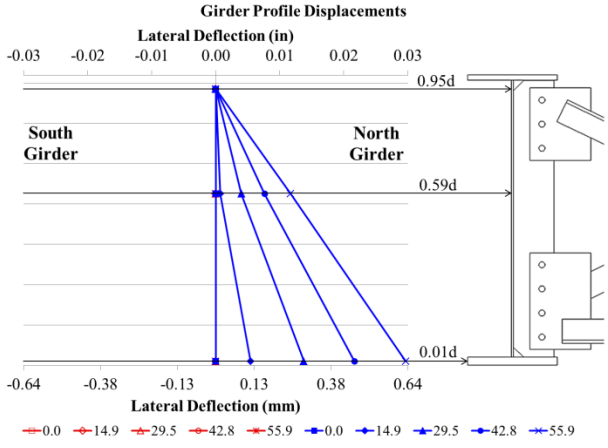

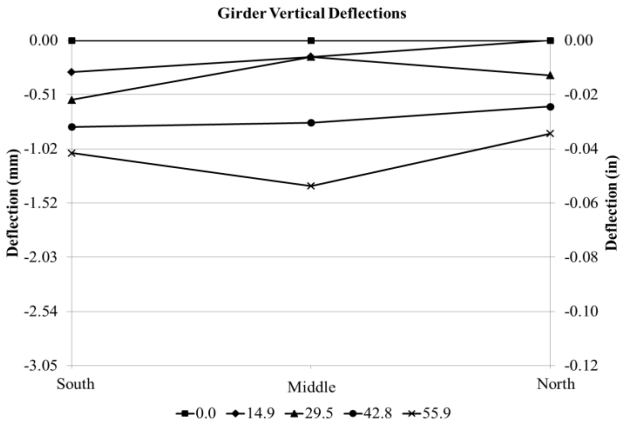

Figure E. 17: Static (150000 Cycles) 09.18.2012 - Without Retrofit

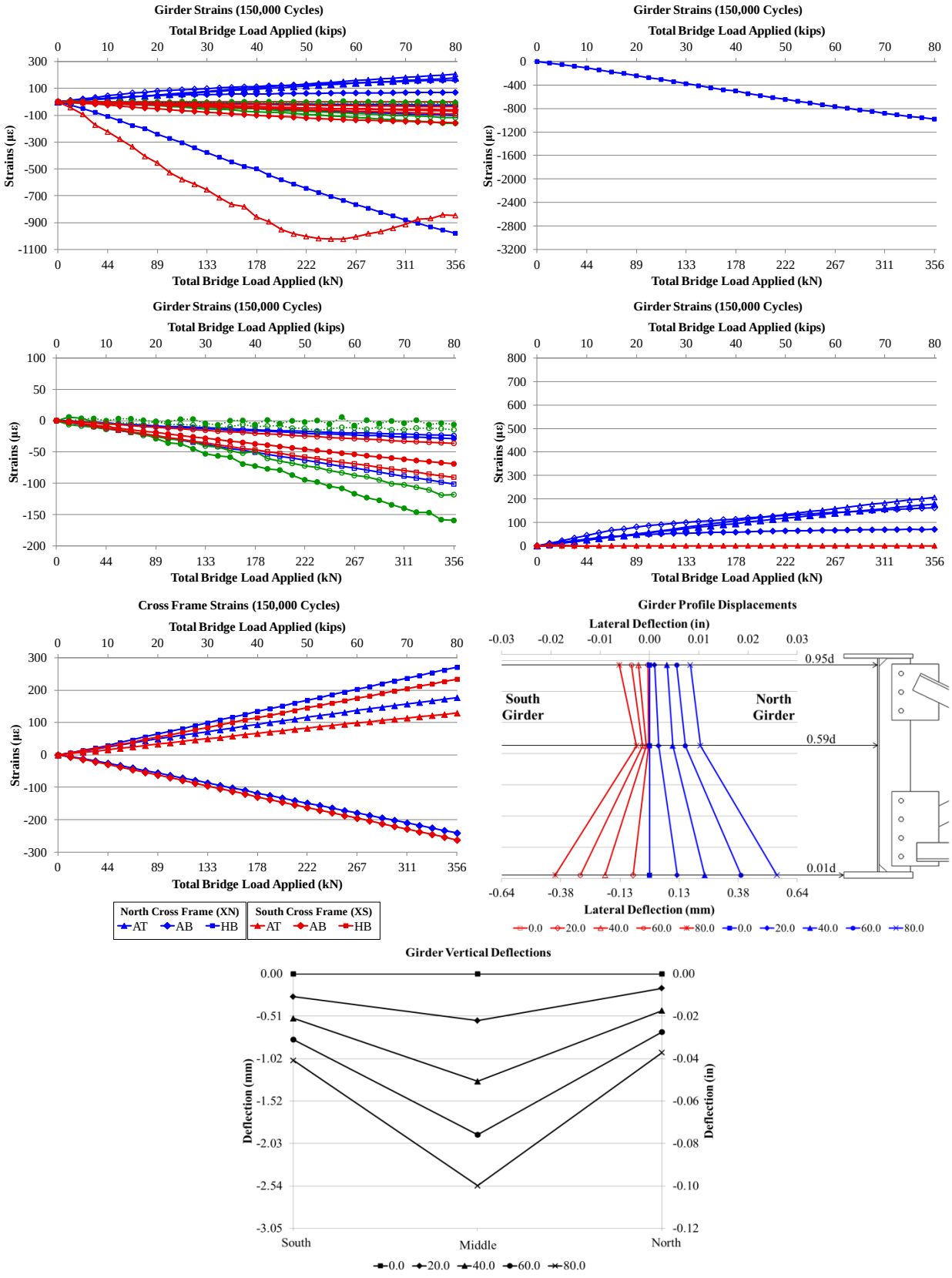

Figure E. 18: Static (150000 Cycles) 9.27.2012 – With Retrofit

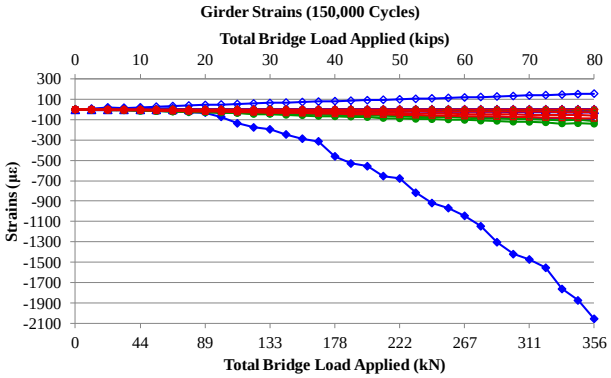

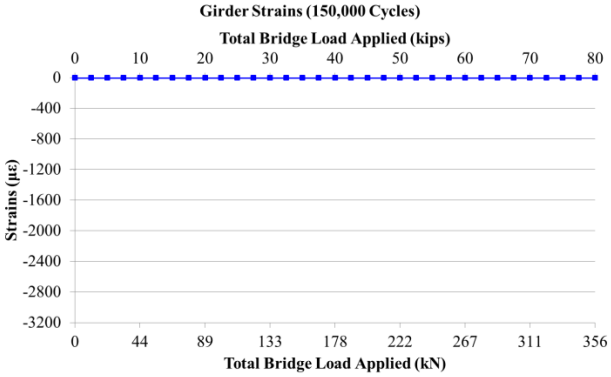

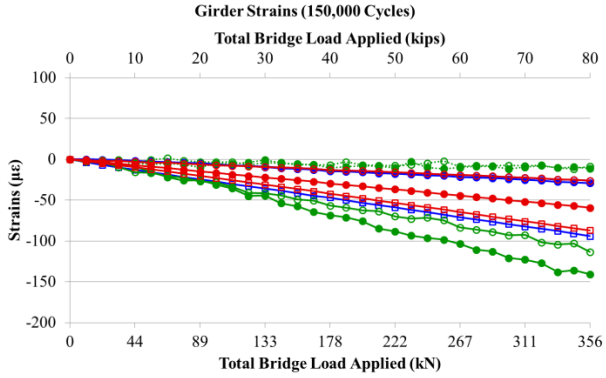

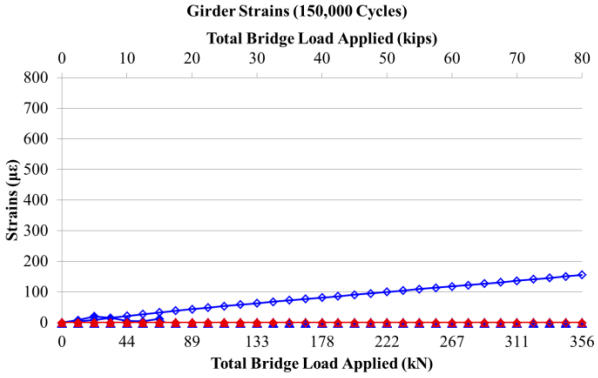

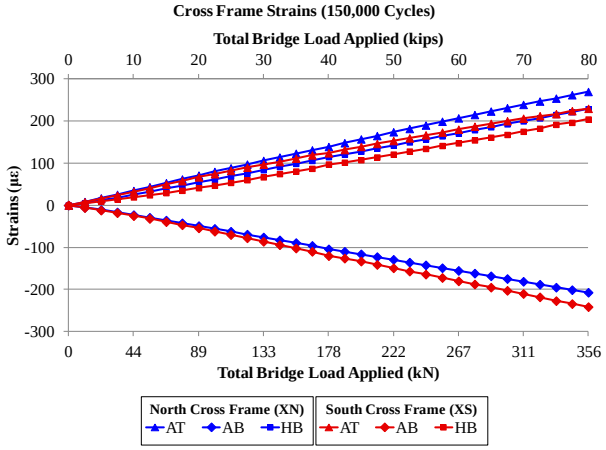

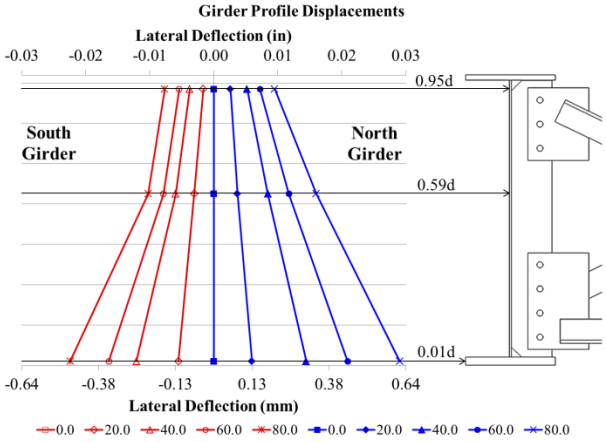

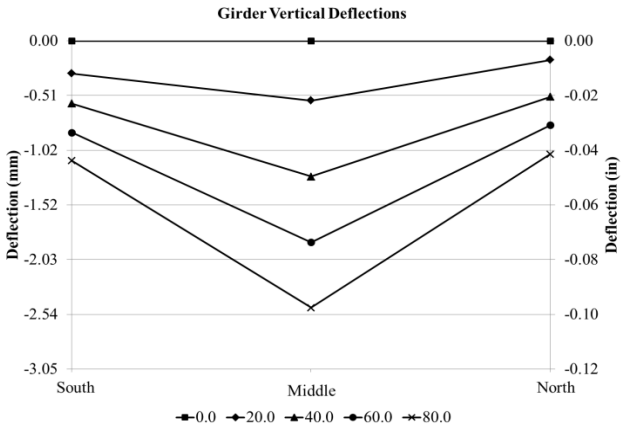

Figure E. 19: Static (1350000 Cycles) 12.07.2012– Without Retrofit

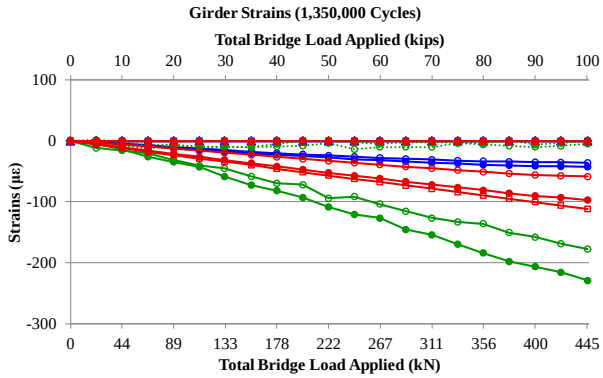

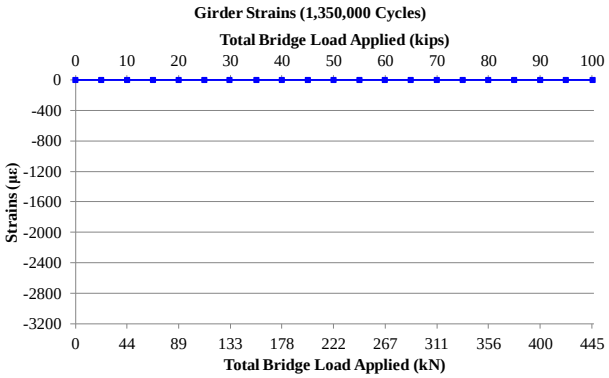

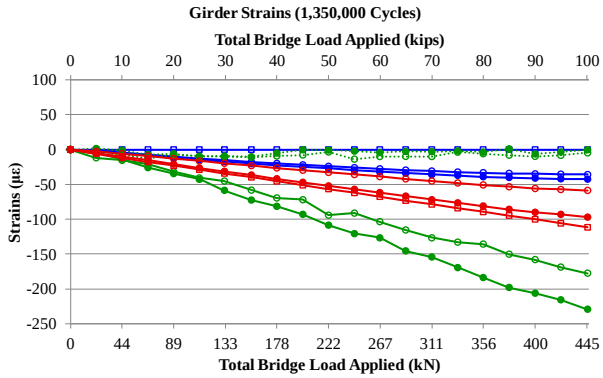

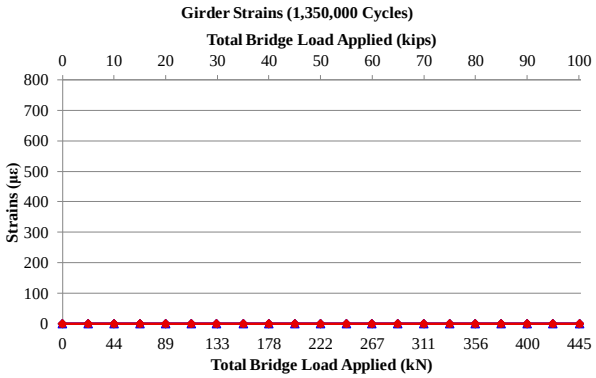

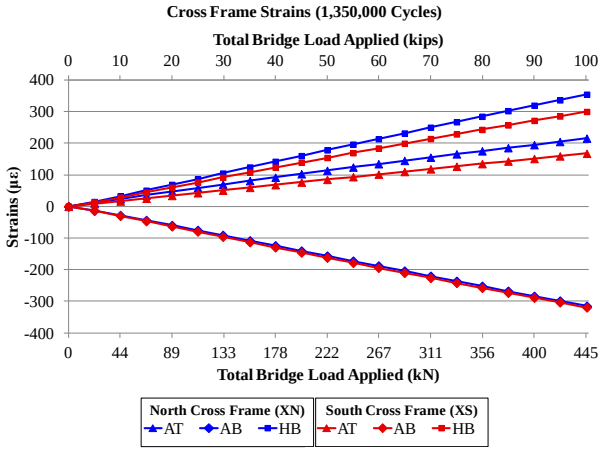

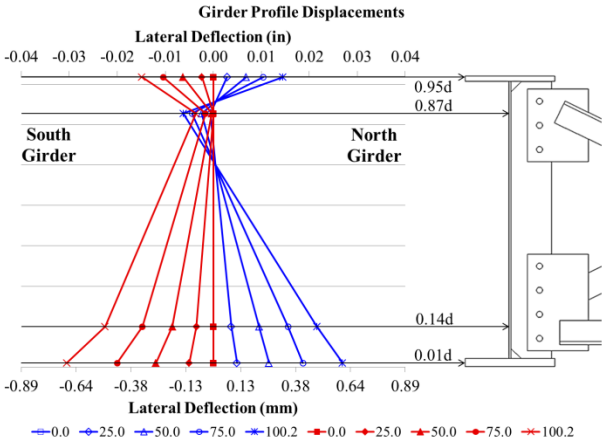

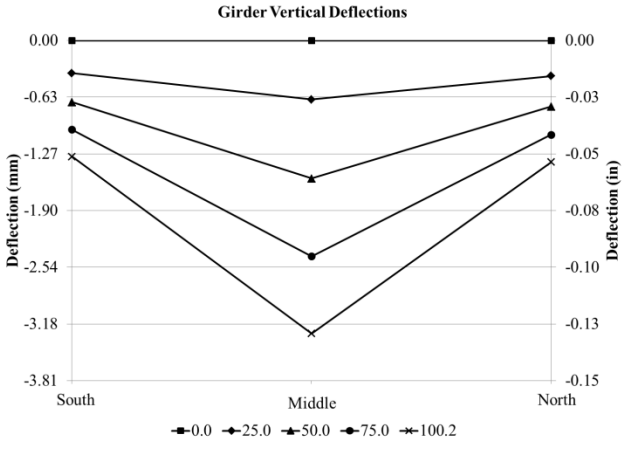

Figure E. 20: Static (1350000 Cycles) 12.07.2012 – With Retrofit

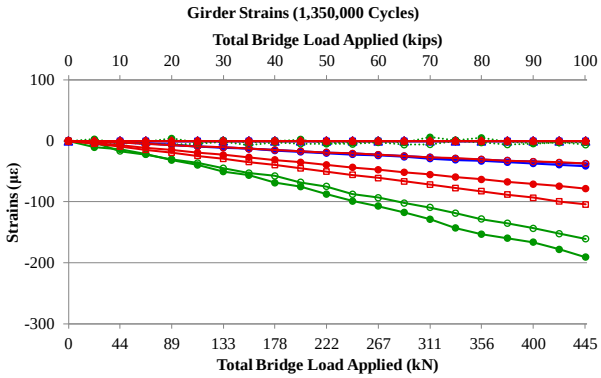

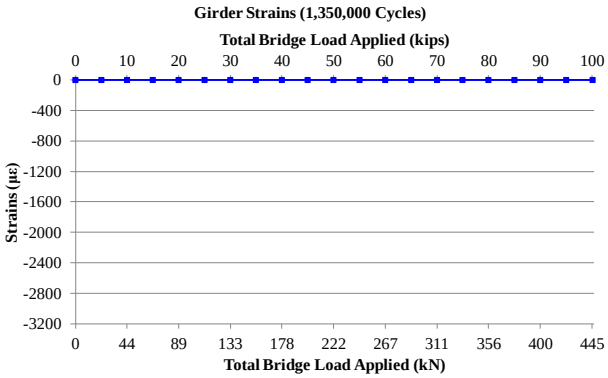

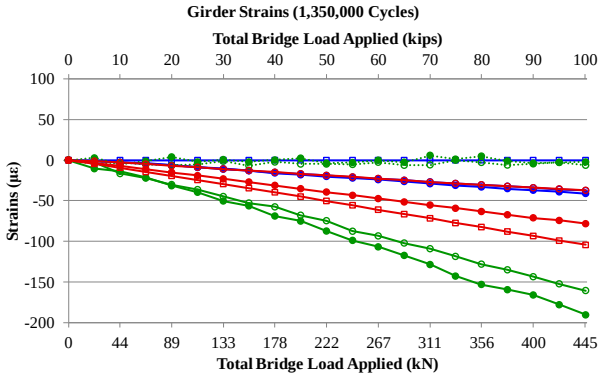

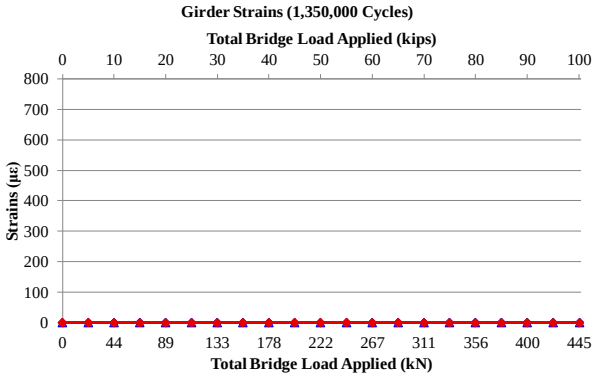

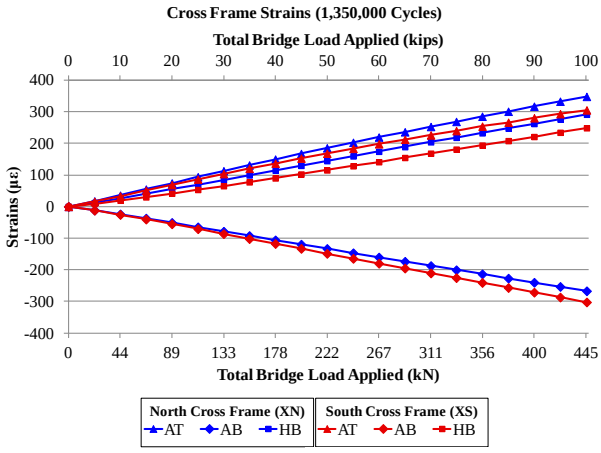

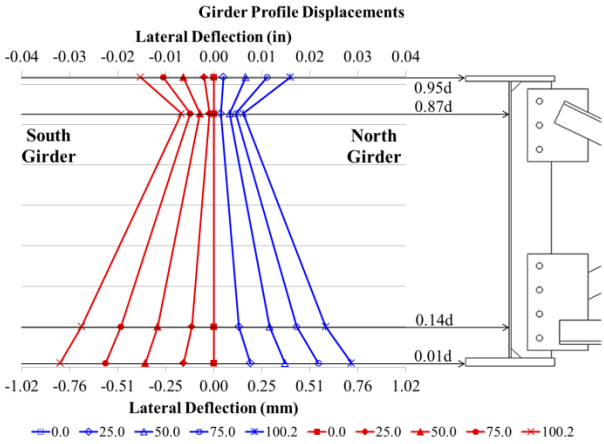

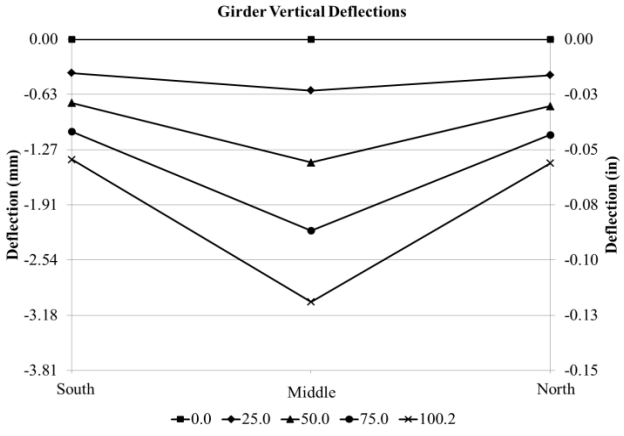

Figure E. 21: Static (2550000 Cycles) 12.21.2012 – With Retrofit

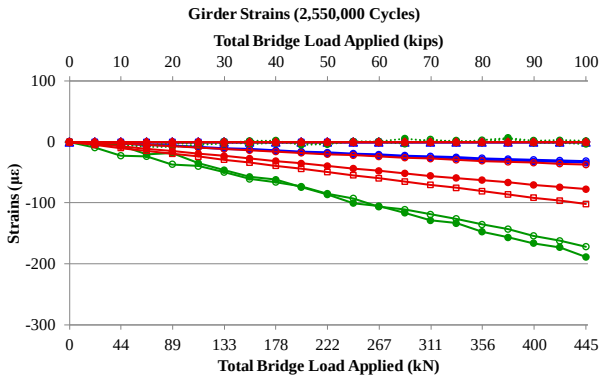

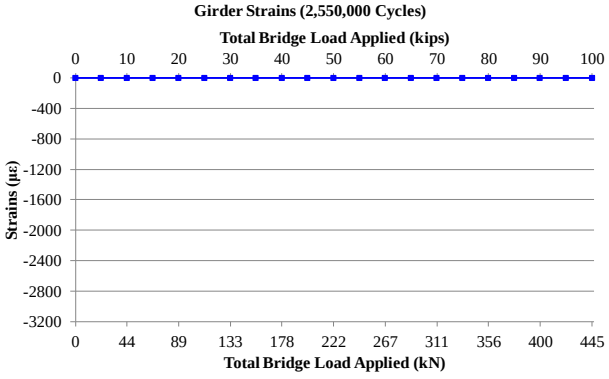

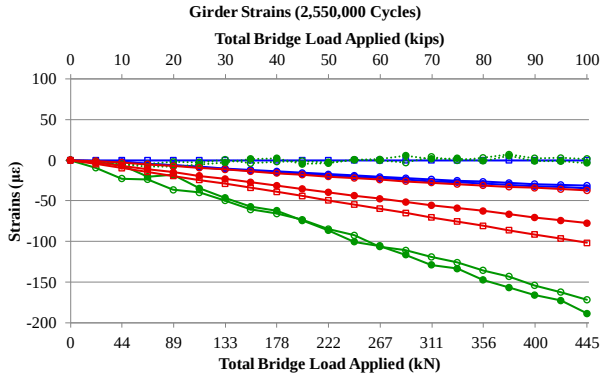

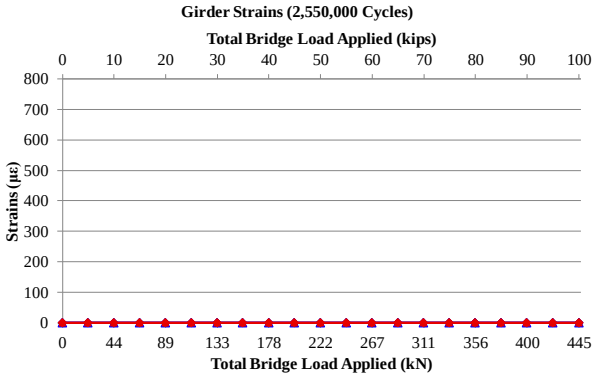

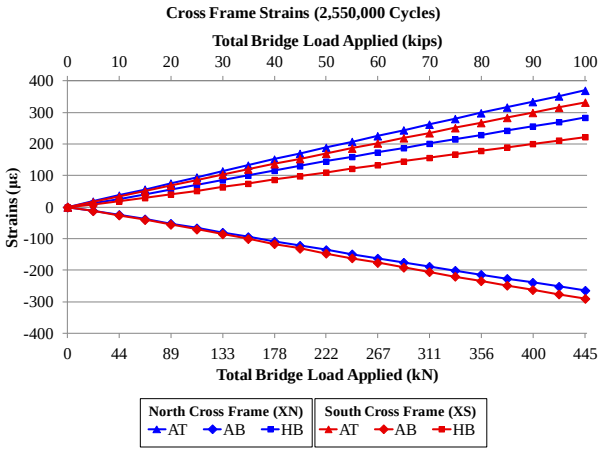

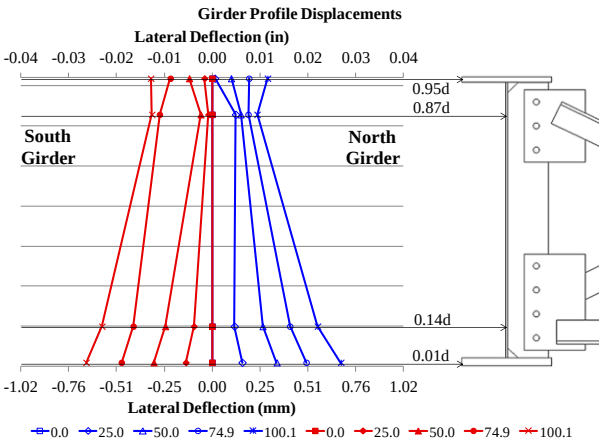

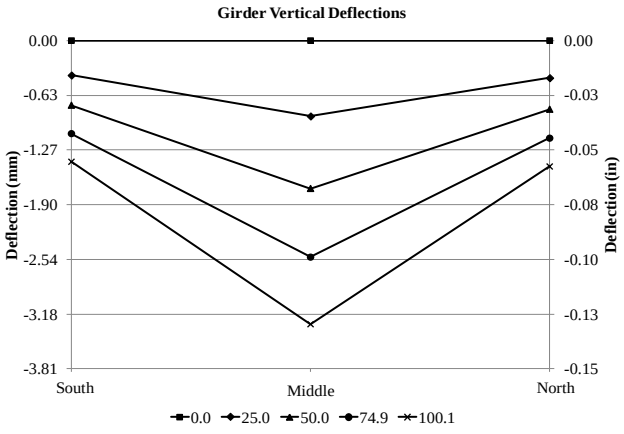

Figure E. 22: Static (2550000 Cycles) 12.21.2012 – Without Retrofit

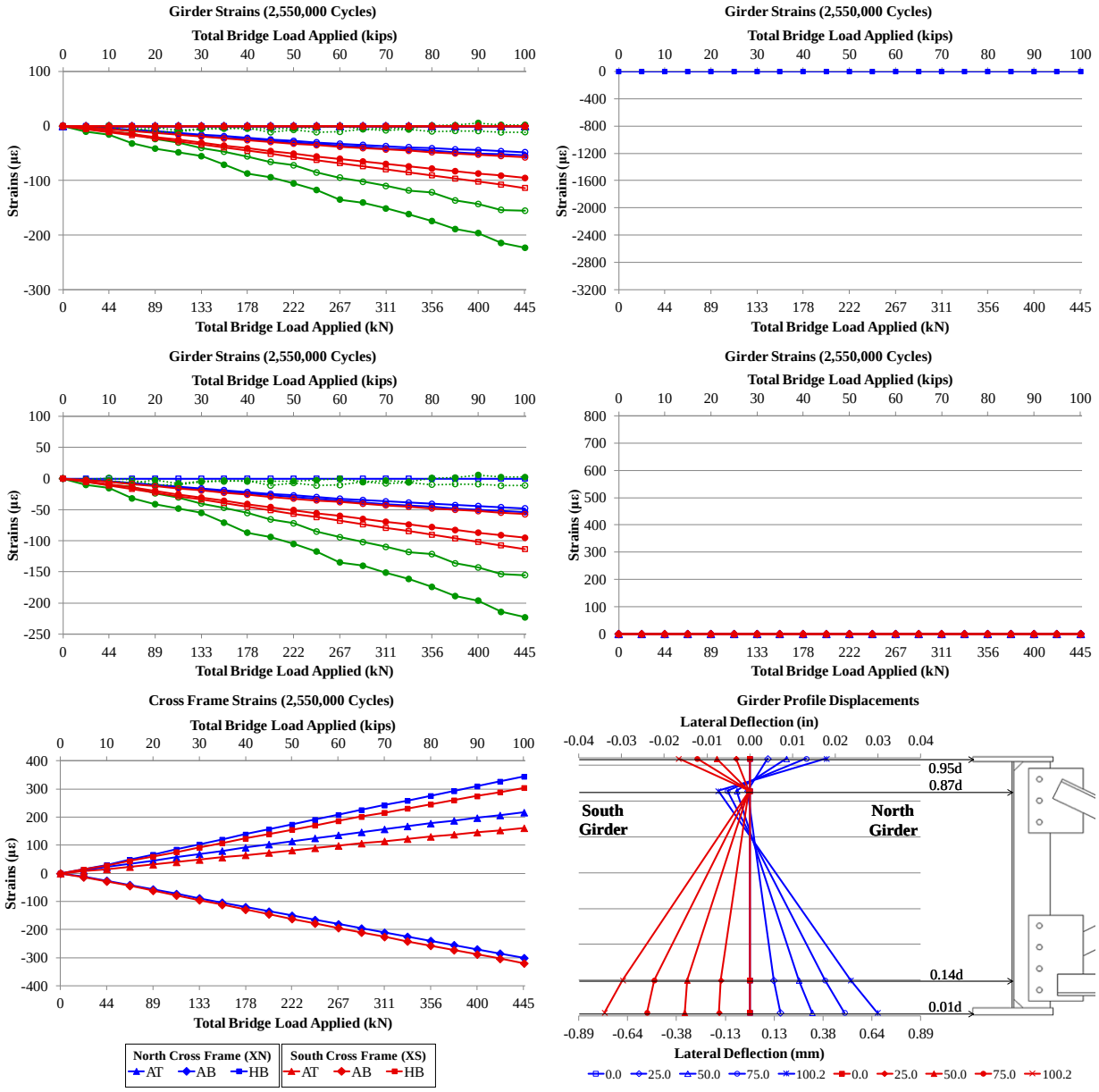

Figure E. 23: Static (2550000 Cycles) 01.03.2013 - Without Retrofit Drilled Holes

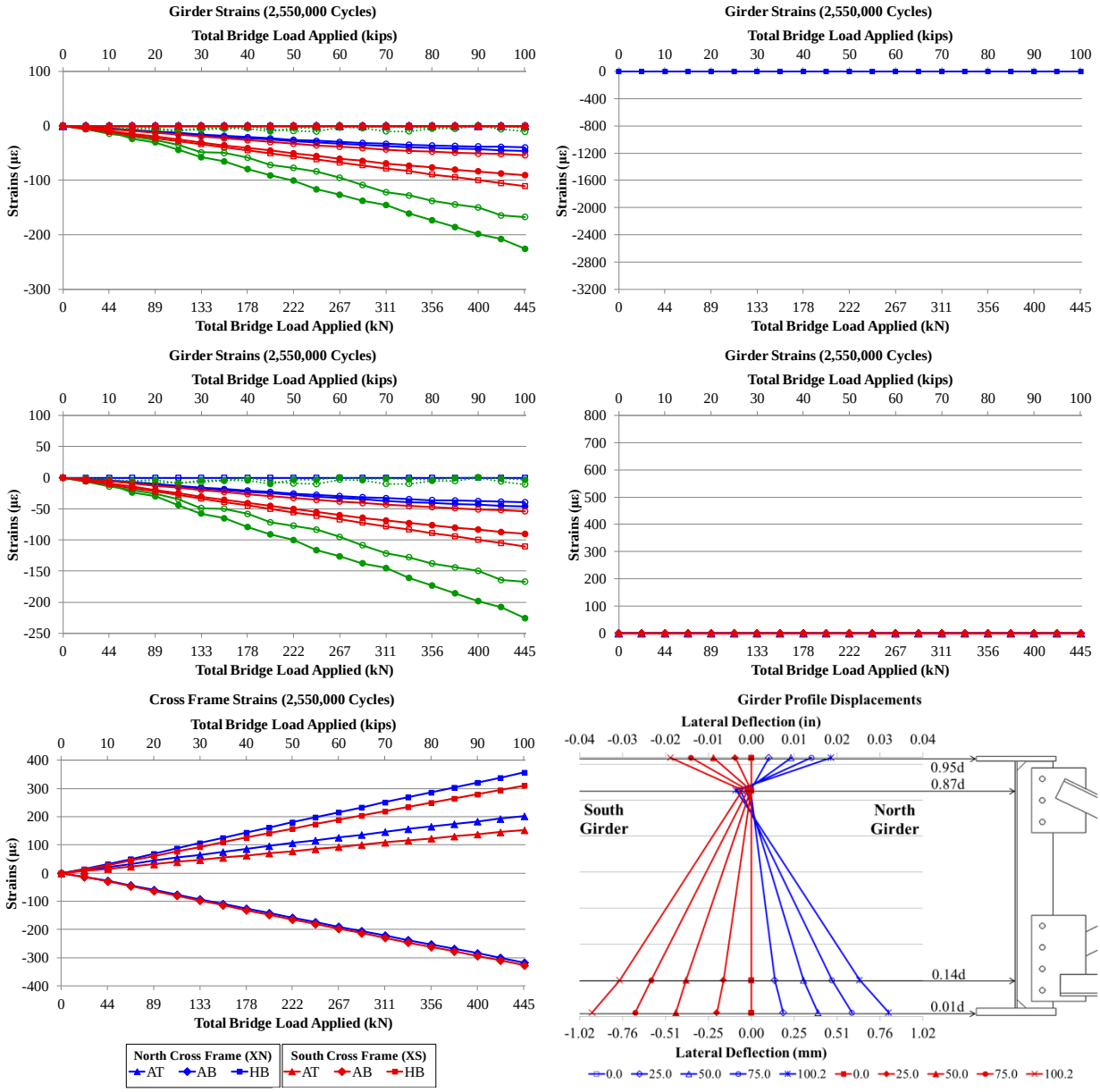

Figure E. 24: Static (2550000 Cycles) 01.04.2013 - With Retrofit Drilled Holes

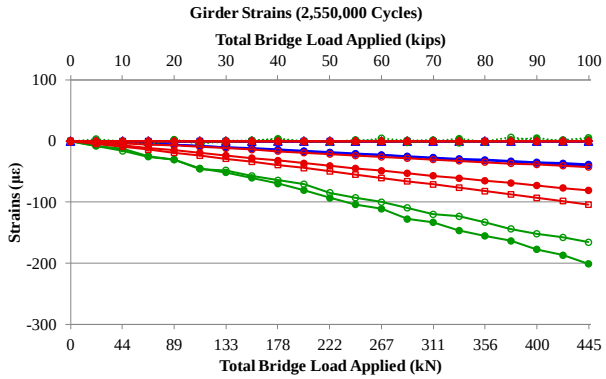

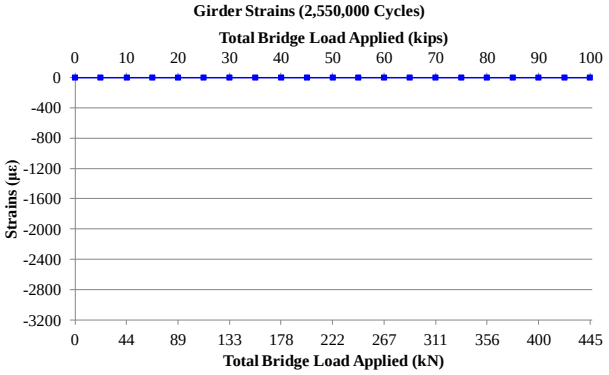

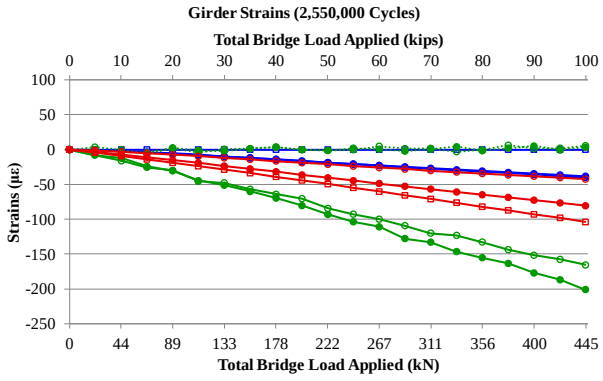

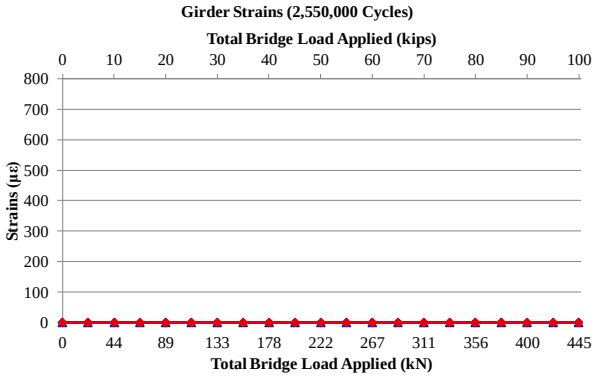

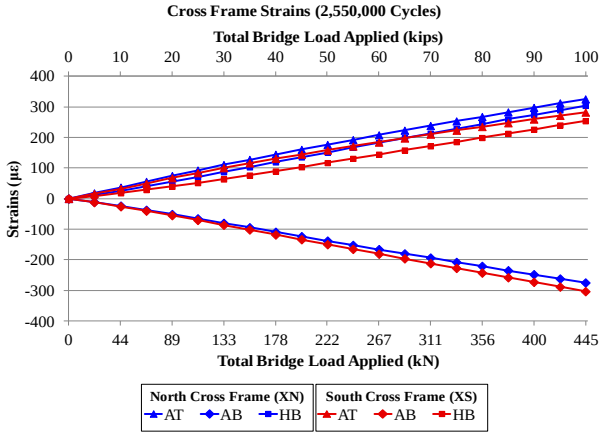

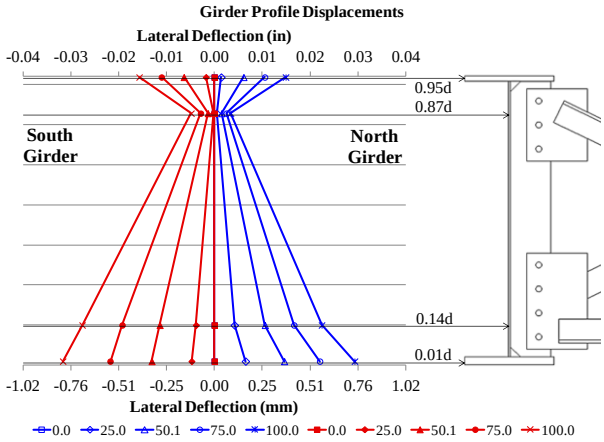

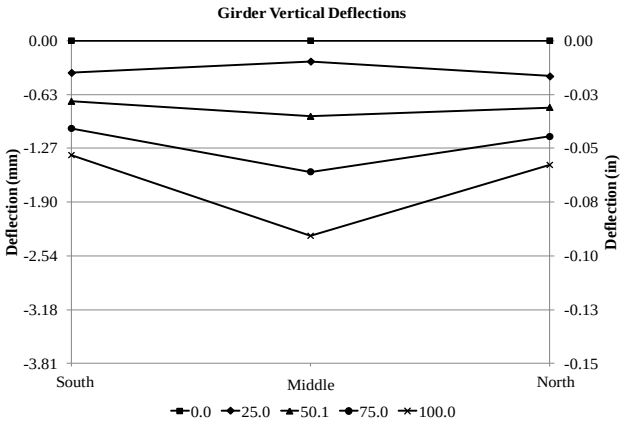

Figure E. 25: Static (3611097 Cycles) 01.17.2013 - With Retrofit Cracked Cross Frame Drilled Holes

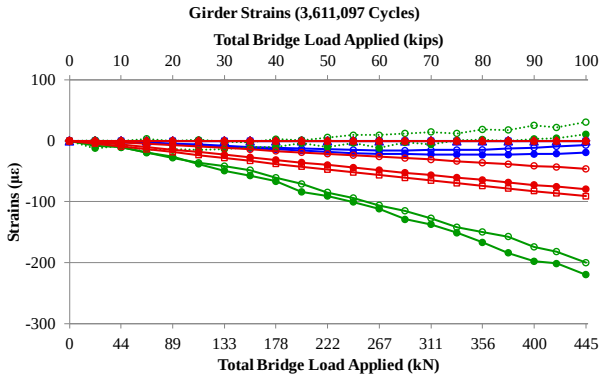

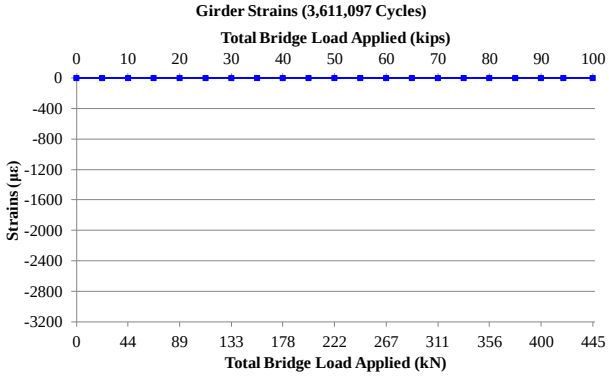

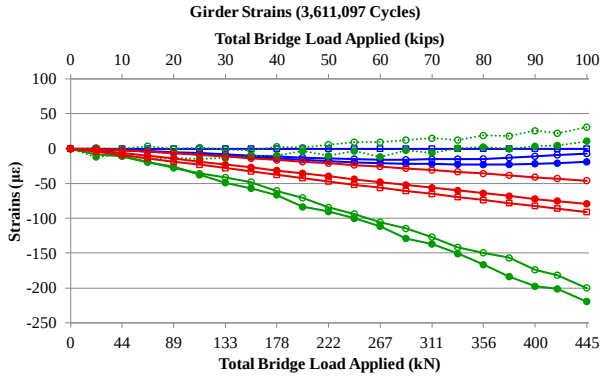

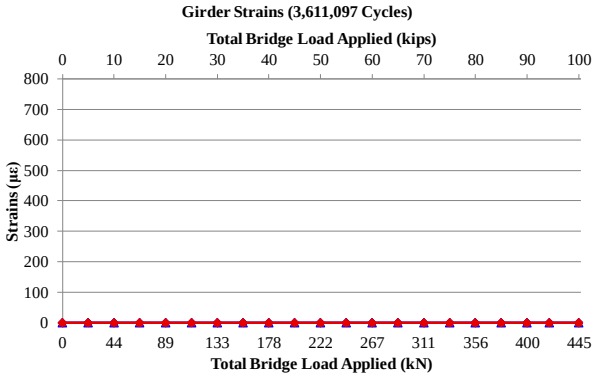

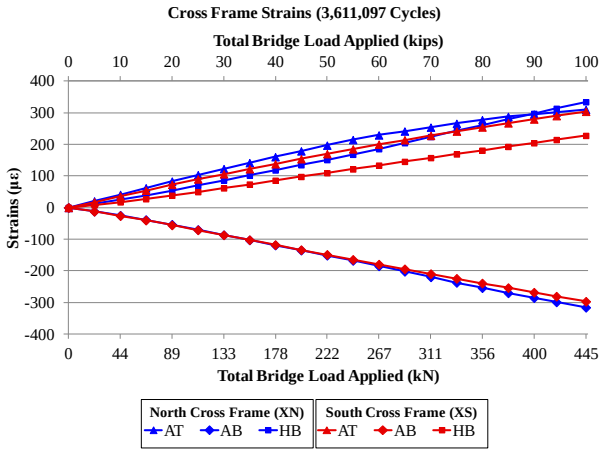

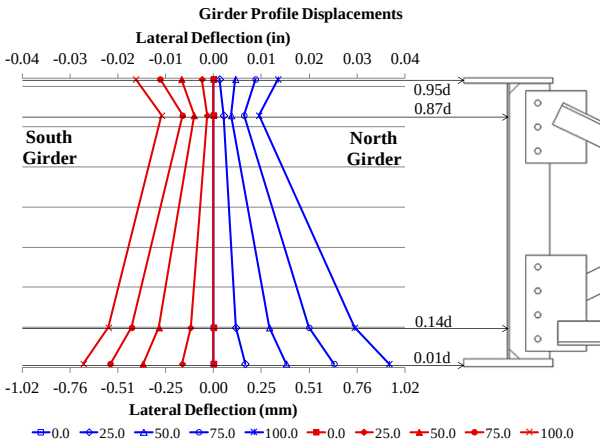

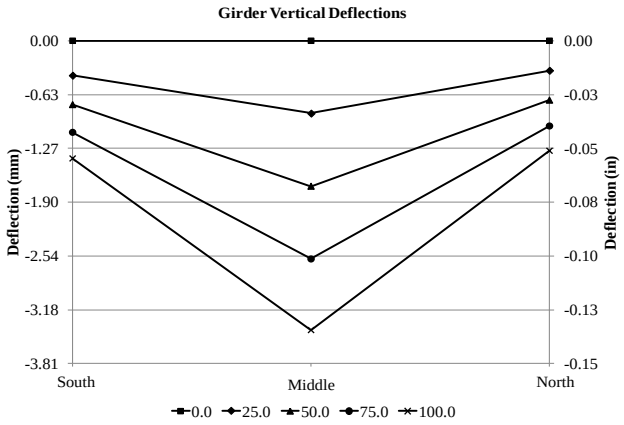

Figure E. 26: Static (3611097 Cycles) 01.22.2013- With Retrofit New Crossframe 0.5in Hole

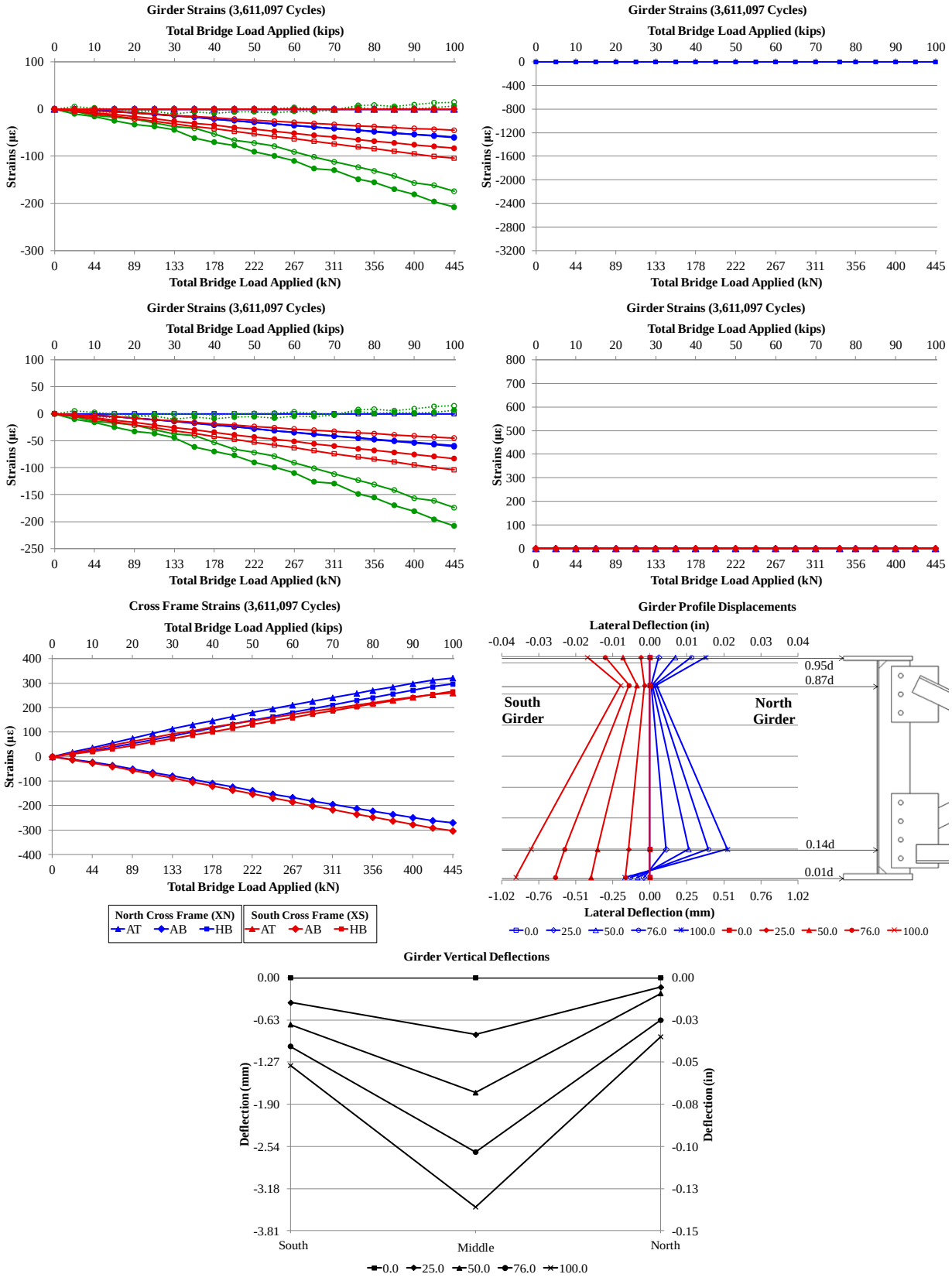

Figure E. 27: Static (3611097 Cycles) 01.22.2013 - Without Retrofit New Crossframe 0.5in Hole

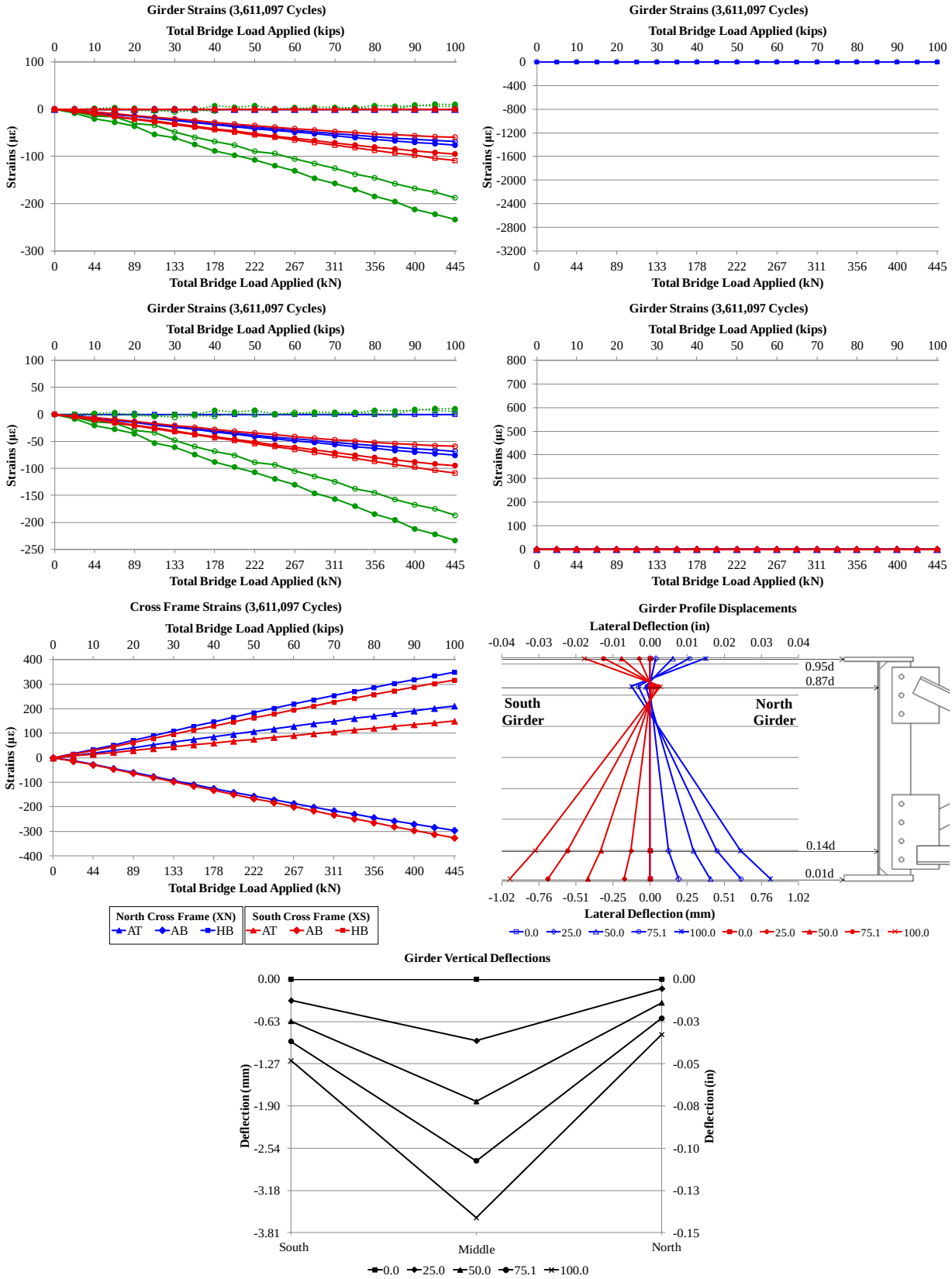

Figure E. 28: Static (3611097 Cycles) 01.22.2013 - Without Retrofit New Crossframe

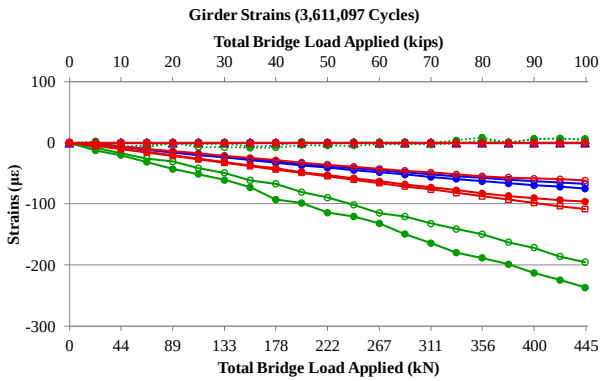

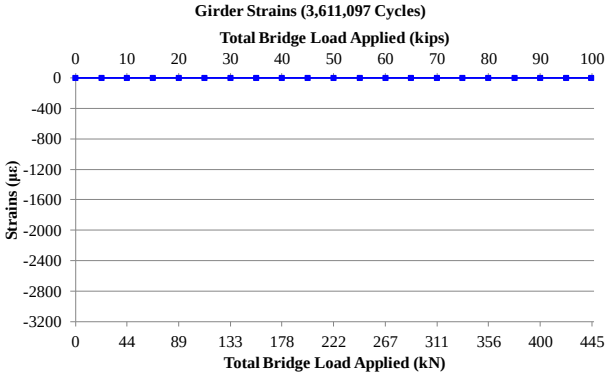

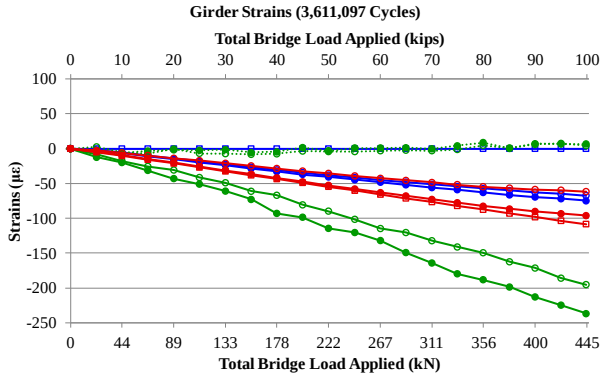

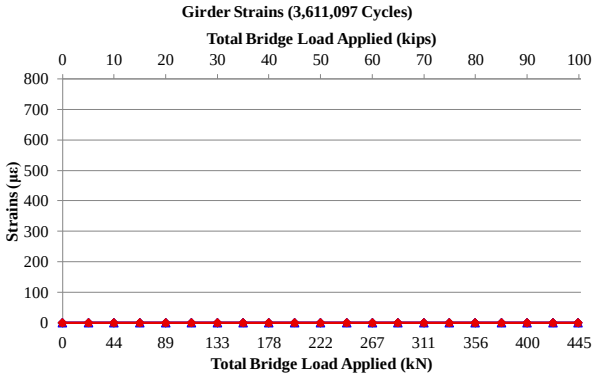

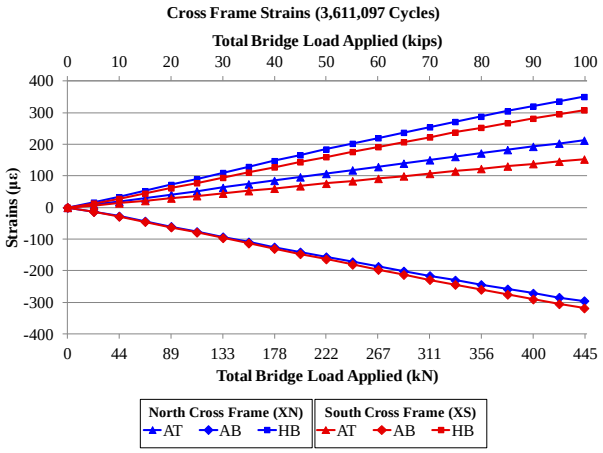

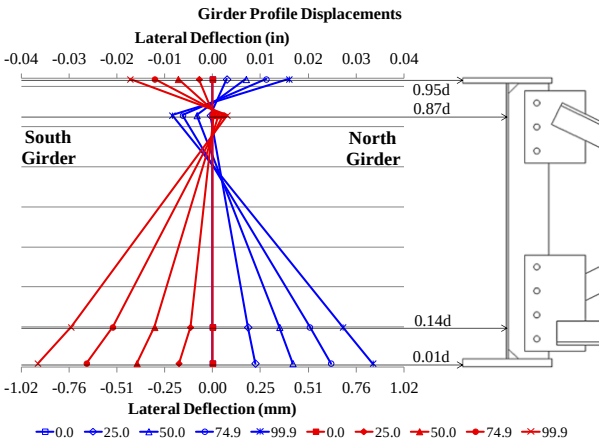

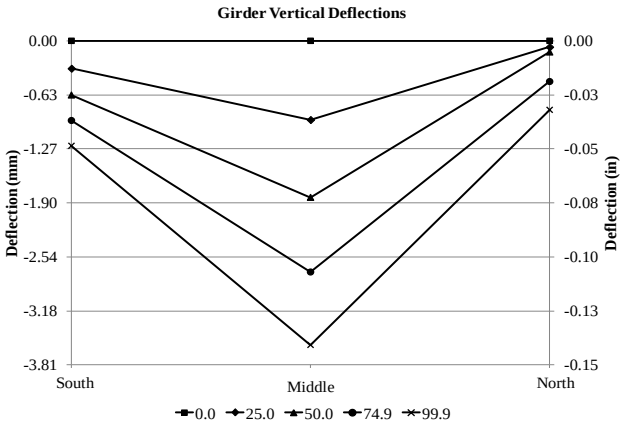

Figure E. 29: Static (4811097 Cycles) 02.15.2013 - Without Retrofit

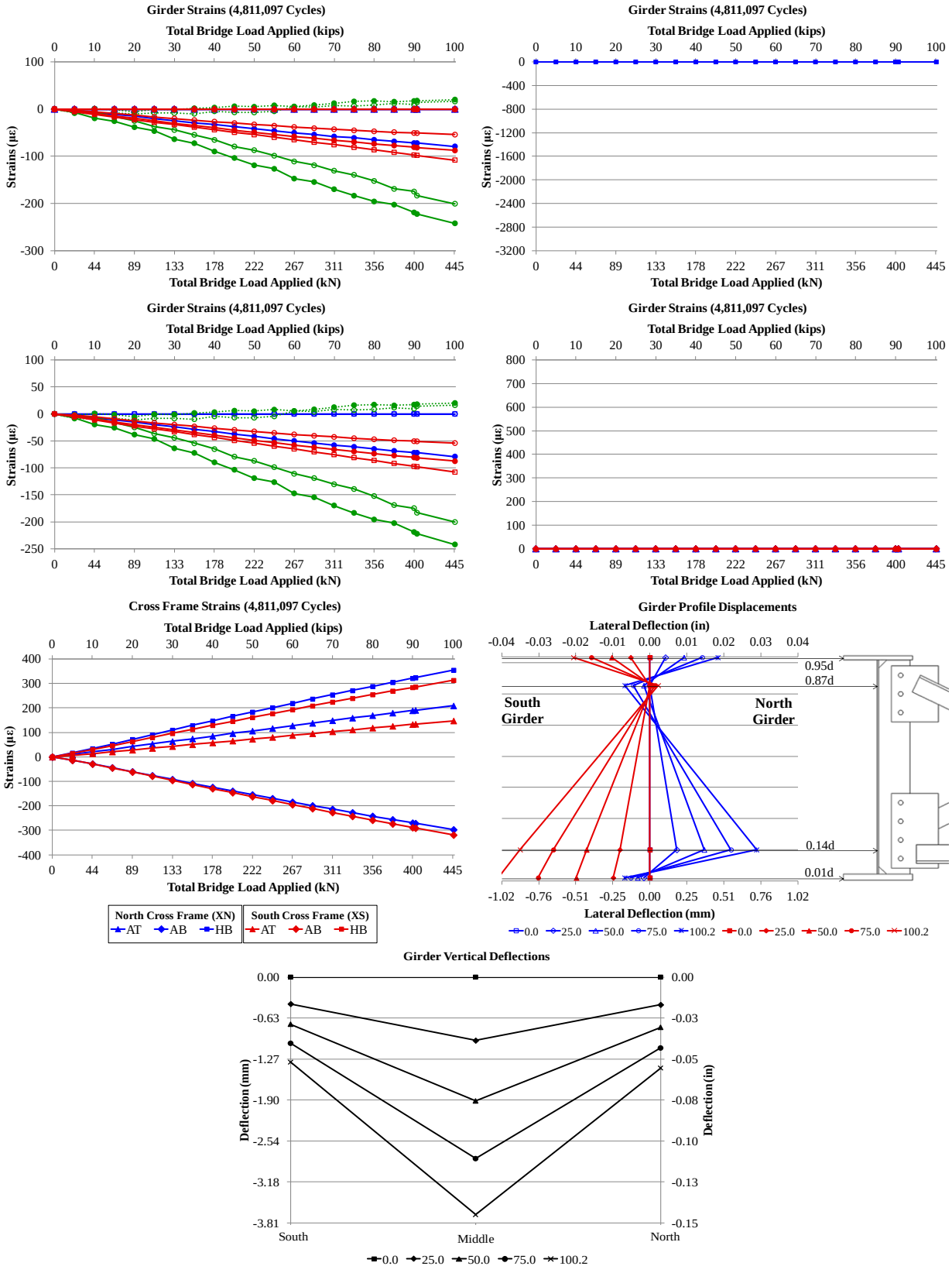

Figure E. 30: Static (4811097 Cycles) 02.15.2013 - With Retrofit

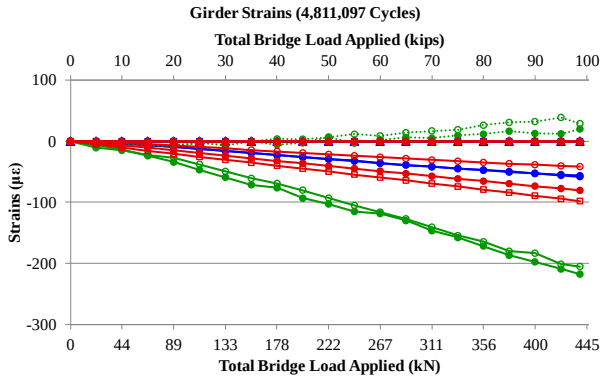

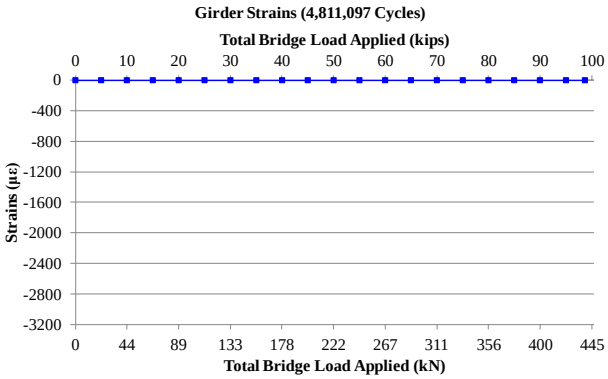

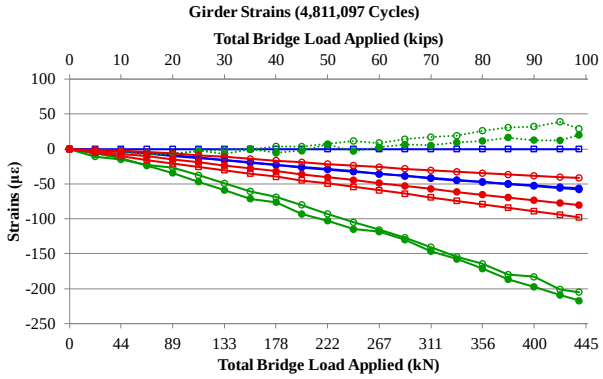

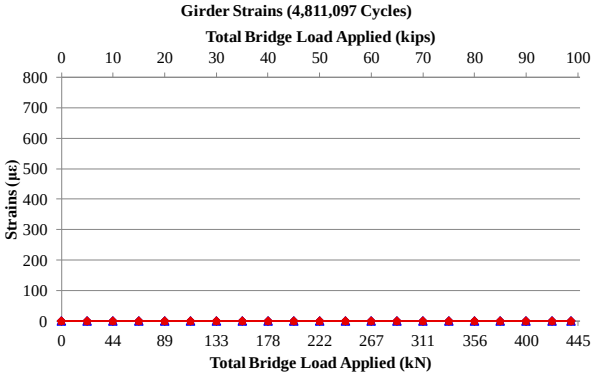

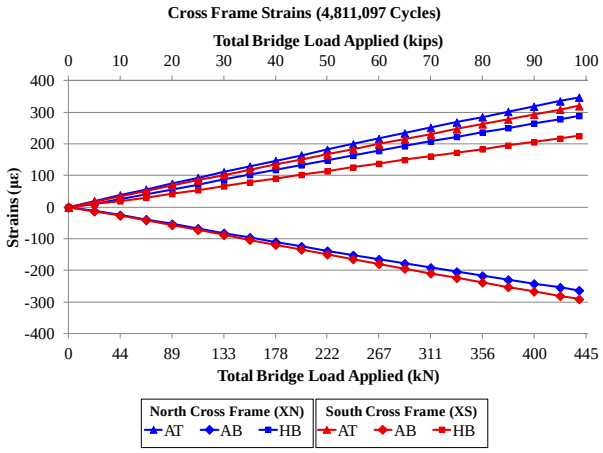

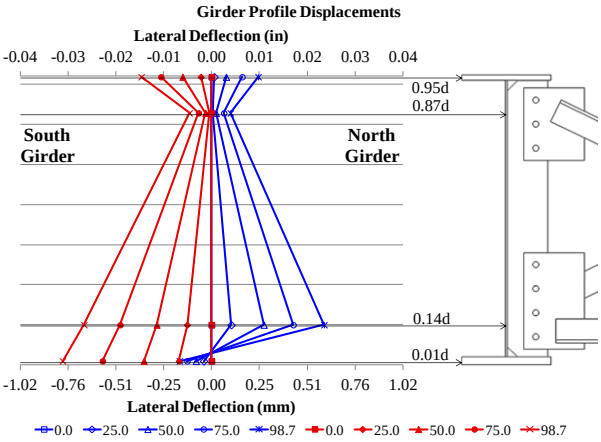

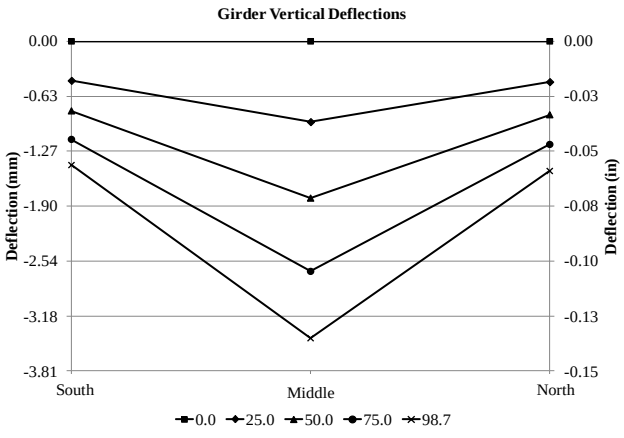

Figure E. 31: Static (6011097 Cycles) 04.16.2013 - With Retrofit

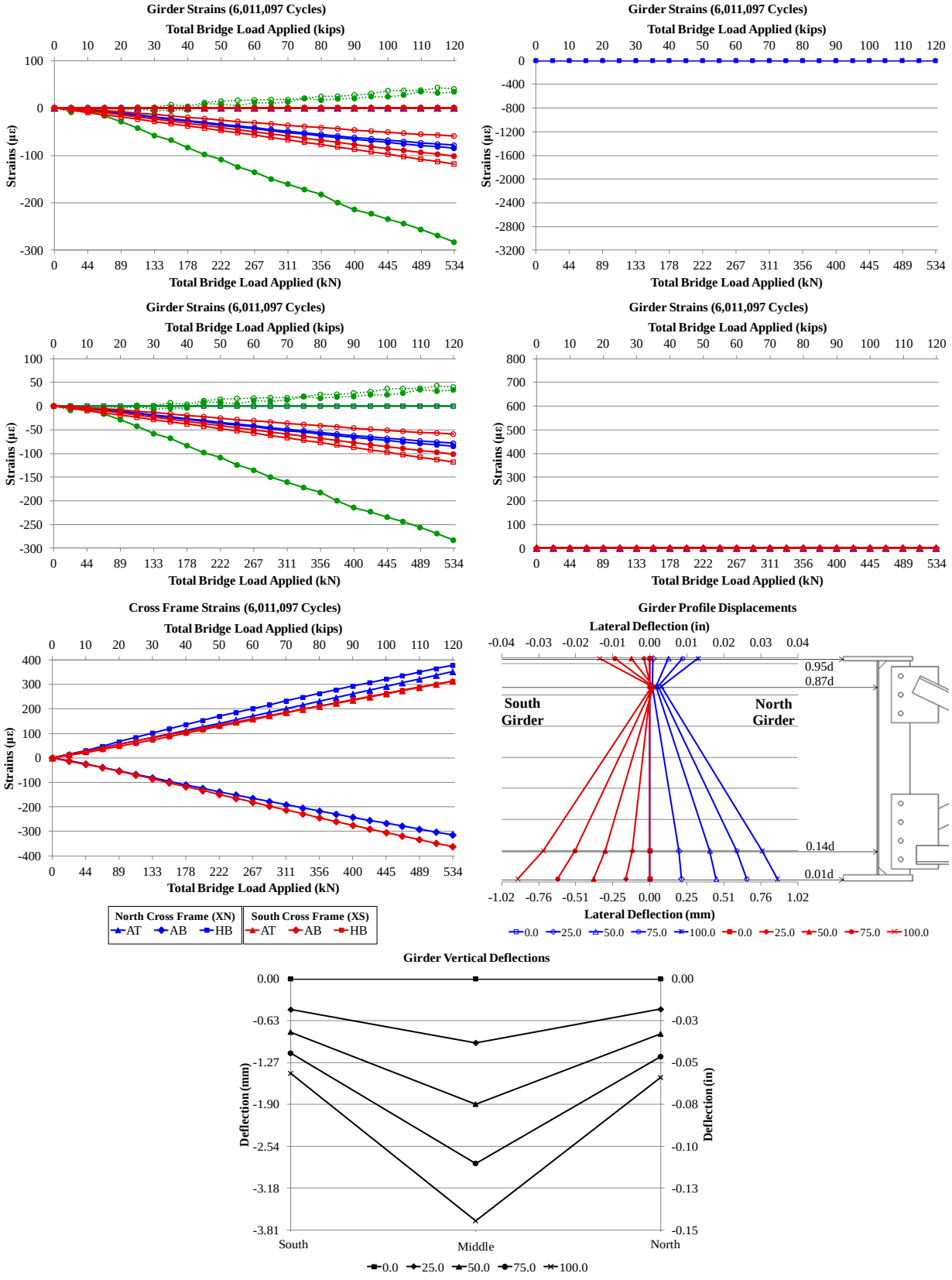

Figure E. 32: Static (6011097 Cycles) 05.20.2013 - Without Retrofit

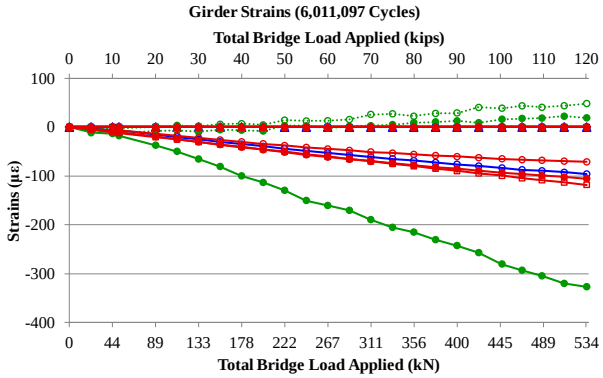

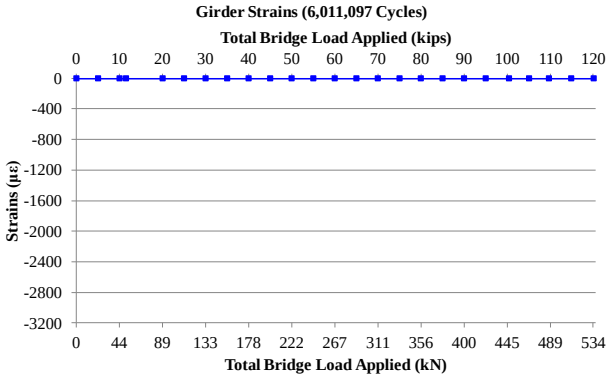

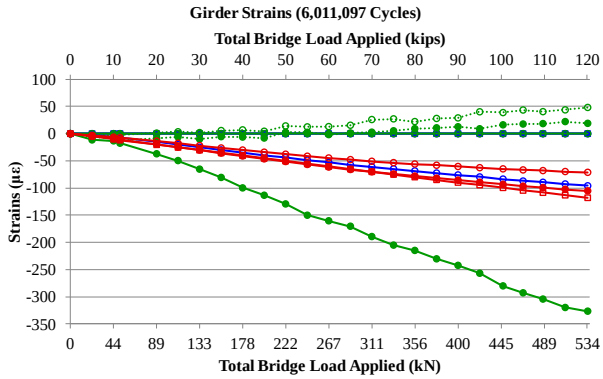

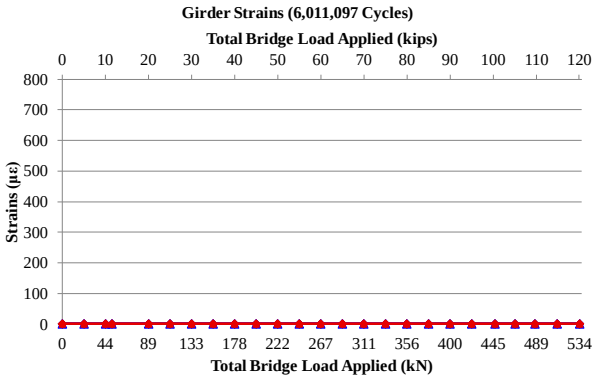

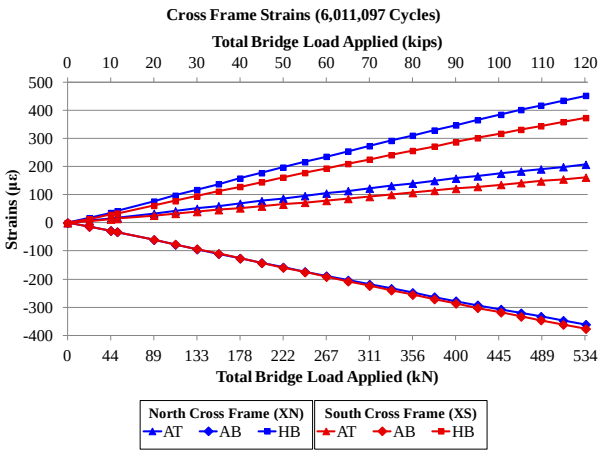

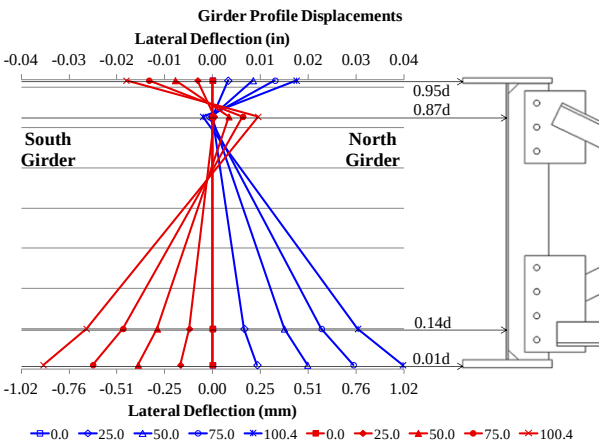

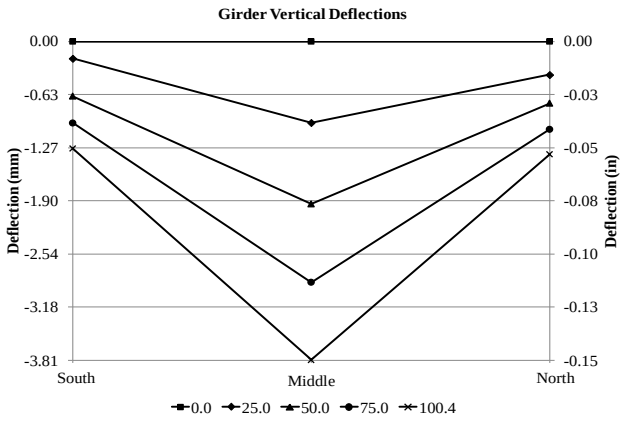

EXPERIMENTAL LOG

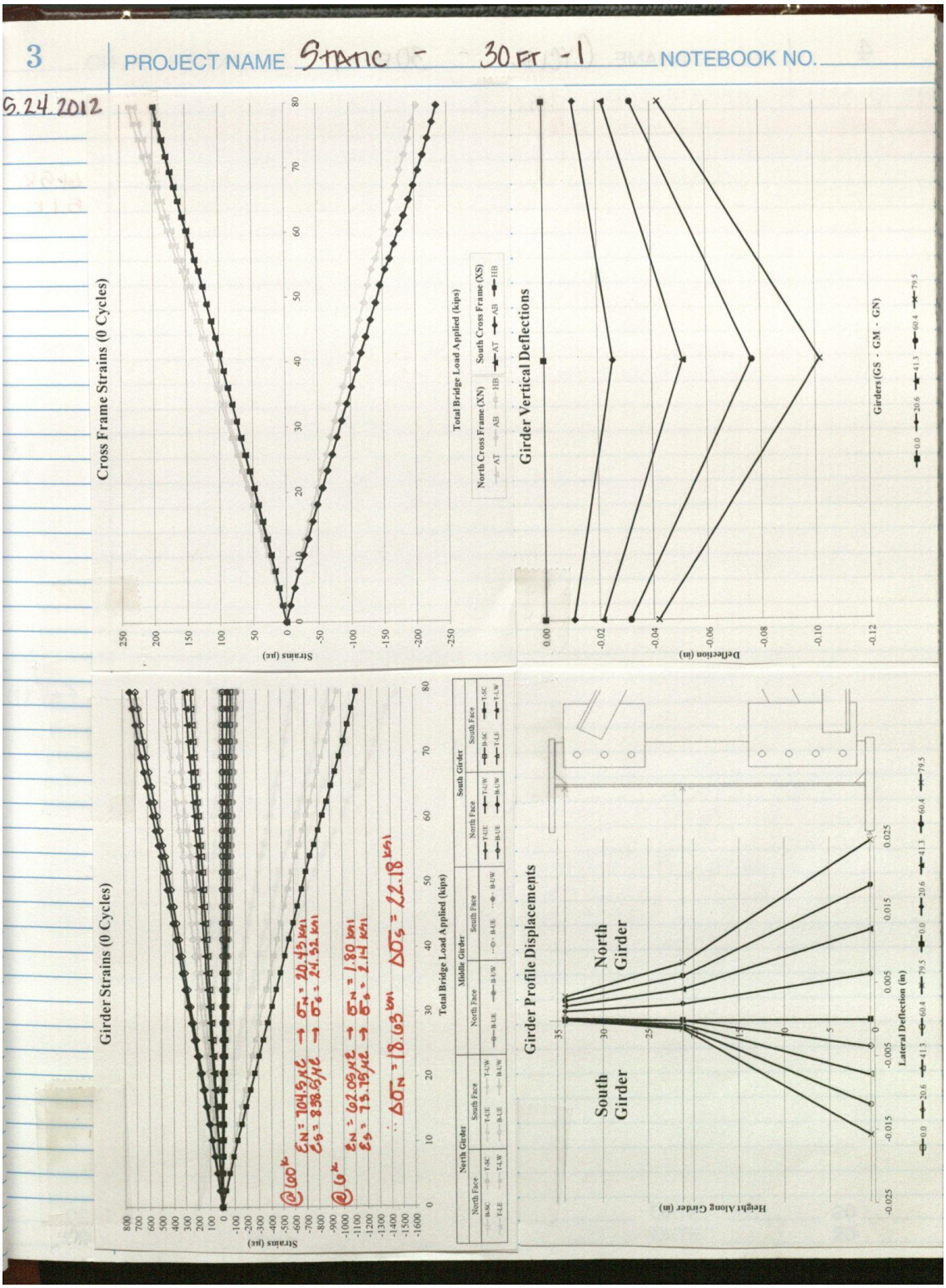

4 PROJECT NAME Cyclic - 30ft-1 NOTEBOOK NO. 5

05.24.2012 (10:54)

15000 CYCLES, 1 Hz (TOTAL 15000)

DISPLACEMENT MAX 0.127 IN → 0.145 IN
MIN 0.013 IN

FORCE MEAN 33.4 K MAX 60.8 K → 61.9 K
AMPL. 27.3 K MIN 6.0 K → 5.1 K

DATA: * MTS SPECIMEN 10:54 → 30ft-1 Cyclic (15000) 05.24.2012
STATIC BEGIN 9:53 → 30ft-1 Static Begin 05.24.2012
CYCLIC BEGIN 10:52 → 30ft-1 Cyclic Begin 05.24.2012
CYCLIC END 15:01 → 30ft-1 Cyclic End 05.24.2012
STATIC END 16:13 → 30ft-1 Static End 05.24.2012

* ACTUAL TIME SHOWN... FILE TIME IS 10:37

NO CRACK DETECTED VISUALLY

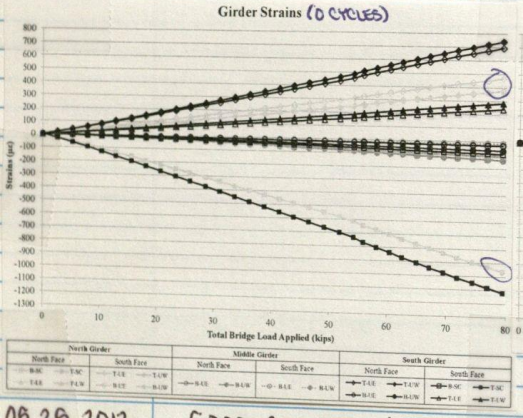

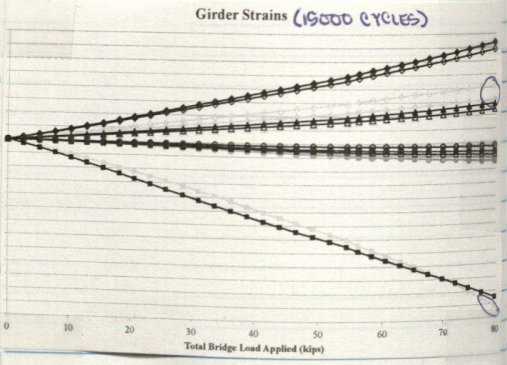

05.29.2012 (10:31)

(12:16)

05.25.2012 (10:32)

5000 CYCLES, 1 Hz (TOTAL 20000)

DISP MAX 0.125 IN → 0.133 IN
MIN 0.010 IN

FORCE MEAN 33.7 K MAX 63.1 K
AMPL. 27.9 K → 27.9 K MIN 4.8 K

DATA: * MTS SPECIMEN 10:32 → 30ft-1 Cyclic (5000) 05.25.2012
CYCLIC END 11:56 → 30ft-1 Cyclic End 05.25.2012
STATIC END 12:10 → 30ft-1 Static End 05.25.2012

* FILE TIME = 10:15

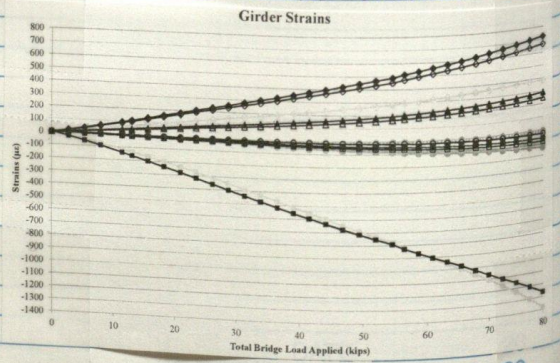

SIGNATURE
READ AND UNDERSTOOD DATE 20

5

PROJECT NAME _____ NOTEBOOK NO. _____

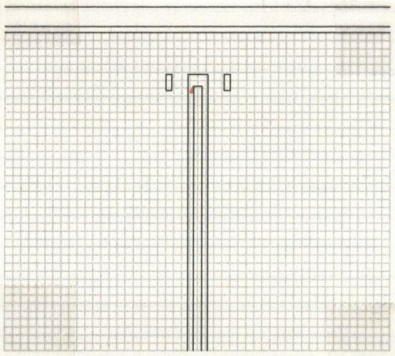

$\frac{1}{8}$ IN CRACK IN NORTH GIRDER, SOUTH FACE, WEST OF STIFFENER.

CRACK IN WELD AT JUNCTURE BETWEEN WELD AND STIFFENER PROPAGATING DIAGONAL FROM CORNER AS SHOWN
CRACK ON OPPOSITE SIDE OF ANGLE FRAMING IN

05.29.2012 (10:31) 5000 CYCLES, 1 HZ (TOTAL 25,000)

DISP MAX 0.128 IN → 0.130 IN
MIN 0.010 IN

FORCE MEAN 32.8 K → 33.4 K MAX 61.6 K → 62.4 K
AMPL 27.7 K MIN 4.6 K → 4.4 K

DATA: * MTS SPECIMEN 10:31 → 30FT-1 CYCLIC (@5000) 05.29.2012
CYCLIC END 12:18 → 30FT-1 CYCLIC-a END 05.29.2012
* FILE TIME = 10:13
PREVIOUS CRACK NOT SEEN USING PENETRANT

(12:16) 5000 CYCLES, 1 HZ (TOTAL 30,000)

DISP MAX 0.134 IN
MIN 0.014 IN

FORCE MEAN 33.9 K MAX 63.3 K
AMPL 28.0 K MIN 5.4 K → 5.2 K

DATA: * MTS SPECIMEN 12:16 → 30FT-1 CYCLIC (b30000) 05.29.2012
CYCLIC END 13:41 → 30FT-1 CYCLIC-b END 05.29.2012
STATIC END 13:53 → 30 FT-1 STATIC-b END 05.29.2012
* FILE TIME = 11:59

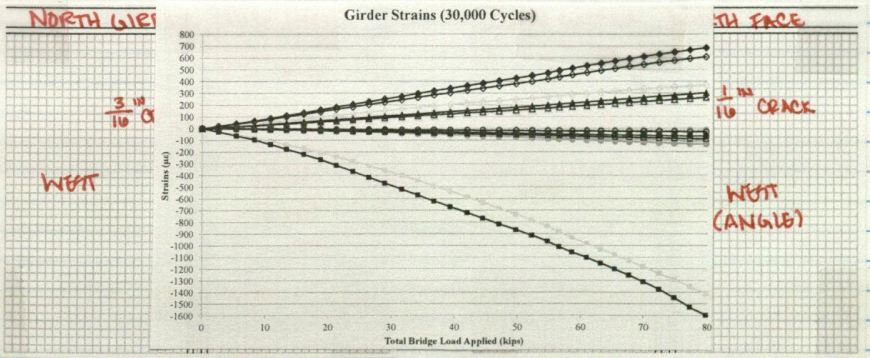

SIGNATURE _____ DATE _____ 20 _____
READ AND UNDERSTOOD _____ DATE _____ 20 _____

6 PROJECT NAME _____ NOTEBOOK NO. _____ 7

(14:00) 5000 CYCLES, 1 HZ (TOTAL 35,000)

DISP MAX 0.134 IN → 0.135 IN
MIN 0.019 IN → 0.016 IN

FORCE MEAN 33.3 K → 33.5 K MAX 61.8 K
AMPL. 27.8 K → 27.7 K MIN 5.9 K → 4.8 K

DATA: * MTS SPECIMEN CYCLIC 14:00 → 15:24 30FT-1 CYCLIC (C5000) 05.29.2012
CYCLIC END → 30FT-1 CYCLIC-C END 05.29.2012

* FILE TIME: 13:42

NORTH GIRDER, SOUTH FACE

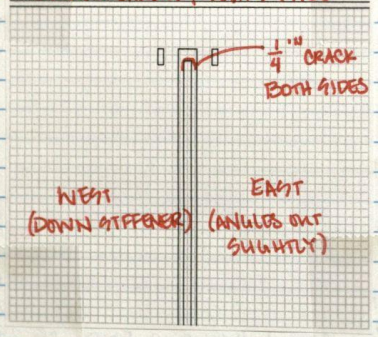

NO CHANGE IN SOUTH GIRDER CRACKS

05.31.2012 (10:45)

05.30.2012 (11:54) 10000 CYCLES, 1 HZ (TOTAL 45,000)

DISP MAX 0.128 IN → 0.141 IN
MIN 0.007 IN → -0.003 IN

FORCE MEAN 34.0 K → 34.0 K MAX 63.4 K → 68.7 K
AMPL. 29.3 K → 31.7 K MIN 3.2 K → 1.2 K

DATA: * MTS SPECIMEN CYCLIC 11:54 → 13:43 30FT-1 CYCLIC (Q10000) 05.30.2012
CYCLIC END → 30FT-1 CYCLIC-Q END 05.30.2012
~~STATIC END → 30FT-1 STATIC-Q END 05.30.2012~~

* FILE TIME: 11:37

5000 CYCLES

NO CHANGE IN NORTH GIRDER CRACKS

SOUTH GIRDER, NORTH FACE

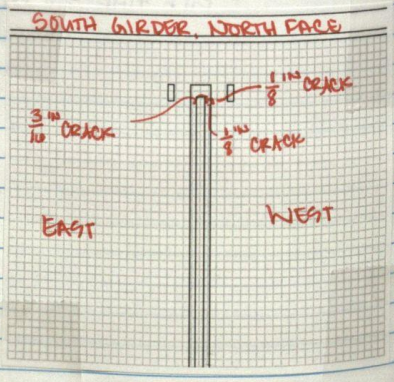

SIGNATURE _____
READ AND UNDERSTOOD _____ DATE _____ 20__
DATE _____ 20__

OOK NO. 7 PROJECT NAME NOTEBOOK NO.

10,000 CYCLES

NORTH G

1/4 IN CRACK

WEST

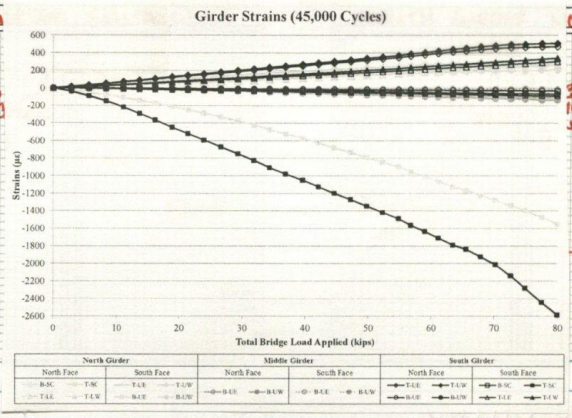

NORTH FACE

3/16 IN CRACK

1/4 IN CRACK

WEST

05.31.2012 (10:49) 15,000 CYCLES, 1 HZ (TOTAL 60,000)

DISP MAX 0.126 IN → 0.121 IN

MIN 0.001 IN → 0.014 IN

FORCE MEAN 34.4 K → 33.7 K MAX 62.0 K → 59.7 K

AMPL 26.9 K → 29.1 K MIN 6.9 K → 8.2 K

DATA: * MTS SPECIMEN 10:45 → 30FT-1 CYCLIC (@15000) 05.31.2012

STATIC BEGIN 10:12 → 30FT-1 STATIC-0 BEGIN 05.31.2012

CYCLIC END 15:18 → 30FT-1 CYCLIC-0 END 05.31.2012

STATIC END 15:30 → 30FT-1 STATIC-0 END 05.31.2012

* FILE TIME: 10:28

ADJUSTED TUNING

ORIGINAL FORCE P: 0.07 I: 0.006 D: 0.0002 F: 0.0 512HZ

NEW FORCE P: ~~0.03~~ 0.04 I: 0.006 D: 0.0001 F: 0.0003 512HZ

ORIGINAL DISP. P: 12 ; I: 0.005 ; D: 0.0001, 512HZ

5000 CYCLES

NORTH GIRDER, SOUTH FACE

1/4 IN CRACK

3/16 IN CRACK

WEST

EAST

SOUTH GIRDER, NORTH FACE

1/4 IN CRACK

3/16 IN CRACK

1/4 IN CRACK

EAST

WEST

SIG.

READ AND UNDERSTOOD DATE 20

10000 CYCLES

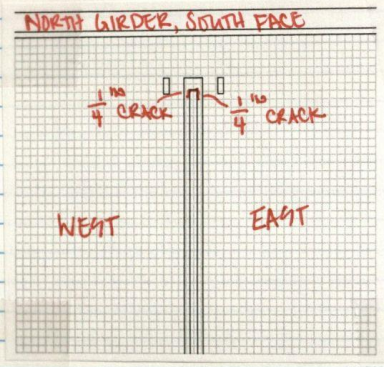

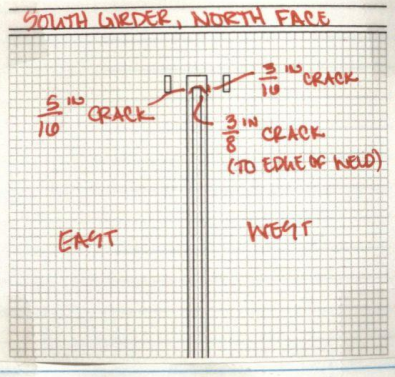

15000 CYCLES

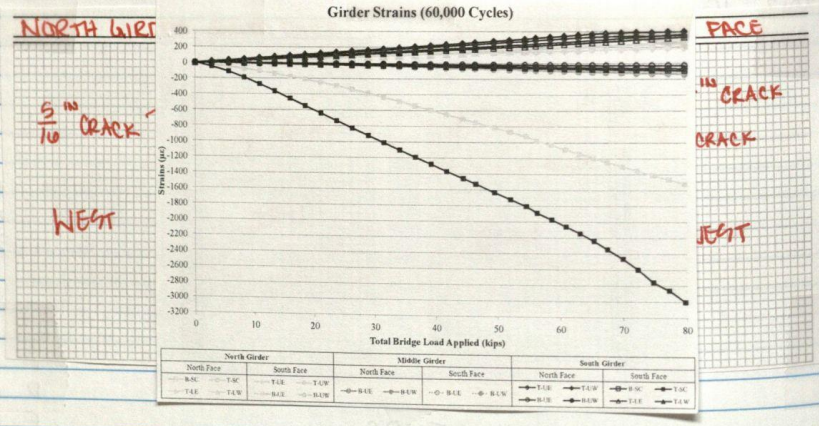

06.01.2012 (11:25)

15000 CYCLES, 1 HZ (TOTAL 75,000)

DISP. MAX 0.123 IN → 0.119 IN
MIN 0.007 IN → 0.004 IN

FORCE MEAN 33.7K → 33.4 K MAX 61.3K → 61.2K
AMPL. 27.7K → 27.5K MIN 3.7K → 5.4K

DATA: * MTS SPECIMEN 11:25 → 30FT-1 CYCLIC (@5000) 06.01.2012
CYCLIC END 15:36 → 30FT-1 CYCLIC-a END 06.01.2012
STATIC END 15:46 → 30FT-1 STATIC-a END 06.01.2012
* FILE TIME: 11:07

SIGNATURE _____
READ AND UNDERSTOOD _____ DATE _____ 20__
DATE _____ 20__

PROJECT NAME _____ NOTEBOOK NO. _____

5000 CYCLES

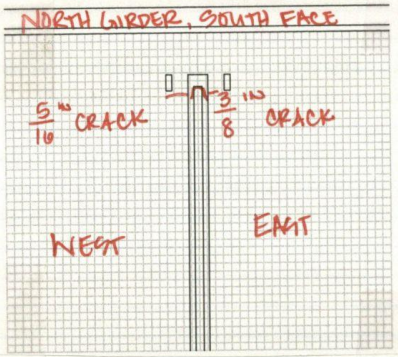

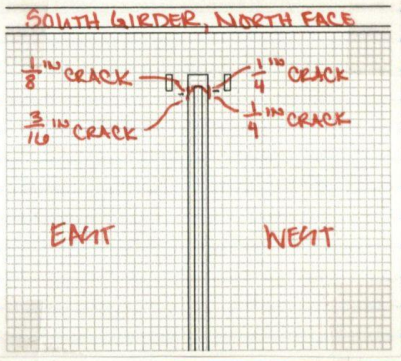

10000 CYCLES

NO CHANGE IN NORTH GIRDER CRACKS

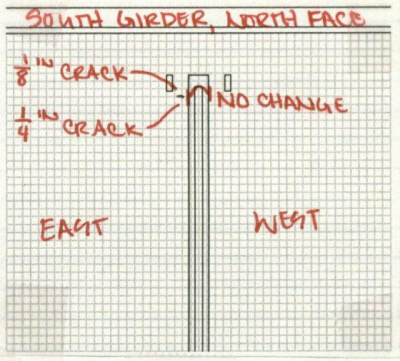

15000 CYCLES

NO CHANG
GIRDER

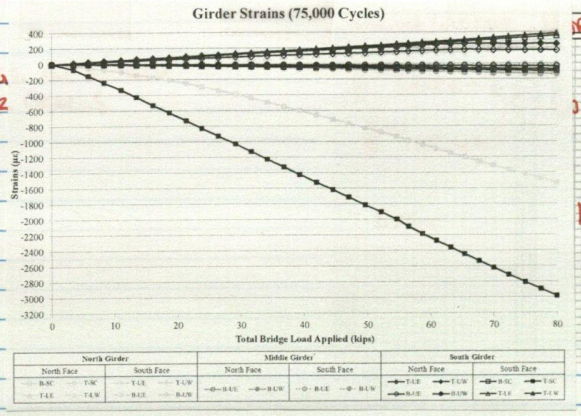

SIGNATURE _____ DATE _____ 20 _____
READ AND UNDERSTOOD _____ DATE _____ 20 _____

10

PROJECT NAME _____ NOTEBOOK NO. _____

11

06.04.2012
(11:15)

15000 CYCLES, 1Hz (TOTAL 90,000)

DISP MAX 0.122IN → 0.129IN
MIN 0.011IN → 0.005IN

FORCE MEAN 33.2K MAX 60.3K → 61.7K
AMPL 26.3K → 26.8K MIN 6.8K → 4.9K

ADJUSTED FORCE P-GAIN TO 0.05

DATA: * HIS SPECIMEN 11:15 → 30FT-1 CYCLIC (@5000) 06.04.2012
CYCLIC END 15:38 → 30FT-1 CYCLIC-a END 06.04.2012
STATIC END 15:55 → 30FT-1 STATIC-a END 06.04.2012

* FILE TIME: 10:58

06.05.2012
(10:10)

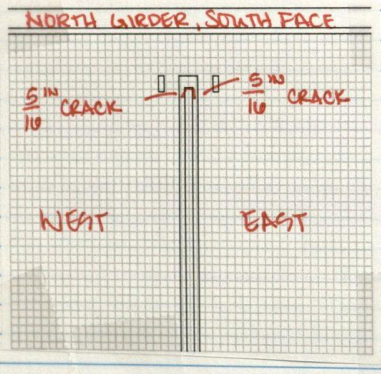

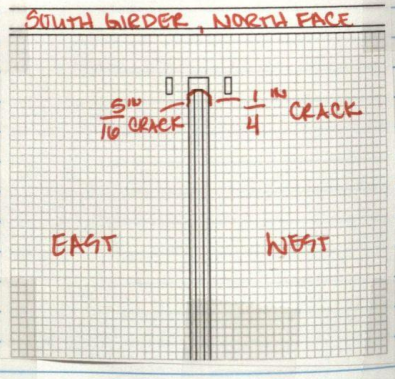

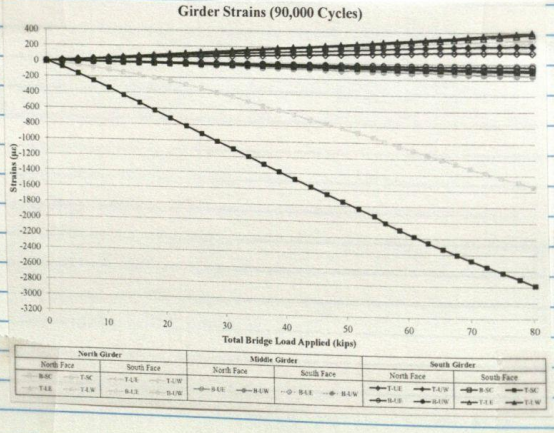

SIGNATURE _____
READ AND UNDERSTOOD _____ DATE _____ 20__
DATE _____ 20__

OK NO. 11 PROJECT NAME NOTEBOOK NO.

06.09.2012 (10:10) 15000 CYCLES, 1 HR (TOTAL 105,000)

DISP MAX 0.129 IN
MIN 0.011 IN

FORCE MEAN 33.2K MAX 60.4K
AMPL 26.0K MIN 5.8K

DATA: * MTS SPECIMEN 10:10 → 30FT-1 CYCLIC (@15000) 06.09.2012
CYCLIC END 14:22 → 30FT-1 CYCLIC-a END 06.09.2012
STATIC END 14:34 → 30FT-1 STATIC-a END 06.09.2012

* FILE TIME: 9:54

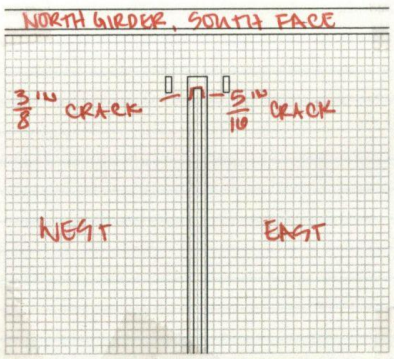

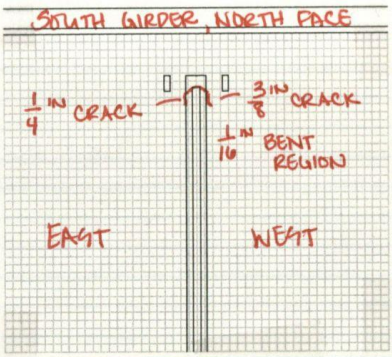

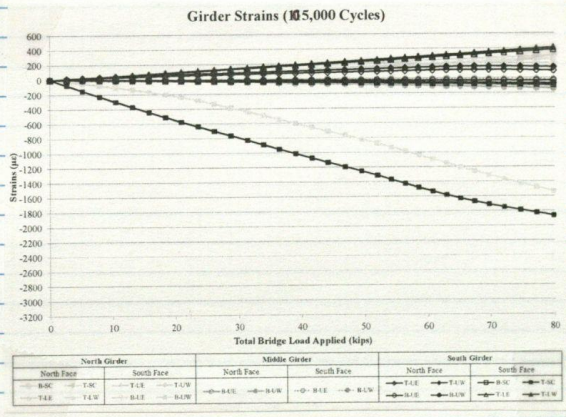

SIGNATURE DATE 20
READ AND UNDERSTOOD DATE 20

(14:39) 10000 CYCLES, 1HZ (TOTAL 115,000)

DISP MAX 0.133IN
MIN 0.017IN → 0.015IN

FORCE MEAN 33.4K → 32.9K MAX 60.5K
AMPL 26.9K → 26.4K MIN 6.1K → 5.9K

DATA: * MTS SPECIMEN 14:39 → 30FT-1 CYCLIC (b10000) 06.05.2012
* FILE TIME: 14:18

06.06.2012 (11:10) 5000 CYCLES, 1HZ (TOTAL 120,000)

DISP MAX 0.124IN → 0.133IN
MIN 0.009IN → 0.007IN

FORCE MEAN 33.8K
AMPL 26.2K → 28.1K MAX 60.1K → 65.9K
MIN 5.9K → 4.4K

DATA: * MTS SPECIMEN 11:10 → 30FT-1 CYCLIC (a5000) 06.06.2012
CYCLIC END 12:31 → 30FT-1 CYCLIC-a END 06.06.2012
STATIC END 12:46 → 30FT-1 STATIC-a END 06.06.2012
* FILE TIME: 10:53

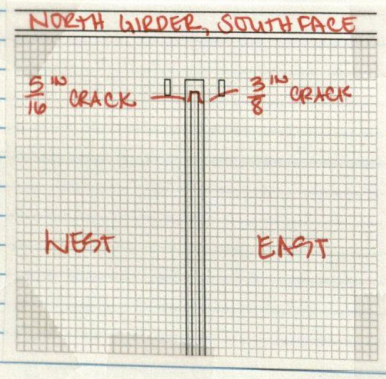

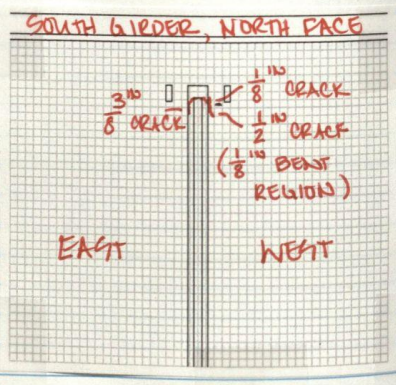

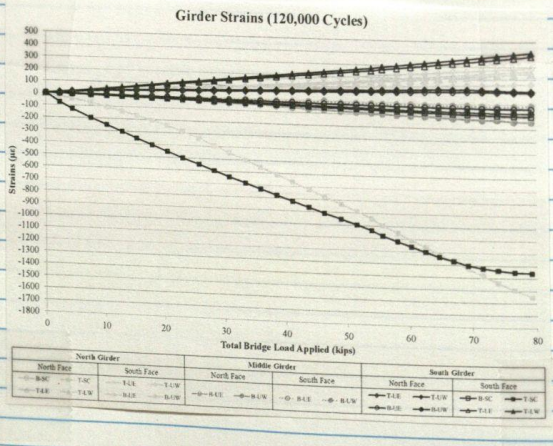

SIGNATURE _____
READ AND UNDERSTOOD _____ DATE _____ 20__
DATE _____ 20__

OOK NO.

→ 5.9k
.05.2012

→ 65.9k
→ 4.4k
)6.06.2012
e.06.2012
)6.06.2012

TH FACE
" CRACK
" CRACK
EAST
EGION)
VEST

20
20

13

PROJECT NAME _____ NOTEBOOK NO. _____

(12:49) 135000 CYCLES, 1 Hz (TOTAL 135,000)

DISP MAX 0.138 IN → 0.135 IN
MIN 0.011 IN → 0.003 IN

FORCE MEAN 33.8 K → 33.0 K MAX 62.2 K → 66.3 K
AMPL 28.9 K → 30.9 K MIN 5.0 K → 1.3 K

DATA : * MTS SPECIMEN 12:49 → 30 FT-1 CYCLIC (b135000) 06.06.2012
CYCLIC END 17:01 → 30 FT-1 CYCLIC-b END 06.06.2012
STATIC END 17:10 → 30 FT-1 STATIC-b END 06.06.2012

* FILE TIME :
AT 5700 CYCLES → ADJUSTED P-GAIN TO 0.04
FORCE MAX 67.8 K
MIN 1.8 K

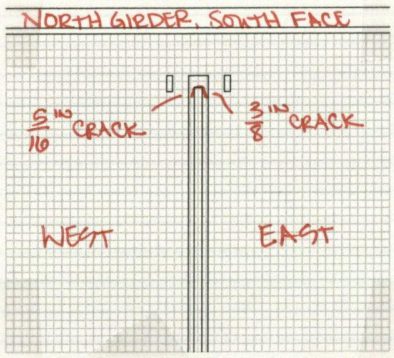

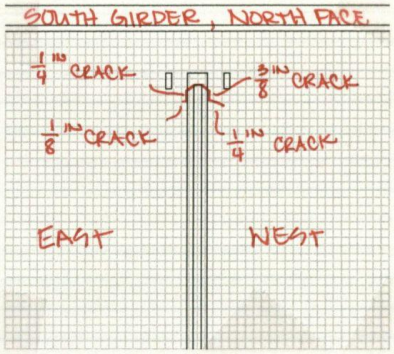

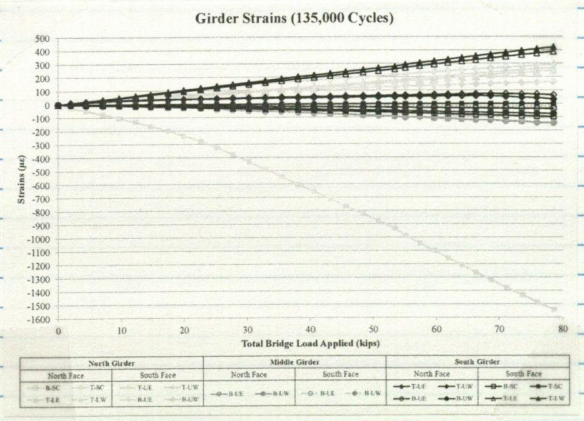

LOST : G3-S T-SC (POSSIBLE START OF CRACK ON BACK SIDE → THROUGH CRACK)

SIGNATURE _____ DATE _____ 20
READ AND UNDERSTOOD _____ DATE _____ 20

06.07.2012 (9:44)

15000 CYCLES, 1 HZ (TOTAL 150,000)

DISP MAX 0.130IN → 0.139IN
MIN 0.005IN

FORCE MEAN 32.9K → 33.6K MAX 63.6K → 65.1K
AMPL 27.8K → 28.9K MIN 3.8K → 3.3K

DATA: *MTS SPECIMEN 9:44 → 30FT-1 CYCLIC (@15000) 06.07.2012
CYCLIC END 13:38 → 30FT-1 CYCLIC-a END 06.07.2012
STATIC END 14:11 → 30FT-1 STATIC-a END 06.07.2012

*FILE TIME: 9:26

AT 4900 CYCLES → ADJUSTED P-GAIN TO 0.03
FORCE MAX 80.6K
MIN -0.2K
→ DISPLACEMENT P-GAIN TO 6

NO CHANGE IN NORTH GIRDER CRACKS

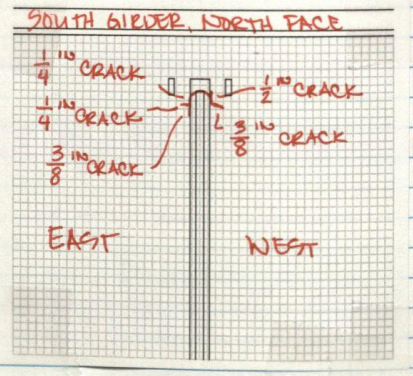

09.27.2012

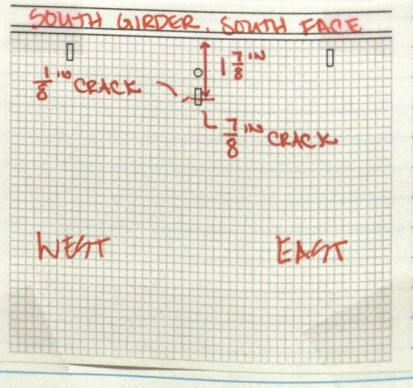

SIGNATURE
READ AND UNDERSTOOD DATE 20
DATE 20

K → 65.1K
K → 3.3K
.07.2012
7.2012
7.2012

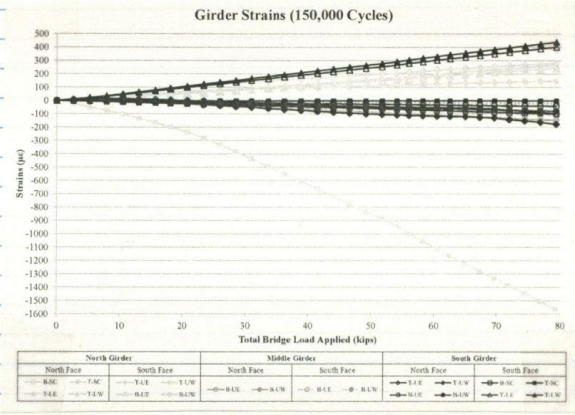

GAUGE CHANGES: G9-S T-9C MOVED 1" EAST AND 1" DOWN
→ G9-S T-9E
G9-S T-LE REPLACED
G9-N T-LE REPLACED
STRING POTS 1-6 REPLACED LVDTS 1-6

DATA: STATIC 14:09 → 30FT-1 STATIC 09.18.2012

RETROFIT APPLIED → TOP WEB GAP, N & S
- ANGLES
- BACKPLATE 60-60K

09.27.2012 5000 CYCLES, 2 HZ (RETROFIT 5000, TOTAL 155,000)

DISP	MAX 0.119 IN		
	MIN 0.010 IN		
FORCE	MEAN 33K	MAX 60.9K	
	AMPL 25.6K	MIN 6.8K	

DATA: * MTS SPECIMEN 13:53 → 30FT-1 CYCLIC (5000) 09.27.2012
STATIC BEGIN 8:48 → 30FT-1 STATIC 09.27.2012
* FILE TIME: 13:35
ADJUSTED FORCE P-GAIN TO 0.07

SIGNATURE DATE 20
READ AND UNDERSTOOD DATE 20

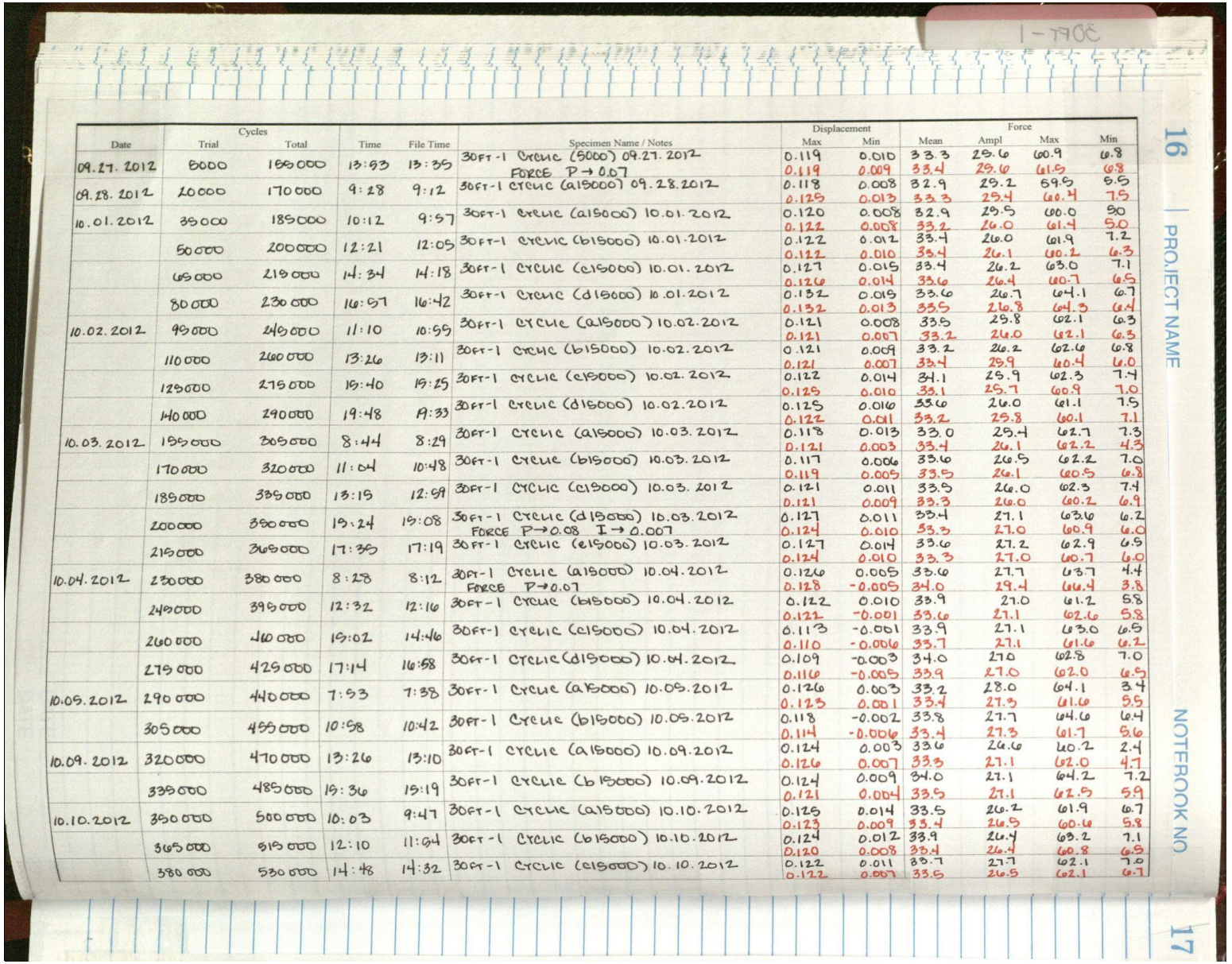

1-190E

16 | PROJECT NAME NOTEBOOK NO. 17

Date	Cycles Trial	Cycles Total	Time	File Time	Specimen Name / Notes	Displacement Max	Displacement Min	Force Mean	Force Ampl	Force Max	Force Min
09.27.2012	5000	185000	13:53	13:35	30FT-1 CYCLIC (5000) 09.27.2012 FORCE P→0.07	0.119	0.010	33.3	29.6	60.9	6.8
						0.119	0.009	33.4	29.6	61.5	6.8
09.28.2012	20000	170000	9:28	9:12	30FT-1 CYCLIC (a15000) 09.28.2012	0.118	0.008	32.9	29.2	59.5	5.5
						0.125	0.013	33.3	29.4	60.4	7.5
10.01.2012	35000	185000	10:12	9:57	30FT-1 CYCLIC (a15000) 10.01.2012	0.120	0.008	32.9	29.5	60.0	5.0
						0.122	0.008	33.2	26.0	61.4	5.0
	50000	200000	12:21	12:05	30FT-1 CYCLIC (b15000) 10.01.2012	0.122	0.012	33.4	26.0	61.9	7.2
						0.122	0.010	33.4	26.1	60.2	6.3
	65000	215000	14:34	14:18	30FT-1 CYCLIC (c15000) 10.01.2012	0.127	0.015	33.4	26.2	63.0	7.1
						0.126	0.014	33.6	26.4	60.7	6.5
	80000	230000	16:57	16:42	30FT-1 CYCLIC (d15000) 10.01.2012	0.132	0.015	33.6	26.7	64.1	6.7
						0.132	0.013	33.5	26.8	64.3	6.4
10.02.2012	95000	245000	11:10	10:55	30FT-1 CYCLIC (a15000) 10.02.2012	0.121	0.008	33.5	25.8	62.1	6.3
						0.121	0.007	33.2	26.0	62.1	6.3
	110000	260000	13:26	13:11	30FT-1 CYCLIC (b15000) 10.02.2012	0.121	0.009	33.2	26.2	62.6	6.8
						0.121	0.007	33.4	25.9	60.4	6.0
	125000	275000	15:40	15:25	30FT-1 CYCLIC (c15000) 10.02.2012	0.122	0.014	34.1	25.9	62.3	7.4
						0.125	0.010	33.1	25.7	60.9	7.0
	140000	290000	19:48	19:33	30FT-1 CYCLIC (d15000) 10.02.2012	0.125	0.016	33.6	26.0	61.1	7.5
						0.122	0.011	33.2	25.8	60.1	7.1
10.03.2012	155000	305000	8:44	8:29	30FT-1 CYCLIC (a15000) 10.03.2012	0.118	0.013	33.0	25.4	62.7	7.3
						0.121	0.003	33.4	26.1	62.2	4.3
	170000	320000	11:04	10:48	30FT-1 CYCLIC (b15000) 10.03.2012	0.117	0.006	33.6	26.5	62.2	7.0
						0.119	0.005	33.5	26.1	60.5	6.8
	185000	335000	13:15	12:59	30FT-1 CYCLIC (c15000) 10.03.2012	0.121	0.011	33.5	26.0	62.3	7.4
						0.121	0.009	33.3	26.0	60.2	6.9
	200000	350000	15:24	15:08	30FT-1 CYCLIC (d15000) 10.03.2012 FORCE P→0.08 I→0.007	0.127	0.011	33.4	27.1	63.6	6.2
						0.124	0.010	33.3	27.0	60.9	6.0
	215000	365000	17:35	17:19	30FT-1 CYCLIC (e15000) 10.03.2012	0.127	0.014	33.6	27.2	62.9	6.9
						0.124	0.010	33.3	27.0	60.7	6.0
10.04.2012	230000	380000	8:28	8:12	30FT-1 CYCLIC (a15000) 10.04.2012 FORCE P→0.07	0.126	0.005	33.6	27.7	63.7	4.4
						0.128	-0.005	34.0	29.4	66.4	3.8
	245000	395000	12:32	12:16	30FT-1 CYCLIC (b15000) 10.04.2012	0.122	0.010	33.9	27.0	61.2	5.8
						0.122	-0.001	33.6	27.1	62.6	5.8
	260000	410000	15:02	14:46	30FT-1 CYCLIC (c15000) 10.04.2012	0.113	-0.001	33.9	27.1	63.0	6.5
						0.110	-0.006	33.7	27.1	61.6	6.2
	279000	429000	17:14	16:58	30FT-1 CYCLIC (d15000) 10.04.2012	0.109	-0.003	34.0	27.0	62.8	7.0
						0.116	-0.005	33.9	27.0	62.0	6.5
10.05.2012	290000	440000	7:53	7:38	30FT-1 CYCLIC (a15000) 10.05.2012	0.126	0.003	33.2	28.0	64.1	3.4
						0.123	0.001	33.4	27.9	61.6	5.5
	305000	455000	10:58	10:42	30FT-1 CYCLIC (b15000) 10.05.2012	0.118	-0.002	33.8	27.7	64.6	6.4
						0.114	-0.006	33.4	27.3	61.7	5.6
10.09.2012	320000	470000	13:26	13:10	30FT-1 CYCLIC (a15000) 10.09.2012	0.124	0.003	33.6	26.6	60.2	2.4
						0.126	0.007	33.3	27.1	62.0	4.7
	335000	485000	15:36	15:19	30FT-1 CYCLIC (b15000) 10.09.2012	0.124	0.009	34.0	27.1	64.2	7.2
						0.121	0.004	33.5	27.1	62.5	5.9
10.10.2012	350000	500000	10:03	9:47	30FT-1 CYCLIC (a15000) 10.10.2012	0.125	0.014	33.5	26.2	61.9	6.7
						0.123	0.009	33.4	26.5	60.6	5.8
	365000	515000	12:10	11:54	30FT-1 CYCLIC (b15000) 10.10.2012	0.124	0.012	33.9	26.4	63.2	7.1
						0.120	0.008	33.4	26.4	60.8	6.5
	380000	530000	14:48	14:32	30FT-1 CYCLIC (c15000) 10.10.2012	0.122	0.011	33.7	27.7	62.1	7.0
						0.122	0.007	33.5	26.5	62.1	6.7

Date	Cycles Trial	Cycles Total	Time	File Time	Specimen Name / Notes	Displacement Max	Displacement Min	Force Mean	Force Ampl	Force Max	Force Min	
10.11.2012	395000	545000	9:07	8:51	30FT-1 CYCLIC (a15000) 10.11.2012	0.127	0.007	33.2	26.5	62.0	3.6	
						0.125	0.009	33.4	26.6	61.4	5.5	
	410000	560000	12:04	11:48	30FT-1 CYCLIC (b15000) 10.11.2012	0.123	0.013	33.6	26.5	62.1	7.0	
						0.125	0.008	33.4	26.5	61.2	6.6	
	425000	575000	15:29	15:13	30FT-1 CYCLIC (c15000) 10.11.2012	0.125	0.014	33.7	26.8	61.3	6.5	
						0.124	0.011	33.5	26.5	61.0	6.6	
	440000	590000	1808	1752	30FT-1 CYCLIC (d15000) 10.11.2012	0.126	0.014	34.0	26.6	62.7	7.2	
						0.122	0.010	33.6	26.5	61.2	6.8	
	455000	605000	2034	2017	30 FT-1 CYCLIC (e15000) 10.11.2012	0.124	0.012	34.1	26.7	62.6	6.8	
						0.124	0.009	33.6	26.5	62.6	6.7	
	470000	620000	2353	2336	30 FT-1 CYCLIC (f15000) 10.11.2012	0.126	0.012	33.7	26.7	63.3	7.0	
						0.122	0.008	33.4	26.5	60.9	6.7	
10.12.2012	485000	635000	10:01	9:45	30FT-1 CYCLIC (a15000) 10.12.2012	0.128	0.007	33.7	27.0	62.5	4.0	
						0.126	0.009	33.9	27.3	62.2	5.1	
	500000	650000	12:22	12:06	30FT-1 CYCLIC (b15000) 10.12.2012	0.126	0.012	34.2	27.5	63.5	6.9	
						0.124	0.009	33.9	27.4	62.3	6.1	
	515000	665000	1437	1421	30FT-1 CYCLIC (c15000) 10.12.2012	0.129	0.012	34.3	27.5	64.9	6.5	
						0.125	0.009	33.8	27.6	61.8	5.9	
10.15.2012	530000	680000	9:57	9:42	30FT-1 CYCLIC (a15000) 10.15.2012 FORCE P→0.09	0.115	0.007	33.3	29.7	59.4	6.6	
						0.120	0.000	35.3	27.3	61.5	5.2	
	545000	695000	13:05	12:50	30FT-1 CYCLIC (b15000) 10.15.2012	0.123	0.008	33.4	27.4	62.9	5.9	
						0.124	0.005	33.4	27.4	62.1	5.3	
10.16.2012	560000	710000	11:08	10:53	30FT-1 CYCLIC (a15000) 10.16.2012	0.128	0.013	33.5	27.0	61.4	5.4	
						0.127	0.010	33.3	27.0	61.1	4.8	
	575000	725000	13:16	13:00	30FT-1 CYCLIC (b15000) 10.16.2012	0.128	0.014	33.8	27.0	62.4	6.9	
						0.128	0.012	33.3	26.9	60.8	5.9	
	590000	740000	15:33	15:17	30FT-1 CYCLIC (c15000) 10.16.2012	0.130	0.016	33.5	27.0	62.6	6.9	
						0.130	0.014	33.3	27.0	61.9	5.7	
10.17.2012	605000	755000	10:53	10:38	30FT-1 CYCLIC (a15000) 10.17.2012	0.119	0.007	33.0	26.3	60.6	5.7	
						0.123	0.006	33.1	26.8	61.6	5.4	
	620000	770000	13:22	13:06	30FT-1 CYCLIC (b15000) 10.17.2012	0.125	0.011	33.4	26.9	62.5	6.5	
						0.124	0.008	33.3	27.1	60.6	5.9	
	635000	785000	15:46	15:31	30FT-1 CYCLIC (c15000) 10.17.2012	0.125	0.011	33.5	27.2	62.2	6.1	
						0.124	0.009	33.4	27.3	61.2	5.7	
10.18.2012	650000	800000	8:21	8:06	30FT-1 CYCLIC (a15000) 10.18.2012	0.126	0.014	33.4	26.3	60.4	6.1	
						0.127	0.011	33.2	26.9	62.1	5.5	
	669000	819000	10:38	10:22	30FT-1 CYCLIC (b15000) 10.18.2012	0.127	0.014	33.4	26.8	62.1	6.6	
						0.125	0.001	33.2	27.0	60.8	6.0	
	680000	830000	12:45	12:29	30FT-1 CYCLIC (c15000) 10.18.2012	0.128	0.014	33.6	26.7	62.5	7.3	
						0.124	0.008	33.4	27.0	60.6	6.0	
	830000	980000	14:53	14:38	30FT-1 CYCLIC (d15000) 10.18.2012	0.123	0.012	33.7	26.7	62.5	6.6	
						0.121	0.004	33.5	27.2	61.0	6.2	1711
						0.125	0.004	33.5	27.2	61.1	6.0	842
						0.121	0.000	33.5	27.2	61.0	6.0	11:45
10.19.2012	849000	999000	11:46	11:31	30FT-1 CYCLIC (a15000) 10.19.2012	0.117	0.003	34.1	27.4	62.9	6.5	
						0.115	-0.002	33.5	27.4	61.2	6.0	
	999000	1149000	13:54	13:38	30FT-1 CYCLIC (b15000) 10.19.2012	0.113	0.003	33.7	26.5	62.1	7.2	
						0.116	-0.002	33.5	27.2	61.0	6.0	1650
						0.126	0.001	33.5	27.1	61.9	6.1	

1-7905

2011 0828

Date	Trial Cycles	Total Cycles	Time	File Time	Specimen Name / Notes	Displacement Max	Displacement Min	Displacement Mean	Force Ampl	Force Max	Force Min
10.22.2012	1,010,000	1,160,000	10:01	9:45	30ft-1 cyclic (a15000) 10.22.2012 FORCE P→0.10	0.130	0.014	32.9	26.3	61.3	5.4
	1,029,000	1,179,000	12:50	12:34	30ft-1 cyclic (b15000) 10.22.2012	0.129	0.014	33.2	26.7	61.0	6.3
						0.130	0.014	33.7	27.0	62.1	6.5
						0.129	0.014	33.1	26.8	60.4	6.2
	1,179,000	1,325,000	14:07	14:42	30a-1 cyclic (c15000) 10.22.2012	0.129	0.013	33.8	27.5	62.2	6.3
						0.128	0.011	33.3	27.4	61.0	5.8
						0.128	0.008	33.4	27.4	61.2	5.5
						0.125	0.004	33.4	27.4	61.2	5.7
10.24.2012	1,190,000	1,340,000	11:20	11:04	30ft-1 cyclic (a15000) 10.24.2012 FORCE P→0.09 I→0.009	0.129	0.015	33.6	27.6	61.3	5.5
						0.130	0.011	33.6	28.0	62.6	5.0
	1,200,000	1,350,000	13:43	13:27	30ft-1 cyclic (b10000) 10.24.2012 FORCE P→0.08 I→0.010	0.130	0.014	33.7	27.6	62.9	6.1
						0.133	0.014	33.8	27.5	62.5	6.0

RETROFIT REMOVED

NORTH GIRDER, SOUTH FACE

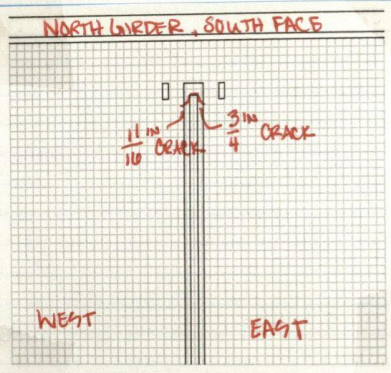

SOUTH GIRDER, NORTH FACE → NO CHANGE

SOUTH GIRDER, SOUTH FACE

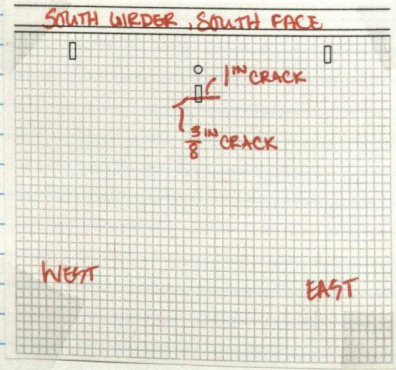

RE _____
D UNDERSTOOD _____ DATE _____
DATE _____

TEBOOK NO.

19

PROJECT NAME

NOTEBOOK NO.

RETROFIT APPLIED
TOP WEB-GAP, N&S
- ANGLES
- BACKPLATE

8-80K

Date	Cycles Trial	Cycles Total	Time	File Time	Specimen Name / Notes	Displacement Max	Displacement Min	Force Mean	Force Ampl	Force Max	Force Min	
12.11.2012	1,500,000	1,500,000	12:02	11:40	30cr-1 CYCLIC (150000) 12.11.2012	0.179	0.003	49.1	37.0	80.5	1.7	
						0.168	0.017	49.0	36.3	82.4	8.5	1440
						0.168	0.014	44.9	36.5	82.6	8.2	2249
						0.163	0.008	44.9	36.4	82.5	8.2	9:39
12.12.2012	300,000	1,800,000	9:41	9:26	30cr-1 CYCLIC (150000) 12.12.2012	0.167	0.015	49.9	36.0	84.4	8.6	
						0.165	0.012	44.8	36.1	82.1	8.3	2:59
						0.166	0.015	45.0	36.2	81.4	8.5	2145
						0.167	0.011	49.0	36.4	82.5	8.5	9:33
12.13.2012	400,000	1,800,000	9:54	9:18	30cr-1 CYCLIC (150000) 12.13.2012	0.172	0.020	45.0	36.3	84.1	8.4	
						0.169	0.017	49.1	36.4	82.0	8.4	1399
						0.169	0.015	49.0	36.1	82.5	8.4	9:27
12.14.2012	600,000	1,990,000	9:34	9:18	30cr-1 CYCLIC (150000) 12.14.2012	0.172	0.022	49.0	36.0	83.0	8.2	
						0.172	0.017	49.0	36.7	83.0	8.10	
						0.171	0.015	49.9	36.7	82.1	7.8	0023
						0.171	0.014	45.0	36.6	82.6	8.1	0939
12.17.2012	700,000	2,100,000	11:41	11:24	30cr-1 CYCLIC (150,000) 12.17.2012	0.170	0.023	44.0	36.0	80.9	8.1	
						0.170	0.011	44.7	36.6	82.2	7.8	1031
						0.169	0.012	44.8	36.8	82.0	8.7	1047
12.18.2012	900,000	2,250,000	11:05	10:49	30cr-1 CYCLIC (150000) 12.18.2012	0.175	0.023	45.0	36.0	83.0	8.9	
						0.169	0.020	44.8	36.5	81.0	8.8	14:00
						0.169	0.014	44.8	36.8	81.7	8.7	10:22
12.19.2012	1,050,000	2,400,000	10:40	10:23	30cr-1 CYCLIC (150,000) 12.19.2012	0.169	0.021	49.1	36.0	82.7	8.9	
						0.160	0.009	44.8	35.5	81.1	8.7	1004
						0.165	0.014	44.8	36.6	82.5	8.9	12:49
12.20.2012	1,200,000	2,580,000	12:52	12:36	30cr-1 CYCLIC (150000) 12.20.2012	0.168	0.024	49.4	36.0	82.7	8.7	
						0.165	0.016	44.8	35.5	81.0	8.7	1027
						0.167	0.013	44.8	36.5	80.7	8.9	9:18
						0.162	0.014	44.8	36.6	81.7	9.0	9:40

SIGNATURE
READ AND UNDERSTOOD

20
20

1-708

RETROFIT REMOVED

EDGE OF CRACK AT EDGE OF OSH

NORTH GIRDER, SOUTH FACE

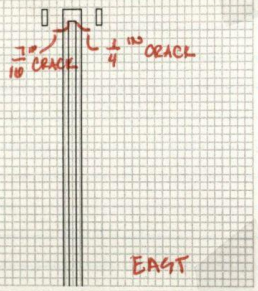

NORTH GIRDER, SOUTH FACE

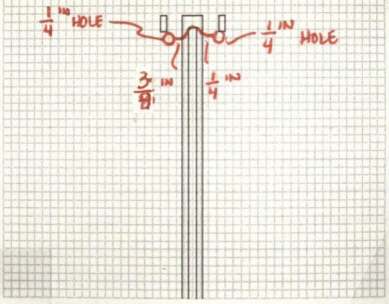

SOUTH GIRDER, NORTH FACE

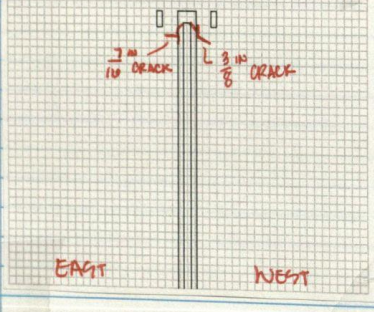

SOUTH GIRDER, NORTH FACE

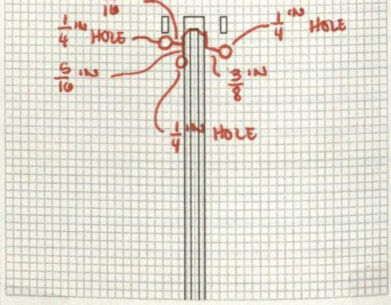

SOUTH GIRDER, SOUTH FACE

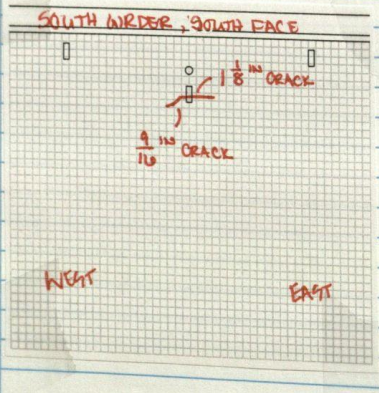

SOUTH GIRDER, SOUTH FACE

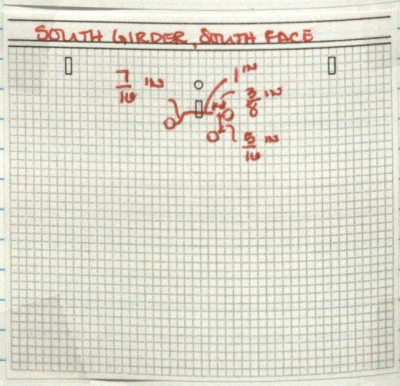

SIGNATURE _____
READ AND UNDERSTOOD _____ DATE _____ 20__
DATE _____ 20__

OOK NO.

21

PROJECT NAME NOTEBOOK NO.

RETROFIT APPLIED

TOP WEB GAP N & S

- ANGLES
- BACK PLATE
- ¼" CRACK STOP HOLES

10=100K

01.10.2013 : NOTICED FAINT CLICKING SOUND AT NORTH GIRDER CROSS FRAME (~ 650,000 CYCLES)

01.17.2013 : NORTH CROSS FRAME BROKEN (1,061,097 CYCLES)

SIGNATURE DATE 20

READ AND UNDERSTOOD DATE 20

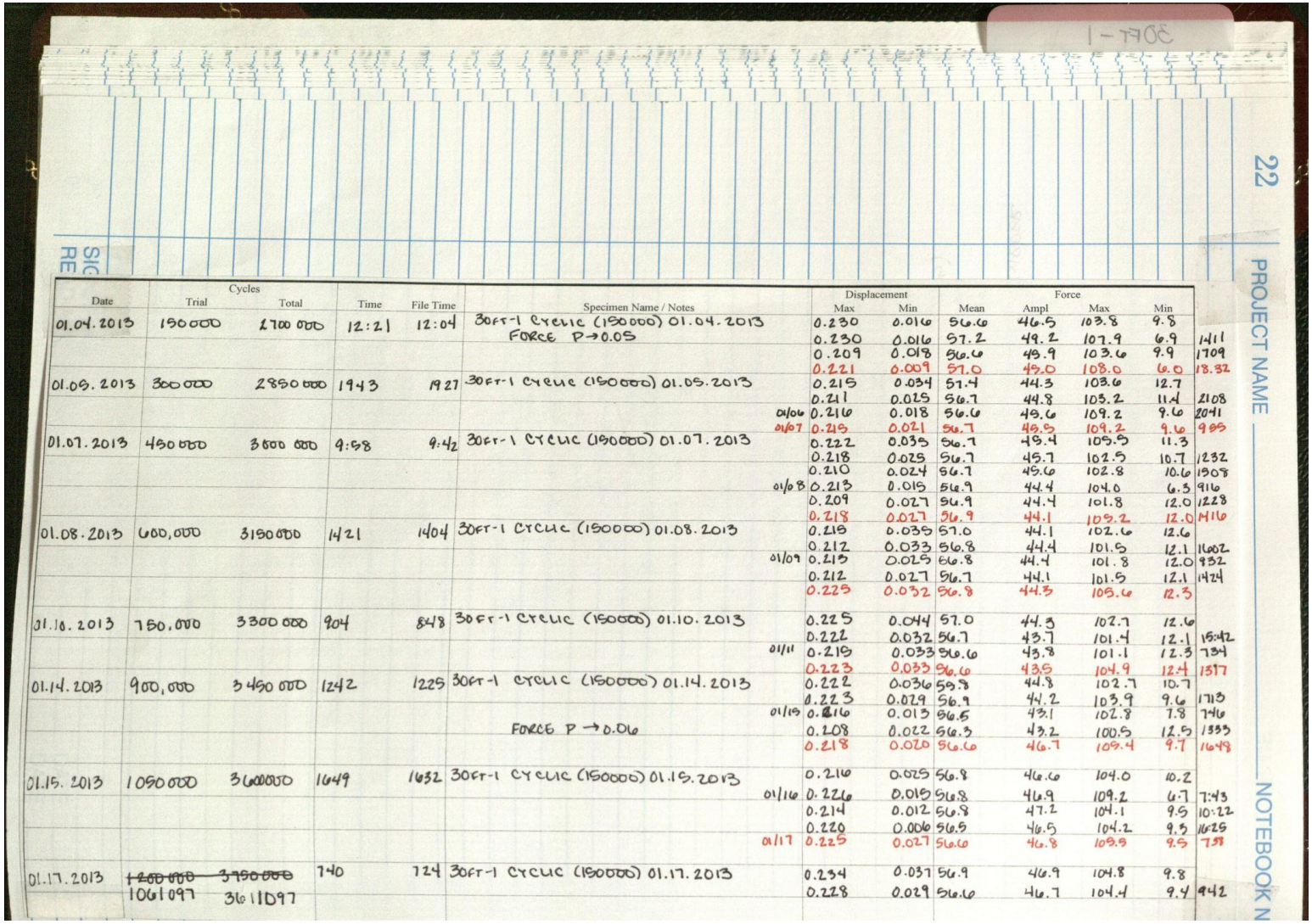

22 PROJECT NAME _____ NOTEBOOK N

SIG
RE

1-T90C

Date	Cycles Trial	Cycles Total	Time	File Time	Specimen Name / Notes		Displacement Max	Displacement Min	Force Mean	Force Ampl	Force Max	Force Min	
01.04.2013	150000	2700000	12:21	12:04	30FT-1 CYCLIC (150000) 01.04.2013 FORCE P→0.05		0.230	0.016	56.6	46.5	103.8	9.8	
							0.230	0.016	57.2	49.2	107.9	6.9	1411
							0.209	0.018	56.6	48.9	103.6	9.9	1709
							0.221	0.009	57.0	49.0	108.0	6.0	18.32
01.05.2013	300000	2850000	1943	1927	30FT-1 CYCLIC (150000) 01.05.2013		0.215	0.034	57.4	44.3	103.6	12.7	
							0.211	0.025	56.7	44.8	103.2	11.4	2108
						01/06	0.216	0.018	56.6	49.6	109.2	9.6	2041
						01/07	0.215	0.021	56.7	48.5	109.2	9.6	985
01.07.2013	450000	3600000	9:58	9:42	30FT-1 CYCLIC (150000) 01.07.2013		0.222	0.035	56.7	49.4	105.5	11.3	
							0.218	0.025	56.7	45.7	102.5	10.7	1232
							0.210	0.024	56.7	49.6	102.8	10.6	1908
						01/08	0.213	0.015	56.9	44.4	104.0	6.5	916
							0.209	0.027	56.9	44.4	101.8	12.0	1223
							0.218	0.027	56.9	44.1	105.2	12.0	1416
01.08.2013	600,000	3150000	1421	1404	30FT-1 CYCLIC (150000) 01.08.2013		0.218	0.035	57.0	44.1	102.6	12.6	
							0.212	0.033	56.8	44.4	101.5	12.1	1602
						01/09	0.215	0.025	56.8	44.4	101.8	12.0	932
							0.212	0.027	56.7	44.1	101.5	12.1	1424
							0.225	0.032	56.8	44.3	105.6	12.3	
01.10.2013	750,000	3300000	904	848	30FT-1 CYCLIC (150000) 01.10.2013		0.225	0.044	57.0	44.3	102.7	12.6	
							0.222	0.032	56.7	43.7	101.4	12.1	15:42
						01/11	0.219	0.033	56.6	43.8	101.1	12.3	734
							0.223	0.033	56.6	43.5	104.9	12.4	1517
01.14.2013	900,000	3450000	1242	1225	30FT-1 CYCLIC (150000) 01.14.2013		0.222	0.036	59.8	44.8	102.7	10.7	
							0.223	0.029	56.9	44.2	103.9	9.6	1713
						01/15	0.216	0.013	56.5	43.1	102.8	7.8	746
					FORCE P→0.06		0.208	0.022	56.3	43.2	100.5	12.5	1333
							0.218	0.020	56.6	46.7	109.4	9.7	1648
01.15.2013	1050000	3600000	1649	1632	30FT-1 CYCLIC (150000) 01.15.2013		0.216	0.025	56.8	46.6	104.0	10.2	
						01/16	0.226	0.015	56.8	46.9	109.2	6.7	7:43
							0.214	0.012	56.8	47.2	104.1	9.5	10:22
							0.220	0.006	56.5	46.5	104.2	9.5	1625
						01/17	0.225	0.027	56.6	46.8	109.9	9.5	758
01.17.2013	~~1200000~~ 1061097	~~3750000~~ 3611097	740	724	30FT-1 CYCLIC (150000) 01.17.2013		0.234	0.037	56.9	46.9	104.8	9.8	
							0.228	0.029	56.6	46.7	104.4	9.4	942

BOOK NO. 23 PROJECT NAME _____ NOTEBOOK NO. _____

RETROFIT REMOVED

NORTH GIRDER, NORTH FACE

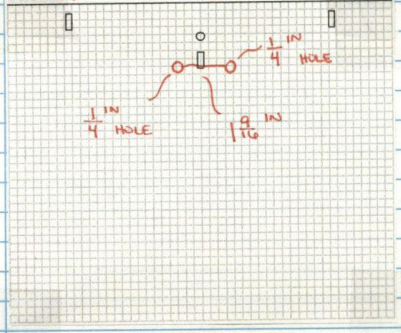

NORTH GIRDER, SOUTH FACE
→ NO CHANGE

SOUTH GIRDER, NORTH FACE

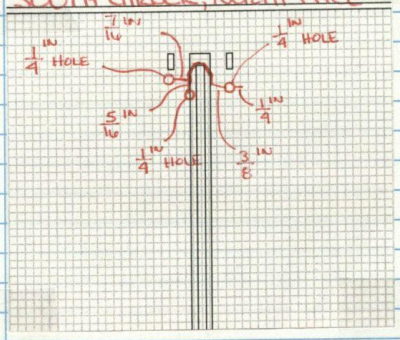

SOUTH GIRDER, NORTH FACE

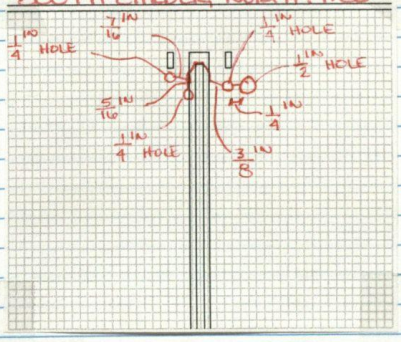

SOUTH GIRDER, SOUTH FACE

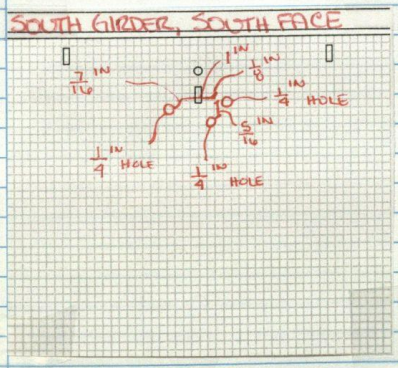

SOUTH GIRDER, SOUTH FACE

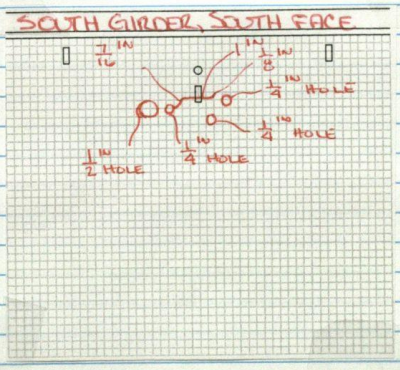

SIGNATURE _____ DATE _____ 20 _____
READ AND UNDERSTOOD _____ DATE _____ 20 _____

01.17.2013 ~~1400000~~ 1001097 ~~3150000~~ 3611097 740 724 3661-1 CYCLIC (180000) 01.17.2013 0.234 0.228 0.037 SG.9 0.029 SG.10 46.9 46.7 104.8 104.4 9.8 9.4 942

24

PROJECT NAME _____ NOTEBOOK NO. _____

RETROFIT APPLIED

TOP WEB WRAP N & S

10 - 100K

- ANGLES
- BACKPLATE
- ¼" HOLES W/ 1 - ½" HOLE ON SOUTH GIRDER, WEST OF STIFFENER

SIGNATURE _____

READ AND UNDERSTOOD _____ DATE _____ 20__

DATE _____ 20__

TTL: 3411.097

TTL: 3,611,097

Date	Cycles Trial	Cycles Total	Time	File Time	Specimen Name / Notes	Displacement Max	Displacement Min	Force Mean	Force Ampl	Force Max	Force Min	Data Time
						0.219	-0.007	56.1	45.6	102.5	10.0	
01.23.2013	150000	3761097	0951	0934	30 FT-1 CYCLIC (150,000) 01.23.2013	0.213	0.022	57.2	46.9	104.1	10.0	1329
						0.212	0.020	56.8	47.0	103.9	9.8	1622
					PAUSED	0.215	0.019	57.3	47.2	104.6	9.1	1713
					01/24	0.219	0.022	56.4	46.4	105.7	9.0	0803
					PAUSED	0.216	0.017	57.3	47.1	105.5	8.5	1701
					01/25	0.222	0.027	57.5	47.7	105.7	9.4	0815
						0.215	0.021	57.4	47.6	105.0	9.6	1102
						0.215	0.021	57.2	47.7	104.8	9.6	1307
					PAUSED	0.217	0.018	56.9	47.2	105.1	9.3	1533 ~ 126965
					01/29	0.211	0.033	56.4	43.6	100.6	11.2	1029
						0.220	0.021	57.1	47.0	105.4	8.3	
						0.218	0.027	57.2	46.8	104.3	10.2	
01.29.2013	300000	3911097	1447	1430	30 FT-1 CYCLIC (150000) 01.29.2013	0.220	0.024	57.2	47.0	105.7	9.3	1804
						0.216	0.025	56.9	46.7	103.8	10.0	1955
					01/30	0.219	0.022	57.1	46.8	104.8	9.5	0812
						0.216	0.023	57.1	46.9	104.0	10.2	1157
						0.217	0.021	57.0	46.6	104.2	9.9	1439
						0.211	0.019	56.9	46.6	103.6	10.2	1740
						0.227	0.019	57.0	46.8	105.6	9.9	
						0.227	0.035	56.9	46.4	104.9	10.7	
01.31.2013	450000	4061097	0827	0810	30 FT-1 CYCLIC (150000) 01.31.2013	0.216	0.026	56.6	46.6	103.3	10.0	1332
						0.220	0.025	57.4	46.0	104.1	9.3	1719
					02/01	0.219	0.021	57.2	46.0	103.6	10.8	0803
						0.216	0.020	57.2	46.2	105.3	10.9	1416
						0.226	0.037	56.3	44.4	104.5	10.2	
02.05.2013	600000	4211097	1042	1026	30 FT-1 CYCLIC (150000) 02.05.2013	0.227	0.032	56.9	45.6	104.9	9.5	1510
					02/06	0.223	0.028	56.6	44.9	102.8	11.0	0926 *
						0.216	0.031	56.6	45.1	101.7	11.4	1103
						0.218	0.035	56.4	44.7	101.1	11.6	1348
						0.220	0.034	56.4	44.5	101.3	11.6	1431
						0.222	0.035	56.8	44.8	102.8	11.7	
02.06.2013	750000	4361097	1431	1415	30 FT-1 CYCLIC (150,000) 02.06.2013	0.221	0.037	56.4	44.7	101.2	11.7	1721
					02/07	0.223	0.032	56.8	44.1	102.1	10.4	1011
						0.224	0.027	57.0	44.0	104.4	8.4	1246
						0.228	0.034	56.7	43.9	103.5	12.5	
						0.225	0.038	55.8	43.2	100.9	10.2	
02.11.2013	900000	4511097	0821	0805	30 FT-1 CYCLIC (150000) 02.11.2013	0.221	0.036	56.5	45.0	101.5	11.5	1215
						0.223	0.020	56.7	45.9	103	9.0	1639
					02/12	0.225	0.030	56.7	45.0	103.7	9.7	0834
						0.224	0.031	56.7	45.1	104.2	11.0	
						0.223	0.032	56.8	44.9	102.3	9.7	
02.12.2013	1050000	4661097	1307	1250	30 FT-1 CYCLIC (150000) 02.12.2013	0.221	0.036	56.7	45.2	101.8	11.6	16216
						0.222	0.037	56.8	45.1	101.9	11.5	1950
					02/13	0.224	0.031	56.6	44.9	102.2	11.2	1112 **
						0.223	0.033	56.5	45.0	101.9	11.2	1340
						0.227	0.036	56.5	44.7	102.7	11.5	

*123194 - FAINT CLICKING ON INT. GIRDER

** - LOUD " " SOUTH GIRDER

PROJECT NAME

NOTEBOOK NO. 27

Date	Cycles Trial	Cycles Total	Time	File Time	Specimen Name / Notes	Displacement Max	Displacement Min	Force Mean	Force Ampl	Force Max	Force Min	Data Time
02.14.2013	1200000	4811047	0738	0721	30 FT-1 CYCLE (USD000) 02.14.2013	0.229	0.038	564	45.3	102.0	10.7	1519
						0.228	0.032	565	44.7	102.3	9.1	2333
						0.225	0.034	566	44.9	102.3	10.9	0822
					02/15	0.222	0.029	565	45.1	102.4	10.9	1023
						0.218	0.028	565	45.2	101.9	11.5	
						0.229	0.028	564	45.8	104.4	10.6	

RETROFIT REMOVED

NORTH GIRDER, NORTH FACE → NO CHANGE

NORTH GIRDER, SOUTH FACE → NO CHANGE

SOUTH GIRDER, NORTH FACE → NO CHANGE

SOUTH GIRDER, SOUTH FACE

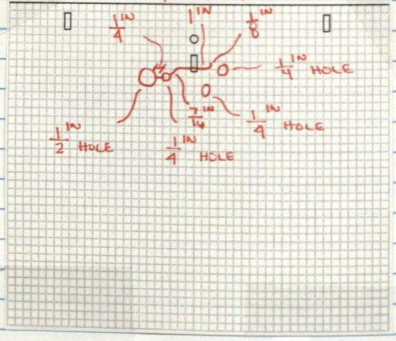

SIGNATURE

READ AND UNDERSTOOD DATE 20

DATE 20

BOOK NO. 27

PROJECT NAME _____ NOTEBOOK NO. _____

RETROFIT APPLIED

TOP WEB GAP N & S 12 - 120 K

- ANGLES
- BACKPLATE
- $\frac{1}{9}$ IN HOLES W/ 1 - $\frac{1}{2}$ IN HOLE ON SOUTH GIRDER, WEST OF STIFFENER

SIGNATURE _____ DATE _____ 20 _____

READ AND UNDERSTOOD _____ DATE _____ 20 _____

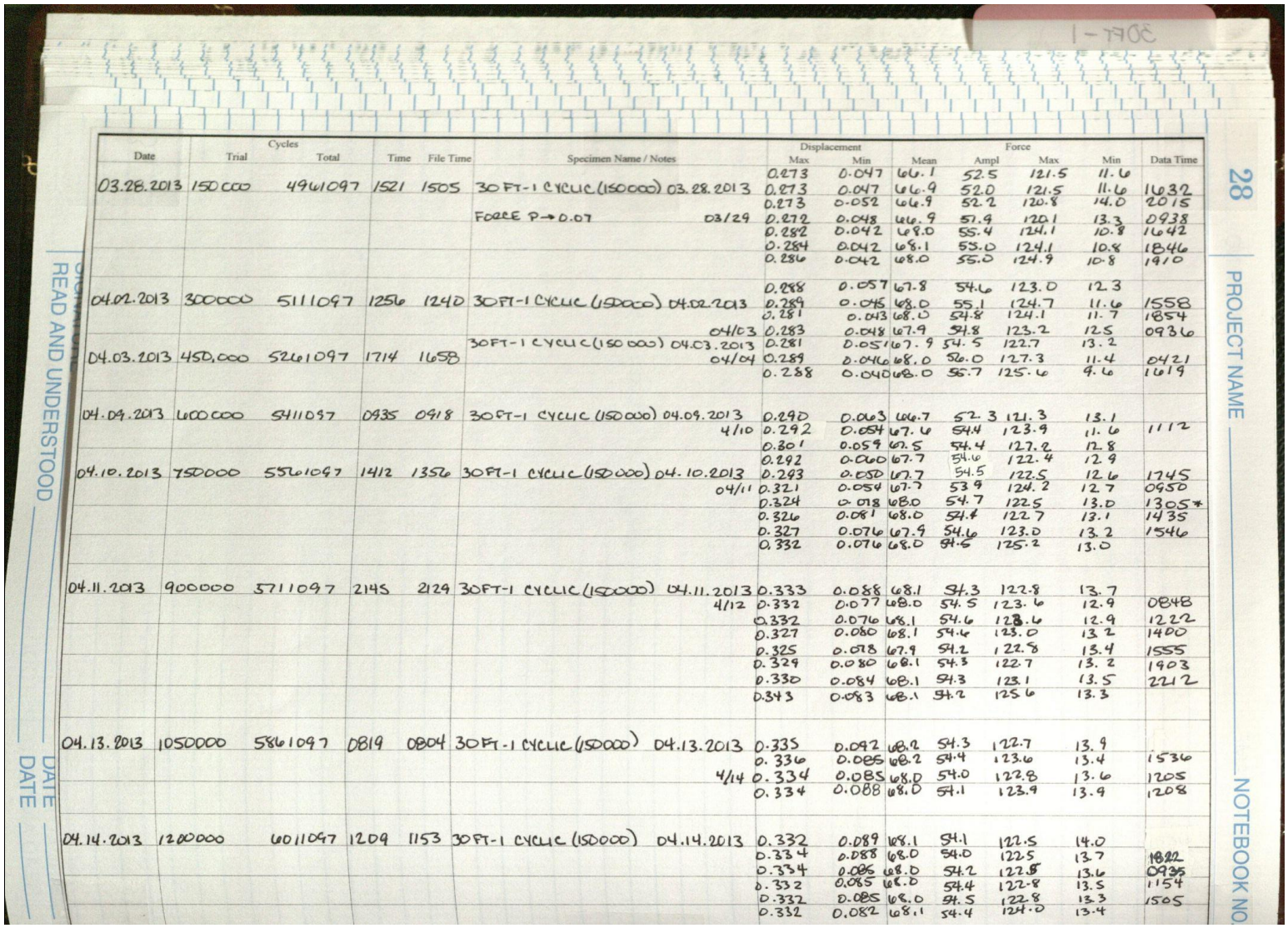

Date	Trial	Cycles Total	Time	File Time	Specimen Name / Notes	Displacement Max	Displacement Min	Force Mean	Force Ampl	Force Max	Force Min	Data Time
						0.273	0.047	66.1	52.5	121.5	11.6	
03.28.2013	150 000	4961097	1521	1505	30 FT-1 CYCLIC (150000) 03.28.2013	0.273	0.047	66.9	52.0	121.5	11.6	1632
						0.273	0.052	66.9	52.2	120.8	14.0	2015
					FORCE P→0.07 03/29	0.272	0.048	66.9	51.9	120.1	13.3	0938
						0.282	0.042	68.0	55.4	124.1	10.8	1642
						0.284	0.042	68.1	53.0	124.1	10.8	1846
						0.286	0.042	68.0	55.0	124.9	10.8	1910
						0.288	0.057	67.8	54.6	123.0	12.3	
04.02.2013	300000	5111097	1256	1240	30FT-1 CYCLIC (150000) 04.02.2013	0.289	0.045	68.0	55.1	124.7	11.6	1558
						0.281	0.043	68.0	54.8	124.1	11.7	1854
					04/03	0.283	0.048	67.9	54.8	123.2	12.5	0936
					30FT-1 CYCLIC (150 000) 04.03.2013	0.281	0.051	67.9	54.5	122.7	13.2	
04.03.2013	450,000	5261097	1714	1658	04/04	0.289	0.046	68.0	56.0	127.3	11.4	0421
						0.288	0.040	68.0	56.7	125.6	9.6	1619
04.09.2013	600 000	5411097	0935	0918	30FT-1 CYCLIC (150 000) 04.09.2013	0.290	0.063	66.7	52.3	121.3	13.1	
					4/10	0.292	0.054	67.6	54.4	123.9	11.6	1112
						0.301	0.059	67.5	54.4	127.2	12.8	
						0.292	0.060	67.7	54.6	122.4	12.9	
04.10.2013	750000	5561097	1412	1356	30FT-1 CYCLIC (150000) 04.10.2013	0.293	0.050	67.7	54.5	122.5	12.6	1745
					04/11	0.321	0.054	67.7	53.9	124.2	12.7	0950
						0.324	0.078	68.0	54.7	122.5	13.0	1305*
						0.326	0.081	68.0	54.4	122.7	13.1	1435
						0.327	0.076	67.9	54.6	123.0	13.2	1546
						0.332	0.076	68.0	54.5	125.2	13.0	
04.11.2013	900000	5711097	2145	2124	30FT-1 CYCLIC (150000) 04.11.2013	0.333	0.088	68.1	54.3	122.8	13.7	
					4/12	0.332	0.077	68.0	54.5	123.6	12.9	0848
						0.332	0.076	68.1	54.6	123.6	12.9	1222
						0.327	0.080	68.1	54.4	123.0	13.2	1400
						0.325	0.078	67.9	54.2	122.8	13.4	1555
						0.329	0.080	68.1	54.3	122.7	13.2	1903
						0.330	0.084	68.1	54.3	123.1	13.5	2212
						0.343	0.083	68.1	54.2	125.6	13.3	
04.13.2013	1050000	5861097	0819	0804	30FT-1 CYCLIC (150000) 04.13.2013	0.335	0.092	68.2	54.3	122.7	13.9	
						0.336	0.085	68.2	54.4	123.6	13.4	1536
					4/14	0.334	0.085	68.0	54.0	122.8	13.6	1205
						0.334	0.088	68.0	54.1	123.9	13.9	1208
04.14.2013	1200000	6011097	1209	1153	30FT-1 CYCLIC (150000) 04.14.2013	0.332	0.089	68.1	54.1	122.5	14.0	
						0.334	0.088	68.0	54.0	122.5	13.7	1822
						0.334	0.086	68.0	54.2	122.8	13.6	0935
						0.332	0.085	68.0	54.4	122.8	13.5	1154
						0.332	0.085	68.0	54.5	122.8	13.3	1505
						0.332	0.082	68.1	54.4	124.0	13.4	

BOOK NO.

29

PROJECT NAME RETROFIT REMOVED

NOTEBOOK NO.

												10:22	
D.334	0.088	48.0	54.0	122.5	13.7							09:35	
D.334	0.086	48.0	54.2	122.8	13.6							11:54	
D.332	0.085	48.0	54.4	122.8	13.5								
D.332	D.085	48.0	54.5	122.8	13.3							15:05	
D.332	D.082	48.1	54.4	124.0	13.4								

4 | 5/8 CLICKING - MIDDLE GIRDER, PAINT CLICKING IN EST. GIRDER

NORTH GIRDER, NORTH FACE

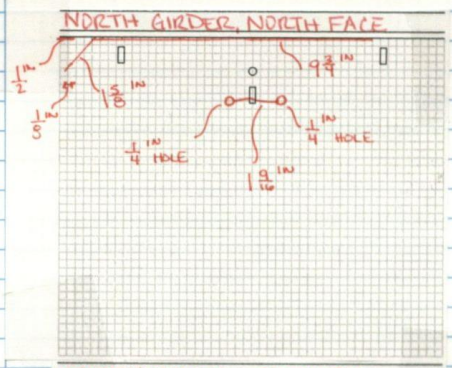

NORTH GIRDER, SOUTH FACE

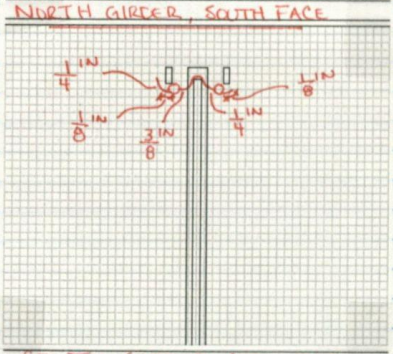

SOUTH GIRDER, NORTH FACE

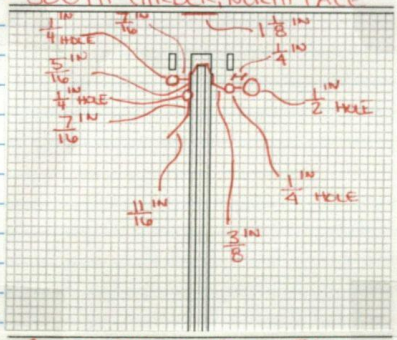

SOUTH GIRDER, SOUTH FACE

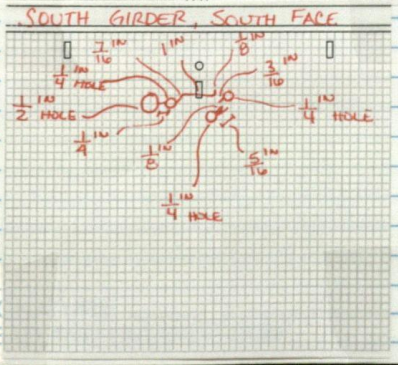

SIG

RE

DATE 20

DATE 20

APPENDIX REFERENCES

Nagati, D. (2012). "Repair of Steel Bridge Girders Damaged by Distortion-Induced Fatigue." Master's Thesis, University of Kansas.